Universitat Politècnica de València
Departamento de Máquinas y Motores Térmicos

UNIVERSITAT
POLITÈCNICA
DE VALÈNCIA

Study of different Exhaust Gas Recirculation configurations and their impact on turbocharged spark ignition engines

Doctoral Thesis
Presented by:
Rafael Pitarch Berná
Directed by:
Dr. Joaquín De La Morena Borja

Valencia, June 2023

Doctoral Thesis

Study of different Exhaust Gas Recirculation configurations and their impact on turbocharged spark ignition engines

Presented by: Rafael Pitarch Berná
Directed by: Dr. Joaquín De La Morena Borja

Tribunal:

President: Dr. Benjamín PLÁ
Secretary: Dr. Francisco V. VERA
Vocal: Dr. Octavio ARMAS

External Evaluators:

Dr. Francisco V. VERA
Dr. Miguel Ángel REYES
Dra. Reyes GARCÍA CONTRERAS

Valencia, June 2023

A mis padres, hermana y yayos,
que han sido mi apoyo y ejemplo.

Impossible is not a fact. It's an opinion.
Impossible is not a declaration. It's a dare.
Impossible is potential. Impossible is temporary.
Impossible is nothing.
Muhammad Ali

Without data, you're just
another person with an opinion.
William Edwards Deming

Resumen

Esta tesis doctoral se encuadra en el contexto de una creciente concienciación y preocupación en la sociedad por la contaminación y su efecto sobre la salud de las personas, así como la influencia de los gases de efecto invernadero en el cambio climático. En este sentido, el sector transporte no ha sido una excepción, y se ha legislado para regular tanto las emisiones contaminantes como las de efecto invernadero de manera cada vez más estricta, retando continuamente a las empresas del sector y fabricantes de motores a aumentar la eficiencia y limpieza de sus sistemas propulsivos.

Este trabajo tiene por objetivo estudiar el impacto que tienen distintos sistemas de recirculación de gases de escape (exhaust gas recirculation o EGR) en un motor de encendido provocado, de inyección directa, sobrealimentado, con distribución variable y dentro de la tendencia del downsizing. Cabe resaltar que el motor bajo estudio es un modelo sin EGR empleado actualmente en aplicaciones de transporte por carretera de turismos utilitarios, por lo que el proyecto ha estado en todo momento ligado a la actualidad del sector, y los avances y descubrimientos de los estudios aquí presentados pueden resultar de una enorme utilidad y ser empleados en aplicaciones reales.

Estos sistemas de recirculación de gases de escape pretenden aumentar la eficiencia de los motores de encendido provocado con el objetivo de reducir la desventaja que estos presentan con respecto a los motores de encendido por compresión, mientras que se mantienen los niveles de emisiones. Dicha desventaja en eficiencia radica principalmente en una menor relación de compresión del motor de encendido provocado para evitar la autoignición y en el uso del dosado estequiométrico para el correcto funcionamiento del postratamiento.

En una primera aproximación, se implementa un circuito de EGR de baja presión para analizar el efecto que tiene la dilución con gases de escape en el funcionamiento del motor, la calibración óptima y el funcionamiento del postratamiento. Para ello, se desarrolla una metodología de diseño de experimentos en varios puntos de operación del motor en régimen estacionario con el objetivo de obtener el consumo especifico mínimo. En dicho diseño de experimentos, las variables son la distribución variable de admisión y escape, el tiempo de ignición a través de la chispa y la tasa de EGR. De esta manera, se obtienen los parámetros de calibración y la tasa de EGR óptima para cada punto, obteniendo mejoras notables en consumo de combustible y por lo tanto en emisiones de dióxido de carbono. Después, se estudia la interacción entre los gases de escape recirculados y los residuales internos que no han podido barrerse del ciclo anterior, y la influencia de diluir con más EGR o con más IGR, pues la composición y temperatura entre ambos difiere notablemente. Estos residuales juegan un papel muy importante a baja carga debido a la alta presión de escape respecto a la de admisión, y pueden regularse con el sistema de distribución variable. Por último, se analiza el problema de dilución espontánea inducido por la condensación de parte del vapor de agua presente en el gas de escape recirculado. Cuando estas gotas de agua condensadas se acumulan y entran en el cilindro, pueden provocar inestabilidades que afectan a la eficiencia y las emisiones.

En la segunda etapa del proyecto, y una vez implementado el circuito de baja presión y analizados sus beneficios, se pretende explorar las distintas opciones que existen para llevar a cabo la dilución con EGR. Para ello, se instala en el motor un circuito de EGR de alta presión y posteriormente otro de baja presión en el que los gases de escape se extraen antes del postratamiento, de manera que la composición de los gases es más parecida a la de los residuales internos. Se realiza el mismo barrido de EGR con cada circuito en los distintos puntos de operación y se comparan los sistemas dos a dos en términos de combustión, emisiones, balance de energía y eficiencia, siendo el sistema común en ambas comparativas el circuito de baja presión tradicional.

Abstract

This PhD-Thesis is framed in the context of a growing awareness and concern in society about pollution and its effect on people's health, as well as the influence of greenhouse gases on climate change. In this sense, transportation has not been an exception, and legislation has been created to regulate both polluting emissions and greenhouse gases in an increasingly strict manner, continually challenging companies in the sector and engine manufacturers to increase efficiency and cleanliness of their propulsive systems.

The objective of this work is to study the impact that different exhaust gas recirculation (EGR) systems have on a spark ignition, direct injection, turbocharged engine, with a variable timing and within the downsizing trend. It should be noted that the engine under study is mass-produced without EGR and is currently used in passenger utility cars, so the project has been always linked to current events in the sector, and the advances and discoveries of the studies presented here can be useful in real applications.

These exhaust gas recirculation systems aim to increase the efficiency of spark ignition engines, reducing the disadvantage they present with respect to compression ignition engines, while maintaining emission levels. Said disadvantage in efficiency lies mainly in a lower compression ratio in order to avoid autoignition and in the use of stoichiometric operation for the optimal operation of the aftertreatment system.

In a first approach, a low-pressure EGR circuit is implemented to analyze the effect that exhaust dilution has on engine performance, optimum calibration and aftertreatment performance. A methodology for the design of experiments is developed and applied at several steady state operating conditions with the aim of obtaining the minimum specific fuel consumption. In this design of experiments, the variables are the intake and exhaust timing, ignition through spark timing and EGR rate. In this way, the optimal calibration parameters and EGR rate for each condition are obtained, with notable improvements in fuel consumption and therefore in carbon dioxide emissions. Then, the interaction between the recirculated exhaust gases and the internal residuals that could not be swept from the previous cycle is studied, together with the influence of diluting with more EGR or IGR, since the composition and temperature between the two differ significantly. These residuals play a very important role at low load due to the high exhaust pressure relative to the intake side, and can be regulated with the variable valve timing system. Finally, the problem of spontaneous dilution induced by condensation of part of the water vapor present in the recirculated exhaust gas is analyzed. When these condensed water droplets accumulate and enter the cylinder, instabilities can appear, affecting efficiency and emissions.

In the second stage of the project, and once the low-pressure circuit has been implemented and its benefits analyzed, it is intended to explore the different options that exist to carry out the dilution with EGR. To do this, a high-pressure EGR circuit and another low-pressure one are installed in the engine. The second low-pressure EGR circuit differs from the first one in the extraction of the exhaust gases, upstream the aftertreatment, so that the composition of the gases is more similar

to that of the IGR. The same EGR sweep is performed with each circuit at different operating conditions and the systems are compared two by two in terms of combustion, emissions, energy balance and efficiency, the common system in both comparisons being the traditional low-pressure circuit.

Resum

Aquesta tesi doctoral s'enquadra en el context d'una creixent conscienciació i preocupació en la societat per la contaminació i el seu efecte sobre la salut de les persones, així com la influència dels gasos d'efecte d'hivernacle en el canvi climàtic. En aquest sentit, el transport no ha sigut una excepció, i s'ha legislat per a regular tant les emissions contaminants com les d'efecte d'hivernacle de manera cada vegada més estricta, reptant contínuament a les empreses del sector i fabricants de motors a augmentar l'eficiència dels seus sistemes propulsius.

Aquest treball té per objectiu estudiar l'impacte que tenen diferents sistemes de recirculació de gasos d'escapament (exhaust gas *recirculation o EGR) en un motor d'encesa provocada, d'injecció directa, sobrealimentat, amb distribució variable i dins de la tendència del downsizing. Cal ressaltar que el motor sota estudi és un model sense EGR empleat actualment en aplicacions de transport per carretera de turismes utilitaris, per la qual cosa el projecte ha estat en tot moment lligat a l'actualitat del sector, i els avanços i descobriments dels estudis presentats poden resultar d'una enorme utilitat i ser emprats en aplicacions reals.

Aquests sistemes de recirculació de gasos d'escapament pretenen augmentar l'eficiència dels motors d'encesa provocada amb l'objectiu de reduir el desavantatge que aquests presenten respecte als motors d'encesa per compressió, mantenint els nivells d'emissions. Aquest desavantatge en eficiència radica principalment en una menor relació de compressió del motor d'encesa provocada per a evitar l'autoignició i en l'ús del dosatge estequiomètric per al correcte funcionament del postractament.

En una primera aproximació, s'implementa un circuit de EGR de baixa pressió per a analitzar l'efecte que té la dilució amb gasos d'escapament en el funcionament del motor, el calibratge òptim i el funcionament del postractament. Per a això, es desenvolupa una metodologia de disseny d'experiments en diversos punts d'operació del motor en règim estacionari amb l'objectiu d'obtindre el consum específic mínim. En aquest disseny d'experiments, les variables són la distribució variable d'admissió i escapada, el temps d'ignició a través de l'espurna i la taxa de EGR. D'aquesta manera, s'obtenen els paràmetres de calibratge i la taxa de EGR òptima per a cada punt, obtenint millores notables en consum de combustible i per tant en emissions de diòxid de carboni. Després, s'estudia la interacció entre els gasos d'escapament recirculats i els residuals interns que no s'han pogut extraure del cicle anterior, i la influència de diluir amb més EGR o amb més IGR, perquè la composició i temperatura dels dos difereix notablement. Aquests residuals juguen un paper molt important a baixa càrrega a causa de l'alta pressió d'escapament respecte a la d'admissió, i poden regular-se amb el sistema de distribució variable. Finalment, s'analitza el problema de dilució espontània induït per la condensació de part del vapor d'aigua present en el gas d'escapament recirculada. Quan aquestes gotes d'aigua condensades s'acumulen i entren en el cilindre, poden provocar inestabilitats que afecten l'eficiència i les emissions.

En la segona etapa del projecte, i una vegada implementat el circuit de baixa pressió i analitzats els seus beneficis, es pretén explorar les diferents opcions que existeixen per a dur a terme la dilució amb EGR. Per a això, s'instal·la en el motor

un circuit de EGR d'alta pressió i posteriorment un altre de baixa pressió en el qual els gasos d'escapament s'extrauen abans del postractament, de manera que la composició dels gasos és més semblant a la dels residuals interns. Es realitza el mateix anàlisi de EGR amb cada circuit en els diferents punts d'operació i es comparen els sistemes dos a dos en termes de combustió, emissions, balanç d'energia i eficiència, sent el sistema comú en les dos comparatives el circuit de baixa pressió tradicional.

Agradecimientos

Antes de comenzar con el grueso del documento, me gustaría dedicar este espacio a todas las personas que han formado parte de esto. Estoy seguro de que sin ellas, esta tesis no habría sido posible.

En primer lugar dar las gracias a Joaquín De La Morena, mi director de tesis. Fue uno de mis profesores favoritos durante la carrera por su manera de transmitir la materia y su cercanía, además de impartir una de mis asignaturas preferidas, Combustión. Durante estos cuatro años, ha sabido dirigir mi trabajo en CMT de la mejor manera posible, siempre pendiente de mí pero dándome un espacio y una libertad a la de hora de desarrollar los proyectos y la tesis que casan a la perfección con mi manera de ser y de trabajar. Es por esto que me he sentido enormemente afortunado, más aún comparando mi situación con otras que conozco de primera mano. Además, Joaquín siempre ha sabido aportar esa idea o enfoque distintivos, arrojando luz al problema cuando no encontrábamos respuesta.

Dar las gracias también a Vicente Esteve. Creo que no podría haber mejor técnico de sala para todos los ensayos y montajes que hemos hecho a lo largo de estos años. Siempre de un buen humor contagioso, atento a cada detalle y con una paciencia a prueba de bombas. Siempre he valorado mucho lo difícil de su trabajo, más aún en ese breve de espacio de tiempo en que me tocó ensayar sin él. También agradecer a David González, un titán en todos los aspectos. Nuestras tesis han ido de la mano desde el primer día, compartiendo motor, ensayos y a veces análisis. Sin él, seguramente estaría lanzando simulaciones en GT-Power todavía. Echaré de menos nuestros adjetivos "panteriles". Tanto David como Antonio Jiménez han sido más amigos que compañeros de trabajo y una vía de escape con quien comentar cualquier situación o anécdota. Dar las gracias también a todos los alumnos con los que hemos hecho trabajos finales, por su aportación al análisis y por permitir ponerme a prueba como tutor, en especial a Francisco, María y Nuria. También a todos los compañeros de despacho que he tenido, sobre todo a André, Elena, Enrique y Juancho.

En el aspecto personal, no podría olvidarme de mis padres, mis yayos y mi hermana. Mis padres, Gloria y Rafa, han sido un apoyo fundamental en todos los aspectos, transmitiéndome sus valores y su forma de entender la vida, además de ser un ejemplo de amor diario. Agradecerles que siempre me han proporcionado la estabilidad, la perspectiva y los medios necesarios, incluso en la distancia, especialmente en los momentos más difíciles. Ambos han demostrado tesón, diligencia, una entrega infatigable y un valor y afán de superación enormes. De igual forma, mi hermana Paula y mis yayos, Gloria y Manuel, han sido vitales en mi día a día, ayudándome de la mejor manera posible y siendo mis segundos padres. Sin todos ellos, nada de esto habría sido posible y perdería el sentido celebrar cualquier éxito conseguido en la vida.

Disclaimer

Rafael Pitarch Berná is co-author of the publications listed below, together with several members of the I.U. CMT-Motores Térmicos and directly supervised by Prof. Joaquín de la Morena Borja. The PhD-Candidate position of last signatory of the organization in the publications is justified by the CMT-Motores Térmicos protocol of signing, based on seniority. These publications are the result of the different researching activities developed during the course of the candidate's doctorate and part of the publications needed in order to fulfill it. For the sake of fluent reading and to maintain a coherent structure, these publications are not explicitly cited every time that a part of it is used for this document, despite figures, discusions and explanations may be directly extracted from the publications. The objective of this disclaimer is to justify the similarity of the previous work with this document and the lack of direct citation. The list of publications is the following:

1. Piqueras P., De la Morena J. De, Sanchis E. J. and Pitarch R. "Impact of Exhaust Gas Recirculation on Gaseous Emissions of Turbocharged Spark-Ignition Engines". *Applied Sciences*, pp. 1-17, 2020.
2. Galindo J., Climent H., De la Morena J., Pitarch R., Guilain S. and Besancon T. "A methodology to study the interaction between variable valve actuation and exhaust gas recirculation systems for spark-ignition engines from combustion perspective". *Energy, Conversion and Management*, Vol. 250, 2021.
3. Galindo J., Navarro R., De la Morena J., Pitarch R. and Guilain S. "On combustion instability induced by water condensation in a low-pressure exhaust gas recirculation system for spark-ignition engines". *Energy*, Vol. 261, 2022.
4. Galindo J., Navarro R., De la Morena J., Pitarch R. and Guilain S. "Influence of the low-pressure exhaust gas recirculation injection point on engine performance". *Proceedings of the Institution of Mechanical Engineers, Part D: Journal of Automobile Engineering*, 2022.

Table of Contents

Index of Figures

Index of Tables

Nomenclature

Latin

a	Speed of sound
A	Area
$a-d$	Correlation coefficients
$A-E$	NIST polynomial coefficients
B	Engine bore
C	Carbon
$C1-C2$	Woschni constants
CH_4	Methane
CO	Carbon monoxide
CO_2	Carbon dioxide
c_p	Specific heat capacity at constant pressure
c_R	Crank radius
c_v	Specific heat capacity at constant volume
d	Delta
D	Mass diffusivity
Da	Damköhler number
$E40$	Ethanol fuel blend of 40%
$F1$	Formula 1
Fr	Fuel/Air equivalence ratio
H	Hydrogen
H_2	Molecular hydrogen
H_2O	Water
HC	Unburnt hydrocarbon
$H_mC_nO_p$	General formulation for hydrocarbons

i	Thermodynamic cycles per engine revolution
I	Turbulent intensity
Ka	Karlovitz number
L	Length
L_{inte}	Integral length
L_T	Taylor length scale
m	Mass
$\dot{m}_i$	Mass flow of the species i
M_i	Manufacturer averaged fleet mass
M_O	European fleet averaged mass
n	Engine speed
N_2	Nitrogen molecule
NH_3	Ammonia
NO	Nitrogen monoxides
NO_2	Nitrogen dioxides
NO_x	Nitrogen oxides
O	Oxygen
O_2	Oxygen molecule
OH	Hydroxyl radical
P	Pressure
PM	Particulate matter emissions
PN	Particulate number
r	Compression ratio
r_L	Connecting rod length
R_u	Universal gas constant
S	Engine stroke
S_L	Laminar burning speed
SO_x	Sulfur oxides
t	Temperature divided by 1000
T	Temperature
THC	Total hydrocarbon emissions
US	United states
U_t	Local turbulent fluctuation speed
V	Volume

w	Specific humidity
W	Work
x	Piston position

Greek

α	Temperature exponent for laminar flame speed
β	Pressure exponent for laminar flame speed
γ	Isentropic exponent
δ	Thickness of the flame front
Δ	Variation
η	Efficiency
η_c	Compressor efficiency
η_e	Break efficiency
η_v	Volumetric efficiency
θ	Crank angle
λ	Air/Fuel equivalence ratio
λ_K	Kolmogorov scale
π	Pi number
ρ	Density
τ	Ignition delay
τ_x	Characteristic time of the x subscript

Subscripts and superscripts

0	Relative to standard conditions
1	Relative to upstream the compressor conditions
2	Relative to downstream the compressor conditions
$2'$	Relative to intake manifold conditions
3	Relative to upstream the turbine conditions
4	Relative to downstream the turbine conditions
a	Relative to after
air	Relative to fresh air conditions
amb	Relative to ambient conditions
atm	Relative to atmospheric conditions
b	Relative to the conditions of the burnt mixture
$comb$	Relative to the combustion process
$cond$	Relative to condensed phase

cooler	Relative to the EGR cooler
cc	Relative to the combustion chamber
cyl	Relative to the conditions inside of the cylinder
disp	Relative to displaced volume
dry	Relative to dry conditions
e	Relative to equilibrium conditions
EGR	Relative to EGR
exh	Relative to exhaust conditions
exp	Relative to experimental conditions
f	Relative to the flame front
in	Relative to intake conditions
inte	Relative to the integral scale
isen	Relative to isentropic conditions
K	Relative to the Kolmogorov scale
L	Relative to laminar conditions
m	Number of hydrogens in a hydrocarbon
mix	Relative to mixture between air and EGR
n	Number of carbons in a hydrocarbon
o	Number of oxygens in a hydrocarbon
O_2	Relative to molecular oxygen
out	Relative to outlet conditions
R	Relative to reaction time
rad	Relative to radical
real	Relative to real conditions
req	Relative to required
sat	Relative to saturation conditions
spark	Relative to spark timing conditions
t	Relative to turbulent conditions
ub	Relative to the conditions of the unburnt mixture
v	Relative to volumetric parameters
vap	Relative to vapor conditions
w	Relative to the in-cylinder walls
WCAC	Relative to WCAC conditions

Acronyms

0D	Zero-dimensional
1D	One-dimensional

AMF	Air mass flow
ANN	Artificial neuronal network
aTDC	After top dead center
BDC	Bottom dead center
BMEP	Brake mean effective pressure
BSFC	Brake specific fuel consumption
bTDC	Before top dead center
CA	Crank angle
CAXX	Referred to the crank angle where XX% of the heat has been released
CAD	Crank angle degree
CFD	Computational fluid dynamics
CI	Compression ignition
CLD	Chemiluminescence detector
COMB	Combustion
COV	Coefficient of variation
CR	Compression ratio
CVCC	Compound vortex controlled combustion
D-EGR	Dedicated exhaust gas recirculation
DI	Direct injection
DISI	Direct injection spark ignited
DOC	Diesel oxidation catalyst
DoE	Design of experiments
DPF	Diesel particulate filter
ECU	Electronic control unit
EGR	Exhaust gas recirculation
EIVC	Early intake valve closing
EMAX	Maximum error
EVC	Exhaust valve closing
EVO	Exhaust valve opening
EXH	Exhaust
FE	Fuel efficiency
FID	Flame ionization detector
FM	Friction multiplier
FMEP	Friction mean effective pressure

FSI	Fuel stratified injection
GDI	Gasoline direct injection
GPF	Gasoline particle filter
GTDI	Gasoline turbocharged direct injection
GWP	Global warming potential
HCCI	Homogeneous charge compression ignition
HP	High pressure
HRR	Heat release rate
HT	Heat transfer
HTM	Heat transfer multiplier
IGR	Internal gas recirculation
IMEP	Indicated mean effective pressure
IMPO	Integral of modulus of pressure oscillations
IND	Indicated
IUFC15	Inrets urban fluid court 15 driving cycle
IVC	Intake valve closing
IVO	Intake valve opening
JTD	Jet turbo diesel
LHV	Lower heating value
LIVC	Late intake valve closing
LP	Low pressure
MAPE	Mean absolute percentage error
MAPO	Maximum amplitude of pressure oscillations
MFB	Mass fraction burnt
MGU-H	Motor generator unit-heat
MIVEC	Mitshubishi innovative valve timing and electronic control system
MPD	Magnetopneumatic detector
MPE	Mean percentage error
MPS	Mean piston speed
MW	Molecular weight
NDIR	Non-dispersive infrared detector
NEDC	New European driving cycle
NMHC	Non-methane hydrocarbons
NMVOC	Non-methane volatile organic compounds

NVO	Negative valve overlap
OCM	Overall convection multiplier
ON	Octane number
PFI	Port fuel injection
PhD	Doctor of Philosophy
PISI	Port injection spark ignited
PLIF	Planar laser-induced fluorescence
PMEP	Pumping mean effective pressure
ppm	Parts per million
RCM	Rapid compression machine
RDC	Real driving cycles
RGF	Residual gas fraction
RH	Relative humidity
RICE	Reciprocating internal combustion engine
rpm	Revolutions per minute
SCR	Selective catalytic reduction aftertreatment system
SI	Spark ignition
TDC	Top dead center
TDI	Turbocharged direct injection
TFSI	Turbocharged fuel stratified injection
TOC	Time of combustion
TWC	Three-way catalyst
VANOS	Variable Nockenwellen Steuerung (Variable Camshaft Timing)
VCR	Variable compression ratio
VGT	Variable geometry turbine
VNT	Variable nozzle turbine
VTEC	Variable valve timing and lift electronic control
VVEL	Variable valve event and lift
VVT	Variable valve timing
VVT-i	Variable valve timing inteligence
WCAC	Water charge air cooler
WLTP	Worldwide harmonized light vehicles test procedure
WOT	Wide open throttle

Chapter 1

Introduction

Contents

1.1 Historical introduction

Reciprocating internal combustion engines (RICE) are used extensively for many purposes since their invention more than a century ago. If a date had to be set for the birth of modern engines, the date would be 1876, when Nikolaus August Otto applied for a patent entitled *Gasmotor*, which was obtained in the name of Gasmotorenfabrik Deutz AG with the number DE 532. The four-stroke cycle under which this engine operated is now known as the Otto Cycle, named after its inventor (US Patent No. 194,047, dated August 14, 1877).

The Otto engine was the result of centuries of evolution, since the first milestones date back to prehistory with the invention of the fire piston, a Southeast Asian device used to kindle fire using a piston to achieve a rapid and adiabatic compression of air. Also in Asia, between centuries IX and XIII, gunpowder appears as the first known chemical explosive, and was used for rocketry and pyrotechnics. Much later, in 1780, Alessandro Volta invents a toy gun that shoots a cork by means of an explosion of a mixture of oxygen and hydrogen ignited by an external energy input.

The first antecedents of RICE were undoubtedly the steam engines developed in the 18th century during the first industrial revolution. This machines are considered the first capable of producing mechanical energy with an acceptable efficiency.

During the course of the XIX century, there were many innovations, among which stand out those coming from Jean Joseph Etienne Lenoir and Alphonse Beau de Rochas. In 1860, Lenoir patented an engine without previous compression of the load (Patent US 31 722). Few years later, in 1862, Beau de Rochas established the importance of compressing the load before combustion and obtained the first known patent of a four-stroke engine (Patent FR 52593).

In 1864, Eugen Langen and Nikolaus August Otto founded the aforementioned company Gasmotorenfabrik Deutz AG, in which Gottlieb Daimler and Wilhelm Maybach also worked. Two years after the Otto engine, Dugald Clerk developed the first spark ignition (SI) engine with a two-stroke cycle. In 1882, James Atkinson patented the engine with Atkinson cycle. The difference between these two is the decoupling of the compression and expansion ratios.

In 1885, Daimler mounted a gasoline engine in collaboration with Maybach on a two-wheeled vehicle, giving birth to the motorcycle. Finally, in 1886 Karl Benz produced the first ever automobiles powered by a four-stroke cycle gasoline engine, as the one in Figure 1.1.

With the aim of getting as close as possible to the ideal Carnot cycle [1], Rudolf Diesel patented in 1892 the concept of the engine that today bears

Figure 1.1. *Karl Benz's first automobile powered by a gasoline engine, 1886.*

his name. The idea was to keep a constant pressure during the expansion stroke, so fuel had to be injected while burning. In this way, only air was compressed instead of a mixture of air and fuel. The indicator diagram of both thermodynamic cycles, Otto and Diesel, are depicted in Figure 1.2.

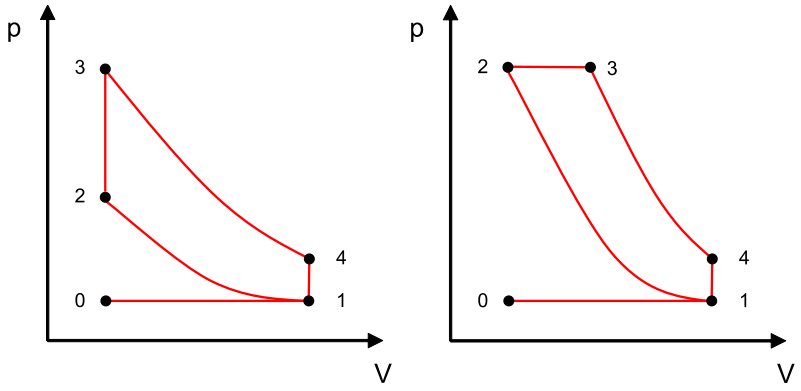

Figure 1.2. *P-V diagram of Otto (left) and Diesel (right) cycles.*

On the one hand, Otto proposed a cycle based on 6 processes:

- 0-1: Intake of gas at isobaric condition.

- 1-2: The gas undergoes an isentropic compression.
- 2-3: Isochoric heat input. Increase of pressure.
- 3-4: The gas undergoes an isentropic expansion.
- 4-1: Isochoric residual heat transfer. Decrease of pressure.
- 1-0: Exhaust of gas at isobaric condition.

On the other hand, Diesel proposed a change in process 2-3 so that the heat input was at isobaric conditions, whereas in the Otto cycle it is at isochoric conditions.

In 1902, Louis Renault obtained a patent for a centrifugal compressor for turbocharging and Leon Levavasseur invented a mechanical system for gasoline injection. In 1905, Alfred Buchi patented a turbocharged engine with a turbine powered by exhaust gases.

Warlike conflicts brought enormous development of RICE, with great advances such as the implementation of turbochargers to a Renault spark-ignited engine for fighter planes during World War I (1914-1918). Turbocharged spark-ignited engines with direct injection (DI) were commonly used in the course of the World War II (1939-1945), even having variable valve timing systems.

Jonas Hesselman presented the first spark ignition gasoline engine with a direct injection system in 1925. Mercedes contributed with the first diesel car on serial production in 1936, the Mercedes 260D shown in Figure 1.3, and the first turbocharged vehicle in 1978, the Mercedes 300SD.

Figure 1.3. *Mercedes 260D, first diesel production passenger car, 1936.*

In 1952, Bosch developed the first gasoline direct injection system for production cars, and Felix Wankel successfully builds the eccentric rotary

engine in 1957, known as Wankel engine. A few years later, in 1961, Bendix introduced the first electronic controlled injection system, the *Electrojector*. A year later, in 1962, General Motors went a step further with the Oldsmobile Jetfire, the first car with a gasoline engine to ever equip a turbocharger, the scheme of which is in Figure 1.4.

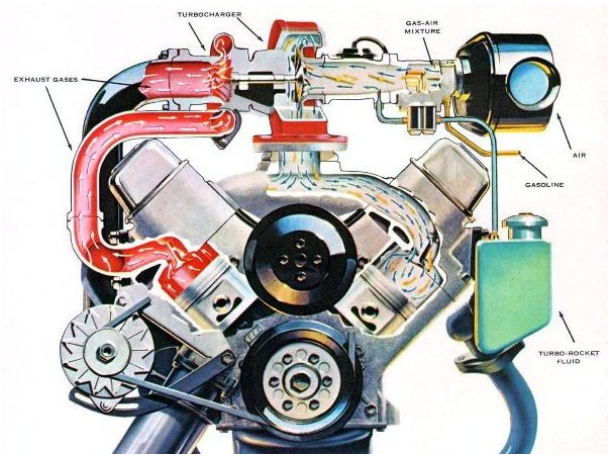

Figure 1.4. *Jetfire's turbocharged SI engine, 1962.*

A special mention has to be made here to Lancia, a brand that has earned a place in the heart of car lovers due to its designs and achievements. Lancia was a pioneer by being the first company to ever: sell a car with a monocoque, offer a five-speed gearbox, sell a car with supercharging and turbocharging on the same engine, develop the first electric roof spoiler or sell the first car with a V6 engine.

The first variable valve timing system for serial production cars came from the hand of Alfa Romeo in 1980, and the electronic injection system with lambda control and TWC (Three-Way Catalyst) appeared for the first time in 1983.

In 1989, the Volkswagen Group presents a turbocharged direct injection (TDI) diesel engine for passenger cars, and Alfa Romeo in 1997 put on the market the first diesel engine with *common rail*, the 156 JTD (Jet Turbo Diesel). Figure 1.5 shows some of the most important milestones in the development of RICE.

Diesel and Otto laid the foundations of the two most widespread engine typologies in vehicle production before the beginning of the 20th century.

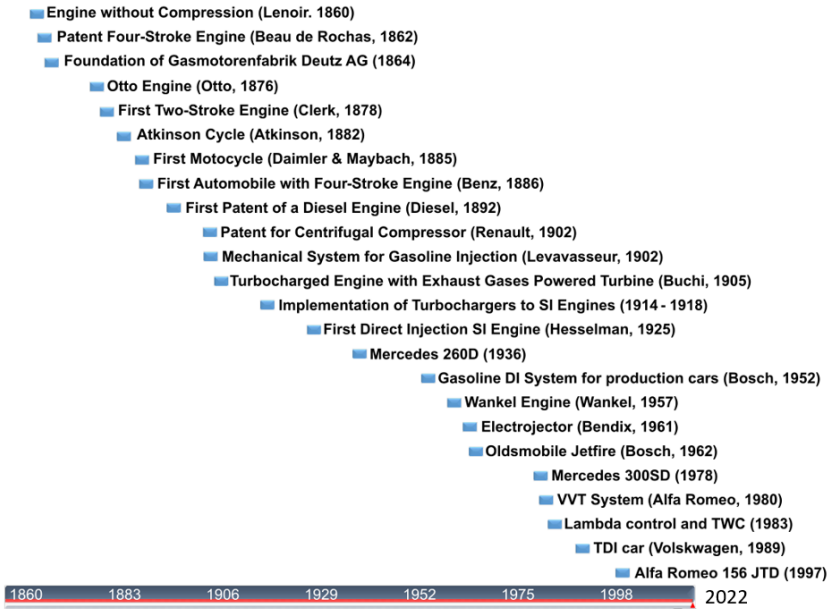

Figure 1.5. *Timeline of RICE evolution.*

Most research and developments since then have been based on the cycles they proposed.

To carry out Diesel's idea, the fuel must be injected while burning, which makes it necessary for the engine to operate in diffusion combustion. This requires high pressure and temperature conditions that allow the atomization and evaporation of the fuel, so fuel needs to be injected when compression is ending and at the beginning of the expansion, after top dead center (TDC). On the other hand, combustion in SI engines is premixed, and is initiated by an external energy input, so that combustion begins around the spark plug and spreads in all directions. As it is premixed, the formation of the mixture must be done during intake and compression strokes, so that the mixture is as homogeneous as possible at spark event to ensure stability. The conditions around the spark plug, mainly composition, temperature and turbulence, can vary the in-cylinder pressure significantly. This phenomenon is known by the name of cyclic dispersion, a characteristic of the SI engines that does not appear in diesel engines, and that can be aggravated by dilution phenomena like lean operation, with lambda greater than one, or exhaust gas recirculation (EGR).

Regarding ignition and fuel used, in CI (Compression Ignition) engines the fuel must be easily ignited, which translates into a high cetane number. As for

the SI, fuel must be of difficult autoignition, so that it is possible to control the start of combustion with the spark event and avoid autoignition and knock.

The regulation of the load in diesel engines must be in a qualitative way, that is, injecting more or less fuel, so that there is always an excess of oxygen. In this way, load control means intake or boost pressure and lambda control, normally operating with values greater than one. On the other hand, the regulation of the load in gasoline engines must be quantitative, that is, changing the amount of air and injecting the fuel to operate with lambda equal to unity for the proper operation of the TWC. A throttle valve becomes mandatory to operate at low loads, and it is responsible for the lower efficiency in this area of the engine map with respect to a diesel engine, since an increase in pumping losses is observed. The higher efficiency of a diesel engine, especially at low loads, is also justified by the higher compression ratio that these engines usually have due to the need to reach given conditions of pressure and temperature to ignite the mixture that has been formed after atomization. This is also reflected in the higher break mean effective pressure (BMEP) . In gasoline engines, the compression ratio is limited by knock phenomena at high load, so variable compression ratio systems could be of great interest.

The difficulty in maintaining a proper, efficient and clean diffusion combustion at high engine speeds is a handicap for diesel engines, which typically have a lower engine speed limit than similar SI engines. This is reflected in the mean piston speed (MPS), which can be up to 10 m/s lower. For this reason, most competition and sports car applications the engines equipped are usually SI, since one of the ways to obtain more power is to directly increase the maximum engine speed.

On the emissions side, the TWC on SI engines is able to significantly reduce the engine-out emissions with the disadvantage from the efficiency perspective of operating at lambda one. However, lean operation and diffusion flame on CI engines means more complexity in the aftertreatment system to meet the standards since the ideal conditions are given for the formation of nitrogen oxides, particulate matter and smoke.

The main differences between the two types of engine, both four-stroke, are synthesized in Table 1.1.

These engines were a revolution in the transportation industry due to their simplicity, robustness, durability and versatility. In addition, the use of fossil fuels with high calorific power gives these engines a great autonomy, as well as high energy density and specific power. Many studies have been carried out over the years in search of improvements to all systems and components, as well as durability and performance [2–11].

Table 1.1. *Main differences between four-stroke CI and SI engines.*

Magnitude	**Compression Ignition**	**Spark Ignition**
Ignition	Autoignition	Spark plug
Mixture	Compression and expansion	Intake and compression
Load regulation	Qualitative	Quantitative
Fuel	High cetane number	High octane number
Compression ratio [-]	12 - 24	8 - 14
max BMEP [bar]	25	25
MPS [m/s]	13 - 15	19 - 25
Lambda [-]	$>$1.05	1

The development of RICE has been subject to the needs and requirements of society at all times. In this way, the first developments and improvements during and after World War II were focused on increasing the performance that these engines offered as well as their durability and reliability. The 1970s energy crisis brought with it greater concern in the industry about reducing fuel consumption, with smaller and more efficient engines being built.

The enormous growth in vehicle traffic led to an increase in the number of health and environmental problems. Many articles and publications already related those health problems to pollutant emissions from engines, as well as the consequences that the accumulation of these elements in the atmosphere could have [12–21]. The problem of climate change became more and more one of the major concerns of the population, causing a paradigm shift in the development of engines around the world guided by the appearance of the first emission regulations.

The control of pollutant emissions became, together with the improvement of efficiency, the most important factor in engine development. From the economic point of view, the crude oil price fluctuations and the predictions of depletion of known reserves push the sector to seek the highest possible efficiency from power plants and processes. Moreover, an increase in efficiency is directly related to carbon dioxides reduction, a greenhouse gas, since its production is proportional to fuel consumption.

In this way, in the 60s and 70s the first simple measures began to be implemented in California such as control over carbon monoxide emissions

at idle speed and crankcase gases. These measures expanded later to the rest of the US and Europe. Since then, regulations began to focus more on unburned hydrocarbon (HC) emissions and carbon monoxides (CO) during normal operation of the engine with the first reglamented driving cycles. In the 70s, the United States also regulated nitrogen oxides (NO_x) emissions together with smoke for diesel engines.

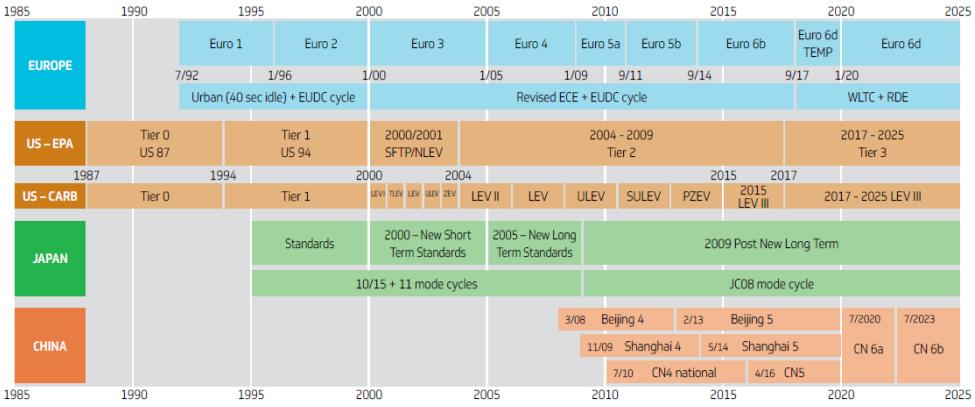

Figure 1.6. *Evolution of the emission standards and driving cycles used in several regions for passenger vehicles. Source: Delphi Technologies [22].*

Over the years, the tightening of standards led to more complex systems to comply with the rules, like the implementation of TWC in gasoline engines, which forced the elimination of the carburetor for a better control over lambda and the lead in gasolines. The name of the TWC comes from the three main pollutants it tries to reduce: NO_x, CO and HC. Carbon monoxides and hydrocarbons are oxidized to water and carbon dioxide, whereas nitrogen oxides are reduced to molecular nitrogen and oxygen. In diesel engines, the use of direct injection systems and turbocharging spread rapidly. The flexibility of injection systems was enough to meet regulations for many years, but as regulations further tightened, more and more complex aftertreatment systems were required. The use of EGR became widespread in diesel engines for NO_x reduction and the use of a SCR (Selective Catalytic Reduction), a DPF (Diesel Particle Filter) and a DOC (Diesel Oxidation Catalyst) is now common. Despite the concatenation of systems, the forthcoming regulations are a challenge in terms of control and emissions for CI engines, offsetting the advantage that these engines have in terms of efficenciy compared to SI engines due to the increased cost.

Local conditions of each country or community such as laws, taxes, availability and fuel price and the average standard of living have resulted in one type of engine predominant over the other in every age and area of the world. In Japan, increased taxes and emission regulations, first for NO_x, and later for soot, caused a reduction in the profit margin that a diesel powered car had thanks to its lower consumption, greatly reducing its popularity. Similar events happened in the US, with more strict regulations for emissions than Europe and lower fuel prices, making people less worried about fuel economy. The two facts limited the impact of diesel engines in the market, also reducing the offer by brands in the automotive sector.

In Europe, during the 70s and 80s, CI engines gained popularity over SI engines [23] due to their durability and efficiency despite the emissions. Nevertheless, as emission standards appeared and tightened, the scales balanced with a CI and SI distribution of roughly 50-50 nowadays, probably due to the following reasons:

- **Extra cost of aftertreatment systems:** as aforexplained, to accomplish with emission standards, CI engines have needed more complex and expensive systems over the years, while for SI engines the TWC is still sufficient.
- **The damaged image of the diesel:** the famous Dieselgate case damaged the image of the diesel engine worldwide together with various bad practices carried out by brands in the automotive sector.
- **Taxes:** in Spain, for example, increased diesel taxes have decreased the population's interest in this engine in favor of the SI engine. In appearance, this measure is taken from an environmental perspective, favoring engines with lower emissions. However, it also ended up being a way to collect more taxes in three ways: higher taxes on diesel fuels, more SI engines sold with their respective higher registration tax compared to CI engine equipped cars and more fuel sold for SI engines, which is also slightly more expensive, due to higher consumption from SI engines and greater number of vehicles.
- **Differences between real and homologated emissions:** large differences have been detected between real and registered emissions during certification, deteriorating even further the diesel position. This fact has promoted changes in the homologation cycles. The WLTP (World Harmonized Light-duty Vehicle Test Procedure) and the RDC (Real Driving Cycles) replace the well-known NEDC (New European

Driving Cycle) in order to better represent a real driving situation during homologation. Therefore, more complex and expensive vehicles are expected in the future.

Emission regulations in Europe are different depending on the type of vehicle. The evolution of these standards for passenger cars and both engine typologies are shown in Figure 1.7, clearly showing a reduction trend over the years. The emission limits for HC and particulate matter (PM) have been multiplied by ten and the emission limits for NO_x by 5 to better observe trends.

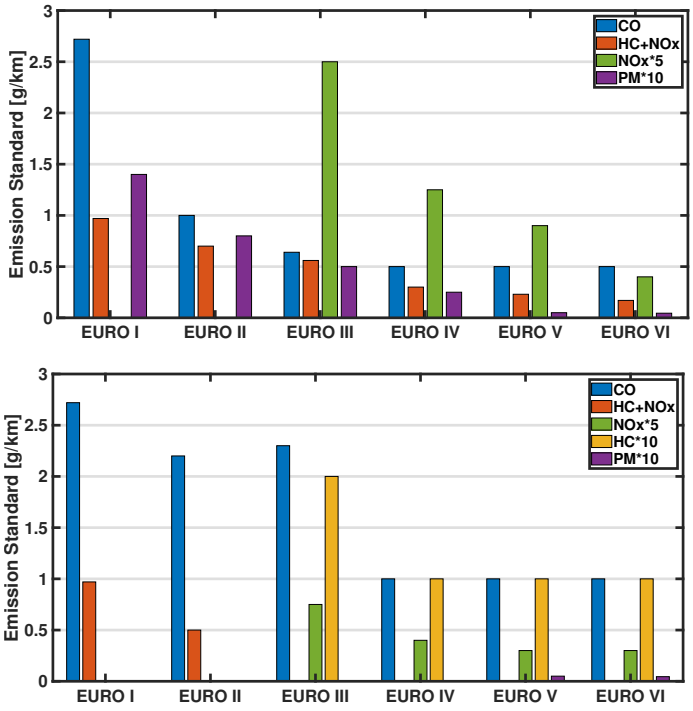

Figure 1.7. *Emission regulations evolution for CI (upper figure) and SI (lower figure) engines in Europe.*

The tightening of emissions regulation is even more evident on area charts, as the ones shown in Figure 1.8. In these graphs, the X-axis represents NO_x emissions (positive direction) and CO emissions (negative direction), whereas the Y-axis represents PM emissions (positive direction) and $HC+NO_x$ emissions (negative direction), all in g/km. The colour of the area represents the Euro regulation. It is worth noting the late incorporation of PM restrictions to the SI regulations with Euro V, which are kept constant with Euro VI.

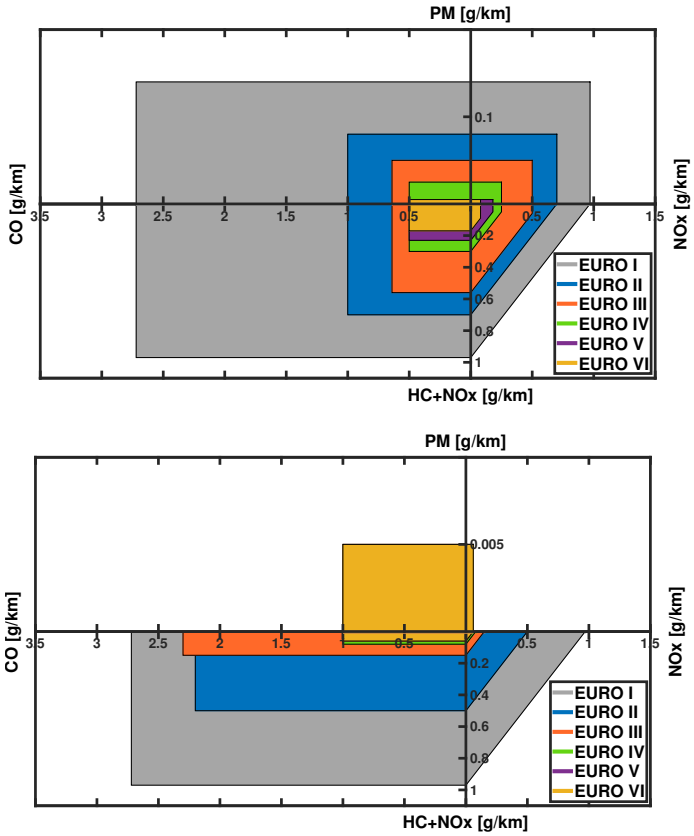

Figure 1.8. *Emission regulations chart for CI (upper chart) and SI (lower chart) engines in Europe.*

Since carbon dioxides (CO_2) are not considered a pollutant emission, it is not included in the regulations previously presented. Nonetheless, carbon dioxide is a greenhouse gas which has an important impact on global warming and ocean acidification [24]. Despite its index of global warming potential (GWP) is set to 1, which is much lower than other gases like methane with 21 or nitrous oxide with 296, the huge amount of carbon dioxide produced in comparison makes this gas the largest contributor to the greenhouse effect, as shown in Figure 1.9. Over the last 150 years, CO_2 concentration has increased from 270 to over 400 parts per milion (ppm). Scientists at Mauna Loa Observatory in Hawaii have monitored the carbon dioxide concentration since 1960 (Figure 1.10), noticing a growth in the slope of the curve [25].

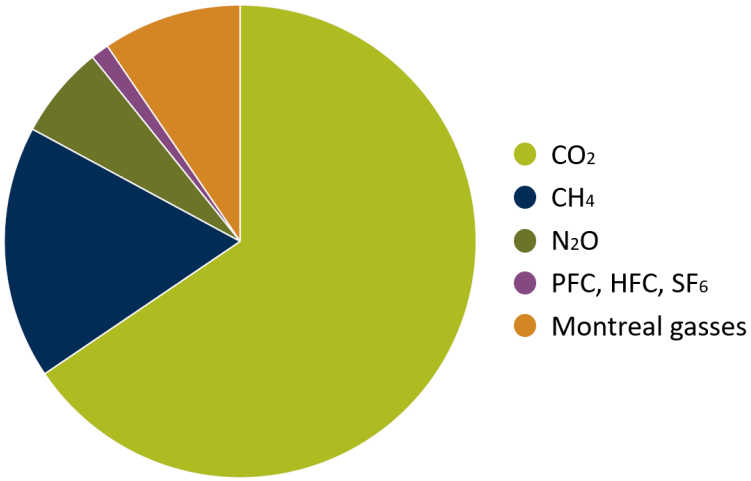

Figure 1.9. *Contribution of different greenhouse gases to total greenhouse gas concentration in 2014. Source: EEA [26].*

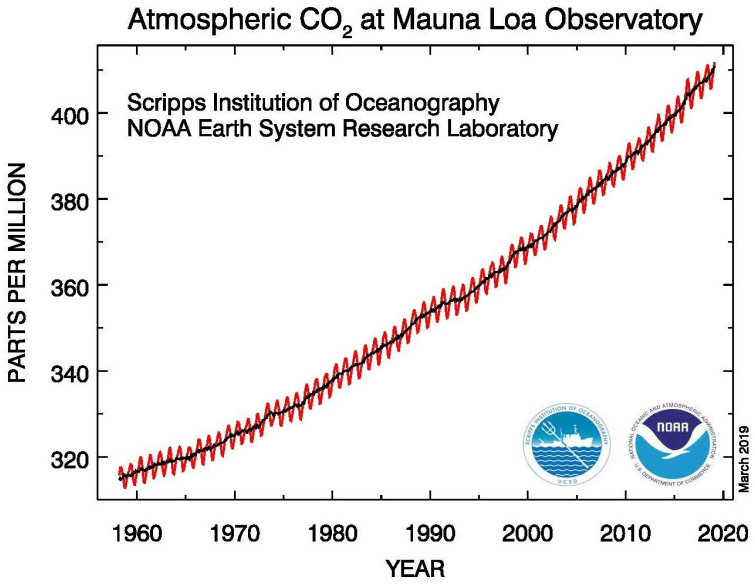

Figure 1.10. *CO_2 concentration evolution over the last 60 years. Source: [25].*

For this reason, the European Union sets an individual CO_2 target for each manufacturer based on the averaged fleet mass for several vehicle typologies.

Until 2021, the CO_2 emission limit for each fleet is computed following Equation 1.1.

$$CO_{2,target} = Target + a \cdot [M_i - M_O] \tag{1.1}$$

The parameters of Equation 1.1 are defined in Table 1.2, where M_O is the European fleet averaged mass from the last three years, and M_i is the manufacturer averaged fleet mass.

Table 1.2. *Values for CO_2 emission limit calculation.*

Vehicle	**Year**	**Target** [g/km]	**a** [g/km/kg]	**Mo** [kg]
	2012 - 2015	130	0.0457	1372
Passenger	2016 - 2018	130	0.0457	1392.4
Cars	2019	130	0.0457	1392.88
	2020	95	0.0333	1392.88
Light	2014 - 2017	175	0.093	1706
Commercial	2018	175	0.093	1766.4
Vehicles	2020	147	0.096	1766.4

From 2021 to 2024, manufacturers will calculate their CO_2 reference target with Equation 1.2, based on their perfomance in 2020 with the WLTP, and their performance and target in 2020 with the NEDC.

$$WLTP_{target} = WLTP_{2020} \cdot \frac{NEDC_{2020.target}}{NEDC_{2020.CO_2}} \tag{1.2}$$

The CO_2 target from 2021 to 2024 for the manufacturer is computed with Equation 1.3.

$$CO_{2,target} = WLTP_{target} + a \cdot [(M_i - M_O) - (M_{i,2020} - M_{O,2020})] \tag{1.3}$$

In this equation, a is the coeffienct in Table 1.2 for 2020, M_O is the mass used as a for the year in question, $M_{O,2020}$ is the mass used as a reference for

2020 defined in Table 1.2, M_i is the averaged mass of the company for the year and $M_{i,2020}$ is the averaged mass of the company in 2020.

If the averaged CO_2 of the fleet, computed as explained depending on the year, is above the specific target, penalties apply for an excess in emissions. Penalties are as follow:

- From 2012 to 2018: 5€ for the first gram, 15€ for the second gram, 25€ for the third gram and 95€ for the fourth gram onwards over the target per vehicle sold.
- From 2019: 95€ per gram over the target per vehicle sold.

The nature of this regulation, which penalizes those manufacturers above their limit by fleet and not by car model individually, has motivated the research and promotion of hybrid and electrical concepts even more, since these are considered low or null emissions vehicles because the carbon dioxides coming from the electric energy production is not computed. Electric and hybrid configurations are capable of reducing local emissions, becoming a great alternative for cities and receiving very good publicity from governments and organizations [27]. However, higher costs from production perspective, lower power densities and the real impact that electricity production can have on emissions are limiting factors. A considerable increase in the use of electric vehicles would bring with it a growing demand for energy production, translating into the need to build more nuclear power plants if the use of electric vehicles becomes widespread. Other problems normally related to electric vehicles are: autonomy, recharging time, infrastructures, enormous electricity demands at night or the added difficulty to charge the vehicle in the absence of own garage and park on the street.

For hybrid powertrains, some studies have found a temperature drop of about 150 °C [28] that could cause the aftertreatment to go below the light-off temperature, increasing the emissions for the next engine start as reported in [29–31]. For this reason, the control over emissions formation will still be crucial in future electrified applications.

Sivak et al. [32] carried a study to compute the impact that a pure electric vehicle could have on emissions. Electricity production has many sources with different efficiencies from pollutant emission and CO_2 production perspective, and each country obtains energy with different combinations of these sources depending on many factors. In this study, an equivalent fuel consumption is calculated with respect to the carbon dioxides that would be emitted according to the different sources of electricity production used in different countries around the world. Results showed that the equivalent fuel consumption is

strongly dependent on the energy sources used, being the most efficient nuclear, wind and hydro. Fuel consumptions vary notably from almost 0 L/100 km, being very clean vehicles, to values above 8 L/100 km, so CO_2 emissions are similar to most SI engines. Most countries are at values between 3 and 5 L/100 km, which are common fuel consumption values in CI engines. Therefore, there is a need to account for the real emissions from hybrid and electric vehicles from the point of view of useful emission regulations.

Figure 1.11 shows the average CO_2 emissions of different types of vehicles depending on their energy source. First, the difference in average efficiency between gasoline and diesel engines is evident with the higher carbon dioxide emissions from petrol cars at the exhaust. When comparing with plug-in hybrid electric vehicles with renewable sources, these slightly reduce total CO_2 emissions, mainly due to the reduction at the exhaust. This improvement could come from the synergy produced by the hybrid system, allowing the RICE to work in more efficient areas of the engine map. A full electric vehicle with renewable sources would suppress the CO_2 exhaust emissions, achieving the lowest emissions. However, the low energy density of these sources would make it impossible for a large number, if not all the vehicles in the world, to work only from renewable sources. In this sense, a more realistic electric vehicle based on the average electricity production in Europe is shown. Carbon dioxides from this vehicle would increase with respect to the previous one, achieving almost levels of plug-in and diesel vehicles, due to emissions coming from fuel (electricity) production. Therefore and with this information, it is possible to expect a growth in the emissions of a plug-in vehicle that will work with this combination of energy sources instead of with renewable sources only. Finally, the example of an electric vehicle powered with energy from coal burning is shown, achieving the highest CO_2 emissions of all and highlighting the importance of taking into account the sources of energy production as stated in [32].

In addition to account for the real emissions of all types of vehicles, it is necessary to take into account the contributions of the different sectors to the emissions production. In order words, the share by sector of each pollutant should be an important factor when legislating. Figure 1.12 shows the contribution of the transport sector to different pollutants. According to this, the transport sector is the major responsible for NO_x emission with a 58% of the total, but it is not for CO, PM, SO_x (sulfur oxides) nor NMVOC (Non-Methane Volatile Organic Compounds).

In terms of CO_2, Figure 1.13 shows that the major contributor to carbon dioxides production is the energy sector with a 73.2%. This sector includes

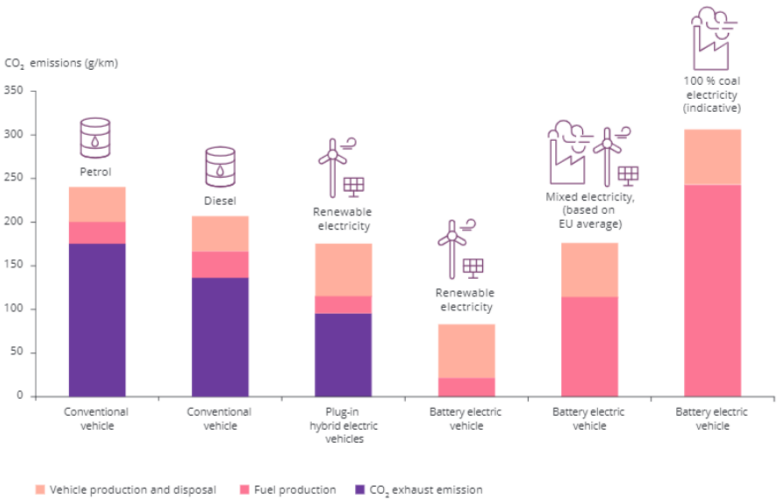

Figure 1.11. *Comparison of CO_2 emissions for different powertrain typologies and energy sources. Source: EEA [33].*

the production of energy for industry and the use in buildings as major responsibles, assigning to road transport sector only a 11.9% share of the total.

The context in which we find ourselves is positioning the SI engine as an attractive alternative either by itself or combined with electrical systems. All the new technologies that are being investigated and incorporated into these engines nowadays aim to reduce the gap in efficiency with respect to diesel engines and keep the level of emissions. The introduction of direct injection, turbocharging and downsizing has meant positive advances in terms of reducing consumption. One of the paths to follow to achieve even greater efficiencies in SI is through dilution in combustion, either by lean burn, EGR or stratification.

Figure 1.12. *Transport and non-transport share of different pollutant emissions. Source: EEA [34].*

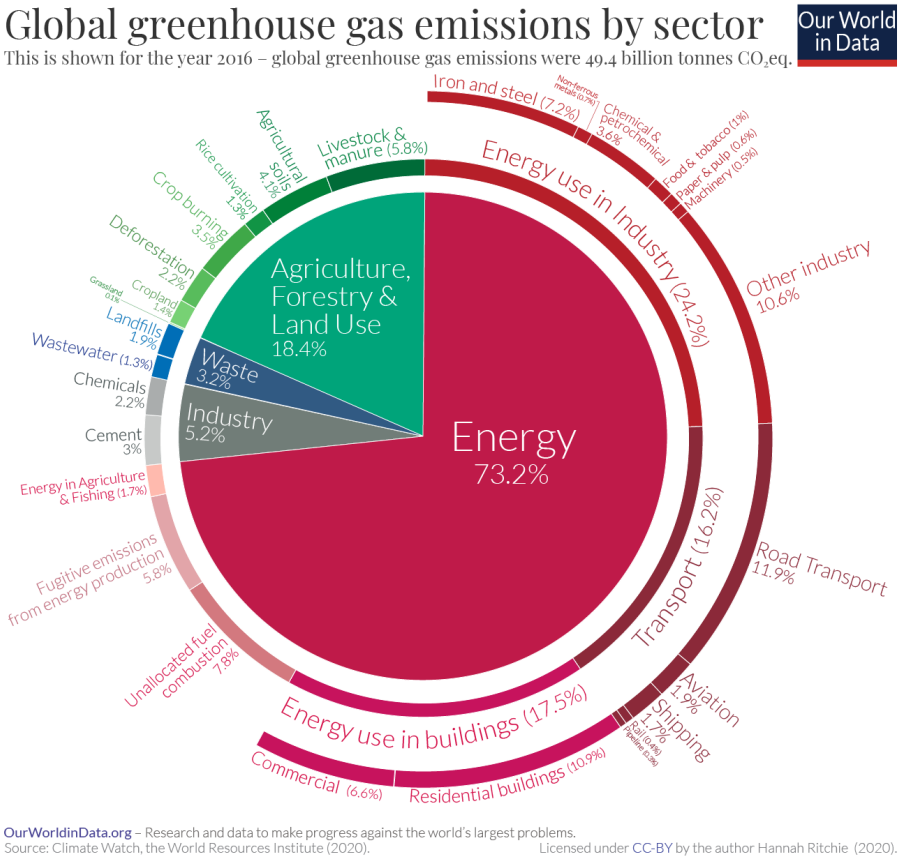

Figure 1.13. *Global greenhouse gases emitted by sector for the year 2016. Source: Our World in Data [35].*

1.2 Context

The incipient increase in the global temperature of the planet caused by climate change [36] together with the high levels of pollution in large cities is making people more aware of the problem of climate change and pollution. From the transport industry, these problem are addressed with emission standards, which tighten as years go by [37]. The fact of having more and more restrictive emission standards and the shortage and price variability of fossil fuels has made the sector to focus on reducing fuel consumption and pollutant emissions from their power plants.

In this regard, the two most widespread engine typologies show important differencies. The emissions control is simpler and cheaper for spark-ignited engines than for compression engines, and it is expected that more complex and expensive aftertreatment systems will be needed in the future with the more realistic driving cycles [38, 39]. This is putting all eyes on the gasoline engine as an alternative for the future, both as the main powertrain system or combined with electrification. For hybrid configurations, the emissions control could be affected by the temperature drop below light-off, increasing emissions on subsequent starts [29–31]. For fully electric powertrains, other problems arise such as the lower power densities, autonomy, batteries life and recharging time, infrastructures or huge electricity demands, as well as the need to account for the real emissions from electricity production.

However there is a big gap in efficiency in favor of the compression ignition engine due to the load control and the knock limited compression ratio in gasoline engines [40–43]. For this reason, some technologies are being developed to reduce this gap [44] while keeping the emissions level like the use of direct injection [45–48], downsizing [49–52], and variable valve actuation [53–55]. The aforementioned technologies will be explained in detail in section 2.3.

A spark-ignited gasoline engine with all the mentioned technologies for fuel economy implemented has been tested in this PhD-Thesis in order to assess the potential and drawbacks that this trend has. The objectives and methodology followed are described hereafter.

1.3 Objectives and methodology

The main objective of this PhD-Thesis is to assess and compare the effects of the different EGR strategies on performance, combustion, emissions and management of SI gasoline engines. To reach this goal, other objectives were defined during the course of the studies:

- To study the tolerance of the engine to the inclusion of EGR and the influence on the optimal valve actuation and spark timing calibration with respect to no EGR operation.
- To understand the different effects from the composition and temperature of recirculated gases on combustion evolution by means of the analysis of the characteristic times of the cumulative heat release.
- To analyse the effects of EGR introduction on the energy balance: the effect on pumping work, combustion development, heat transfer losses, knock and enrichment suppression.
- To assess the problem of sudden dilution induced by condensation of the water present in the exhaust gases of a low-pressure EGR circuit.
- To understand the main potential and limitations of different EGR applications in turbocharged multi-cylinder engines, such as the low-pressure POST and PRE TWC, high-pressure and internal residuals, analysing the effect on engine-out emissions, reciculability and efficiency.

To complete the proposed objectives, a gasoline turbocharged direct injection (GTDI) engine has been installed on a test bench with all the state-of-the-art fuel efficiency technologies for gasoline engines. In this sense, a VVT (Variable Valve Timing) system was useful to control the load and the concentration of IGR (Internal Gas Residuals) and two prototype cooled EGR lines were installed, one for a LP-EGR (Low-Pressure) circuit and the other for a HP-EGR (High-Pressure) circuit. Another LP-EGR circuit was mounted, called PRE, changing the extraction point of the exhaust gases from downstream to upstream the TWC. A 1D model was also built and validated in the GT-Power environment with experimental tests to predict the engine behaviour and several parameters that were difficult to measure as the HP-EGR rate and the concentration of IGR.

As a starting point, a DoE was performed in several engine points defined by the engine speed and load. The parameters of the DoE were the LP-EGR rate, the spark timing and the VVT setting on both intake and exhaust. In the search for efficiency, the spark timing was set based on the CA50, which was monitored online, to achieve values between 7 and 10 CAD after top dead center (aTDC) as explained in [41, 56]. With this DoE, it was possible to analyse the tolerance of the engine to EGR inclusion depending on the calibration and the operating point, as well as to optimize the calibration with and without EGR. Besides, a comparison between the LP-EGR and IGR strategies was made through the energy balance and on the emissions side.

Following the condensation topic, the engine was mounted on a climatic chamber to easily control the ambient and cooling temperatures and evaluate the instabilities produced by EGR condesation in the WCAC (Water Charge Air Cooler).

Later, the same engine points were tested with the HP-EGR and the PRE system in order to compare it with the POST LP-EGR. The calibration of the VVT was kept constant at the optimal for the LP-EGR, and the spark timing adjusted with the same criteria. In this way, another possible study would be a comparison between systems with the optimal calibration for each.

1.4 Document structure

In this subsection, a review and description of the present document is made to summarize the content.

Chapter 1 has detailed an historical introduction about reciprocating internal combustion engines together with the main objectives proposed and the methodology followed. Lastly, the document structure is described.

Chapter 2 is a review of the current knowledge that intends to give the reader a fundamental understanding of the main topics related to this PhD-Thesis and the state of the art. In this sense, the standard SI gasoline engine is explained from the intake and exhaust lines and valve actuation, boosting, the typical SI combustion process and the abnormal combustion together with the main pollutants and their formation mechanisms. Besides, a description of the main technologies to increase the efficiency of SI engines is made, focusing on the exhaust gas recirculation strategies.

Chapter 3 is a review of the experimental and theoretical tools that were used at some point for this PhD-Thesis. On the experimental side, the engine and the experimental set-up are detailed, together with the two test benches employed. On the theoretical side, the 1D engine model, the psychrometric model used for condensation assessment and the tests processing are explained together with thermodynamic and in-cylinder pressure signal calculations.

Chapter 4 focuses on analyzing the impact that LP-EGR has on engine efficiency. To do so, the EGR tolerance and influence of calibration are examined, studying also combustion and emissions when comparing LP-EGR to IGR by decoupling the effects of composition and temperature of the recirculated gases. Moreover, the problem of dilution induced by water condensation is analysed.

Chapter 5 presents a comparison between EGR systems two-by-two. First, the already analysed LP-EGR circuit presented in Chapter 4 is compared to

the HP-EGR circuit from a combustion, efficiency and emissions perspective. Later, the same LP-EGR circuit, called POST, is compared with a similar approach to the PRE system, another LP-EGR circuit where the exhaust gas is extracted upstream the TWC.

Chapter 6 is a summary of the findings and conclusions of all studies and the potential advantages and drawbacks of EGR inclusion in SI gasoline engines. Furthermore, future studies are proposed to continue the research line presented in this PhD-Thesis.

Bibliography

[1] Carnot S. *Réflexions sur la puissance motrice du feu et sur les machines propres à développer cette puissance.* Bachelier, 1824.

[2] Goering C. E. and Fry B. "Engine durability screening test of a diesel oil/soy oil/alcohol microemulsion fuel". *Journal of the American Oil Chemists Society*, Vol. 61 n^o 10, pp. 1627–1632, 1984.

[3] Bird G. L. "Ford 2.5 liter direct injection naturally aspirated diesel engine". *Proceedings of the Institution of Mechanical Engineers. Part D, Transport engineering*, Vol. 199 n^o 2, pp. 113–122, 1985.

[4] Kamo R., Bryzik W. and Glance P. "Adiabatic engine trends-worldwide". *SAE Technical Paper n. 870018*, 1987.

[5] Brandi F. K., Wünsche P. and Gschweltl E. "Design strategies for low noise engine concepts". *SAE Technical Paper n. 911070*, 1991.

[6] Ohgami E., Ohsawa N. and Saito T. "Nissan's new V8 and L4 aluminum cylinder block - Design and production". *SAE Technical Paper n. 910431*, 1991.

[7] Kleinschmidt P. and Schmidt F. "How many sensors does a car need?". *Sensors and Actuators: A. Physical*, Vol. 31 n^o 1-3, pp. 35–45, 1992.

[8] Barron M. B. and Powers W. F. "The role of electronic controls for future automotive mechatronic systems". *IEEE/ASME Transactions on Mechatronics*, Vol. 1 n^o 1, pp. 80–88, 1996.

[9] Wandell J. L. "Shot peening of engine components". *American Society of Mechanical Engineers, Internal Combustion Engine Division (Publication) ICE*, Vol. 29, pp. 101–108, 1997.

[10] Kohany T. and Sher E. "Using the 2nd law of thermodynamics to optimize variable valve timing for maximizing torque in a throttled SI engine". *SAE Technical Paper n. 1999-01-0328*, 1999.

[11] Bybee K. "Reliable electronics for high-temperature downhole applications". *JPT, Journal of Petroleum Technology*, Vol. 52 n^o 7, pp. 56–57, 2000.

[12] Santodonato J., Basu D. and Howard P. "Health effects associated with diesel exhaust emissions, literature review and evaluation". *National Academy of Sciencies, Engineering and Medicine*, n^o EPA/600/1-78/063, 1978-11.

[13] EPA U.S. *The benefits and costs of the clean air act from 1990-2010.* 1999.

[14] Davidson C. I., Phalen R. F. and Solomon P. A. "Airborne particulate matter and human health: A review". *Aerosol Science and Technology*, Vol. 39 n^o 8, pp. 737–749, 2005.

[15] Pope C. A. and Dockery D. W. "Health effects of fine particulate air pollution: Lines that connect". *Journal of the Air and Waste Management Association*, Vol. 56 n^o 6, pp. 709–742, 2006.

[16] Bernstein L., Bosch P., Canziani O., Chen Z., Christ R. and Riahi K. *Synthesis Report. Intergovernmental Panel on Climate Change 2007.* 2007.

[17] Hill J., Polasky S., Nelson E., Tilman D., Huo H., Ludwig L., Neumann J., Zheng H. and Bonta D. "Climate change and health costs of air emissions from biofuels and gasoline". *Proceedings of the National Academy of Sciences of the United States of America*, Vol. 106 n^o 6, pp. 2077–2082, 2009.

[18] Smith K. R., Jerrett M., Anderson H. R., Burnett R. T., Stone V., Derwent R., Atkinson R. W., Cohen A., Shonkoff S. B., Krewski D., Pope C. A., Thun M. J. and Thurston G. "Public health benefits of strategies to reduce greenhouse-gas emissions: health implications of short-lived greenhouse pollutants". *The Lancet*, Vol. 374 n^o 9707, pp. 2091–2103, 2009.

[19] Vijayaraghavan K., Lindhjem C., DenBleyker A., Nopmongcol U., Grant J., Tai E. and Yarwood G. "Effects of light duty gasoline vehicle emission standards in the United States on ozone and particulate matter". *Atmospheric Environment*, Vol. 60 n^o 2012, pp. 109–120, 2012.

[20] Kim K. H., Kabir E. and Kabir S. "A review on the human health impact of airborne particulate matter". *Environment International*, Vol. 74, pp. 136–143, 2015.

[21] Zhang M., Chen W., Shen X., Zhao H., Gao C., Zhang X., Liu W., Yang C., Qin Y., Zhang S., Fu J., Tong D. and Xiu A. "Comprehensive and high-resolution emission inventory of atmospheric pollutants for the northernmost cities agglomeration of Harbin-Changchun, China: Implications for local atmospheric environment management". *Journal of Environmental Sciences (China)*, Vol. 104, pp. 150–168, 2021.

[22] Delphi Technologies. "Worldwide emissions standards, Passenger cars and light duty vehicles". *Delphi informative booklet*, 2019/2020.

[23] Cames M. and Helmers E. "Critical evaluation of the European diesel car boom - Global comparison, environmental effects and various national strategies". *Environmental Sciences Europe*, Vol. 25 n^o 1, pp. 1–22, 2013.

[24] Happer W. "The Truth About Greenhouse Gasses". *The Global Warming Policy Foundation*, n^o 3, pp. 2–6, 2011.

[25] Oceanic National and Administration Atmospheric. "Trends in Atmospheric Carbon Dioxide". *ESRL Global Monitoring Division*, 2019.

[26] European Environment Agency. "Contribution of different greenhouse gases to the overall greenhouse gas concentration". *Data and Maps*, 2017.

[27] Dong X., Wang B., Yip H. L. and Chan Q. N. "CO_2 Emission of Electric and Gasoline Vehicles under Various Road Conditions for China, Japan, Europe and World Average - Prediction through Year 2040". *Applied Sciences*, Vol. 9 n^o 11, pp. 2295, Jun 2019.

[28] Knorr T., Ellmer D., Baensch S. and Schatz A. ""Optimization of the 48 V Hybrid Technology to Minimize Local Emissions in the RDE"". In *27th Aachen Colloquium Automobile and Engine Technology*, October 2018.

[29] Pham A. and Jeftic M. "Characterization of Gaseous Emissions from Blended Plug-In Hybrid Electric Vehicles during High-Power Cold-Starts". *SAE Technical Papers*, Vol. 2018-01-0428 n^o 2018-01-0428, pp. 1–9, 2018.

[30] Yamada H., Inomata S. and Tanimoto H. "Particle and VOC Emissions from Stoichiometric Gasoline Direct Injection Vehicles and Correlation Between Particle Number and Mass Emissions". *Emission Control Science and Technology*, Vol. 3 n^o 2, pp. 135–141, 2017.

[31] Zinola S., Raux S. and M Leblanc. "Persistent Particle Number Emissions Sources at the Tailpipe of Combustion Engines". *SAE Technical Papers*, Vol. 2016-01-2283 n^o 2016-01-2283, pp. 1–10, 2016.

[32] Sivak M. and Schoettle B. "Fuel sources for electricity in the individual countries of the world and the consequent emissions from driving electric vehicles". *Sustainable Worldwide Transportation*, 2017.

[33] European Environment Agency. *The European environment - state and outlook 2020. Knowledge for transition to a sustainable Europe*, volume 60. 2020.

[34] *The contribution of transport to air quality - TERM 2012: Transport indicators tracking progress towards environmental targets in Europe*. Number 10. 2012.

[35] Ritchie H. and Roser M. "CO_2 and Greenhouse Gas Emissions". *Our World in Data*, 2017.

[36] Kolodziej C. P., Pamminger M., Sevik J., Wallner T., Wagnon S. W. and Pitz W. J. "Effects of Fuel Laminar Flame Speed Compared to Engine Tumble Ratio, Ignition Energy, and Injection Strategy on Lean and EGR Dilute Spark Ignition Combustion". *SAE International Journal of Fuels and Lubricants*, Vol. 10 n^o 1, pp. 82–94, 2017.

[37] Shu G., Pan J. and Wei H. "Analysis of onset and severity of knock in SI engine based on in-cylinder pressure oscillations". *Applied Thermal Engineering*, Vol. 51 n^o 1-2, pp. 1297–1306, 2013.

[38] Sjerić M., Taritaš I., Tomić R., Blažić M., Kozarac D. and Lulić Z. "Efficiency improvement of a spark-ignition engine at full load conditions using exhaust gas recirculation and variable geometry turbocharger - Numerical study". *Energy Conversion and Management*, Vol. 125, pp. 26–39, 2016.

[39] Pinterits M. *EU National Greenhouse Gas Inventory Report May 2014*. Number 09. 2014.

[40] Piqueras P., De la Morena J., Sanchis E. J. and Pitarch R. "Impact of Exhaust Gas Recirculation on Gaseous Emissions of Turbocharged Spark-Ignition Engines". *Applied Sciences*, pp. 1–17, 2020.

[41] Galindo J., Climent H., De la Morena J., Pitarch R., Guilain S. and Besancon T. "A methodology to study the interaction between variable valve actuation and exhaust gas recirculation systems for spark-ignition engines from combustion perspective". *Energy, Conversion and Management*, Vol. 250, 2021.

[42] Galindo J., Navarro R., De la Morena J., Pitarch R. and Guilain S. "On combustion instability induced by water condensation in a low-pressure exhaust gas recirculation system for spark-ignition engines". *Energy*, Vol. 261, pp. 125122, 2022.

[43] Teodosio L., De Bellis V. and Bozza F. "Fuel Economy Improvement and Knock Tendency Reduction of a Downsized Turbocharged Engine at Full Load Operations through a Low-Pressure EGR System". *SAE International Journal of Engines*, Vol. 8 n^o 4, pp. 2015–01–1244, 2015.

[44] Bourhis G, Chauvin J, Gautrot X and de Francqueville L. "LP EGR and IGR compromise on a GDI engine at middle load". *SAE International Journal of Engines*, Vol. 6 n^o 1, pp. 67–77, 2013.

[45] Boccardi S., Catapano F., Costa M., Sementa P., Sorge U. and Vaglieco B. M. "Optimization of a GDI engine operation in the absence of knocking through numerical 1D and 3D modeling". *Advances in Engineering Software*, Vol. 95, pp. 38–58, 2016.

[46] Potteau S., Lutz P., Leroux S., Moroz S. and Tomas E. "Cooled EGR for a Turbo SI Engine to Reduce Knocking and Fuel Consumption". *SAE Technical Papers*, 2007.

[47] Takaki D., Tsuchida H., Kobara T., Akagi M., Tsuyuki T. and Nagamine M. "Study of an EGR system for downsizing turbocharged gasoline engine to improve fuel economy". *SAE Technical Papers*, Vol. 1, 2014.

[48] Francqueville L. and Michel J. B. "On the Effects of EGR on Spark-Ignited Gasoline Combustion at High Load". *SAE International Journal of Engines*, Vol. 7 n^o 4, pp. 1808–1823, 2014.

[49] Zhang Z., Wang T., Jia M., Wei Q., Meng X. and Shu G. "Combustion and particle number emissions of a direct injection spark ignition engine operating on ethanol/gasoline and n-butanol/gasoline blends with exhaust gas recirculation". *Fuel*, Vol. 130, pp. 177–188, 2014.

[50] Wei H., Zhu T., Shu G., Tan L. and Wang Y. "Gasoline engine exhaust gas recirculation - A review". *Applied Energy*, Vol. 99, pp. 534–544, 2012.

[51] Shen K., Li F., Zhang Z., Sun Y. and Yin C. "Effects of LP and HP cooled EGR on performance and emissions in turbocharged GDI engine". *Applied Thermal Engineering*, Vol. 125 n^o x, pp. 746–755, 2017.

[52] Leduc P., Dubar B., Ranini A. and Monnier G. "Downsizing of Gasoline Engine: an Efficient Way to Reduce CO_2 Emissions". *Oil & Gas Science and Technology*, Vol. 58 n^o 1, pp. 115–127, 2003.

[53] Agarwal11 D., Singh S. K. and Agarwal A. K. "Effect of Exhaust Gas Recirculation (EGR) on performance, emissions, deposits and durability of a constant speed compression ignition engine". *Applied Energy*, Vol. 88 n^o 8, pp. 2900–2907, 2011.

[54] Kumano K. and Yamaoka S. "Analysis of knocking suppression effect of cooled egr in turbo-charged gasoline engine". *SAE Technical Papers*, Vol. 1, 2014.

[55] Fontana G. and Galloni E. "Variable valve timing for fuel economy improvement in a small spark-ignition engine". *Applied Energy*, Vol. 86, pp. 96–105, 2009.

[56] Lavoie G. A., Ortiz-soto E., Babajimopoulos A., Martz J. B. and Assanis D. N. "Thermodynamic sweet spot for high- efficiency , dilute , boosted gasoline engines". *International Journal of Engine Research*, Vol. 14 n^o 3, pp. 260–278, 2012.

Chapter 2

Literature Review

Contents

2.1 Introduction

Spark-ignited engines are the predominant alternative in the world for passenger cars and most applications since the first vehicles began to be marketed [1]. During the 70s and 80s, compression-ignition engines started gaining popularity over SI engines due to higher efficiencies, government aids and increased fuel prices [2]. Similar trends were observed in Japan and the U.S., but the introduction of stricter emissions regulations reduced the impact that this engine typology would have on the market. The higher emission level of CI engines for nitrogen oxides and particulate matter and the more expensive aftertreatment required to comply with regulations made these regions of the world to see this engine as a no future technology.

In a similar manner, SI engines have regained popularity over the last years in Europe probably favored by the introduction of the Euro V and VI emission standards. Since the beginning of the new century, the research on SI engines has been mainly centered on reducing the gap in efficiency with respect to compression engines. To this concern has also been added the need to further reduce pollutant emissions. All this has led to the development of both active and passive solutions, which have meant a technological leap forward. Combustion chamber designs, direct injection, EGR, GPF (Gasoline Particle Filter), downsizing and boosting are probably the most important.

In this sense, this chapter aims to review the most important aspects of a traditional SI engine based on a four-stroke cycle used in the automotive industry and provide the reader a certain knowledge level of the basic elements and processes. The chapter is divided into two topics. In the first part, the traditional SI engine is described with its peculiarities, advantages and drawbacks. The main systems and elements on the air management side, the traditional SI combustion process and the main mechanisms of pollutant formation are explained. After that, the main technologies focused on improving efficiency, performance and reducing exhaust emissions that are being used nowadays or will be in the future are reviewed. The last section of this chapter is only focused on the different exhaust gas recirculation architectures and the implications and singularities of each.

2.2 The standard SI engine

RICE are power plants that extract mechanical work oxidizing a volatile fuel that is mixed with an oxidant such as air. Spark-ignited engines are classified within internal combustion engines, since the combustion process

occurs within the fluid running through it, and reciprocating due to the movement by which the machine extracts the work.

The two most widespread types of RICE, the spark ignition and the compression ignition engines, are based historically on the Otto and the Diesel cycle respectively. These two engine typologies mainly differ on the mixture ignition method, among other characteristics. Naturally, the ignition method also influences the type of fuel required and different characteristics of the engine. For spark-ignited engines, the fuel must be hardly auto-igniting, so that the ignition moment can be controlled. Several fuels as hydrogen, ethanol, natural gas, liquefied petroleum gas or gasoline meet this characteristic.

The main application of both CI and SI engines is the automotive industry, more specifically operating with four-stroke cycles instead of two-stroke cycles. Four-stroke cycles have the following stages: intake, compression, expansion and exhaust, as shown in Figure 2.1, so a cycle is completed in two crankshaft revolutions. In an engine with a two-stroke cycle, the exhaust and intake take place in the same stroke in a process known as scavenging. The most common applications for two-stroke engines are small engines such as mopeds, modeling and tools (normally SI engines) or large vessels, railways or stationary engines (normally CI engines). The great majority of engines in the automotive industry are four-stroke engines. More details on engine strokes and valve events will be explained in the section 2.2.1.2.

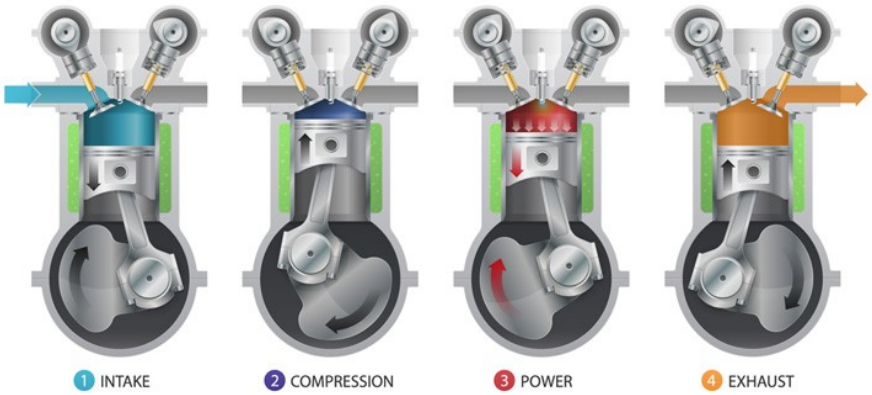

Figure 2.1. *Diagram of the phases of a four-stroke cycle.*

A diferentiation can also be done between air-cooled and water-cooled engines. However, the vast majority of engines have been water-cooled for several decades. Another classification depends on the number and

arrangement of cylinders, since cylinders can be grouped in different ways and orientations. The chosen arrangement mainly depends on the occupied space due to the cylinder size, the number of cylinders, the need and ease for cooling, accessibility for maintenance, engine application and its performance. Some of the most used configurations are depicted in Figure 2.2.

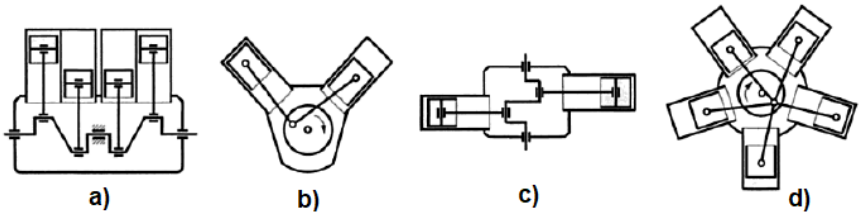

Figure 2.2. *Different cylinder arrengements: a) In-line; b) V-shape; c) Horizontally opposed; d) Radial. Source: Adapted from [3].*

Other less used configurations are: W-shaped, H-shaped, double crankshaft and opposed cylinders. Whereas the majority of engines in the automotive industry are in-line, most engines for motorsport and sport cars have used V-shaped engines, like both in Formula 1 and MotoGP. The case of Moto GP is curious, since in this category V-shaped and in-line engines coexist, something similar to what happened to atmospheric and boosted engines in F1 for many decades. Automotive companies have made cylinder arrangements and their designs a recognizable brand, as with the BMW R boxer engine, the Porsche boxer engine or the W engine from Bugatti. The Wankel engine deserves a special mention here although it does not fall within the RICE, since it is not reciprocating but rotary. Many companies have built Wankel engines, Mazda being practically the only one that continues to bet on this engine typology today.

This first section of this chapter is subdivided in three parts. The first subsection explains the systems and functioning of the intake and exhaust lines and load regulation, including valve actuation, boosting and aftertreatment of a traditional SI gasoline engine. In the second subsection, the combustion process of a regular SI engine is explained with its different phases and peculiarities. In the third subsection, the formation of the main pollutants regulated in Europe are explained.

2.2.1 Air management

Air management in engines is of vital importance since it is responsible for the renewal of the load. This system includes the introduction of fresh

air into the cylinders and its subsequent extraction from the engine once the air has been burned with fuel. It is also a very important branch of study given the influence it has on performance, efficiency, emissions, stability and smooth operation. Air management include the intake and exhaust lines with its respective systems, valve actuation, exhaust gas recirculation and boosting.

2.2.1.1 Intake line

With the purpose of supplying to the engine the needed amount of air, the intake line runs from the air filter in contact with ambient air to the intake runners. The air filter is an essential element of the engine. It ensures that the air that reaches the cylinders to mix with the fuel is completely clean and free of impurities, thus avoiding any possible damage.

In the case of boosted engines, the next item in the intake line is the compressor, either from a supercharger or a turbocharger. It must be said that if the engine is equipped with an EGR system, a choke valve may be placed at the junction of the exhaust gas with the fresh air in order to better control the pressure difference between the points of the EGR line, thus increasing the recirculated rate. The compressor is responsible for increasing the air pressure and thus the amount of oxygen admitted, also increasing the temperature. Having heated the air is a potential loss of volumetric efficiency due to the lower density, so in most turbocharged and supercharged engines, a cooler is located downstream the compressor. The fact of lowering donw the temperature of the air at almost constant pressure would further increase the density of the charge, and would also reduce knock probability in SI engines. Both water-to-air and air-to-air heat exchangers can be used, the first one being the most used in downsized engines. These water-air coolers often use separate water circuits from engine cooling to achieve lower temperatures [4]. Due to the long route involved in having a compressor and intercooler, the use of intake manifolds integrated with the intercooler, also called WCAC, has spread [5–8]. In this way, the possible lag coming from such a large volume in the intake line is reduced and packing is improved. In addition, air bypass lines can be found to prevent the flow from passing through the compressor at different operating points, for example to avoid surge.

In gasoline engines, the air flow, thus the engine load, is controlled by the main throttle, which is usually placed just before the intake manifold. In this way, the throttle controls the intake manifold pressure by choking, allowing more or less flow to pass through the runners into the cylinders. This way of controlling the volumetric efficiency supposes an efficiency loss at partial

loads due to the increase in pumping work, which is reflected in a higher fuel consumption compared to CI engines.

The intake manifold is the last element of the intake line, placed upstream the runners and the intake valves. The manifold design is of crucial importance and depends on the number and arrangement of cylinders, as well as the application that the engine will have. During the intake stroke, a rarefaction wave is generated and transmitted along the intake duct until it is reflected due to a certain discontinuity. In the case of an open end, the rarefaction wave is reflected as an overpressure wave, as shown in Figure 2.3.

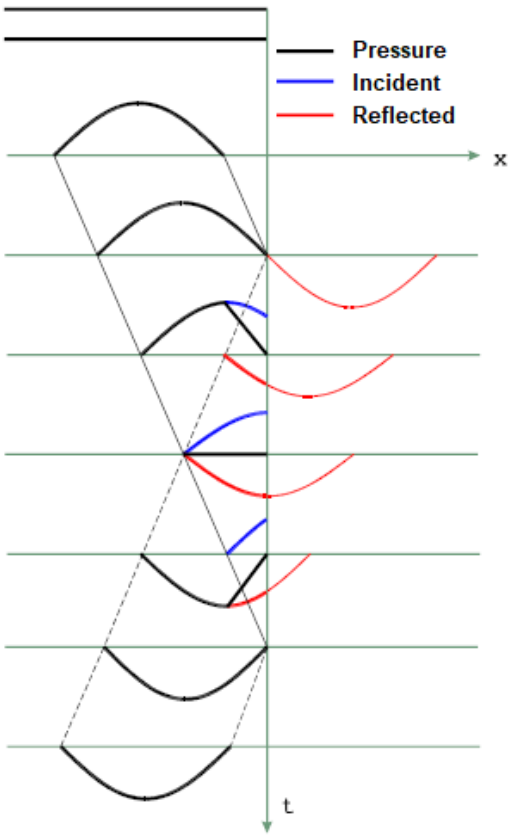

Figure 2.3. *Waves reflection by an open end. Source: Adapted from [3].*

In the case of a single cylinder, the overpressure wave then travels back to the intake runners, and if the intake valves are still open it causes a pressure

increase in the last part of the intake stroke, helping cylinder filling. It is possible to calculate the time (Equation 2.1) and angular (Equation 2.2) gap between both waves assuming acoustic waves:

$$\Delta t = \frac{2 \cdot L}{a} \tag{2.1}$$

$$\theta = 360 \cdot n \cdot \Delta t \tag{2.2}$$

where L is the characteristic length that the wave travels, a is the in air speed of sound and n is the engine regime. The time gap between both waves is constant, but the angular gap depends on the engine speed. The maximum effect of this reflected wave occurs when the peak of the wave reaches the valve around bottom dead center (BDC), at around 90°C from the intake valve opening. In this way, it is possible to define a perfect length for a given engine speed, also called tuning, as shown in Equation 2.3:

$$L = \frac{a \cdot \Delta t}{2} = \frac{a \cdot \theta}{2 \cdot 360 \cdot n} = \frac{90 \cdot a}{720 \cdot n} = \frac{a}{8 \cdot n} \tag{2.3}$$

In the case of a multi-cylinder engine, all the intake ducts are joint to a common manifold or tube. In this case, the rarefaction wave produced by the cylinder is reflected in the duct junction but its amplitude is less than that produced by an open end. The diameter of the ducts and the intake manifold volume affects the amplitude of the waves. For large volumes, of order of several times the engine displacement, there is a reflection almost like that of an open end, and a little volume produces a very slight reflection. The rarefaction wave may be reflected in other elements of the intake line, producing several overpressure waves if the volume of the element is enough. These waves would reach the intake valve at different times. The design of all the lengths and volumes affecting this phenomenon is known as intake tuning. Moreover, the optimal relationship between the engine frequency and the manifold frequency depends on the number of cylinders in the manifold. The firing order greatly influences the tuning of the manifold, since the rarefraction wave can prevent the filling of other cylinders. For example, for three and six cylinders, the second reflection of a cylinder is added to the rarefaction of the next cylinder in the firing order. There is a significant overlap in the intake strokes of consecutive cylinders in a four-cylinder engine, making it difficult to get a significant resonance effect and making firing order a non-random parameter.

2.2.1.2 Intake and exhaust valve actuation

The valve system act as the inlet and outlet doors of the cylinder. The four strokes shown in Figure 2.1 ideally are as follow:

- **Intake stroke:** intake valves open at TDC with the exhaust valves closed, and the piston begins its downstroke towards BDC, thus creating a sufficient depression for gases to enter. Intake valves close upon reaching BDC.
- **Compression stroke:** the piston moves upwards to TDC with both valves closed, compressing the air admitted in the previous stroke in a closed and decreasing volume. Somewhere near TDC, the spark plug actuates, developing the combustion process that will be explained in Section 2.2.2.
- **Expansion stroke:** the piston starts moving towards down to BDC aided by the high level of pressure promoted by the heat released. In this stroke, most of the work is obtained.
- **Exhaust stroke:** with the piston placed at BDC, the exhaust valves open and there is a first discharge due to the high pressure inside the cylinder. There is a second discharge of burnt gases that is induced by the piston moviing towards TDC. The exhaust valves close and the cycle begins with a new intake stroke.

In practice, the fluid dynamic characteristics of gases and the time required to achieve an effective lift of the valves increase the complexity of the processes aforementioned. Therefore, the valve events are advanced and delayed, both intake and exhaust, with the aim of improving the efficiency of the processes and the engine itself. In this sense, four valve events are redefined: IVO (Intake Valve Opening), IVC (Intake Valve Closing), EVO (Exhaust Valve Opening) and EVC (Exhaust Valve Closing) as shown in Figure 2.4.

The IVO is advanced with respect to TDC, so the intake phase starts during the last part of the exhaust stroke of the previous cycle, to allow gases to enter the cylinder sooner, once the exhaust pressure has dropped significantly. The IVC is delayed with respect to BDC, reducing the effective compression ratio and allowing more air coming into the cylinder. Although the cylinder begins to move upwards and could expel part of the gases already introduced, the inertia of the gases and wave phenomena explained in Section 2.2.1.1 are capable of continuing to fill the cylinder. After compression and combustion,

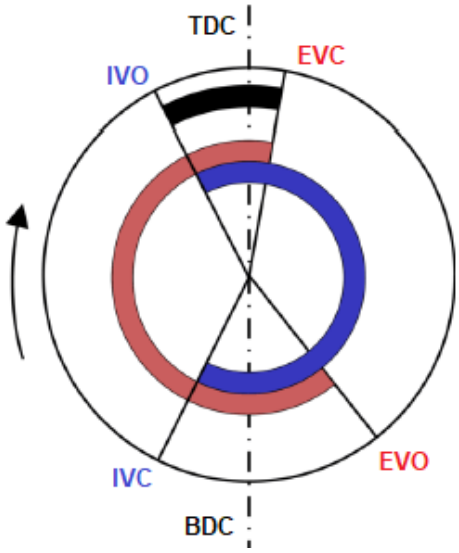

Figure 2.4. *Valve timing diagram of a four-stroke engine.*

the EVO is advanced with respect to BDC. This delay would reduce pumping losses due to the reduced exhaust pressure. However, there is a decrease in the useful expansion stroke, which can lead to a loss in work produced, so there should be a balance between both effects. The intake valves will open again for the next cycle whereas the exhaust stroke is coming to an end and the EVC is delayed with respect to TDC. The coexistence of both valves open at the same time is called valve overlap and has several effects. Depending on the delta pressure across the valves, valve overlap can help the scavenging process, even leading to short-circuiting, a highly undesirable effect as a lot of work has been invested in getting those gases into the cylinder. In other circumstances, burned gases may travel to the intake line, usually being reintroduced once the exhaust valves are closed. Besides, there is a risk of contact between the valves and the piston that must be avoided. If there is no valve overlap, it is called negative valve overlap (NVO). A generic duration in CAD of the intake (in blue) and exhaust (in red) processes, together with the valve overlap (in black) are shown in Figure 2.4. The optimal value for valve advances and delays is very dependent on the point of the map, mainly speed and load, since it is a key factor on volumetric efficiency and pumping losses. Besides, it also affects combustion due to the change in residuals concentration. However, it is clear that lower valve overlaps are better for low speeds, and higher valve overlaps are better for high engine speeds and sports applications. In order to

optimize the engine in the whole map, variable valve actuation systems have been developed, which will be explained later.

The effect of the number of valves, or what is the same, the area of the section, is also a factor to keep in mind. As the engines have been developed, in general and depending on the application, the number of valves has increased from one to two of each, being the four valves per cylinder the most extended configuration. However, three valves at intake have also been used in certain engines. Figure 2.5 shows the dependence of volumetric efficiency and pumping losses with respect to engine speed and the section of intake and exhaust valves. The volumetric efficiency is greatly influenced by the intake valve section, with a minimum effect of pumping losses. With exhaust valves, the opposite happens, affecting more pumping losses than volumetric efficiency.

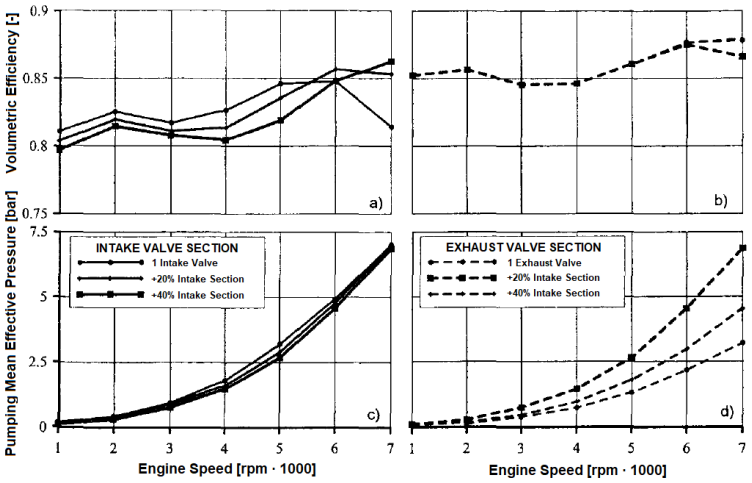

Figure 2.5. *Effect of the intake and exhaust valves section and engine speed on load renewal parameters: a) Volumetric efficiency depending on intake valve section; b) Volumetric efficiency depending on exhaust valve section; c) Pumping mean effective pressure depending on intake valve section; d) Pumping mean effective pressure depending on exhaust valve section. Source: Adapted from [3].*

2.2.1.3 Exhaust line

The exhaust system is in charge of extracting the gases produced by combustion and extracting them from the engine to the atmosphere. Once the exhaust valves are open, the exhaust gases leave the cylinder, uniting the gas from the different cylinders in the exhaust manifold. Note than the same tuning effect explained in 2.2.1.1 also applies for the exhaust system. When

the exhaust valves open, an overpressure wave is generated, which travels and reflects, giving rise to a wave that helps to empty the cylinder. However, tuning effects on volumetric efficiency are lower, as well as the effect on performance.

If the engine is turborcharged, the next item in the exhaust line is the turbine. The exhaust manifold is sometimes integrated into the turbine volute, as is the case with the engine under study in this document. Other engines have an integrated exhaust manifold in the head of the cylinders for reduced exhaust temperatures, thus reducing the need for enrichment at high loads. The most widespread types of turbine are wastegate and VGT (Variable Geometry Turbine), also named as VNT (Variable Nozzle Turbine). As the name suggests, the wastegate has a valve to change the quantity of exhaust gas that goes throught the turbine to control the turbocharger. In the case of VGT, the rack position is changed in order to vary the relative position of the stator blades. In this case, all flow goes always through the turbine. More details on boosting are given in Section 2.2.1.4

After the turbine, the exhaust gases are at a lower temperature and pressure on the way to the aftertreatment system. However, several studies are pointing out the potential improvement that putting the aftertreatment before the turbine would suppose to reduce the emission of pollutants at low temperatures and cold start [9–11]. The typical aftertreatment system of a nowadays SI gasoline engines consist of a TWC. Lately, the use of a GPF has been studied [12–19], mainly because of to the use of direct injection, EGR and the new emission standards. In some cases, also a NO_x trap has also been used, mostly for lean operation. The aftertreatment systems in SI gasoline engines used to be a two-way catalyst for carbon monoxide and hydrocarbon emissions reduction, and expanded to three-way catalysts in the early 80s to also reduce NO_x. Its size, price and efficiency surely make the TWC the best possible aftertreatment for gasoline engines, and hence it has been used for so many years. The best operating condition for the TWC is oscillating around stoichiometric conditions, where the conversion of all three contaminants is maximum. In this situation, there is enough oxygen in the exhaust to oxidize HC and CO and it is possible to reduce NO_x. Figure 2.6 shows the conversion efficiency with respect to air-fuel ratio for the three species.

The implementation of a TWC forces SI engines to operate under stoichiometric conditions to maintain high efficiency levels. This is translated into lower efficiencies than CI engines, which in addition to operate under lean conditions, do not need to use throttle and therefore have lower pumping losses. However, this drawback is compensated since CI engines require much more complex and expensive aftertreatment systems. Furthermore, it

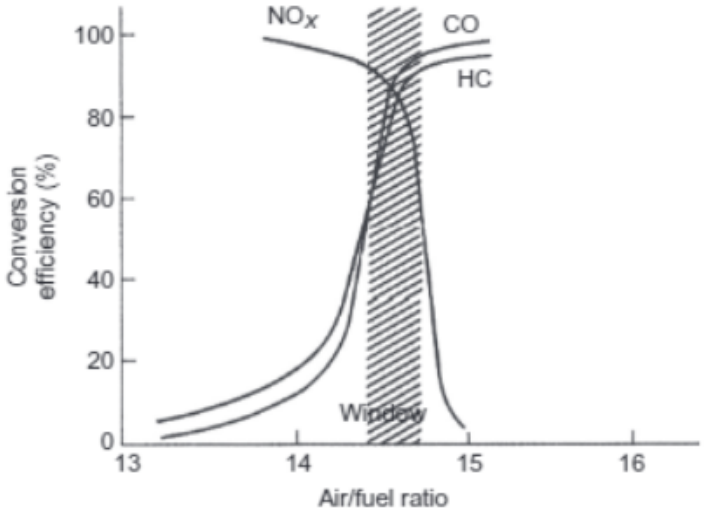

Figure 2.6. *Conversion efficiency of the TWC with respect to air-fuel ratio for NO_x, HC and CO. Source: [20].*

is expected that the trend in the cost and complexity of CI aftertreatment will be increasing, making diesel cars as expensive as hybrid and electric [21].

In the case of having an EGR system, a valve to control the rate of recirculated gas may be placed at some point of the exhaust line. Its position depends on the EGR system used, differentiating between high and low pressure systems, clean or dirty.

If the exhaust gas undergoes a cooling process, a water-to-air cooler is normally placed between the EGR valve and the junction with fresh air. The effect on engine operation and the different EGR systems will be explained in Section 2.3.6 and 2.4.

A muffler is normally the last item placed before reaching the atmosphere in the exhaust line. The purpose of the muffler is to attenuate the noise generated by the engine by reducing the speed of the gases and absorbing the sound waves or canceling them by interference with the reflected waves, with similar phenomena to those explained for intake and exhaust tuning.

2.2.1.4 Boosting

Despite the fact that boosted SI engines exist since the beginning of the 20th century, boosted engines for the automotive industry have always been related to CI engines. In gasoline engines, boosting has been used throughout history especially for sports applications, since massive application was a challenge mainly due to knock control. With the improvements in control techniques and downsizing, boosting in SI engines is becoming more and more common.

Boosting is mainly divided into two types: turbocharging and supercharging. The turbocharger is a compressor attached to a turbine by a shaft. This turbine extracts the energy from the exhaust gases, which would otherwise be lost. The flux diagram of a turbocharger is shown in Figure 2.7. In the case of supercharging, the compressor is driven by the engine

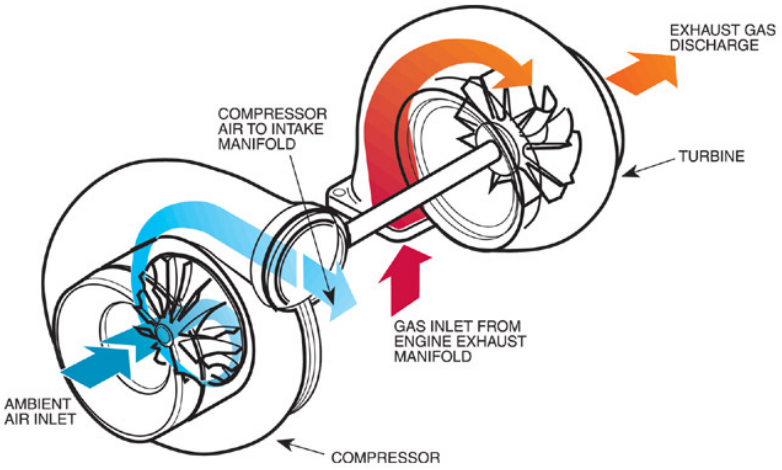

Figure 2.7. *Flux diagram of a turbocharger.*

The use of a turbocharger has an advantage from an efficiency point of view as it takes advantage of the enthalpy of the burned gases. In addition, the use of a supercharger implies a loss of energy in the engine shaft. However, a great benefit is found with the use of a supercharger when it comes to reaction time. Known as turbocharger lag, it is the time taken to accelerate the turbogroup, something that does not happen with superchargers. The size and weight of

the turbine plays a fundamental role here since the lag mainly depends on the inertia of the turbocharger. Turbocharger lag has been reduced over the years, being very small nowadays but very important in the past. Nowadays, electric powered systems as the ones used in F1 (MGU-H) are being implemented to accelerate the turbocharger, thus reducing or supressing lag, or directly driving the compressor as a supercharging system. The case of the Renault 5 Turbo is very famous, a car from the 80s that suffered a lot from lag, causing an abrupt surge of power that caught many off guard.

Currently, there are engines that combine these two technologies simultaneously, as the Volkswagen's 1.4 TFSI (Turbocharged Fuel Stratified Injection) engine, to have a quick reaction from the engine and a good low end torque by means of a supercharger, and also have a high power thanks to a bigger turbocharger. Several turbochargers are also being implemented in some applications, both in parallel or serial configuration, to obtain fast torque responses and high power. In the case of parallel configuration, each turbocharger is normally used to feed a bank of cylinders, as in the Ferrari 488 GTB or the F8 Tributo. For the serial configuration, all turbochargers feed the same cylinders. For example, BMW has launched a tri-turbo engine, available in their 5 Series, X5 and X6 and an engine with four turbochargers for the 7 Series. However, most boosted applications use a single stage turbocharger configuration, as in the engine under study in this document. A more extensive explanation of the different turbocharger configurations can be found in [22].

2.2.2 The SI premixed combustion

Among the different types of combustion that exist, gasoline engines are within the premixed turbulent. This type of combustion is normally divided into four phases [23]: spark ignition and lag, flame kernel formation, premixed turbulent combustion and flame termination or quenching.

During the first two phases, only 5 to 10% of the heat is released and a little pressure increase with respect to motoring cycles is observed, thus not much useful work is obtained. During the third phase, combustion speeds up, burning the vast majority of the mixture to about 90% of the heat release and increasing the in-cylinder pressure to its peak value, delivering work. The remaining unburned mixture is consumed during the flame termination with a pressure decrease [24]. The combustion phases, the pressure evolution inside the cylinder of a fired and a motoring cycle and the fuel burn fraction of a fired cycle are shown in Figure 2.8.

There are several combustion chamber arrengements in direct injection spark-ignited engines that are normally classified into three categories

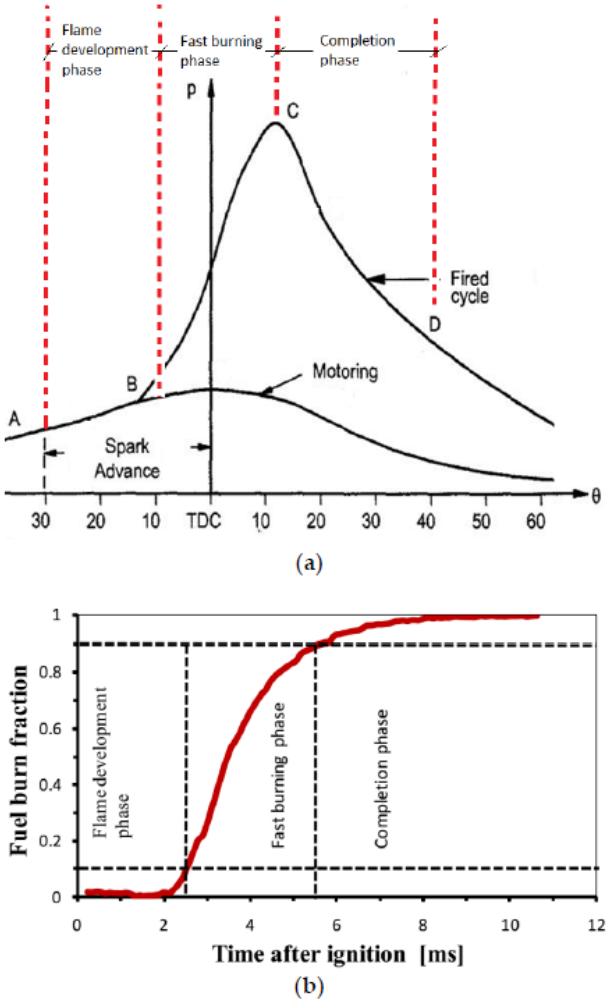

Figure 2.8. *Combustion phases in SI engines shown in: (a) pressure evolution with CAD for a fired cycle compared to motoring cycle; (b) accumulative heat release rate. Source: [25].*

depending on the mechanism that govern the mixture formation: guided by air, wall and spray. The three categories can be seen in Figure 2.9.

In the wall and air-guided configurations, the fuel injector is normally directed to the spark position and in a far position to it, so the in-cylinder flow structures or the interaction with the piston control the mixture process. In the case of spray-guided configurations, spark and the fuel injector are usually

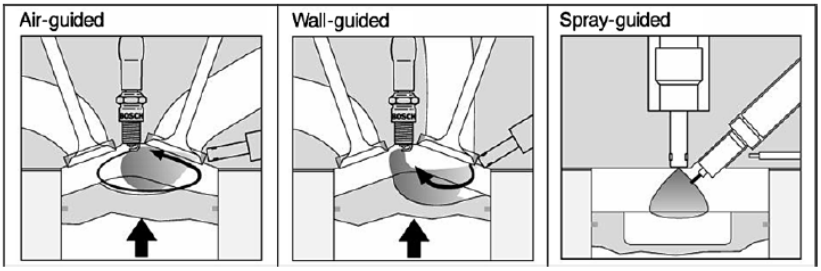

Figure 2.9. *DISI arrengements of the combustion chamber. Source: [26].*

placed very close to provide a good fuel preparation and ignition. In the first stages of DI spark-ignited engines development, the wall-guided system was predominant [27], but spray-guided has gained prominence in recent years due to fuel economy improvements, lower hydrocarbon and soot emissions and the possibility to operate in further stratified conditions [28–30].

2.2.2.1 Spark event and ignition lag

The combustion process on gasoline engines starts with an external energy input that must be sufficient in intensity and duration to give rise to the start of combustion. This fact imposes two clear demands on the fuel to be used and the type of mixture. First, the fuel must be resistant to auto-ignition so that spontaneous ignition does not occur, in order to ensure that the process starts at the desired time. Second, there must be a premix of the air and fuel to ensure homogeneity and the proper advance of the flame front.

The spark ignition process has been deeply detailed [3, 31–35]. The formation process of the spark is divided into several phases:

- **Pre-breakdown:** the gas in the gap between electrodes acts an electrical insulator. When the electric potential reaches values of the order of 15 kV, electrons increase their energy and start moving towards the anode. Current increases as other gas molecules ionize.
- **Breakdown:** in about 1-10 ns, the current is increased to around 200 A, the voltage drops to around 50-100 V and the process is self-sustaining. A narrow channel of about 40 µm is initially formed with high levels of energy. A huge increase in temperature increases the pressure inside the channel, causing a sudden expansion with shock waves. This energy transfer to plasma is about 95% efficient.

- **Arc discharge:** lower voltage levels, around 50 V, are found for the system to be able to maintain it. In this phase the thermal dissociation of gas molecules dominates. The cathode acts as a hot spot and part of it melts and vaporizes, causing deterioration. Temperatures in the channel drop and the plasma expands and exothermic reactions begin to occur, producing a flame that spreads.

- **Glow discharge:** after this, current drops to levels of a around 100 mA. Temperature in the channel drops to around 3000 K and the efficiency of energy transfer to gas decreases. Most energy stored in the system is discharged in this phase.

2.2.2.2 Flame kernel formation

The kernel is the name given to a small spherical shaped volume inside the unburned region of the combustion chamber where the reaction is starting. These initial states of combustion are always developed under laminar conditions, with a smooth advance of the flame front. To ensure a stable development of the combustion, this flame kernel must have a minimum size, normally related to that of the gap between electrodes, to overcome different sources of heat lossesas stated in [36]. Highly deformated surfaces and heat losses affect negatively the consumption of all reactants, since the flame front may quench. In this sense, the strength of the vortex is a dominant factor as explained by Xiong et al. [37] and Eichenberger et al. [38]. Many studies have tried to visualize the flame ignition and kernel development by different methods [39–43].

Many parameters could affect the development of the flame kernel created due to the ignition process, as well as its ability to finally form a self-sustaining flame front capable of consuming all reactants. Local conditions of temperature, heat losses, lambda and mixture homogeneity around the spark plug are some of the main possible disturbances, together with turbulence. Given that turbulence is a complex phenomenon with a strong random component, conditions around the spark plug can vary notably between cycles as show in Figure 2.11, leading to cyclical variations [44] that affect torque and power stability, combustion, efficiency and emissions [45, 46]. Other parameters that can affect are the geometry and the ignition system.

2.2.2.3 Premixed turbulent combustion

The analysis of the turbulent combustion depends on a series of dimensionless numbers, namely: Reynolds, Damköhler and Karlovitz. The

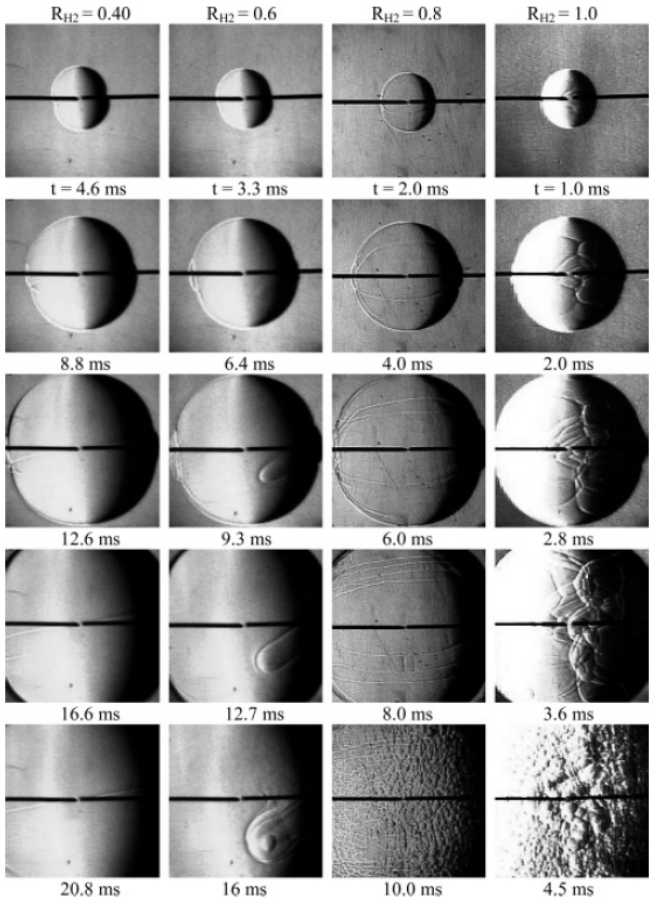

Figure 2.10. *Initial flame kernel development visualization through Schlieren technique for natural gas - hydrogen mixtures at several hydrogen fractions and stoichiometric operation. Source: [42].*

Reynolds number compares inertial and viscous forces. To better understand the Damköhler and Karlovitz numbers, several parameters must be defined. As there are two characteristic lengths of the turbulence, two characteristic times are also defined: the mixing or diffusion time referred to the macroscale (integral scale), τ_{inte}, and the mixing or diffusion time referred to the microscale (Kolmogorov scale), τ_K. Both times can be compared to the characteristic reaction time, τ_R. In this sense, the Damköhler number, Da, compares τ_{int} with τ_R (Equation 2.4), whereas the Karlovitz number, Ka, compares τ_R with τ_K (Equation 2.5).

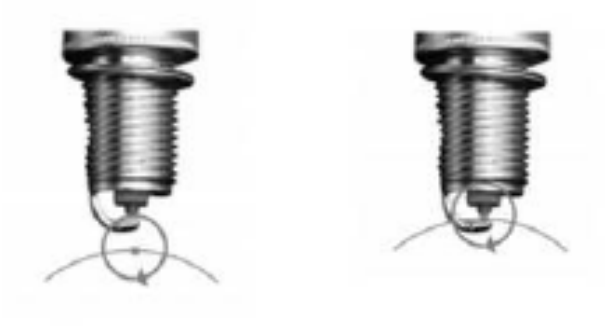

Figure 2.11. *Turbulence conditions around the spark plug causing cyclical variations. Source: Adapted from [3].*

$$Da = \frac{\tau_{inte}}{\tau_R} = \frac{L_{inte}/I}{\delta/S_L} \tag{2.4}$$

$$Ka = \frac{\tau_R}{\tau_K} = \frac{\delta/S_L}{\lambda_K/I} \tag{2.5}$$

where L_{int} refers to the characteristic length of the macroscale, I refers to the turbulent intensity, δ is the thickness of the flame front, S_L is the combustion speed in laminar conditions and λ_K is the spatial Kolmogorov scale. Depending on this analysis, the flame is in a determined regime [47, 48]. The Borghi diagram proposed in [49] and [50] is shown in Figure 2.12:

The most interesting area for spark ignition engines is between the corrugated and thickened wrinkled flames, being both regimes with Damköhler numbers beyond the unit. The boundary between these regimes is placed, for some authors [52], at Karlovitz number equal to one. For some others, it is when λ_K equals δ. The difference between both regimes lies in the addition of small sized fluctuations into the flame front, forcing it to expand. In this way, corrugated flamelets have a higher level of turbulence compared to wrinkled flames, promoting the formation of pockets. This pockets are small bags of burned mass within the fresh mixture that are able to increase combustion rates due to a bigger surface area of the flame front. For greater turbulence levels, λ_K is smaller than δ, there is a transition to thickened wrinkled flames and fluctuations enter the flame front, making it larger. In this sense, combustion speed is somehow related to turbulence intensity. However, the interaction between these local turbulences that increase the flame front and the charge

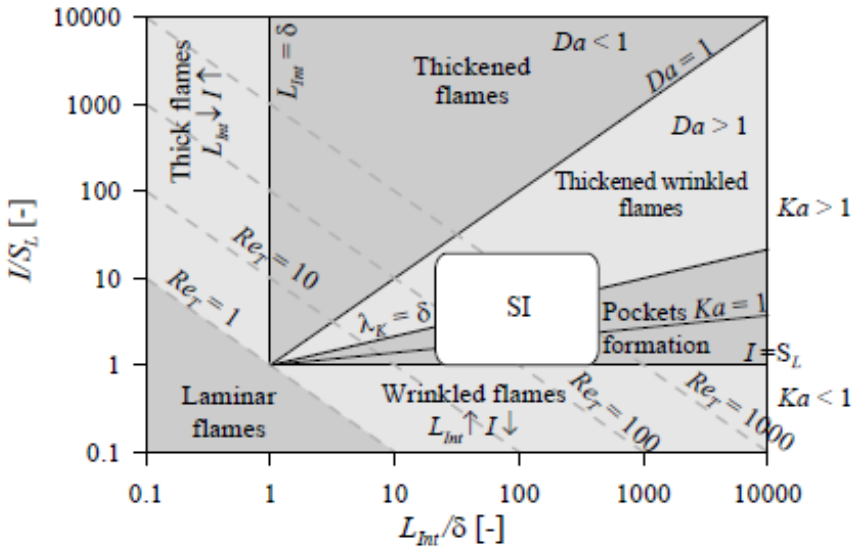

Figure 2.12. *Borghi diagram and typical position of a SI engine. Source: [51].*

motion inside the cylinder is a very complicated process [53]. Large eddies would disturb the flame front and increase heat losses, quenching the flame in extreme cases. Besides, it has been demonstrated that the eddies generated during the intake stroke do not last enough to enhance combustion, and are dissipated during compression. It is the eddies generated during compression from the breaking of the swirl and tumble motions that most affect the burn rate.

The premixed turbulent combustion can be explained through a two-zone entrainment model, as the one proposed by Keck et al. [54]. The rate of unburned mass entrained but not yet burned, dm_{ub}, is shown in Equation 2.6:

$$\frac{dm_{ub}}{dt} = \rho_{ub} \cdot A_f \cdot U_t - \frac{dm_{ub}}{\frac{L_t}{S_L}} \tag{2.6}$$

where U_t is the local turbulent fluctuation speed at which the flame front area, A_f, advances and ρ_{ub} refers to the unburned gases density. The entrained gas is burned at a rate that depends on L_t, the length scale for turbulent conditions. Hence, the burning rate, dm_b, is the result of the sum of the unburned mass and the laminar combustion, as shown in Equation 2.7:

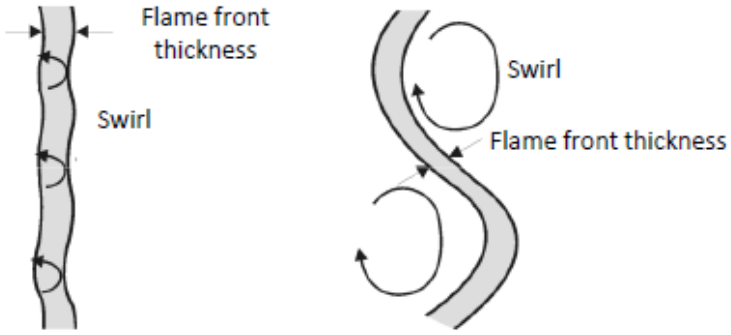

Figure 2.13. *Differences between thickened flame (left) and disorted flame (right) due to the size relationship between turbulence and the thickness of the flame front. Source: [51].*

$$\frac{dm_b}{dt} = \rho_{ub} \cdot A_f \cdot S_L + \frac{dm_{ub}}{\frac{L_t}{S_L}} \tag{2.7}$$

With Equations Equation 2.6 and Equation 2.7 and assuming quasi-steady conditions, so the rate of unburned mass entrained is zero, the burn rate is simplified to Equation 2.8:

$$\frac{dm_b}{dt} = \rho_{ub} \cdot A_f \cdot (S_L + U_t) \tag{2.8}$$

For quasi-steady combustion, the burning speed is the contribution of the laminar speed and the speed of the local turbulent fluctuation, $S_L + U_t$. For very slow laminar flames, the diffusion time, ${L_t}^2/D$, would be comparable or larger than the burning time, L_t/S_L, so this model would not be useful and the flames would be thickened like. Note that D is the mass diffusivity.

2.2.2.4 Flame termination

During the first phase of the expansion stroke, about 90 to 95% of the mixture has been consumed and the flame front reaches the nooks and crannies of the chamber, near the geometric limits marked by the wall of the cylinder and the piston. At this stage, the volume of the chamber is still very small. The last portion of the mixture, also called end-gas, burns very slowly due to proximity to walls. These metal walls can increase heat losses due to its temperature, slowing down the reaction speed and the putting an end to combustion.

The contribution of this end-gas to the amount of work delivered is very little due to the moment in which the heat is released and the small fraction of mixture that remains unburned. However, the end-gas has undergone a compression process and high temperatures, so there is a risk of autoignition and knock, that would not be a destructive phenomenon at flame termination, causing only slight pressure variations [24] and affecting smooth operation.

2.2.2.5 Autoignition: abnormal combustion

The autoignition of the mixture is a totally undesirable phenomenon in gasoline engines that can lead to knock. This event can occur when the mixture is at high pressure and temperature during a time that allow it to ignite, before the spark event or the flame front reaches that portion of the gas. It also happens when the mixture finds a hot spot acting as a second spark plug. Naturally, the more unburned gas there is, the more dangerous it is. The autoignition event normally occurs at the final stages of combustion, in the end-gas.

When different points of the combustion chamber autoignite, there is a temperature and pressure increment in the cylinder, growing the burn rate, as can be observed in the heat release rate (HRR), in a process that can be highly destructive [55–57]. Besides, the higher temperature and pressure, and the clash between the different flame fronts that would be generated can cause pressure waves as shown in Figure 2.14 that propagate violently at the speed of sound [58]. These oscillations in pressure, proportional to the amount of autoignited gas, would break the thermal layer that protect the piston and cylinder wall, with the corresponding damage on the surface made by the high temperature. This effect can cause early deterioration and material melting. Moreover, the pressure gradient can damage the mechanisms of the engine, producing the characteristic noise [59] that gives its name to the phenomenon. However, detecting the knock and its different levels is not always an easy task and many methods have been developed for this [60, 61].

When the mixture is under certain conditions of temperature and pressure, several chain reactions begin and after a certain time, combustion occurs [63, 64]. This time is the autoignition delay time (τ).

The appearance of knock is greatly influenced by many parameters as fuel, fuel-air ratio, oxygen concentration, intake pressure and temperature or engine speed and load, among others. Normally, increasing the engine load, and therefore the pressure and temperature, reduces the ignition delay, as well as stoichiometric operation [65]. Reduced oxygen concentration would reduce reactivity, increasing the delay time. Increased engine speed would reduce

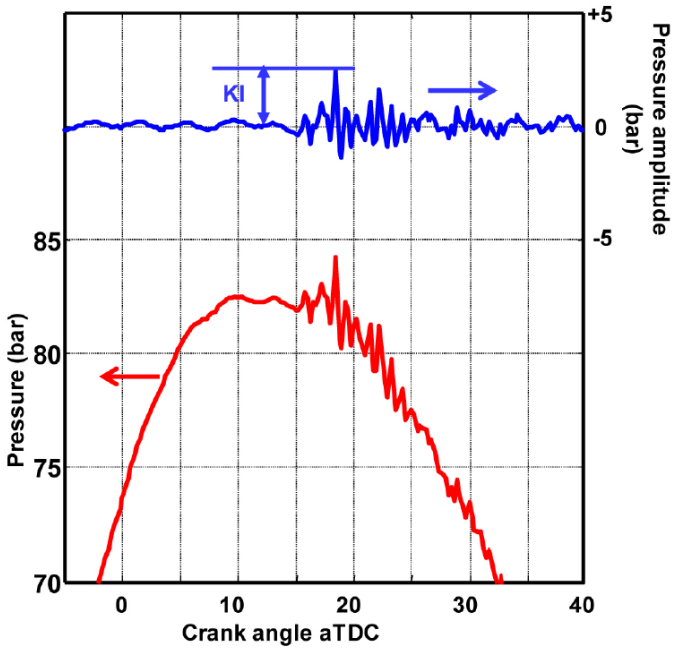

Figure 2.14. *Pressure oscilations on the instantaneous in-cylinder pressure evolution (red) and pressure amplitude variation (blue). Source: [62].*

knock events, since there are reduced timescales. The fuel is characterized by the octane number (ON), which greatly influences the capicity of the fuel to resist autoignition.

In this sense, mapping of the ignition delay has been made for several fuels and conditions of temperature and pressure, as the one shown in Figure 2.15, normally in the RCM (Rapid Compression Machine). Certain experimental correlations have also been investigated, using as input parameters both conditions and the octane number of the fuel [62, 66–69].

2.2.2.6 Factors affecting combustion

There are many factors that can affect the development of combustion that has been explained above. First, the design parameters like the location and number of spark plugs, the geometry, or the number and area of the valves, as well as the shape of the ducts, among others. In this section, a brief review of several factors affecting combustion will be made.

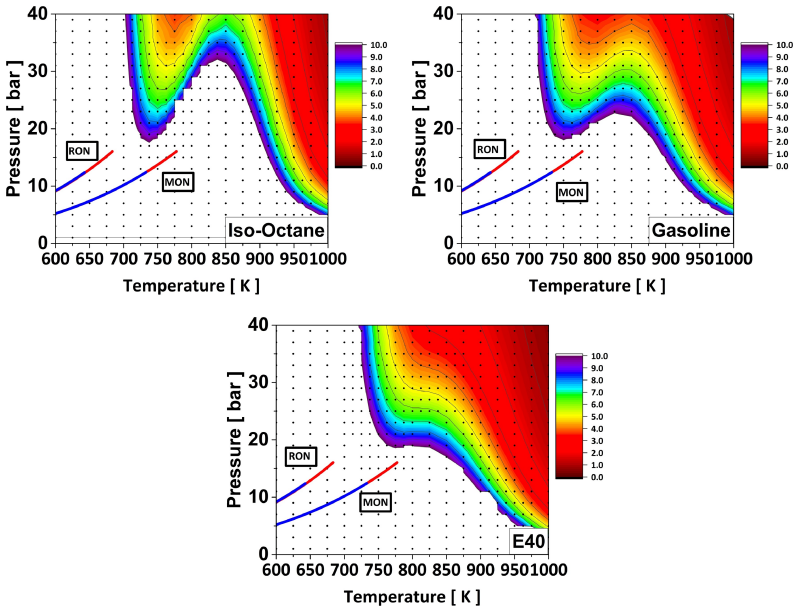

Figure 2.15. *Autoignition delay time maps in function of pressure and temperature for iso-octane (left upper graph), gasoline (right upper graph) and E40 (lower graph). Source: [70].*

Spark advance

The instant of ignition is, of course, a key part in the combustion process [71] and the appearance and mitigation of knock. The spark advance can change the amount of mixture burned before and after TDC, changing the work developed during the cycle. Moreover, advancing or delaying the spark event can change the peak pressure value and the IMEP (Indicated Mean Effective Pressure), thus changing efficiency [72]. When advancing the spark event, more and more mixture is burned before TDC, increasing the maximum temperature and pressure. However, more heat transfer losses are observed. Naturally, pressure and temperature do not rise indefinitely with spark advance, observing a fall from a certain value. Excesive spark advance would lead to misfires or to a early pressure rise, difficulting the movement of the piston during compression. For small spark advances, the pressure rise occurs too late and the maximum benefit is not taken. Exhaust temperature is be affected by late spark timing. Between the two extreme situation, none of them convenient, there is an optimum value for efficiency and torque output, as shown in Figure 2.16.

However, combustion centering is not always possible, since knock can appear, forcing the engine to work at a non-optimal combustion centering [73].

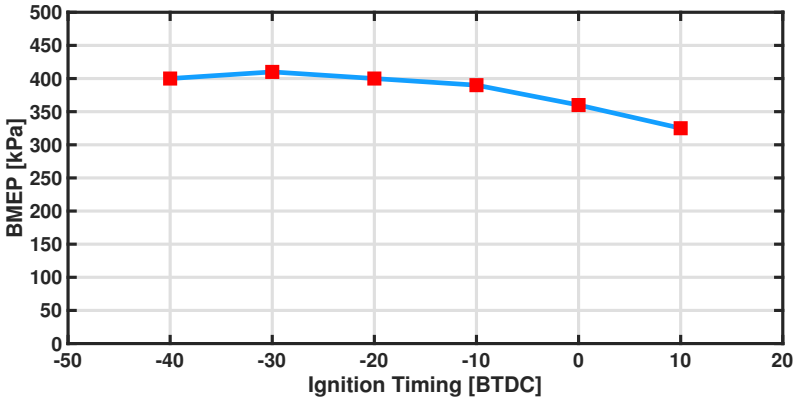

Figure 2.16. *Ignition timing effect on BMEP. Source: Adapted from [74].*

Engine speed

For greater engine speeds, the CAD for the laminar phases of combustion also increases, since at these combustion stages the flame speed is almost constant. This effect results in increased CAD needed to burn all the mixture, despite the fact that the turbulence also scales with the regime, but not necessarily linearly, depending on the design of the combustion chamber and intake pipes. Therefore, the spark event needs to be advanced to keep combustion centering. The spark advance with respect to the engine speed was traditionally made by a centrifugal device, but nowadays it has been replaced by electronic control. In addition, the probability of knock is usually decreased with a shorter residence time.

Engine load

For SI engines, the RGF (Residual Gas Fraction) is normally increased at low and partial loads compared to high loads. This is explained by the reduced intake pressure and increased difference between exhaust and intake pressure, which makes the scavenging process more difficult. An excesive concentration of RGF could reduce the overall combustion speed, therefore it is necessary to increase the spark advance. Similar effects occur when the concentration of RGF is not only due to IGR but also due to EGR [75]. For higher or full

engine loads, RGF are reduced, and higher temperatures and pressures occur, increasing the knock probability. All effects lead to decreasing spark advance. However, very late sparks could increase exhaust temperature, which is also a major limit in this area of the map [73].

Fuel-air ratio

Stoichiometric or slightly rich operation of the engine is the provide the best possible combustion in SI engines, since the higher combustion temperatures are expected. This is explained by the ease with which the flame front finds favorable areas to continue spreading. For equivalence ratios greater than 1.2 and for lean operation, temperatures drop. However, lean operation is a hot spot as under certain conditions it can allow better combustion centering. The flammability limits for both excess and under-fuel must also be taken into account.

Ambient conditions

The ambient conditions that most affect combustion are temperature, pressure and humidity. For lower ambient temperatures, a reduction in both laminar and turbulent flame speeds is expected. However, the effect is small. A reduction in ambient pressure can significantly change the combustion in naturally aspirated engines by reducing the trapped mass. Proportionally, heat losses would have a greater weight, reducing temperatures and therefore the combustion rate. The effect of humidity is due to the increased presence of inerts, reducing the reactivity and the temperature, thus the combustion speed.

2.2.3 Pollutant emissions formation in SI engines

The gasoline normally used in SI engines is a product obtained by distillation of petroleum, and it is a combination of hundreds of individual hydrocarbon chains from C_4, like butanes and butenes, to C_{11}, like methylnaphthalene, with a final H-C ratio of around 1.6-1.9. In a perfect stoichiometric combustion with gasoline, all the oxygen contained in the air would completely oxidize the fuel, leading to the formation of water (H_2O) and carbon dioxides. Nitrogen (N_2) present predominantly in the air would continue unchanged. However, different intermediate products from combustion appear sice it is not a perfect process but incomplete. The objective of this section is to evaluate the main pollutants produced by SI engines that

are regulated nowadays: carbon monoxide, unburned hydrocarbons, nitrogen oxides and particulate matter. Note that carbon dioxide is not considered a pollutant since it is a final product of combustion. In addition to explaining its formation, it is intended to furnish knodledge about the effect that each pollutant has on the human and environmental health, as well as the general trends observed in these emissions when using exhaust recirculation.

2.2.3.1 Carbon dioxides

Carbon dioxide is generated as a final product of combustion and it is known as one of the main contributors to greenhouse effect, as shown in Figure 1.9. The GWP index is defined as the amount of heat that a greenhouse gas can absorb in the atmosphere compared to CO_2. Following this definition, the GWP of carbon dioxide is set to 1, while the potential of other gases such as nitrous oxide or methane are 296 and 21 respectively. However, the amount of carbon dioxide produced and emitted is much higher in comparison.

The two factors that can affect the emission of carbon dioxides from an engine are: efficiency and fuel composition. Since carbon dioxide emission is directly linked with fuel consumption, all strategies focused on increasing efficiency would also reduce CO_2 emissions. Regarding fuel composition and assuming a generic fuel molecule as $H_mC_nO_p$, the H-C (m/n) and O-C (p/n) ratios of the fuel molecule are key factors. Increasing these two ratios is translated into lower carbon concentrations, thus lower CO_2 formation potential, as shown in Figure 2.17. Fuels like carbon monoxide, methane or hydrogen could be good options to reduce carbon dioxides emissions. Nontheless, traditional fuels are increasingly being combined with biofuels [76, 77], that can be distinguished between first and second generation [3].

The addition of EGR to the fresh mixture would greatly affect the emission of carbon dioxides. Exhaust recirculation is a strategy that, in addition to reducing nitrogen dioxide, notably reduces heat losses within the cylinder as well as the need for fuel enrichment and the knock probability at high loads in SI engines. At partial loads, greater openings of the valves are needed so also pumping losses are reduced. All this makes EGR a system capable of improving efficiency, thus reducing the fuel needed and consequently the carbon dioxide emitted. However, for a given quantity of fuel, the higher concentration of CO_2 means that more heat is released, linked to higher efficiency, as explained in Equation 2.10 and Equation 2.11. Carbon dioxide production is also influenced by dissociation to carbon monoxide, normally presenting these two compounds inverse trends [5].

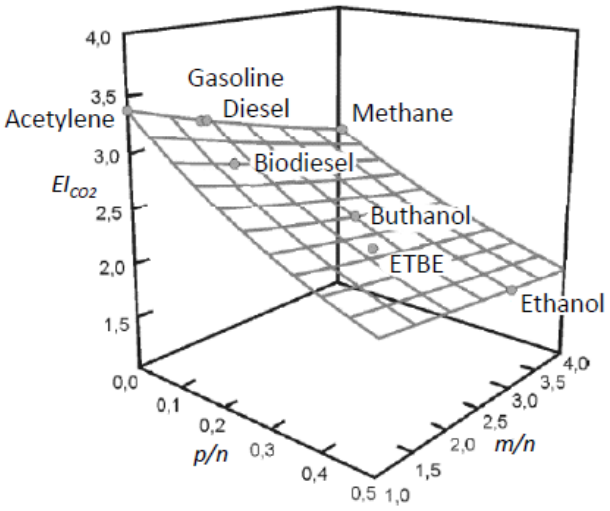

Figure 2.17. *Impact of fuel formulation on the emission index of CO. Source: [51].*

2.2.3.2 Carbon monoxides

Carbon monoxide is a compound formed in the intermediate steps of the combustion reaction, prior to the complete the oxidation of carbon. The mechanism is as explained in Equation 2.9:

$$RadH \rightarrow Rad \rightarrow RadO_2 \rightarrow RadCHO \rightarrow RadCO \rightarrow CO \tag{2.9}$$

where Rad represents a radical. Apart from incomplete combustion, CO is also formed from CO_2 dissociation when temperature rises beyond 2000 K.

$$CO + \frac{1}{2}O_2 \rightarrow (1-\beta)CO_2 + \beta CO + \frac{\beta}{2}O_2 \tag{2.10}$$

where β represents the fraction of CO_2 that dissociates. For $\beta = 1$, there is no reaction thus no heat is released. For $\beta = 0$, maximum heat is released so that temperature and pressure rise at their most [78]. Equation 2.11 shows the complete oxidation of CO.

$$CO + \frac{1}{2}O_2 \rightarrow CO_2 + heat \tag{2.11}$$

Carbon monoxide, apart from an undesirable pollutant, represents a loss of energy that has not been used in the engine, since it is a fuel capable of releasing

heat as shown in Equation 2.11. CO is mostly dependent on the equivalence ratio, which is evident in Figure 2.19, obtaining maximum concentrations when operating with a lack of oxygen under rich conditions. These makes CO emissions more important in SI engines. Same conditions are found if locally rich regions appear in the mixture. This is the case of heterogeneities in the mixture, during load transient due to lambda control and engine start-up, when intentionally lambda is set to rich. Another formation mechanism of carbon monoxide is flame quenching, when the flame front reaches the piston or cylinder wall, freezing the reaction. The concentration of carbon monoxide is governed by the balance between the formation processes and the oxidation reactions, these being much slower than the formation ones. In a gasoline engine, the rapid drop in temperature normally freezes the reaction before reaching equilibrium in the CO oxidation reactions.

This gas is odorless, colorless and poisonous due to its capacity to combine with hemoglobin, replacing oxygen in the blood. Symptoms on humans exposed to this gas include headache, chest pain and dizziness. Long exposure periods or high concentrations can lead to unconsciousness, arrhythmias, seizures or eventually death in extreme cases. Figure 2.18 shows the saturation of hemoglobin in percentage with respect to the exposure time. Between 10 and 40%, severe headaches and reduced mental alertness are expected. Between 40 and 50%, vomiting and collapse. Beyond that, coma and death. Many deaths have been reported in the past due to charcoal-burning and motor vehicle exhaust in closed or poorly ventilated places, making clear the importance of reducing this emission. Fortunately, today's emission levels have reduced this type of incidents [79].

As aforexplained, CO production depends on the kinectics of the carbon monoxide transformation to carbon dioxide almost at the end of combustion, so these two compounds usually follow a trade-off. When operating with EGR, the oxygen concentration reduction would shift the equilibrium of the reaction to more CO production, naturally. However, the reduced in-cylinder temperature due to increased presence of inerts and higher ratio of specific heat values would reduce the dissociation of CO_2 to CO and the kinetics of the oxidation reaction are reduced [5]. These two opposite effects have led to different conclusions about the effect of EGR on CO emissions, depending on the specific characteristics of the experiment. Several studies have found a potential to reduce this pollutant with exhaust recirculation [5], whereas some others had the opposite conclusion [81, 82] or just found variations [83]. Changes on the spark timing [81, 83] or valve events can also vary CO production. For greater EGR rates, combustion instabilities are expected [45], increasing carbon monoxides.

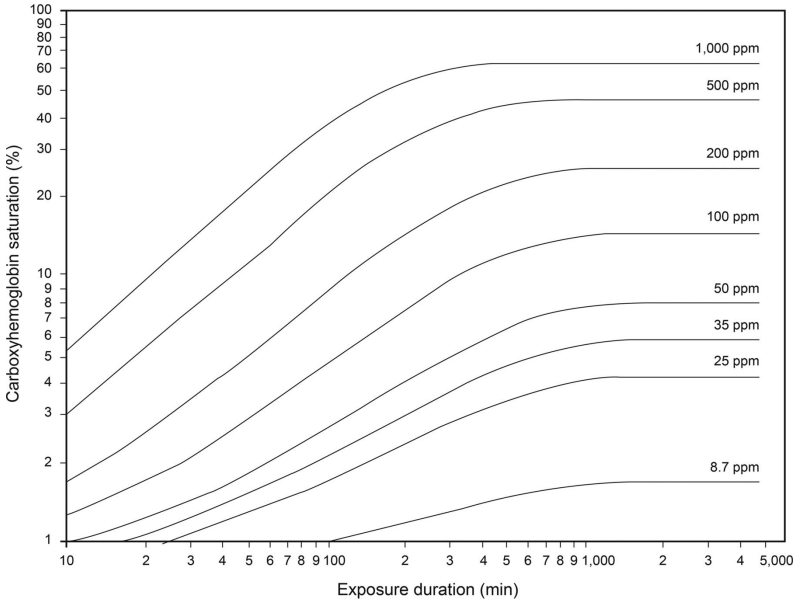

Figure 2.18. *Saturation of hemoglobin in percentage with respect to the exposure time to CO. Source: Adapted from [80].*

2.2.3.3 Unburned hydrocarbons

Unburned hydrocarbons are the result of an imperfect combustion process, therefore they are also considered a loss of energy due to heat that is not released. Since unburned hydrocarbons are formed at different stages of combustion and in different degrees of oxidation of the fuel, their composition is highly variable. The engine operating condition, the geometry of the different parts involved and the fuel composition also play an important role on HC formation.

The mechanisms that contribute the most to HC formation are:

- **Fuel-air ratio:** there is a strong dependency between HC emissions and fuel-air ratio, which is evident in Figure 2.19. The lowest possible HC emissions are achieved with slightly lean operation, allowing a good mixture between oxygen and fuel. When the engine is running with lambdas below one, there is a lack of oxygen to react with the fuel, thus increasing the pollutants related with partial combustion, HC and CO. Rich conditions can also be found during start-up and load transitions due to lambda control.

For lean operation, bad combustion could appear, also increasing HC emissions. At the extremes the flammability limits could be reached, resulting in missfire and and therefore the maximum hydrocarbon emission.

- **Incomplete combustion:** despite running under stoichiometric conditions, combustion is not perfect due to several factors. Poor mixing between oxygen and fuel can cause certain fuel particles not to find the oxygen necessary to burn.

  Another factor of incomplete combustion is the well-known flame quenching. When the front gets to the limits of the combustion chamber, the temperature drops and the reaction freezes due to lower reactivity, thus leaving a small volume of mixture unburned. This same phenomenon happens during the expansion stroke due to a temperature and pressure reduction that slows down the combustion, finally quenching the flame. High concentrations of residuals can increase the likelihood of this happening, as well as the presence of EGR, which reduces oxygen concentration and combustion temperature.

- **Crevice volumes:** small spaces in the chamber can be filled with the mixture during the compression stroke and early combustion stages, for example, those volumes between the piston and cylinder. Typically, up to 3% of the mixture could be introduced into these gaps, but this strongly depends on the chamber design, rings, piston and tolerances. The relative position between the compression ring and the spark plug also plays a role, since closer positions would translate into greater ease of burning the mixture there. Note that piston rings are one of the main contributors to crevice volumes, even more in cold conditions due to differences in thermal expansion, being the responsible of up to 80% of these emissions. The pressure drop experienced during the expansion stroke would allow that part of the mixture housed in these volumes to return to the chamber and burn, at least partially.

- **Leakages:** part of the mixture that is forced into the volumes sorrounding the valves may leak through it as pressure in increased by compression and combustion.

- **Valve overlap:** during the time both valves are open at the same time, short-circuiting can occur, specially in PFI (Port Fuel Injection) engines. Since the cylinder inlet and outlet are open, there is a possible path for the mixture to follow which will end up with unburned hydrocarbons in the exhaust line. This problem can be solved with a variable valve

actuation system, to reduce or supress the valve overlap, or with a direct injection system to inject after EVC. This is a much more important factor on two-stroke engines, in which the scavenging process manages the renewal of the load.

- **Deposits:** porous structures formed by depositis in the combustion chamber can cause the absorption during the compression stroke of a fraction of the hydrocarbons present in the mixture. When the pressure drops, the absorbed hydrocarbons are released and expelled to the exhaust. Boosted engines or with high compression ratio usually suffer more from this problem. The chamber geometry and the use of fuel with additives can reduce the formation of deposits, as well as enhanced flow motion.

- **Oil:** the continuous relative movement that exists between the piston and the cylinder makes lubrication necessary to avoid friction and wear of the components, as well as the fusion of the material. The presence of an oil layer on the walls in order to lubricate can cause an effect similar to that of fuel deposits previously explained. Engines using propane the importance of this mechanism is reduced since propane is insoluble in oils.

  Furthermore, small droplets of oil can become part of the combustion, an issue that can be aggravated by the wear caused by aging, increasing the tolerances and the size of the oil layer. Oil is tipically a heavier combination of hydrocarbons than fuel, so combustion speed decreases as oil concentration increases, facilitating the appearance of unburned hydrocarbons.

The main issue with hydrocarbon emissions is the reaction that may occur in pressence of nitrogen oxides and sunlight when they are in contact in the atmosphere. This reaction forms ozone at ground level, a component of photochemical smog which is a widespread air pollutant in urban areas. Ozone is a gas that can irritate eyes and damage the respiratory system. Moreover, some hydrocarbons are toxic for humans and capable of causing several types of tumors.

As with CO emissions, the reduction on oxygen concentration and combustion temperature that is obtained with the use of EGR would decrease the kinetics of the oxidation reactions of hydrocarbons, reducing combustion speed and producing incomplete combustions, thus leading to increased HC emissions as demonstrated by previous studies [84, 85]. The addition of EGR

above a certain limit, as already explained, can cause instabilities [45] that also increase this type of emissions.

2.2.3.4 Nitrogen oxides

Nitrogen oxides are a set of chemical compounds that come from the interaction between oxygen and nitrogen, namely nitrogen monoxide (NO) and nitrogen dioxide (NO_2), the latter being produced to a lesser extent. Major factors affecting NO_x formation are described below:

- **Combustion temperature:** nitrogen oxides formation is directly related to peak temperature during combustion [86], since high activation energies are needed to dissociate oxygen and the bonds of nitrogen. As the burning rate increases, so do the flame temperatures, thus increasing NO_x formation. Also flame quenching can influence the formation of NO_x, reducing this emission notably [87].

- **Fuel-air ratio:** the abundance of oxygen is a key factor to form nitrogen oxides. For lean operation conditions, there is a fraction of oxygen that would not react with the fuel, and if tempeature is high enough, nitrogen oxides will formate. On the one hand, the efficiency advantage of lean operation is offset by the penalty in NO_x emissions [88]. On the other hand, slightly rich operation will increase the combustion temperature in a certain range, so the formation of NO_x depends on the balance between the increase in temperature and the shortage of oxygen, interfering with H and OH radicals [89]. For further enrichment, both temperature and oxygen concentration are reduced, decreasing nitrogen oxides formation.

These two effects are well sumarized by the simplified Zeldovich mechanism [90–92] in Equation 2.12, which assumes that NO formation is in equilibrium:

$$\frac{d[NO]}{dt} = \left(\frac{6 \cdot 10^{16}}{T^{0.5}}\right) \cdot exp\left(\frac{-69096}{T}\right) \cdot [O_2]_e{}^{0.5} \cdot [N_2]_e \tag{2.12}$$

where $[O_2]_e$ and $[N_2]_e$ refer to the concentration of oxygen and nitrogen respectively assuming chemical equillibrium, and $[NO]$ denotes the instantaneous molar concentration of nitric oxide. This mechanism also allows a perfect understanding of the reduction in NO_x that is obtained when using EGR, which has been extensively proven [93–95]. Exhaust recirculation implies a double reducing effect on NO_x:

1. **Dilution**: the higher amount of inert gases inside the cylinder is translated into reduced oxygen concentration and reactivity.

2. **Thermal**: the addition of gases with greater heat capacities reduces the temperature inside the combustion chamber.

In general, HC and NO_x emissions follow opposite trends with most engine parameters, following a trade-off in which almost everything that favors efficiency (i.e. high pressures and temperatures, faster combustions, etc.) will reduce HC and increase NO_x. Exhaust gas recirculation, which at first was used to reduce NO_x in diesel engines, also increases HC. Figure 2.19 shows the evolution of the three mean emissions with the fuel-air equivalence ratio.

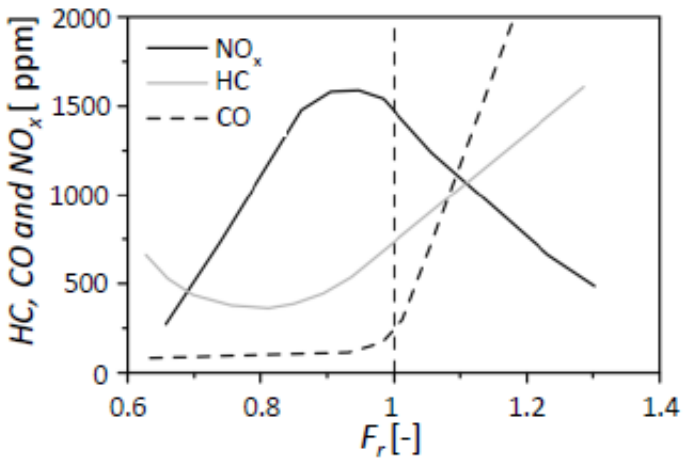

Figure 2.19. *Main exhaust emissions depending on the fuel-air equivalence ratio. Source: [3].*

Figure 2.20 presents soot and NO_x formation in a gray diagram, where darker means higher concentration of the species, with respect to the ratio of fuel to air and temperature, confirming that NO_x emissions are increased with higher temperatures, beyond 2200 K, and lean operation. These conditions are easily found in CI and stratified GTDI engines. In the case of a traditional SI engine, the position on this diagram would be almost fixed around equivalence ratio equal to 1 and temperatures between 2400 and 2600 K. In the case of stratified operation or CI engines, several conditions of this diagram will occur due to the inhomogeneities present on the mixture.

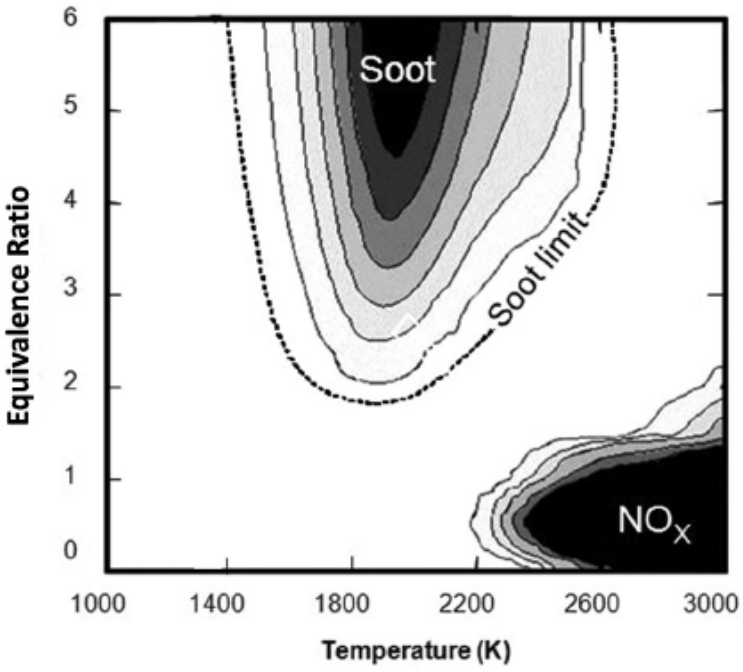

Figure 2.20. *Soot and NO_x formation depending on temperature and equivalence ratio. Source: Adapted from [96].*

The emission of NO_x into the atmosphere has different effects on the environment. First, its effects on humans and animals include irritated eyes and lungs, asthma, headaches and reduced resistance to diseases [97]. Seocond, it affects ozone, generating photochemical smog and increasing the solar ultraviolet radiation that passes the ozone layer. Second, its combination with the water present in clouds results in acid rain, polluting clear water, corroding metals and damaging lands, trees and plants [98].

2.2.3.5 Particulate matter

Particulate matter emissions from RICE are normally divided into two groups: volatile and solid. The volatile particles, typically nanoparticle size, are formed by nucleation of several components, that normally include sulfuric acid, with water. When it comes to solid particles, usually described as soot, are mainly carbonaceous agglomerations. The different particles form the well-known accumulation and nucleation modes, depending on the number and size distribution.

Particulate matter emissions have historically been a problem in CI engines [99], having been almost negligible in SI engines, since the conditions needed to form particles are seldom found in PFI engines. However, the development of GDI (Gasoline Direct Injection) engines has transferred this problem to SI engines. Many studies have reflected the increase in PM emissions in GDI engines compared to PFI [100–105]. Given that this concern has arisen in SI engines only in recent years, the knowledge of this type of emissions in gasoline engines is much lower than in diesel. In this sense, the knowledge acquired about particles during the development of CI engines over the years is not fully applicable to GDI engines, since the latter normally produce less and smaller engine-out particles [106–108].

Direct injection engines typically generate two effects that are linked to PM emissions. First, the heterogeneity of the mixture, increasing the area in which the local ratio of fuel and air is greater than the stoichiometric. In Figure 2.20 it can be seen how, effectively, the formation of soot occurs in mixtures or regions with fuel-air equivalence ratio beyond 2. In this situation, the lack of oxygen makes the formation of CO_2 impossible, even CO, causing carbon atoms to agglomerate in carbonaceous particles with HC and other traces of absorbed components, with sizes from 10 to 80 nm [32]. The second effect is the appearance of fuel deposits on the walls or the piston, which are also considered heterogeneities. Cold start conditions are also a problem for PM emissions, since rich operation is needed and temperatures are relatively low, affecting combustion.

With the arrival and spread of direct injection systems in SI engines, the use of wall spray guided chambers [109] has been reduced, since PM emissions are difficult to reduce with this configuration to Euro VI levels. Wall wetting [110] becomes a major problem with this configuration, and the only possible solution is to change the specifications of the injector.

Kayes et al. [111] coducted a study about the effects that different engine parameters have on the emission of PM, confirming the strong dependence of particle emissions with the ratio of fuel to air, as reported in Figure 2.20. Mininum particle mass and number were obtained with fuel-air ratios within 10% of stoichiometric operation, increasing more than 3 times when moving a 30% or more away from stoichiometric. Changes on oil or coolant temperatures, exhaust recirculation or spark timing also influences due to intake and in-cylinder temperature variations, as well as the operating point.

Figure 2.21 shows a comparison in PM emissions between: two vehicles with a spark ignition engine and traditional port fuel injection (PISI), two compression ignition engine, one of them with a diesel particle filter and a

spark ignition engine with direct-injection (DISI). All vehicles underwent the same driving cycle at different ambient temperatures. Results demonstrate a clear increase in the emission of particles from the DISI engine vehicle compared to those with PFI. Moreover, the lowest possible emission is found with the use of DPF, whereas the highest is found with a CI engine without DPF. A clear trend to increase emissions with the reduction of ambient temperature is also observed.

The effects of these emissions on the environment are mainly alterations in the climate and visibility. On the health side, effects do not depend on a specific component, but on the combination of them, together with the particle size and concentration [112]. Kim et al. [113] stated the danger of small inhalable particles, with longer residence times and increased acidity, which are able to penetrate into lower airways. The exposure to this pollutant can cause respiratory [113] and cardiovascular [114] problems, cancer [115] and increaed death rates [112]. From a toxicological and epidemiological approach, PM emissions are most likely to be responsible for carcinogenic problems, rather than a selection of individual carcinogenic pollutants [116].

The use of EGR also influences the formation of particles, and adds the problem of having particles circulating through the intake line, which can cause damage to the compressor, for example. Alger et al. [117] studied the effect of exhaust recirculation on particle emissions at high load. A substantial reduction on PM number and mass was observed, since with EGR it was possible to supress enrichment. Zhang et al. [118] observed similar trends, with a reduction on the peak particle number and a shift in its distribution towards smaller particles with EGR. The accumulation mode was increased whereas the nucleation mode was reduced [119].

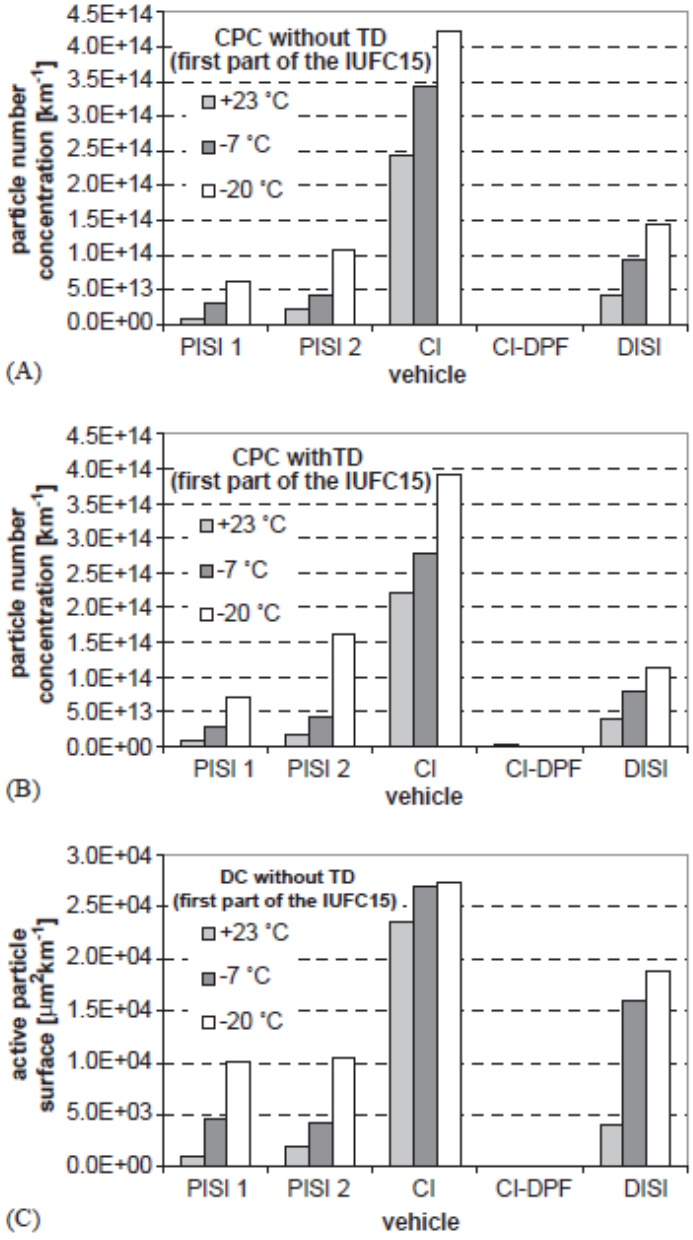

Figure 2.21. *Particle emission comparison for different vehicle types for the IUFC15 driving cycle at different ambient temperatures. Source: [107].*

2.3 Technologies to improve efficiency in SI engines

The growing concern about the shortage of fossil fuels and the need to give concrete answers to address the problem of climate change [120], as well as the large number of vehicles that circulate in urban areas today, which can cause serious health problems due to their polluting emissions, has made that emission regulations are increasingly strict [121].

During the last decades, vehicle manufacturers in Europe have complied with consumption and emissions regulations through the majority sale of diesel vehicles, whose greater efficiency compared to gasoline engines translates into lower fuel consumption. However, the new emission regulations, with more realistic driving cycles [77], will require even more expensive and complex aftertreatment systems for diesel engines [122]. Furthermore, the famous dieselgate scandal has markedly damaged the image and reputation of diesel engines. In this context, the efficiency of SI engines is becoming one of the main targets of engine development, owing to a lower pollutant emissions except for carbon dioxide. For this reason, different strategies [123] arise with the aim of increasing efficiency [124] and reducing the gap that exists in this regard with respect to CI engines while keeping the emission level [125–127].

2.3.1 Direct injection

During the course of World War II, direct injection spark-ignited engines were very common for war planes. However, it was not until the late 90s that direct injection was applied to SI engines for automotive applications. Japanese companies were pioneers in this regard, bringing electronic direct injection systems to the market by the hand of Mitsubishi, Nissan and Toyota.

Injecting the fuel into the cylinder produces a charge cooling effect since the fuel evaporates by absorbing part of the heat in the cylinder, as has been reported in many studies [126, 128, 129]. This effect is much greater than in port fuel injection engines, since the heat absorption in these engines takes place at the intake manifold and ports.

The reduction of the in-cylinder temperature is translated into reduced knock probability, allowing a better combustion centering. For high load operation, a better combustion centering would also reduce exhaust temperature, thus reducing or supressing enrichment [130–132]. Moreover, reduced knock introduces the possibility to increase the compression ratio (CR) [133], directly increasing efficiency. Several brands, as Toyota and Mazda, have increased the compression ratio of their atmospheric gasoline engines mainly thanks to the effects of direct injection.

Besides, the control of the fuel-air ratio can be more flexible with DI systems, allowing stratified operation (explained in Section 2.3.2.2) and a potential reduction of pumping losses is observed at partial loads [134]. Direct injection can provide a better fuel efficiency than similar PFI engines, especially if downsizing and turbocharging are also used [135, 136]. Alkidas et al. [137] made a comparison between the efficiency of a DI engine and a PFI engine by decoupling different effects. Results are shown in Figure 2.25, with positive contributions to fuel economy for DI engines coming from reduced heat transfer losses (HT), better properties in the air and fuel mixture (PROP) and the possibility to increase the compression ratio (CR). However, combustion (COMB) and friction losses (FRICT) worsened with the direct injection system. The sum of all contributors resulted in a 15% improvement of the brake efficiency in favor of direct injection.

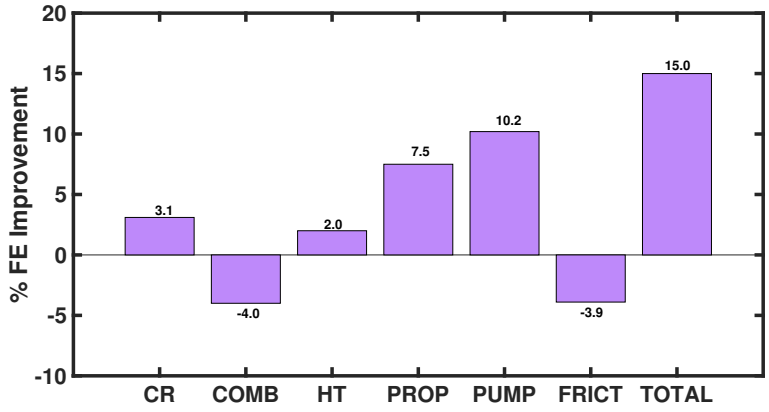

Figure 2.22. *Fuel economy improvements from different sources comparing DI and PFI engines. Source: Adapted from [137].*

The higher efficiency achieved with DI engines clearly reduces the emission of carbon dioxides [138–140], one of the major contributors to the greenhouse effect. However, DI reduces the available mixing time with respect to PFIs, and depending on the injection time it can be really short. This shortened time causes a greater heterogeneity in the mixture, leading to a possible reduction in the combustion efficiency. The heterogeneities on the mixture would increase, as explained in Section 2.2.3, the main pollutants affected by rich operation. Carbon monoxides are normally increased with DI compared to typical PFI engines, as reported by [141]. Many studies have shown increased particulate emissions with the use of direct injection in comparison with port fuel injection [118, 140, 142–149]. Even when fuel is injected during the first stages of the

intake stroke, there can be evaporation and mixture problems, and impinging of the fuel on the surfaces may occur, generating more solid particles than PFI engines [102, 103, 150–152].

The clear increase in certain emissions with direct injection, especially PM, has led to research on techniques to reduce them. The most outstanding techniques nowadays are the use of multiple injections as in diesel engines, increasing the temperature of the cooling system during cold starts or the addition of a GPF to the aftertreatment system. Since the particles formed by SI engines differ from those of CI engines, there have also been numerous studies on the impact of these emissions on health and the environment.

2.3.2 Alternative combustion concepts

2.3.2.1 Lean combustion

This strategy is based on moving away from stoichiometric operation and developing combustion with an excess of air, as in CI engines. Lean operation was used during the decade of the 70's and 80's in spark-ignited engines. However, the appearance and hardening of emission regulations reduced the impact of this strategy due to the need to use more complex after-treatment systems. This is explained by the reduced efficiency of TWC when the mixture is not stoichiometric, as can be seen in Figure 2.19. When there is an excess of oxygen in the exhaust, the efficiency of NO_x conversion is decreased remarkably. In this way, it would be necessary to use an oxidizer and a nitrogen oxides reduction system, losing the advantage in aftertreatment price and simplicity over compression engines. This problem practically caused the disappearance of this technique in gasoline engines until the arrival of direct injection systems and stratification [128, 153].

Dilution through lean operation is a proven strategy to increase efficiency due to several reasons. Compared to stoichiometric operation, pumping work can be less important, particularly at low and partial loads. Besides, the reduction in the reactivity of the mixture causes a temperature drop that improves heat losses and reduces knocking probability, allowing a better centering of the combustion at high loads [154] and the possibility to operate with higher CR. A high compression air diluted engine was used to complete several driving cycles in [155], reducing fuel consumption between a 6 and 10% depending on the driving cycle. Nonetheless, excessive dilution could lead to problems with combustion stability and flammability limits, leading to misfiring and flame quenching [156]. For this reason, most of the research on this topic is focused on increasing the burning lean limit [157], for example with enhaced flow motion as in [158], where the effects of increased tumble to

expand the combustion range of lean combustion were studied, resulting in a 5.7% fuel consumption improvement.

On the emissions side, hydrocarbons and carbon monoxides can be reduced compared to stoichiometric operation due to the increased oxygen availability [131]. In terms of nitrogen oxides, the greater availability of oxygen is a factor that can increase the NO_x emission, while the reduction in temperature obtained with dilution tends to reduce them. However, despite being able to achieve a reduction in engine-out emissions, aftertreatment systems are still needed to comply with regulations, needing an specific aftertreatment system.

This dilution strategy has also been compared with EGR dilution by different authors. As explained, both dilution strategies can reduce exhaust temperatures and autoignition problems with a different impact in emissions and efficiency. Xie et al. [90] proposed a dilution coefficient to compare both techniques, showing that changes on combustion speed are lower with air dilution than with EGR, so further dilution can be achieved. Air dilution produced lower HC and CO concentrations and higher NO_x emissions than EGR. Both strategies increased efficiency with a slight advantage for air dilution.

2.3.2.2 Stratification

Stratification of the charge in SI engines is a way of operating with a lean mixture but with a locally rich region nearby the spark plug that ensures the ignition and propagation of the flame [141, 159–161]. The concept is based on direct injection systems and a wall-guided combustion in the past, and a spray-guided in the latest applications since wall and piston wetting can increase emissions. Injection occurs in the last stages of compression to ensure the heterogeinity of the charge, and the spray is directed and concentrated in the surroundings of the spark plug [162]. The major purpose of stratification is to achieve a greater burning lean limit at low loads.

The first investigations on stratification are from the hand of Ricardo and Hesselman in the decade of the 20's. Later, in the 70's, Honda released their CVCC (Compound Vortex Controlled Combustion) engine, which had a good market share for several years. Toyota developed and launched the D-4 engine in 1996 [163], a stratified DISI engine, and the second generation in 1999 [164, 165]. Fuel economy improvements under the Japanese driving cycle were excellent [166].

Nowadays, many brands of the automotive sector have launched their own stratified charge spark-ignited engine. For example, BMW with the N55

engine, Mercedes with the M256, Renault with the F5R and Volkswagen with the fuel stratified injection (FSI) engines.

Research on this topic has shown the enormous importance of the injection and spark timing on emissions production, stability and performance. Oh et al. [153] tested a DISI engine under stratified lean combustion and used visualization techniques. Stable combustion was found limited by the injection timing due to misfiring, and the smoke emissions were increased as injection was retarded. The PLIF (Planar Laser-Induced Fluorescence) spray visualization demonstrated the stratification of the mixture with a locally rich region nearby the spark plug and both mixing and premixed combustion.

2.3.2.3 Pre-chamnber ignition

Another combustion concept that has been widely studied in the past few years is the pre-chamber ignition system or also called turbulent jet ignition [167]. The core of this concept is the division of the cylinder in two areas, a pre-chamber and a main chamber, coupled by a set of orifices. The pre-chamber normally represents approximately 2% of the cylinder volume at TDC to achieve the best tradeoff between combustion performance and heat transfer losses [168]. During the compression stroke, the gases will transfer from the main chamber to the pre-chamber pushed by the action of the piston motion. The flow through the orifices creates a highly turbulent flow field in this pre-chamber at the moment of the spark activation, promoting the ignition and initial flame kernel propagation. As combustion develops, stagnation pressure and temperature increase rapidly inside the pre-chamber, inducing a high velocity discharge of the flames and/or active components through the connecting orifices [169]. Therefore, each of the jets produced by this discharge act as an ignition point for the fair-fuel mixture inside the main chamber. In this way, it is possible to develop high velocity and stable combustion even at lean or ultra-lean conditions (equivalence ratio up to 0.3).

Two main configurations have been proposed for this concept. The most simple one is the passive or homogeneous pre-chamber system. It operates by creating a homogeneous fuel-air mixture in the manifold or the intake stroke. Therefore, both pre-chamber and main chamber operate at the same equivalence ratio, and the limit for lean operation is related to the ignition inside the pre-chamber itself. Instead, in the active or stratified system, an additional fuel injector (normally gaseous) is placed inside the pre-chamber and allows to maintain stoichiometric conditions inside this volume regardless the condition of the rest of the cylinder. This allows to work at leaner conditions overall, but at the expense of higher cost and complexity of the combustion

system. In any of the two systems, the design of the orifices connecting both volumes is critical for the successful operation of the engine. In particular, parameters such as the number and size of the orifices [170] or their orientation [171, 172] have shown to have the highest impact in combustion performance.

2.3.3 Variable valve actuation

Valve events explained in Section 2.2.1.2, namely IVO, IVC, EVO and EVC, have a direct impact on many parameters that affect engine performance, behavior and exhaust emissions. Traditionally, these events were set constant in timing and duration for all engine operating conditions. Since the perfect timing and duration of these events can change depending on the engine operating conditions, variable valve actuation systems were developed to allow these parameters to be adjusted according to the engine speed and load. With variable valve actuation systems, it is possible to change real duration of both intake and exhaust strokes and so the scavenging process. Besides, it is possible to change the volumetric efficiency, thus being able to operate with less throttling and reduce pumping losses among other benefits [173–178].

To obtain the best possible efficiency, the settings of the variable valve actuation should change as follow. For low and part loads, the settings of the variable valve system are adjusted to minimize pumping losses while obtaining a good indicated efficiency from combustion, since this system can change the concentration of residuals. Strategies as Atkinson and Miller cycles, explained below, appear as good options to maximize engine performance. At higher loads and low engine speeds, the trend could be to increase the valve overlap, increasing volumetric efficiency and reducing IGR thanks to a favored scavenging process, with higher intake than exhaust pressures and an elongated process. Knock probability can also be reduced with a delayed intake valve thanks to a decreased dynamic compression of the charge. For high loads and high engine speeds, the overlap is reduced to avoid any short-circuiting. Since downsized engines are normally designed to provide a good response at low speeds with small turbines, at higher engine speeds there is a high exhaust pressure that can increase pumping. Note that the EVO can change drastically the exhaust temperature at high loads, affecting fuel enrichment for component protection, thus fuel economy. Besides, the valve timing strategy can be different during warm-up operation to optimize fuel consumption or to achieve a faster activation of the aftertreatment system.

Over the last years, many technologies have been developed for variable valve actuation. There are systems capable of changing the valve events timing, as well as the maximum valve lift and profile [179–181]. That is the case of the

Fiat Multiair system [182]. Other simpler systems include only some of these functions. The cam switching system uses several profiles for the valve lift, normally two, and changes between them with an actuator at a given engine speed, as it is in the Honda VTEC (Variable valve Timing and lift Electronic Control) [183, 184]. The oscillating cam system use a oscillating motion in a cam lobe to open an close the valves and by means of a kinematic chain it is able to change the lift of the valve continuously. However, since it is a kinematic chain, the lift depends on the duration of the event, so both cannot be varied independently. Some of the systems based on this technology are the valvematic from Toyota [185], the valvetronic system from BMW [186], the MIVEC (Mitshubishi Innovative Valve Timing and Electronic Control System) from Mitshubishi [187] and the VVEL (Variable Valve Event and Lift System) from Nissan [188]. The eccentric cam drive system works by changing the rotation speed of the cam lobe with an eccentric disc. In this sense, speeding up the lobe during the opening means a shorter duration. This system provides an independent control over lift profile and duration [189] but two eccentric mechanism need to be added to the engine, making it more complex and expensive. There are also systems that operate without a camshaft, so there is a huge flexibility to adjust the valve events on timing and duration [190, 191]. Last but not least, the cam phasing system [192] work with a variator that adjust continuously the position of the cam with respect to the piston position, changing the valve timing. This is the case of the VVT-i (Variable Valve Timing inteligence) from Toyota [166] and VANOS (Variable Nockenwellen Steuerung) from BMW [193], as well as the engine tested in this PhD-Thesis. More information on the different variable valve actuation systems can be found in [194].

2.3.3.1 Miller cycle

The Miller cycle [195, 196] consists of dividing the compression stroke into two parts thanks to the use of the LIVC (Late Intake Valve Closing). At the BDC, when the piston is about to start the compression stroke, the intake valve is open. The first degrees of the compression stroke is made with the intake valves open, expelling part of the air charge out of the cylinder through the intake valves and creating a virtual fifth stroke. The loss of power that this load expulsion supposes is compensated with an increase in the intake pressure, either by opening the throttle or by boosting. The lower dependence on throttle and higher intake pressure is normally translated into reduced pumping losses. The reduced effective compression inside the cylinder would increase the expansion to compression ratio, therefore a thermal efficiency increase may be obtained. The P-V diagram and the T-S diagram for the

Miller cycle are shown in Figure 2.23. Note the increased area enclosed by the cycle compared to Figure 1.2 thanks to the increased expansion to compression ratio. Many studies also call Miller cycle the operation with early intake valve closing (EIVC), since the intake stroke is divided into two parts, one with the intake valve open and the other with the intake valve closed. Note that many studies refer to the Miller cycle incorrectly, and it is usually confused with the Atkison cycle. Both cycles share the same spirit, but it is usually referred to Atkinson when the intake pressure is below atmospheric conditions.

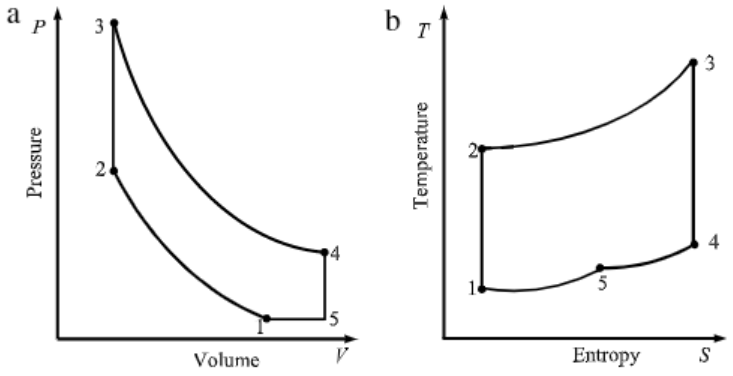

Figure 2.23. *Miller cycle representation: a) P-V diagram; b) T-S diagram. Source: [197].*

Miller cycle has been investigated in many studies with variable valve actuation strategies in downsized gasoline engines in order to increase thermal efficiency. In practice, the Miller cycle shows enormous consumption reduction potential both by 1D simulation [198] and experimentally. A higher BMEP than the Otto cycle can be obtained with Miller cycle, even with a lower compression ratio as stated by [199]. Between 7 and 11% fuel consumption reduction has been reported at high loads by using LIVC and EIVC [200]. At high loads, a benefit from LIVC over EIVC strategy is reported due to reduced knock probability and better pumping losses, whereas at low loads the trend is reversed, and EIVC provides decreased pumping losses than LIVC. However, combustion is slowed down with EIVC with lower temperatures at the end of compression [201].

Cylinder deactivation also arises as a possibility of reducing the total volume displaced by the engine as well as downsizing, reducing throttling thus pumping losses to increase efficiency [202, 203].

2.3.3.2 Atkinson cycle

James Atkinson patented his idea of a cycle back in 1882. The genuine design of the Atkinson cycle united the phases of a four-stroke engine in a single turn of the crankshaft, as in a two-stroke engine. A complex mechanism, as shown in Figure 2.24, allows the piston stroke to be changed alternately, so the intake and compression strokes are shorter than the expansion and exhaust strokes. In this sense, the expansion ratio is greater than the compression ratio, so a great thermal efficiency is achieved at the cost of a power loss. However, this mechanism originally used in the Atkinson engine is not used in real engines, and the application of the Atkinson cycle is made through valve timing strategies, so that an increased expansion to compression ratio can be obtained.

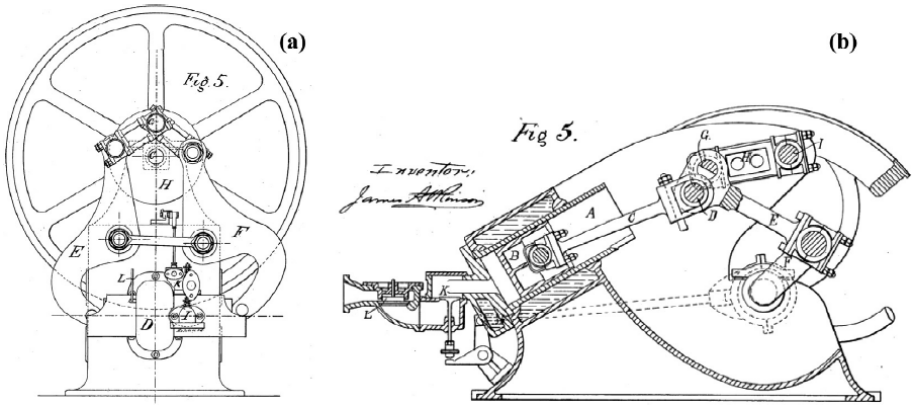

Figure 2.24. *Patent drawing of the genuine Atkinson engine. Source: [204].*

Many studies have explored the application of the Atkinson cycle to gasoline engines with LIVC strategies, observing great improvements in thermal efficiencies [205, 206]. With LIVC, the effective compression of the charge is reduced, and if the expasion stroke remains unchanged, efficiency may be improved. The basis of the Atkinson and the Miller cycles are very similar, but in the Atkinson cycle the intake pressure is below atmospheric, thus at low and part load operation. Numerous studies in the literature refer to the Miller cycle when it is actually Atkinson's.

2.3.4 Variable compression ratio

For the ideal Otto cycle, the efficiency, η, increases with the specific heats ratio, γ, and with the compression ratio, r, as shown in Equation 2.13:

$$\eta = 1 - \frac{1}{r^{(\gamma-1)}} \tag{2.13}$$

For this reason, SI engines are normally designed with the highest possible compression ratio, which is normally limited by knock and exhaust temperature at high loads. However, as depicted in Figure 2.25, the compression ratio could be increased for partial loads to further increase efficiency. In this sense, the variable compression ratio (VCR) systems are used to change this parameter depending on the engine speed and load.

The first engine built and tested with a variable compression ratio dates from 1920 and came from Ricardo. Reputable automotive brands such as Peugeout, Porsche or Nissan have developed their own research on these systems, but VCR systems have not spread significantly to road cars to date. There are three main ways to vary the CR of the engine [207]. First, there is the possibility to change the height of the piston by changing the rod length, as Porsche proposed. A second possibility is to vary the combustion chamber volume, as Saab presented in the year 2000 with an inclinable cylinder head and cylinder [208]. The third possibility is to change the crankshaft geometry. New designs are also being studied as in [209].

Many studies have been conducted to analyze the potential of this system. A variable compression ratio system was tested at several engine loads in [210], showing that VCR benefits can be higher than those from cylinder deactivation or GDI operation. Similar results were found by [211] under different driving cycles. A comparison of different VCR systems was presented in [212] via simulation, showing the potential of VCR technologies.

Variable compression ratio systems have the prospect to increase engine efficiency, and could synergize with other systems like variable valve timing, direct injection, downsizing and EGR to take a major technological leap once the technology is stablished.

2.3.5 Downsizing and boosting

Downsizing is an extended technique that aims for fuel consumption reduction, thus carbon dioxide emission reduction, in gasoline engines [213–215]. The technique consists of reducing the displaced volume by the engine, either with less unit displacement or with fewer cylinders, so less throttling is needed and the engine operates at higher loads, reducing pumping losses. To compensate for the loss in torque and power that comes from a smaller displacement, manufacturers are adding a boosting system to increase BMEP, normally with a turbocharger. This strategy was born at the beginning of the

21st century with the 1.4 TFSI engine from Volkswagen that replaced 1.6 and 2.0 litre atmospheric engines.

Downsizing is not understood without the use of boosting, explained in 2.2.1.4, to increase BEMP and power to naturally-aspirated levels. Boosting pressure and BEMP have evolved to higher values throughout history in combustion engines, from around 12 bar of BMEP in the 60s to 20 in the 80s and to around 23 nowadays. This increase has been accompanied by other evolutions that have resulted in better resistance to higher thermal and mechanical levels, so engines can now withstand higher peak pressures and temperatures.

Due to the regulation of the load in gasoline engines, increasing the load and power means increasing the air mass flow, $\dot{m}_{air}$, which depends on the volumetric efficiency, η_v, displaced volume, V_{disp}, the density of the air, ρ_{air}, the engine speed, n and the number of cycles per revolution, i.

For a downsized engine, V_t is reduced, so the most pretty straight forward way to increase the air mass is through density. Following the ideal gases law, the air density, ρ_{air} is defined by the air pressure, P_{air}, the air temperature T_{air} and the constant of ideal gases R_u.

To increase the density, a compressor is placed in the intake line to rise pressure. However, this process heats up the air charge, which represents a potential loss of density. For this reason, in many applications an intercooler is placed downstream the compressor to drop the temperature at an almost constant pressure, thus increasing further the density. Break mean effective pressure and power, P_e, which are related by the engine speed, both depend on the air density. For GDI engines, a higher density can help the mixture formation and the stratified operation.

The improvement in brake efficiency achieved with downsizing depends strongly on the amount of volume reduction that takes place, so conducted studies have reported several degrees of improvement [216, 217]. Boretti et al. [177] compared a low-tech 4L naturally-aspirated gasoline engine with a downsized high-tech turbocharged gasoline engine, observing a 43% fuel savings in a NEDC cycle. Similar trends were found by Lumsden et al. [218] with a 25% fuel consumption reduction when halving the engine displacement from 2.4 L to 1.2 L.

A problem with downsizing and boosting is that operation with higher loads can lead to increased wear of different elements, affect driveability, cycle to cycle variations and increase fuel enrichment for exhaust temperature control. Besides, higher load operation can lead to increased knock tendency [219], so

a worse combustion phasing and less CR than naturally-aspirated engines are used. Moreover, when downsizing is carried out without changing the number of cylinders but only reducing the unitary displaced volume, a packaging problem may occur due to the injectior, valves and bore sizes.

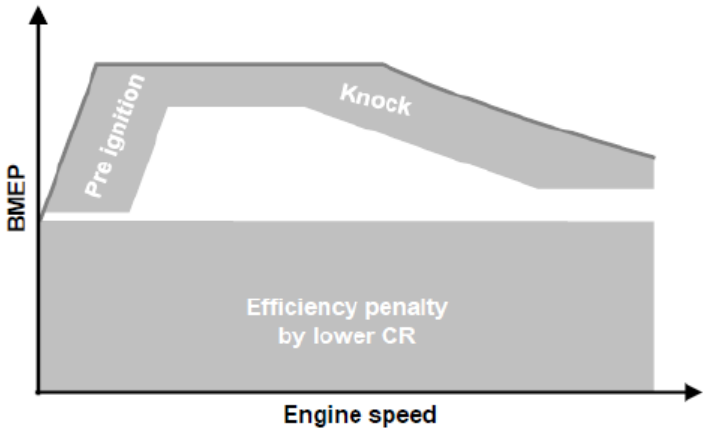

Figure 2.25. *Main problems of downsizing in an engine map. Source: [4].*

A huge effort is being made to address driveability problems as explained in Section 2.2.1.4, with different boosting strategies as the combination of different turbochargers in parallel or in series, combination of turbocharging and supercharging, variable geometries and electric groups [220–223]. The problem with knock, worse combustion phasing and higher temperatures in the exhaust that increase fuel enrichment need to be addressed with other strategies as direct injection, EGR or variable valve actuation systems, among others. In this sense, a new stream of design is emerging, known as rightsizing [196], that preserves the spirit of downsizing but without taking it to extreme levels that pose a problem.

2.3.6 Exhaust gas recirculation

The exhaust gas recirculation strategy, also known as EGR, lays its basis on reintroducing the exhaust gases in the intake line to mix them with fresh air running towards the cylinders. This is a well-known and widely used strategy in CI engines for NO_x emissions reduction. The excess of air and high temperatures due to the higher CR of this engines compared to SI engines, as well as the presence of inhomogeneities in the mixture, are the main causes of the higher NO_x formation of these engines. In this way, the addition of inert

gases to the mixture with the EGR strategy would reduce the temperature, thus the formation of this pollutant.

When EGR began to be used in SI engines, in the decade of the 90's, it was observed that the improvement potential of this strategy went beyond the reduction of nitrogen oxides. Exhaust recycle was investigated in naturally-aspirated engines at partial loads to increase efficiency. At high loads, the maximum power output was reduced since part of the fresh air was replaced with exhaust gases [224].

The addition of inert gases implies an oxigen concentration reduction and increases the heat capacity of the mixture and the ratio of specific heats [83], so these gases are a heat sink, so the combustion temperatures are reduced and so heat losses [225, 226], and achieving a higher ideal thermal efficiency [227–231]. Lower temperatures and oxygen concentration would reduce the formation of NO_x emissions as explained by the simplified Zeldovich mechanism in Equation 2.12. The lower temperatures achieved with a less reactive mixture also reduces the exhaust temperature, allowing a reduction or suppression of the enrichment needed at high loads [226, 232–234] for turbine components protection. Operation at lower combustion temperatures also implies a lower knock risk [73, 235–238], so a better combustion phasing [72, 157] can be achieved or the compression ratio can be further increased [233], both achieving higher efficiencies [227, 239]. However, the lower reactivity of the mixture would reduce the flame speed and induce combustion instabilities [240, 241], being able to reach a deterioration that would overcome the benefits aforexplained [242]. In this sense, several studies have investigated the possibility of reducing these instabilities by different means. Oh et al. [196] showed the synergy between high tumble and EGR with Miller cycle in order to improve stability, achiving an increase in efficiency of 10%. Yu et al. [243] achieved a reduction in the total combustion and induction times when increasing the ratio of ethanol in the mixture, reducing instabilities.

Some of the aforementioned benefits with exhaust gas recirculation can be seen in Figure 2.26. As oxygen concentration is reduced with EGR, a better combustion phasing can be achieved by optimizing the ignition timing and reducing the brake specific fuel consumption (BSFC). Moreover, knock events are delayed and a greater gross indicated work is obtained with lower pumping work.

Besides, together with all the improvements from efficiency perspective, a higher intake pressure is needed to move the exhaust gases and the same amount of air running towards the cylinders to keep the engine load, so at

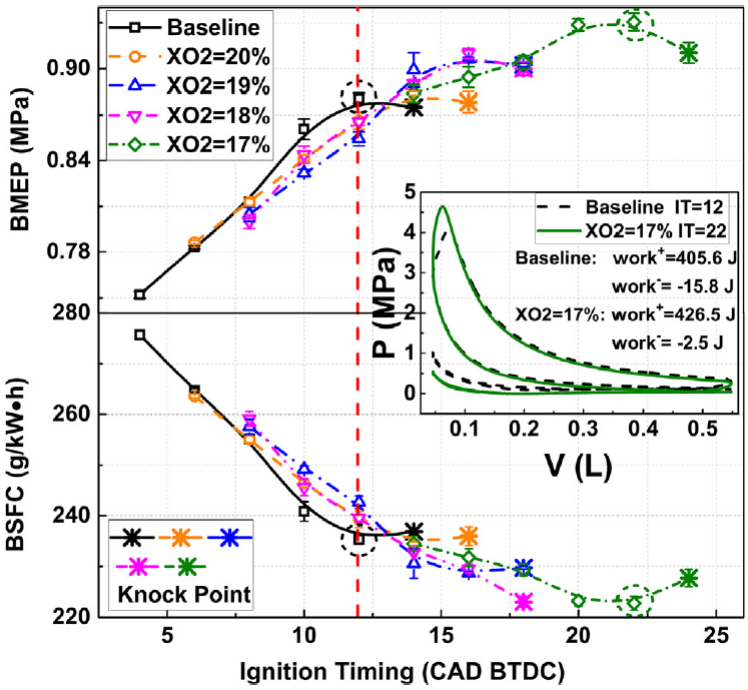

Figure 2.26. *BMEP and BSFC with respect to ignition timing and P-V diagram for different oxygen concentrations. Source: [244].*

partial load the throttled area of the engine map is reduced, thus pumping losses [5, 245–247].

A diagram of the benefits produced by EGR dilution is shown in Figure 2.27 and in section 2.4, further details of the different existing EGR strategies and their implications are given.

From emissions perspective, the trends with HC and NO_x are clear and demonstrated by many studies [248, 249]. The reduction in combustion temperatures and oxygen concentration result in a disminution of the nitrogen oxides [93–95] and an increase of the unburned hydrocarbons [250], following a slowed combustion [84, 85]. The conversion efficiency of the TWC is near 99% for hydrocarbons at stoichiometric operation, downplaying the increase of this pollutant with EGR. However, some studies have shown a potential drop in efficiency of the TWC at low loads for HC and CO with EGR due to lower exhaust temperatures [108].

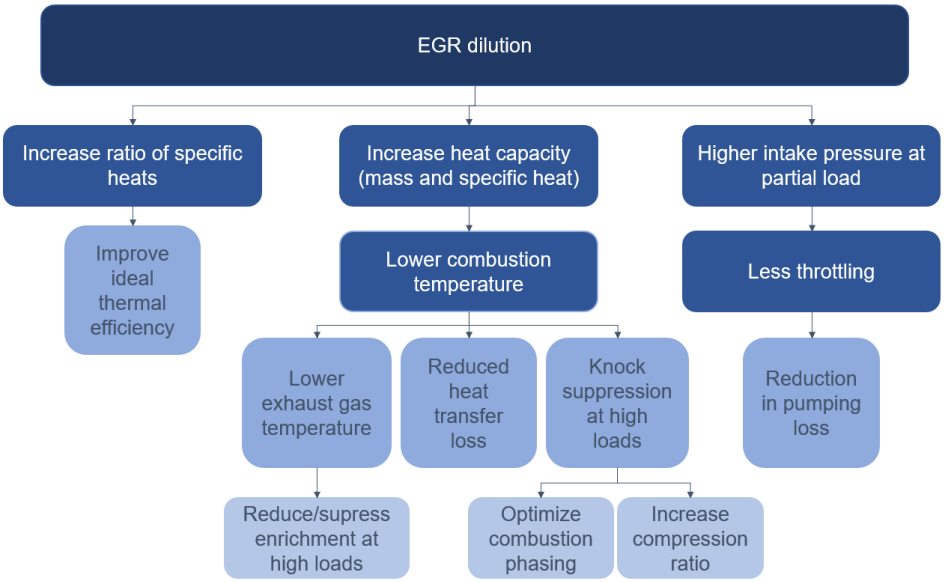

Figure 2.27. *Scheme of the effects of exhaust gas recirculation.*

In terms of CO, the formation of carbon monoxide is dependent on the kinetics of the carbon monoxide to carbon dioxide reaction [5]. Reduced oxygen concentration with EGR would shift the thermal equilibrium to a higher concentration of CO. However, lower combustion temperatures imply less CO_2 dissociating to CO and a reduction in the reaction speed. For particulate matter, a reduction in the peak particle number and finner particle production was found with EGR, increasing the accumulation mode and reducing the nucleation mode [118, 119]. Besides, longer combustions with EGR can result in late oxidation of accumulation mode particulates, reducing them [251].

At high loads, the suppression of enrichment with EGR has also an impact on emissions, reducing notably HC, CO and particulate matter [83, 119, 252]. Besides, without enrichment, the maximum conversion efficiency of the TWC can be achieved with stoichiometric operation, reducing all emissions downstream the aftertreatment [84, 253, 254].

In summary, the potential of the EGR strategy on reducing NO_x, CO and PM emissions while increasing HC emissions is demonstrated. [84, 117, 255, 256]. However, excessive EGR rates can critically affect the combustion initiation and development, affecting combustion stability, producing large

variations between cycles and changing the positive effects that EGR has on efficiency and emissions [45]. In most EGR-related studies, the maximum rate achieved is below 30% [84, 257], needing increased in-cylinder air motion or improved ignition systems to rise the EGR percentage beyond 35% within acceptable operating conditions [117].

2.4 The EGR strategies

As detailed in subsection 2.3.6, the addition of exhaust gases to the fresh mixture has several benefits both from efficiency and emissions perspective, as demonstrated by several studies. Besides, there is great flexibility when implementing this system in the engine, since there are many different configurations. EGR systems can be classified as follows:

- **High-pressure, low-pressure or mixed:** depending on the section of the exhaust line in which the gases are extracted, if upstream or downstream the turbine, and where they are reintroduced, upstream or downstream the compressor.
- **Cooled or hot:** if the exhaust gases undergo a cooling process before mixing with fresh air or not.
- **Clean or dirty:** if the exhaust gas is extracted upstream or downstream the aftertreatment system, fact that can change the composition of the gas.

The most commonly used configurations are cooled low-pressure with clean gases and cooled high-pressure with dirty gases. This is explained by the fact that in gasoline engines, the turbine is always located upstream the aftertreatment, so that in the high-pressure loop the gases are extracted before reaching the TWC. Besides, cooled EGR has become more widespread than hot EGR given the highest efficiency benefit with increased volumetric efficiency [258], also reducing to a greater extent NO_x but increasing HC and cyclic variations compared to hot EGR [91]. The high and low pressure circuits have also been compared by combining both, showing differences in turbocharger operation given the different levels of enthalpy available and the lower pressure ratio that the HP-circuit needed, affecting recirculability and efficiency [239]. In addition, the best strategy can be chosen based on the engine operating conditions as shown in Figure 2.28.

The composition of the gas used is also a variable that has been investigated. For example, Gong et al. [260] performed a study comparing

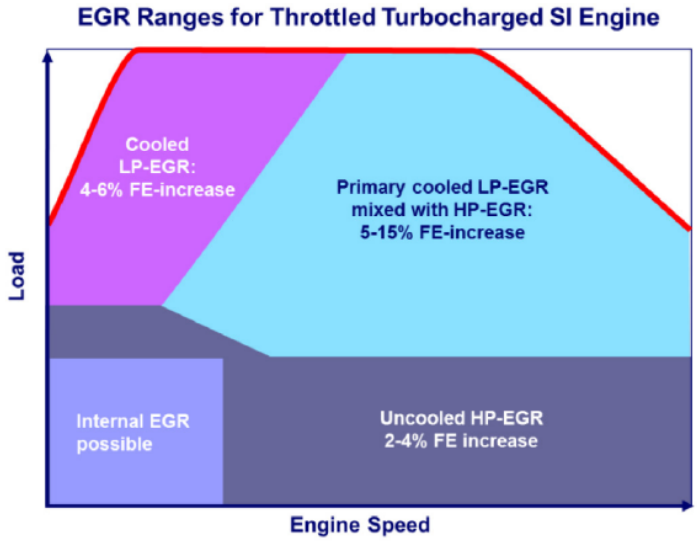

Figure 2.28. *EGR strategy depending on the engine operating conditions. Source: [259].*

different EGR compositions, showing reduced variations of IMEP, soot, carbon monoxides and hydrocarbon emissions when using only CO_2 EGR, while NO_x emissions worsened compared to traditional EGR.

In addition, there are many studies in the literature that refer to a type of EGR called dedicated. Dedicated EGR (D-EGR) is a concept in which the exhaust gas coming from one or more cylinders of a multi-cylinder engine is used to recirculate the exhaust gases [261], as depicted in Figure 2.29. In this sense, the EGR rate only comes from the dedicated cylinders, which are operated at rich conditions, around 1.3 to 1.4 equivalence ratio [262], performing a reformation of the fuel to hydrogen (H_2) and CO [263]. These fuel traces are introduced in all cylinders with EGR, increasing combustion speed, reducing knock probability and extending EGR recirculability thanks to enhanced stability [264, 265]. Alger et al. [266] showed an improvement in emissions and fuel consumption with D-EGR, as well as Robertson et al. [261], who obtained a 10% fuel consumption reduction on US test cycles.

Another posibility to achieve dilution with inert gases is to use the internal residual strategy or IGR. Eventhough it is not exactly exhaust recirculation, its effects are very similar to those coming from EGR and it could be classified as a hot and dirty system. It is worth mentioning that all engines operate with

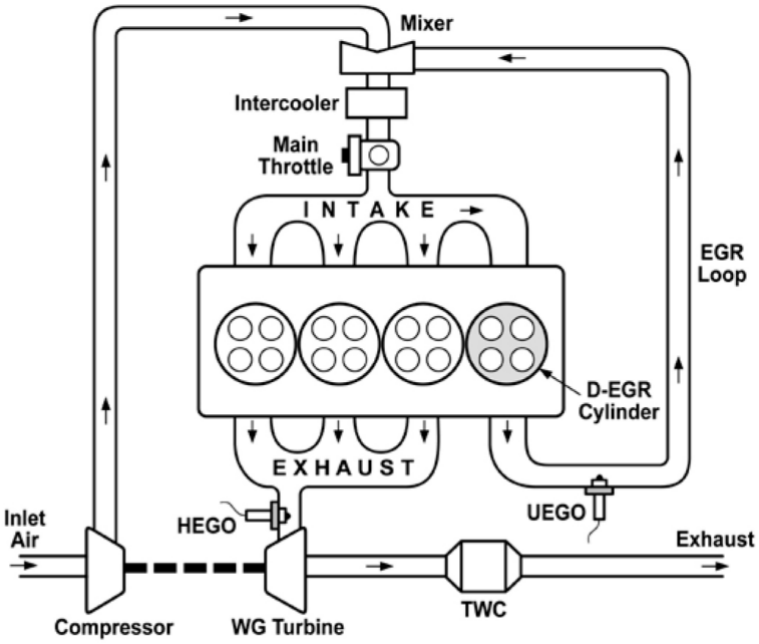

Figure 2.29. *Dedicated EGR scheme of a four cylinder engine. Source: [262].*

some internal gas residual since the scavenging process is never perfect, and when operating also with EGR, the sum of internal gas residual and EGR is called residual gas fraction or RGF.

In this PhD-Thesis, the internal gas residual strategy is investigated together with a cooled low-pressure loop and a cooled high-pressure loop. Moreover, another low-pressure circuit is studied, the main difference with the previous one being the extraction point of the EGR with respect to the TWC.

2.4.1 Internal gas residual

The internal gas residual (IGR) strategy is based on the un-swept residuals, also known as exhaust or internal residuals, from the previous cycle. Although there is not purely a recirculation of gases, this strategy is included in the framework of the EGR due to its similar effects [267]. The concentration of internal residuals is very dependent on the operating conditions, mainly intake and exhaust pressures. When the intake pressure is significantly lower than the exhaust pressure, the scavenging process becomes difficult and even

some back flows through the intake valve may take place. For this reason, internal residuals concentration can be very significant at low loads, and almost negligible at high loads.

The use of a VVT system opens the door to the possibility of modulating the amount of residuals by changing the overlap duration [173]. Typically, for low load operation where the exhaust pressure is considerably higher than the intake pressure, the residual concentration increases with the valve overlap. In the other hand, the residual concentration is reduced for higher loads with increasing valve overlaps. Another technique based on VVT systems to control the residual concentration is the NVO [268, 269]. With this strategy, there is no overlap, which makes the scavenging process as difficult as possible, increasing the IGR concentration in the combustion chamber. The NVO strategy is widely used in homogeneous charge compression ignition (HCCI) applications [270–272].

Several studies have focused their research on the effects of residuals. Szwaja et al. [273] showed the higher temperature of the internal residuals compared to EGR and the different composition that these have also imply distinct effects on combustion and emissions. On the emissions side, reduced NO_x and increased CO and HC were obtained with higher residuals, whereas both the induction and total combustion time were deteriorated with residuals, with the former being much more affected. Malaquias et al. [274] performed a study on different compression ratios and high IGR concentrations, showing a 2% increase in efficiency with reduced pumping. The higher concentration of residuals also decreased combustion speed. On the emissions side, a reduction of up to 40% was obtained for all species. Khoa et al. [275] tested several operating conditions of engine speed and load, proving the combustion temperature and NO_x reduction with IGR. Besides, they showed that the best possible control of residuals was obtained with EIVO and LEVC. Lanzanova et al. [268] used the NVO strategy to increase the IGR concentration, improving pumping and combustion centering at a low engine speed and load condition.

However, the concentration of residuals is a difficult parameter to measure experimentally, so a method to estimate it is required. In many studies, the difficulty in estimating this parameter leads to it being directly ignored as in [276]. The most common methods used to estimate the concentration of residuals are: 1D modeling [277], the equation of state method, the Yun and Mirsky method and the Fitzgerald method [244, 278–280]. In the case of this PhD-Thesis, a 1D model was used to calculate and predict the behaviour of the internal residuals in different engine points depending on the VVT settings, as shown by Galindo et al. [281].

2.4.2 High-pressure system

The high pressure loop, also known as short route, is a very popular configuration that has been used in diesel engines during the last couple of decades. In this configuration, the exhaust gas is extracted before going through the turbine, at high pressure and temperature, and it is introduced downstream the compressor as in the scheme in Figure 2.30.

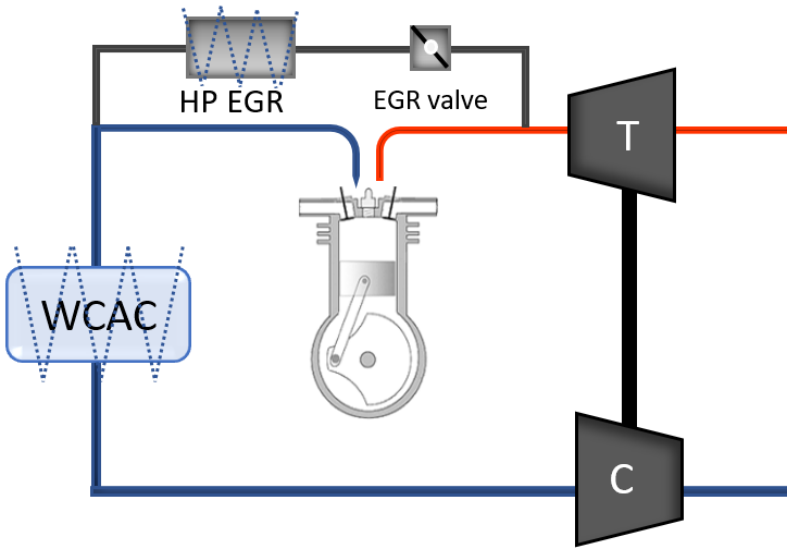

Figure 2.30. *High-pressure EGR loop scheme.*

The EGR flow going from the exhaust to the intake line naturally depends on the delta pressure between the extraction and the injection point. In this sense, recirculating exhaust gases can be difficult at some engine points where the intake pressure is at the level or beyond the exhaust pressure, for example, at high loads and particularly low engine speeds. Some configurations also include a valve to slightly increase the exhaust pressure or to reduce the intake pressure to ensure a sufficient and adequate EGR rate.

In this configuration, the flow through the turbine is reduced, penalizing the turbine power and the low end torque of the engine. This fact would be beneficial at high engine loads, since pumping losses can be reduced via decreased exhaust pressures as observed in [4]. Besides, the HP-EGR system is the most compact design, which makes it easier for brands to integrate it into the engine compartment and provides a faster response under transient conditions.

The high temperatures that can be found upstream the turbine cause the need to use a cooling system before introducing the gases into the intake line to avoid damages or melting of the materials in the intake side, which are normally plastics or aluminum. Cooling is also needed to reduce the knock phenomena in SI engines and to keep the volumetric efficiency. The cooling power required for this EGR system is very high since the temperature drop in some cases goes from 1200 K to below 500 K.

Yu et al. [282] demonstrated the capability of a high-pressure loop on reducing enrichment and knock probability at high and full load operating conditions, obtaining a lower power output as shown by Galloni et al. [283]. A comparison between cooled and hot high-pressure EGR was performed by Xie et al. [90], showing that better combustion centering and improved stability is obtained with cooled gases.

Zamboni et al. [284] compared the LP and the HP strategy, obtaining a greater fuel consumption reduction with HP, mainly related to the pressure gradient across the engine. However, the turbocharger operation was less afected by the LP circuit, which also achieved lower NO_x concentrations due to reduced intake temperatures. In a similar way, Lujan et al. [285] performed a study on the optimal strategy using both LP and HP-EGR, showing that the high-pressure circuit is more suitable for the start of the cycle (cold conditions) given the higher temperatures and fuel consumption benefit obtained with the HP circuit. The low-pressure circuit should be used later in the cycle for NO_x limits, despite the penalty on efficiency.

2.4.3 Low-pressure system

The low-pressure loop consists of extracting the exhaust gases at lower pressures, downstream the turbine and normally once the gases have gone through the TWC, and the injection is upstream the compressor as in Figure 2.31. This configuration has been used recently in diesel engines and may be the future configuration to use widely in gasoline engines.

Since the extraction point is downstream the turbine, the exhaust gases are at lower pressures than in a high-pressure loop, so the pressure difference between the extraction and the injection points of the line is commonly lower in comparison [91]. For this reason, a valve to reduce the intake line pressure or to increase the exhaust line pressure is usually needed. However, at high loads when the intake pressure is higher than the exhaust pressure, specially at low engine speeds, this system is more flexible than the high-pressure route. In transient conditions, the longer distance that the exhaust gas has to travel from the extraction point to the cylinders in the low-pressure loop compared

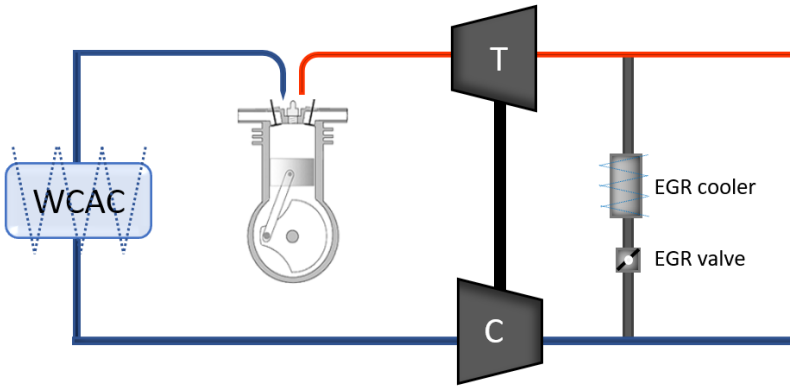

Figure 2.31. *Low-pressure EGR loop scheme.*

to the high-pressure loop would cause a slower engine response. In this sense, the low-pressure system is also know as long route.

Naturally, the exhaust gases in the low-pressure loop are at lower temperatures than in the high-pressure loop due to the expansion process that takes place in the turbine. For this reason, the cooling power needed for this EGR system is much lower. Besides, the exhaust gas and the air mix upstream the intercooler, so the temperature of the mixture is controlled and the exhaust gases are subjected to two cooling processes.

During WOT (Wide Open Throttle) operation, increased boosting is needed to keep the air mass flow and move the exhaust gases. This fact would increse the work delivered by the turbine, increasing the expansion ratio and affecting pumping losses. In the case of the high-pressure loop, less exhaust gases would go though the turbine so the exhaust pressure is reduced together with pumping losses.

Lujan et al. [84] performed a study with a LP-EGR circuit, achieving a fuel consumption reduction at low loads due to pumping and better combustion centering. An improvement in heat losses was also observed. Decreased NO_x and increased HC concentrations were obtained following the reduced combustion temperatures. At high loads, an evident change in the operating point of the turbocharger was observed. In a similar way, Reihaini et al. [286] demonstrated the higher level of boosting needed for LP-EGR, damaging pumping losses.

The catalyst performance with EGR was studied by Bermudez et al. [108], showing a decreased conversion efficiency for hydrocarbons and carbon

monoxides due to the lower oxygen concentration and reduced exhaust temperatures. The reduction in carbon monoxides that occurred at high load was the only fact that compromised nitrogen oxides.

Franken et al. [287] studied the combination of cooled LP-EGR and water injection, showing that both dilution techniques can mitigate knock, thus improving fuel consumption, with a disadvantage for EGR in terms of soot emissions. In the same way, Lattimore et al. [119] showed that at high load, the fuel enrichment suppression that is obtained with EGR promotes a reduction in particles, whereas the main driver at low loads is the ignition timing. For this reason, soot particles can be reduced with moderate EGR rates due to longer combustions, whereas at high EGR rates the dominant factor is the lower temperature, increasing particles [251].

Following the dedicated EGR strategy, Zhao et al. [288] used fuel enrichment with hydrogen and butanol blends in order to obtain more stable conditions with EGR, achieving efficiency and emissions improvements, as in the case of Gainey et al. [289].

2.4.4 Mixed-pressure system

The mixed-pressure loop is a trade-off between the high and the low-pressure loops, since the exhaust gas extraction is done as in the high-pressure system, upstream the turbine, and the injection point is upstream the compressor, as in the low-pressure system. Therefore, advantages and drawbacks from both systems are found. The scheme of a mixed-pressure system is shown in Figure 2.32.

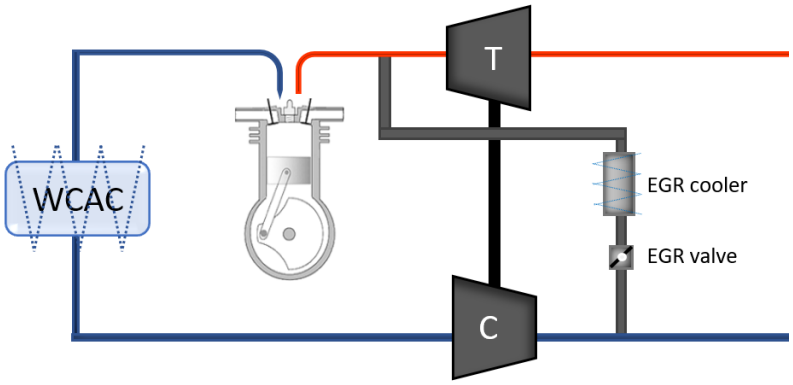

Figure 2.32. *Mixed-pressure EGR loop scheme.*

The lower energy in the turbine due to the extraction of gas limits the operating range of the engine at conditions of high load and low speed, as in the high-pressure loop. Therefore, the maximum power output is reduced [231]. However, the problem of recirculating gases with HP at high engine loads, specially at low engine speeds, disappears when the injection point is at atmospheric pressure, upstream the compressor.

In the mixed-pressure loop, the cooling power needed is between the high and the low-pressure loop. Since the gases are extracted at high temperatures as in the short route, and the injection temperature has to be in the order of the low pressure system, the cooling power is higher than in the low-pressure loop. However, the cooling power needed is lower than in the high-pressure loop since the exhaust gases undergo a second cooling process in the intercooler.

In terms of pumping losses, the same exhaust pressure reduction as in the high-pressure system is observed due to the reduction in the flow that goes through the turbine [4]. Since the exhaust gas is extracted upstream the TWC, the composition is the same as in the high-pressure system, having a higher concentration of pollutants than in the low-pressure loop. In this way, the mixed configuration does not normally apply to diesel engines to prevent that the mixture of hydrocarbons and soot end up clogging the ducts of the compressor in the same way they are responsible of the EGR coolers fouling. Besides, the length from the extraction point to the cylinders is similar to that of the low-pressure system, so this loop has the same transient problems.

The choice of the EGR architecture to use is very dependent on the application and the main objective. In this sense, the internal gas residual strategy, two low-pressure and a high-pressure loop have been investigated and compared in this PhD-Thesis.

Bibliography

[1] International Energy Agency. *Energy Technology Perspectives 2012: Pathways to a Clean Energy System.* 2012.

[2] Cames M. and Helmers E. "Critical evaluation of the European diesel car boom - Global comparison, environmental effects and various national strategies". *Environmental Sciences Europe*, Vol. 25 n^o 1, pp. 1–22, 2013.

[3] Pairy F. and Desantes J. M. *Motores de combustión interna alternativos.* Editorial Reverté and Editorial UPV, 2011.

[4] Glahn C., Kluin M., Konigstein A. and Cloos L. K. "Cooled External EGR - System Optimization of the Cooling and Charging System on a 3-Cylinder Gasoline DI T/C Engine". *In 24th Aachen Colloquium Automobile and Engine Technology*, pp. 189–204, 2015.

[5] Piqueras P., De la Morena J., Sanchis E. J. and Pitarch R. "Impact of Exhaust Gas Recirculation on Gaseous Emissions of Turbocharged Spark-Ignition Engines". *Applied Sciences*, pp. 1–17, 2020.

[6] Song X., Myers J. and Sarnia S. "Integrated Low Temperature Cooling System Development in Turbo Charged Vehicle Application". *SAE International Journal of Passenger Cars - Mechanical Systems*, Vol. 7 n^o 1, pp. 163–173, 2014.

[7] Luján J. M., Climent H., Pla B. and Rivas-Perea M. E. "Exhaust gas recirculation dispersion analysis using in-cylinder pressure measurements in automotive diesel engines". *Applied Thermal Engineering*, Vol. 89, pp. 459–468, 2015.

[8] Garcia J. J. "Exhaust gas condensate corrosion test on low pressure cooling system of aluminum brazed EGR, ACAC and WCAC". *SAE Technical Papers*, Vol. 8, 2012.

[9] Serrano J. R., Piqueras P., De la Morena J. and Ruiz M. J. "Influence of pre-turbine small-sized oxidation catalyst on engine performance and emissions under driving conditions". *Applied Sciences (Switzerland)*, Vol. 10 n^o 21, pp. 1–17, 2020.

[10] García-Afonso O. *Análisis teórico-experimental de la arquitectura pre-turbo de sistemas de post-tratamiento en MCIA.* 2013.

[11] Angiolini E. "Contribution to the understanding of filtration and pressure drop phenomena in wall-flow DPFs". *PhD-Thesis. Universitat Politècnica de València, Departamento de Máquinas y Motores Térmicos*, n^o June, 2017.

[12] Easter J., Fiano A., Bohac S., Premchand K. and Hoard J. "Evaluation of low mileage GPF filtration and regeneration as influenced by soot morphology, reactivity, and GPF loading". *SAE Technical Papers*, Vol. 2019-April n^o April, pp. 1–9, 2019.

[13] Masumitsu N., Otsuka S., Fujikura R., Imai Y. and Endo T. "Analysis of the pressure drop increase mechanism by ash accumulated of coated GPF". *SAE Technical Papers*, Vol. 2019-April n^o April, pp. 1–7, 2019.

[14] Saito C., Nakatani T., Miyairi Y., Yuuki K., Makino M., Kurachi H., Heuss W., Kuki T., Furuta Y., Kattouah P. and Vogt C. D. "New Particulate Filter Concept to Reduce Particle Number Emissions". *SAE Technical Papers*, 2011.

[15] Eakle S., Avery S., Weber P. and Henry C. "Comparison of Accelerated Ash Loading Methods for Gasoline Particulate Filters". *SAE Technical Papers*, Vol. 2018-September, pp. 1–14, 2018.

[16] McCaffery C., Zhu H., Li C., Durbin T. D., Johnson K. C., Jung H., Brezny R., Geller M. and Karavalakis G. "On-road gaseous and particulate emissions from GDI vehicles with and without gasoline particulate filters (GPFs) using portable emissions measurement systems (PEMS)". *Science of the Total Environment*, Vol. 710, pp. 136366, 2020.

[17] Chan T., Meloche E., Kubsh J., Rosenblatt D., Brezny R. and Rideout G. "Evaluation of a Gasoline Particulate Filter to Reduce Particle Emissions from a Gasoline Direct Injection Vehicles". *SAE Int. J. Fuels Lubr.*, Vol. 5 n^o 3, pp. 1277–1290, 2012.

[18] Ko J., Kim K., Chung W., Myung C. L. and Park S. "Characteristics of on-road particle number (PN) emissions from a GDI vehicle depending on a catalytic stripper (CS) and a metal-foam gasoline particulate filter (GPF)". *Fuel*, Vol. 238 n^o October 2018, pp. 363–374, 2019.

[19] Gong J., Stewart M. L., Zelenyuk A., Strzelec A., Viswanathan S., Rothamer D. A., Foster D. E. and Rutland C. J. "Importance of filter's microstructure in dynamic filtration modeling of gasoline particulate filters (GPFs): Inhomogeneous porosity and pore size distribution". *Chemical Engineering Journal*, Vol. 338 n^o November 2017, pp. 15–26, 2018.

[20] Ribbens W. B. *The Basics of Electronic Engine Control*. 2017.

[21] Weernink W. O. "Europeans, Japanese intensify hybrid, diesel debate". *Europe: Automotive News*, Vol. 8, 2003.

[22] Varnier O. "Trends and Limits of Two-Stage Boosting Systems for Automotive Diesel Engines". *PhD-Thesis. Universitat Politècnica de València, Departamento de Máquinas y Motores Térmicos*, 2012.

[23] Hagos F. "Combustion, Performance and Emissions Characteristics of Imitated Syngases in Direct-Injection Sparkigntion Engine.". *PhD-Thesis. Universiti Teknologi Petronas, Seri Iskandar, Malaysia*, 2013.

[24] Pulkrabek W. W. *Engineering Fundamentals of the Internal Combustion Engine*. Upper Saddle River, New Jersey 07548, 1997.

[25] Chala G. T., Abd Aziz A. R. and Hagos F. Y. "Natural Gas Engine Technologies: Challenges and Energy Sustainability Issue". *Energies*, Vol. 11 n^o 11, 2018.

[26] Preussner C., Döring C., Fehler S. and Kampmann S. "GDI: Interaction between mixture preparation, combustion system and injector performance". *SAE Technical Papers*, n^o 724, 1998.

[27] Solomon A. S., Anderson R. W., Najt P. M. and Zhao F. "Direct fuel injection for gasoline engines". *SAE progress in technology series PT - 80*, 2000.

[28] Van Der Wege B. A., Han Z., Iyer C. O., Muñoz R. H. and Yi J. "Development and analysis of a spray-guided DISI combustion system concept". *SAE Technical Papers*, n^o 724, 2003.

[29] Wirth M., Zimmermann D., Friedfeldt R., Caine J., Schamel A. and Storch A. "The next generation of gasoline direct injection: improved fuel economy and optimized system cost". *Advance engine design and performance*, pp. 52–139, 2003.

[30] Schwarz C., Schünemann E., Durst B., Fischer J. and Witt A. "Potentials of the Spray-Guided BMW DI Combustion System Reprinted From : SI Combustion and Direct Injection SI Engine Technology". *SAE International*, Vol. 328 n^o 724, pp. 145–149, 2006.

[31] R. Maly. *Spark Ignition: Its Physics and Effect on the Internal Combustion Engine in Fuel Economy in Road Vehicles Powered by Spark-Ignition Engines.* Hilliard, J. C. and Springer, G. S. Plenum Press, New York, 1984.

[32] Heywood J. B. *Internal combustion engine fundamentals.* McGraw-Hill, 1988.

[33] Sher E. and Keck J. C. "Spark ignition of combustible gas mixtures". *Combustion and Flame*, Vol. 66 n^o 1, pp. 17–25, 1986.

[34] R. Maly. *Initiation and Propagation of Flame Fronts in Lean CH4-Air Mixtures by the Three Modes of Ignition Spark in Fuel Economy in Road Vehicles Powered by Spark-Ignition Engines.* Hilliard, J. C. and Springer, G. S. Plenum Press, New York, 1984.

[35] Kalghatgi G. T. "Spark ignition, early flame development and cyclic variation in I.C. engines". *SAE Technical Papers*, n^o January, 1987.

[36] Ko Y., Arpaci V. S. and Anderson R. W. "Spark ignition of propane-air mixtures near the minimum ignition energy: Part II. A model development". *Combustion and Flame*, Vol. 83 n^o 1-2, pp. 88–105, 1991.

[37] Xiong Y., Roberts W. L., Drake M. C. and Fansler T. D. "Investigation of pre-mixed flame-kernel/vortex interactions via high-speed imaging". *Combustion and Flame*, Vol. 126 n^o 4, pp. 1827–1844, 2001.

[38] Eichenberger D. A. and Roberts W. L. "Effect of unsteady stretch on spark-ignited flame kernel survival". *Combustion and Flame*, Vol. 118 n^o 3, pp. 469–478, 1999.

[39] Sick V., Drake M. C. and Fansler T. D. "High-speed imaging for direct-injection gasoline engine research and development". *Experiments in Fluids*, Vol. 49 n^o 4, pp. 937–947, 2010.

[40] Shahbaz M. A., Shawal S. and Kaiser S. A. "Endoscopic visualization of the early premixed flame kernel in an SI engine by high-speed chemiluminescence imaging and". *Experiments in Fluids*, Vol. March, 2017.

[41] Abd Aziz A. R., Anbese Y. T., Hagos F. Y., Heikal M. R. and Firmansyah. "Characteristics of early flame development in a direct-injection spark-ignition CNG engine fitted with a variable swirl control valve". *Energies*, Vol. 10 n^o 7, 2017.

[42] Huang Z., Zhang Y., Wang Q., Wang J., Jiang D. and Miao H. "Study on flame propagation characteristics of natural gas-hydrogen-air mixtures". *Energy and Fuels*, Vol. 20 n^o 6, pp. 2385–2390, 2006.

[43] Samsudin D., Anuar M. D., Othman S., Manshoor B. and Khalid A. "Application of Schlieren Optical Visualization System in External Combustion and Internal Combustion Engine: A Review". *Applied Mechanics and Materials*, Vol. 773-774 n^o July, pp. 535–539, 2015.

[44] Fansler T. D., Reuss David L., Sick V. and Dahms R. N. "Combustion instability in spray-guided stratified-charge engines: A review". *International Journal of Engine Research*, Vol. 16 n^o 3, pp. 260–305, 2015.

[45] Galloni E. "Analyses about parameters that affect cyclic variation in a spark ignition engine". *Applied Thermal Engineering*, Vol. 29 n^o 5-6, pp. 1131–1137, 2009.

[46] Patterson D. J. "Cylinder pressure variations, a fundamental combustion problem". *SAE Technical Paper n. 290016*, 1966.

[47] Peters N. and Williams F. A. "Premixed combustion in a vortex". *Symposium (International) on Combustion*, Vol. 22 n^o 1, pp. 495–503, 1989.

[48] Peters N. "Laminar flamelet concepts in turbulent combustion". *Symposium (International) on Combustion*, Vol. 21 n^o 1, pp. 1231–1250, 1988.

[49] Abraham J., Williams F. A. and Bracco F. V. "A discussion of turbulent flame structure in premixed charges". *SAE Paper 850345*, 1985.

[50] Borghi R. "Turbulent combustion modelling". *Progress in Energy and Combustion Science*, Vol. 14 n^o 1, pp. 245–292, 1988.

[51] Valero J. "Analysis of the potential of SI lean combustion and CAI combustion in a two-stroke spark-assisted gasoline engine". *PhD-Thesis. Universitat Politècnica de València, Departamento de Máquinas y Motores Térmicos*, 2020.

[52] Williams F. A. "An approach to turbulent flame theory". *Journal of Fluid Mechanics*, Vol. 40 n^o 2, pp. 401–421, 1970.

[53] Hill P. G. and Zhang D. "The effects of swirl and tumble on combustion in spark-ignition engines". *Progress in Energy and Combustion Science*, Vol. 20 n^o 5, pp. 373–429, 1994.

[54] Beretta G. P., Rashidi M. and Keck J. C. "Turbulent flame propagation and combustion in spark ignition engines". *Combustion and Flame*, Vol. 52 n^o C, pp. 217–245, 1983.

[55] Konig, G. Maly R. R. Bradley D. Lau A. K. C. Sheppard C. G. W. "Role of exothermic centres on knock initiation and knock damage". *SAE Technical Paper n. 902136*, 1990.

[56] Fitton, J. Nates R. "Knock erosion in spark-ignition engines". *SAE Technical Paper n. 962102*, 1996.

[57] Nates, R. J. Yates A. D. B. "Knock damage mechanisms in spark-ignition engines". *SAE Technical Paper n. 942064*, 1994.

[58] Konig, G. Sheppard C. G. W. "End gas auto-ignition and knock in a spark ignition engine". *SAE Technical Paper n. 902135*, 1990.

[59] Bradley D. and Kalghatgi G. T. "Influence of autoignition delay time characteristics of different fuels on pressure waves and knock in reciprocating engines". *Combustion and Flame*, Vol. 156 n^o 12, pp. 2307–2318, 2009.

[60] Pla B., De la Morena J., Bares P. and Jiménez I. "Knock Analysis in the Crank Angle Domain for Low-Knocking Cycles Detection". *SAE Technical Papers*, Vol. 2020-April n^o April, pp. 1–11, 2020.

[61] Zhen X., Wang Y., Xu S., Zhu Y., Tao C., Xu T. and Song M. "The engine knock analysis - An overview". *Applied Energy*, Vol. 92, pp. 628–636, 2012.

[62] Hoepke B., Jannsen S., Kasseris E. and Cheng W. K. "EGR Effects on Boosted SI Engine Operation and Knock Integral Correlation". *SAE International Journal of Engines*, Vol. 5 n^o 2, pp. 547–559, 2012.

[63] Westbrook, C. K. Pitz W. J. Leppard W. R. "The autoi-gnition chemistry of paraffinic fuels and pro-knock and anti-knock additives: a detailed chemical kinetic study". *SAE Technical Paper n. 912314*, 1991.

[64] Hirst, S. L. Kirsch L. J. "The application of a hydrocarbon auto-ignition model in simulating knock and other engine combustion phenomena, in: Combustion modeling in reciprocating engines". *New York: Plenum*, 1980.

[65] Warnatz J., Maas U. and Dibble R. W. *Combustion: Physical and chemical fundamentals, modeling and simulation, experiments, pollutant formation*. 2006.

[66] Livengood J. C. and Wu P. C. "Correlation of Autoignition Phenomena in Internal Combustion Engines and Rapid Compression Machines". *5th Symp. (International) on Combustion*, pp. 347–356, 1955.

[67] Douaud A. M. and Eyzat P. "Four-octane-number method for predicting the anti-knock behavior of fuels and engines". *SAE Technical Paper n. 780080*, 1978.

[68] Khaled F., Badra J. and Farooq A. "Ignition delay time correlation of fuel blends based on Livengood-Wu description". *Fuel*, Vol. 209 n^o August, pp. 776–786, 2017.

[69] Radu, B. Martin G. Chiriac R. Apostolescu N. "On the knock characteristics of LPG in a spark ignition engine". *SAE Technical Paper n. 2005-01-3773*, 2005.

[70] Szybist J. P. and Splitter D. A. "Pressure and temperature effects on fuels with varying octane sensitivity at high load in SI engines". *Combustion and Flame*, Vol. 177, pp. 49–66, 2017.

[71] Middleton R. J., Manofsky L. K., Lavoie G. A., Wooldridge M. S., Assanis D. N. and Martz J. B. "The effect of spark timing and negative valve overlap on Spark Assisted Compression Ignition combustion heat release rate". *Proceedings of the Combustion Institute*, Vol. 35 n^o 3, pp. 3117–3124, 2015.

[72] Kakaee A. H., Shojaeefard M. H. and Zareei J. "Sensitivity and effect of ignition timing on the performance of a spark ignition engine: An experimental and modeling study". *Journal of Combustion*, Vol. 2011, 2011.

[73] Splitter D. A. and Szybist J. P. "Experimental investigation of spark-ignited combustion with high-octane biofuels and EGR. 2. Fuel and EGR effects on knock-limited load and speed". *Energy and Fuels*, Vol. 28 n^o 2, pp. 1432–1445, 2014.

[74] Zareei J. and Kakaee A. H. "Study and the effects of ignition timing on gasoline engine performance and emissions". *European Transport Research Review*, Vol. 5 n^o 2, pp. 109–116, 2013.

[75] Amann M., Alger T. and Mehta D. "The Effect of EGR on Low-Speed Pre-Ignition in Boosted SI Engines". *SAE International Journal of Engines*, Vol. 4 n^o 1, pp. 235–245, 2011.

[76] Leiva-Candia D. E., García I. L., Lopez I., Serrano-Herrador J. A. and Dorado M. P. "Descriptive and inferential statistics as an exhaust emission comparative tool between different engine operating conditions and fuels. Application to highly oxidized biodiesel blended with primary alcohols". *Fuel*, Vol. 324 n^o PA, pp. 124453, 2022.

[77] Fernández-Yáñez P., Soriano J. A., Soto F., Armas O., Pla B. and Bermúdez V. "Pollutant emissions from Euro 6 light duty vehicle tested under steady state and transient operation on a roller test bench with hydrogenated paraffinic and biodiesel fuels". *Fuel*, Vol. 323 n^o March, 2022.

[78] Guillemot P. *Les émissions de polluants des moteurs á allumage commandé*. Ecole du Petrole et des Moteurs, 2008.

[79] "Suicidal Carbon Monoxide Poisoning Using Motor Vehicle Exhaust in an Open Space". *Medical Principles and Practice*, Vol. 28 n^o 5, pp. 490–492, 2019.

[80] Hess D. R. "Inhaled carbon monoxide: From toxin to therapy". *Respiratory Care*, Vol. 62 n^o 10, pp. 1333–1342, 2017.

[81] Gu X., Huang Z., Cai J., Gong J., Wu X. and Lee C. F. "Emission characteristics of a spark-ignition engine fuelled with gasoline-n-butanol blends in combination with EGR". *Fuel*, Vol. 93 n^o x, pp. 611–617, 2012.

[82] Agarwal11 D., Singh S. K. and Agarwal A. K. "Effect of Exhaust Gas Recirculation (EGR) on performance, emissions, deposits and durability of a constant speed compression ignition engine". *Applied Energy*, Vol. 88 n^o 8, pp. 2900–2907, 2011.

[83] Marchitto L., Tornatore C., Valentino G. and Teodosio L. "Impact of Cooled EGR on Performance and Emissions of a Turbocharged Spark-Ignition Engine under Low-Full Load Conditions". *SAE Technical Paper*, 2019.

[84] Luján J. M., Climent H., Novella R. and Rivas-Perea M. E. "Influence of a low pressure EGR loop on a gasoline turbocharged direct injection engine". *Applied Thermal Engineering*, Vol. 89, pp. 432–443, 2015.

[85] Duchaussoy Y., Lefebvre A. and Bonetto R. "Dilution interest on turbocharged SI engine combustion". *SAE Technical Papers*, n^o 724, 2003.

[86] Michaels H. C. and Fulper B. K. "Nitrous oxide emission factors for mobile sources USEPA". *In AWMA emissions inventory conference, New Orleans, USA, 1998.*, 1998.

[87] Soltic P. and Hausberger S. "On-Road Emission Measurements and emission modeling results for a tractor-semi trailer in Trans-Alpine operation". *13th International Scienfftic Symposium Transport and Air Pollution Boulder, September 13-15*, 2004.

[88] Ouellette P., Douville B., Hill P. G. and Ursu B. "NOx reduction in a directly injected natural gas engine". *American Society of Mechanical Engineers, Internal Combustion Engine Division (Publication) ICE*, Vol. 31-33 n^o 3, pp. 59–71, 1998.

[89] Szczepanski D. "Factors influencing NOx emissions at Tarong and Stanwell power stations". *PhD-Thesis. The University of Queensland*, 1998.

[90] Xie F., Li X., Su Y., Hong W., Jiang B. and Han L. "Influence of air and EGR dilutions on improving performance of a high compression ratio spark-ignition engine fueled with methanol at light load". *Applied Thermal Engineering*, Vol. 94, pp. 559–567, 2016.

[91] Wei H., Zhu T., Shu G., Tan L. and Wang Y. "Gasoline engine exhaust gas recirculation - A review". *Applied Energy*, Vol. 99, pp. 534–544, 2012.

[92] Sarikoc F., Kettner M., Velji A., Spicher U., Krause A. and Elsaesser A. "Potential of reducing the NO_x emissions in a spray guided DI gasoline engine by stratified exhaust gas recirculation (EGR)". *SAE Technical Papers*, n^o 2006-01-1261, 2006.

[93] Al-Qurashi K., Lueking A. D. and Boehman A. L. "The deconvolution of the thermal, dilution, and chemical effects of exhaust gas recirculation (EGR) on the reactivity of engine and flame soot". *Combustion and Flame*, Vol. 158 n^o 9, pp. 1696–1704, 2011.

[94] Ghazikhani M., Feyz M. E. and Joharchi A. "Experimental investigation of the Exhaust Gas Recirculation effects on irreversibility and Brake Specific Fuel Consumption of indirect injection diesel engines". *Applied Thermal Engineering*, Vol. 30 n^o 13, pp. 1711–1718, 2010.

[95] Ladommatos N., Abdelhalim S. M., Zhao H. and Hu Z. "Effects of EGR on heat release in diesel combustion". *SAE Technical Papers*, Vol. 980184, 1998.

[96] Kalghatgi G. T. "The outlook for fuels for internal combustion engines". *International Journal of Engine Research*, Vol. 15 n^o 4, pp. 383–398, 2014.

[97] Ladommatos N., Abdelhalim S. and Zhao H. "Control of oxides of nitrogen from diesel engines using diluents while minimising the impact on particulate pollutants". *Applied Thermal Engineering*, Vol. 18 n^o 11, pp. 963–980, 1998.

[98] Odell P. R. "Why carbon fuels will dominate the 21st century's global energy economy". *Geopolitics of Energy*, Vol. 26 n^o 3-4, pp. 2–8, 2004.

[99] Fayad M. A., Tsolakis A., Fernández-Rodríguez D., Herreros J. M., Martos F. J. and Lapuerta M. "Manipulating modern diesel engine particulate emission characteristics through butanol fuel blending and fuel injection strategies for efficient diesel oxidation catalysts". *Applied Energy*, Vol. 190, pp. 490–500, 2017.

[100] Aakko P. and Nylund N. "Particle emissions at moderate and cold temperatures using different fuels". *SAE Technical Paper n. 2003-01-3285*, 2003.

[101] Peckham M. S., Finch A. and Campbell B. "Analysis of Transient HC, CO, NOx and CO_2 Emissions from a GDI Engine using Fast Response Gas Analyzers". *SAE International Journal of Engines*, Vol. 4 n^o 1, pp. 1513–1522, 2011.

[102] Braisher M., Stone R. and Price P. "Particle number emissions from a range of European vehicles". *SAE Technical Paper n. 2010-01-0786*, 2010.

[103] Peckham M. S., Finch A., Campbell B., Price P. and Davies M. T. "Study of particle number emissions from a turbocharged gasoline direct injection (GDI) engine including data from a fast-response particle size spectrometer". *SAE 2011 World Congress and Exhibition*, 2011.

[104] Mohr M., Forss A. and Lehmann U. "Particle emissions from diesel passenger cars equipped with a particle trap in comparison to other technologies". *Environmental Science and Technology*, Vol. 40 n^o 7, pp. 2375–2383, 2006.

[105] Catapano F., Di Iorio S., Sementa P. and Vaglieco B. M. "Characterization of ethanol-gasoline blends combustion processes and particle emissions in a GDI/PFI small engine". *SAE Technical Papers*, Vol. 1, 2014.

[106] Ntziachristos L., Amanatidis S., Samaras Z., Janka K. and Tikkanen J. "Application of the pegasor particle sensor for the measurement of mass and particle number emissions". *SAE Technical Papers*, Vol. 2, 2013.

[107] Mathis U., Mohr M. and Forss A. "Comprehensive particle characterization of modern gasoline and diesel passenger cars at low ambient temperatures". *Atmospheric Environment*, Vol. 39 n^o 1, pp. 107–117, 2005.

[108] Bermúdez V., Lujan J. M., Climent H. and Campos D. "Assessment of pollutants emission and aftertreatment efficiency in a GTDi engine including cooled LP-EGR system under different steady-state operating conditions". *Applied Energy*, Vol. 158, pp. 459–473, 2015.

[109] Kawamoto M., Honda T., Katashiba H., Sumida M., Fukutomi N. and Kawajiri K. "A Study of Center and Side Injection in Spray Guided DISI Concept". *SAE Technical Papers*, n^o 724, 2005.

[110] Warey A., Huang Y., Matthews R., Hall M. and Ng H. "Effects of piston wetting on size and mass of particulate matter emissions in a DISI engine". *SAE Technical Papers*, Vol. 2002 n^o 724, 2002.

[111] Kayes D. and Hochgreb S. "Mechanisms of particulate matter formation in spark-ignition engines. 1. Effect of engine operating conditions". *Environmental Science and Technology*, Vol. 33 n^o 22, pp. 3957–3967, 1999.

[112] Davidson C. I., Phalen R. F. and Solomon P. A. "Airborne particulate matter and human health: A review". *Aerosol Science and Technology*, Vol. 39 n^o 8, pp. 737–749, 2005.

[113] Kim K. H., Kabir E. and Kabir S. "A review on the human health impact of airborne particulate matter". *Environment International*, Vol. 74, pp. 136–143, 2015.

[114] Pope C. A. and Dockery D. W. "Health effects of fine particulate air pollution: Lines that connect". *Journal of the Air and Waste Management Association*, Vol. 56 n^o 6, pp. 709–742, 2006.

[115] Stober W. and Abel U. "Lung cancer due to diesel soot particles in ambient air". *International Archives of Occupational and Environmental Health*, Vol. 68, pp. S3–S61, 1996.

[116] Castro A., Götschi T., Achermann B., Baltensperger U., Buchmann B., Felber Dietrich D., Flückiger A., Geiser M., Gälli Purghart B., Gygax H., Kutlar Joss M., Lüthi L. M., Probst-Hensch N., Strähl P. and Künzli N. "Comparing the lung cancer burden of ambient particulate matter using scenarios of air quality standards versus acceptable risk levels". *International Journal of Public Health*, Vol. 65 n^o 2, pp. 139–148, 2020.

[117] Alger T., Gingrich J., Khalek I. A. and Mangold B. "The role of EGR in PM emissions from gasoline engines". *SAE Technical Papers*, Vol. 3 n^o 1, pp. 85–98, 2010.

[118] Zhang Z., Wang T., Jia M., Wei Q., Meng X. and Shu G. "Combustion and particle number emissions of a direct injection spark ignition engine operating on ethanol/gasoline and n-butanol/gasoline blends with exhaust gas recirculation". *Fuel*, Vol. 130, pp. 177–188, 2014.

[119] Lattimore T., Wang C., Xu H., Wyszynski M. L. and Shuai S. "Investigation of EGR Effect on Combustion and PM Emissions in a DISI Engine". *Applied Energy*, Vol. 161 n^o x, pp. 256–267, 2016.

[120] Kolodziej C. P., Pamminger M., Sevik J., Wallner T., Wagnon S. W. and Pitz W. J. "Effects of Fuel Laminar Flame Speed Compared to Engine Tumble Ratio, Ignition Energy, and Injection Strategy on Lean and EGR Dilute Spark Ignition Combustion". *SAE International Journal of Fuels and Lubricants*, Vol. 10 n^o 1, pp. 82–94, 2017.

[121] Shu G., Pan J. and Wei H. "Analysis of onset and severity of knock in SI engine based on in-cylinder pressure oscillations". *Applied Thermal Engineering*, Vol. 51 n^o 1-2, pp. 1297–1306, 2013.

[122] Fayad M. A., Fernàndez-Rodríguez D., Herreros J. M., Lapuerta M. and Tsolakis A. "Interactions between aftertreatment systems architecture and combustion of oxygenated fuels for improved low temperature catalysts activity". *Fuel*, Vol. 229 n^o October 2017, pp. 189–197, 2018.

[123] Joshi A. "Review of Vehicle Engine Efficiency and Emissions". *SAE Technical Papers*, Vol. 2, pp. 2479–2507, 2021.

[124] Luján J. M., Bermúdez V., Dolz V. and Monsalve-Serrano J. "An assessment of the real-world driving gaseous emissions from a Euro 6 light-duty diesel vehicle using a portable emissions measurement system (PEMS)". *Atmospheric Environment*, Vol. 174 n^o July 2017, pp. 112–121, 2018.

[125] Grover, Jr. Ronald O. and Cleary David. "Correlating Measured Combustion Performance with CFD Predicted In-Cylinder Flows for a Spark-Ignition Direct-Injection (SIDI) Engine with Enhanced Charge Motion". *SAE Technical Papers*, Vol. 2013-01-1090, 2013.

[126] Costa M., Catapano F., Sementa P., Sorge U. and Vaglieco B. M. "Mixture preparation and combustion in a GDI engine under stoichiometric or lean charge: an experimental and numerical study on an optically accessible engine". *Applied Energy*, Vol. 180, pp. 86–103, 2016.

[127] Alagumalai A. "Internal combustion engines: Progress and prospects". *Renewable and Sustainable Energy Reviews*, Vol. 38, pp. 561–571, 2014.

[128] Park C., Kim S., Kim H. and Moriyoshi Y. "Stratified lean combustion characteristics of a spray-guided combustion system in a gasoline direct injection engine". *Energy*, Vol. 41 n^o 1, pp. 401–407, 2012.

[129] Alkidas A. C. "Combustion advancements in gasoline engines". *Energy Conversion and Management*, Vol. 48 n^o 11, pp. 2751–2761, 2007.

[130] Teodosio L., De Bellis V. and Bozza F. "Fuel Economy Improvement and Knock Tendency Reduction of a Downsized Turbocharged Engine at Full Load Operations through a Low-Pressure EGR System". *SAE International Journal of Engines*, Vol. 8 n^o 4, pp. 2015–01–1244, 2015.

[131] Grandin B. and Angstrom H. "Replacing Fuel Enrichment in a Turbo Charged SI Engine: Lean Burn or Cooled EGR". *SAE Technical Paper*, 1999.

[132] Shojaeefard M. H., Tahani M., Etghani M. M. and Akbari M. "Cooled EGR for a Turbo Charged SI Engine to Reduce Knocking and Fuel Consumption". *Int. Journal of Automotive Engineering*, Vol. 3 n^o 4, 2013.

[133] Akihisa D. and Daisaku S. "Research on Improving Thermal Effiiency through Variable Super-High Expansion Ratio Cycle". *SAE Technical Paper n. 2003-32-0039*, 2010.

[134] Boccardi S., Catapano F., Costa M., Sementa P., Sorge U. and Vaglieco B. M. "Optimization of a GDI engine operation in the absence of knocking through numerical 1D and 3D modeling". *Advances in Engineering Software*, Vol. 95, pp. 38–58, 2016.

[135] De Bellis V. "Performance optimization of a spark-ignition turbocharged VVA engine under knock limited operation". *Applied Energy*, Vol. 164, pp. 162–174, 2016.

[136] Zaccardi J. M., Pagot A., Vangraefschepe F., Dognin C. and Mokhtari S. "Optimal design for a highly downsized gasoline engine". *SAE Technical Papers*, Vol. 4970, 2009.

[137] Alkidas A. C. and El Tahry S. H. "Contributors to the fuel economy advantage of DISI engines over PFI engines". *SAE Technical Papers*, n^o 724, 2003.

[138] U.S. EPA. "Final rulemaking to establish light-duty vehicle greenhouse gas emission standards and corporate average fuel economy standards". *Joint Technical Support Document*, 2010.

[139] Sakai S. and Rothamer D. "Impact of ethanol blending on particulate emissions from a spark-ignition direct-injection engine". *Fuel*, Vol. 236 n^o October 2018, pp. 1548–1558, 2019.

[140] Fuquan Z., Lai M. C. and Harrington D. L. "Automotive spark-ignited direct-injection gasoline engines". *Prog Energy Combust Sci 25*, pp. 437–562, 1999.

[141] Knop V. and Essayem E. "Comparison of PFI and DI operation in a downsized gasoline engine". *SAE Technical Paper n. 2013-01-1103*, 2013.

[142] Karajalainen P., Pirjola L., Heikkila J., Lahde T., Tzamkiozis T., Ntziachristos L., Keskinen J. and Ronkko T. "Exhaust particles of modern gasoline vehicles: a laboratory and an on-road study". *Atmospheric Environment*, Vol. 97, pp. 262–270, 2014.

[143] Liang B., Ge Y., Tan J., Han X., Gao L., Hao L., Ye W. and Dai P. "Comparison of PM emissions from a gasoline direct injected (GDI) vehicle and a port fuel injected (PFI) vehicle measured by electrical low pressure impactor (ELPI) with two fuels: gasoline and M15 methanol gasoline". *Journal of Aerosol Science*, Vol. 57, pp. 22–32, 2013.

[144] Barone T. L., Storey J. M. E., Youngquist A. D. and Szybist J. P. "An analysis of direct-injection spark-ignition (DISI) soot morphology". *Atmospheric Environment*, Vol. 49, pp. 268–274, 2012.

[145] Hall D. and Dickens C. "Measurement of the number and size distribution of particles emitted from a gasoline direct injection vehicle". *SAE Technical Papers*, 2009.

[146] Momenimovahed A., Handford D., Checkel M. D. and Olfert J. S. "Particle number emission factors and volatile fraction of particles emitted from on-road gasoline direct injection passenger vehicles". *Atmospheric Environment*, Vol. 102, pp. 105–111, 2015.

[147] Karavalakis G., Short D., Vu D., Russell R., Hajbabaei M., Asa-Awuku A. and Durbin T. D. "Evaluating the effects of aromatics content in gasoline on gaseous and particulate matter emissions from SI-PFI and SIDI vehicles". *Environmental Science Technology*, Vol. 49, pp. 7021–7031, 2015.

[148] Yamada H., Inomata S. and Tanimoto H. "Particle and VOC Emissions from Stoichiometric Gasoline Direct Injection Vehicles and Correlation Between Particle Number and Mass Emissions". *Emission Control Science and Technology*, Vol. 3 n^o 2, pp. 135–141, 2017.

[149] Fushimi16 A., Kondo Y., Kobayashi S., Fujitani Y., Saitoh K., Takami A. and Tanabe K. "Chemical composition and source of fine and nanoparticles from recent direct injection gasoline passenger cars: effects of fuel and ambient temperature". *Atmospheric Environment*, Vol. 124, pp. 77–84, 2016.

[150] Price P., Stone R., Oudenijeweme D. and Chen X. "Cold start particulate emissions from a second generation di gasoline engine". *SAE Technical Paper n. 2007-01-1931*, 2007.

[151] Whitaker P., Kapus P., Ogris M. and Hollerer P. "Measures to Reduce Particulate Emissions from Gasoline DI engines". *SAE Technical Paper n. 2011-01-1219*, 2011.

[152] Giechaskiel B., Dilara P. and Andersson J. "Particle Measurement Programme (PMP) light-duty inter-laboratory exercise: Repeatability and reproducibility of the particle number method". *Aerosol Science and Technology*, Vol. 42 n^o 7, pp. 528–543, 2008.

[153] Oh H. and Bae C. "Effects of the injection timing on spray and combustion characteristics in a spray-guided DISI engine under lean-stratified operation". *Fuel*, Vol. 107, pp. 225–235, 2013.

[154] Lumsden G., Eddleston D. and Sykes R. "Comparing lean burn and EGR". *SAE Technical Paper n. 970505*, 1997.

[155] Hiroyuki O., Yasuyuki M., Toshimitsu F. and Masashi M. "Investigation of High-Compression Lean Burn Engine". *SAE Technical Paper n. 871215*, 1987.

[156] Yu C., Kim T., Yi Y., Lee J., Noh S. and Choi K. "Development of kmc 2.4l Lean burn engine". *SAE Technical Paper n. 950685*, 1995.

[157] Ibrahim A. and Bari S. "A comparison between EGR and lean-burn strategies employed in a natural gas SI engine using a two-zone combustion model". *Energy Conversion and Management*, Vol. 50 n^o 12, pp. 3129–3139, 2009.

[158] Saito H., Shirasuna T. and Nomura T. "Extension of Lean Burn Range by Intake Valve Offset". *SAE Technical Paper n. 2013-32-9032*, 2013.

[159] Kume T., Iwamoto Y., Lida K., Murakami M., Akishino K. and Ando H. "Combustion Control Technologies for Direct Injection SI Engine". *SAE 960600*, 1996.

[160] Fraidl G. K., Piock W. F. and Wirth M. "Gasoline Direct Injection: Actual Trends and Future Strategies for Injection and Combustion Systems". *SAE 960465*, 1996.

[161] Wirth M., Piock W. F., Fraidl G. K., Schoeggl P. and Winklhofer E. "Gasoline di engines: The complete system approach by interaction of advanced development tools". *SAE Technical Papers*, n^o 724, 1998.

[162] Mori S. and Shimizu R. "Analysis of EGR cyclic variations in a direct injection gasoline engine by using raman scattering method". *SAE Technical Papers*, n^o 724, 2002.

[163] Harada J., Tomita T., Mizuno H., Mashiki Z. and Ito Y. "Development of Direct Injection Gasoline Engine". *SAE 970540*, 1997.

[164] Kanda M., Baika T., Kato S., Iwamuro M., Koike M. and Saito A. "Application of a new combustion concept to direct injection gasoline engine". *SAE Technical Papers*, Vol. 2000 n^o 724, 2000.

[165] Abe S., Sasaki K., Baika T., Nakashima T. and Fujishiro O. "Combustion analysis on piston cavity shape of a gasoline direct injection engine". *SAE Technical Papers*, n^o 724, 2001.

[166] Sadakane S., Sugiyama M., Kishi H., Abe S., Harada J. and Sonoda Y. "Development of a new V-6 high performance stoichiometric gasoline direct injection engine". *SAE Technical Papers*, Vol. 2005 n^o 724, 2005.

[167] Alvarez Carlos Eduardo Castilla, Couto Giselle Elias, Roso VinÃcius RÃ¼ckert, Thiriet Arthur Braga and Valle Ramon Molina. "A review of prechamber ignition systems as lean combustion technology for SI engines". *Applied Thermal Engineering*, Vol. 128, pp. 107–120, 2018.

[168] Hua Jianxiong, Zhou Lei, Gao Qiang, Feng Zhonghui and Wei Haiqiao. "Influence of pre-chamber structure and injection parameters on engine performance and combustion characteristics in a turbulent jet ignition (TJI) engine". *Fuel*, Vol. 283, 1 2021.

[169] Tanoue Kimitoshi, Kimura Takanori, Jimoto Taishu, Hashimoto Jun and Moriyoshi Yasuo. "Study of prechamber combustion characteristics in a rapid compression and expansion machine". *Applied Thermal Engineering*, Vol. 115, pp. 64–71, 2017.

[170] Gentz Gerald, Thelen Bryce, Gholamisheeri Masumeh, Litke Paul, Brown Adam, Hoke John and Toulson Elisa. "A study of the influence of orifice diameter on a turbulent jet ignition system through combustion visualization and performance characterization in a rapid compression machine". *Applied Thermal Engineering*, Vol. 81, pp. 399–411, 4 2015.

[171] Zhou Lei, Song Yuntong, Hua Jianxiong, Liu Fengnian, Liu Zongkuan and Wei Haiqiao. "Effects of different hole structures of pre-chamber with turbulent jet ignition on the flame propagation and lean combustion performance of a single-cylinder engine". *Fuel*, Vol. 308, 1 2022.

[172] Novella Ricardo, De la Morena JoaquÃn, Pagano Vincenzo and Pitarch Rafael. "Optical evaluation of orifice orientation and number effects on active pre-chamber spark ignition combustion". *Fuel*, Vol. 338, pp. 127265, 2023.

[173] Fontana G. and Galloni E. "Variable valve timing for fuel economy improvement in a small spark-ignition engine". *Applied Energy*, Vol. 86, pp. 96–105, 2009.

[174] Kreuter P., Heuser P., and Schebitz M. "Strategies to Improve SIEngine Performance by Means of Variable Intake Lift, Timing and Duration". *SAE Technical Paper*, 1992.

[175] Wang Y., Conway G. and Chadwell C. "Combined benefits of variable valve actuation and low-pressure egr on si engine efficiency part 2: High load". *SAE Technical Papers*, Vol. 2019-April n^o April, pp. 1–9, 2019.

[176] Sellnau M., Kunz T., Sinnamon J., and Burkhard J. "2-step Variable Valve Actuation: System Optimization and Integration on an SI Engine". *SAE Technical Paper*, 2006.

[177] Boretti A. "Use of Variable Valve Actuation to Control the Load in a Direct Injection, Turbocharged, Spark-Ignition Engine". *SAE Technical Paper 2010-01-2225*, 2010.

[178] Moriya Y., Watanabe A., Uda H. and Kawamura H. "A Newly Developed Intelligent Variable Valve Timing System - Continuously Controlled Cam Phasing as Applied to a New 3 Liter Inline 6 Engine". *SAE Technical Paper*, 1996.

[179] Allen J. and Law D. "Production electro-hydraulic variable valve-train for a new generation of I.C. Engines". *SAE Technical Paper n. 2002-01-1109*, 2002.

[180] Dresner T. and Barkan P. "A review of variable valve timing benefits and modes of operation". *SAE Technical Paper n. 891676*, 1989.

[181] Gould L. A., Richeson W. E. and Erickson F. L. "Performance evaluation of a camless engine using valve actuators with programmable timing". *SAE Technical Paper n. 910450*, 1991.

[182] Palma A., Del Core D. and Esposito C. "The HCCI concept and control, performed with multiair technology on gasoline engines". *SAE Technical Papers*, 2011.

[183] Hosaka T. and Hamazaki M. "Development of the Variable Valve Timing and Lift (VTEC) Engine for the Honda NSX". *SAE Technical Papers*, 1991.

[184] Kojima S. "Development of high-performance and low-emission gasoline engine". *SAE Technical Papers*, Vol. 2008 n^o 724, 2008.

[185] Kinoshita K., Ueda K., Ito F., Shinojima Y., Yanagizawa T., Sakaguchi T. and Yamazaki T. "Development of a Custom Integrated Circuit for Continuously Variable Valve Lift Mechanism System Control". *SAE Technical Paper*, 2008.

[186] Luttermann C., Schunemann E. and Klauer N. "Enhanced VALVETRONIC Technology for Meeting SULEV Emission Requirements". *SAE Technical Paper*, 2006.

[187] Hatano K., Lida K., Higashi H. and Murata S. "Development of a New Multi-Mode Variable Valve Timing Engine". *SAE Technical Papers*, 1993.

[188] Kiga S., Mae Y., Akasaka Y. and Tomogane K. "Development of Innovative Variable Valve Event and Lift (VVEL) System". *SAE Technical Paper*, 2007.

[189] Stone R. "Introduction to Internal Combustion Engines". *4th edition*, 2012.

[190] Lou Z., Wen S., Qian J., Xu H., Zhu G. and Sun M. "Camless Variable Valve Actuator with Two Discrete Lifts". *SAE Technical Paper*, 2015.

[191] Battistoni M., Foschini L., Postrioti, L. and Cristiani M. "Development of an Electro-Hydraulic Camless VVA System". *SAE Technical Paper*, 2007.

[192] Watanabe I., Kawai T., Yonezawa K. and Ogawa T. "The New Toyota 2.0-Liter Inline 4-Cylinder ESTEC D-4ST Engine - Turbocharged Direct Injection Gasoline Engine". *23rd Aachen Colloquium Automobile and Engine Technology*, 2014.

[193] Flierl R. and Klüting M. "The third generation of valvetrains - New fully variable valvetrains for throttle-free load control". *SAE Technical Papers*, Vol. 2000 n^o 724, 2000.

[194] Lou Zheng and Zhu Guoming. "Review of advancement in variable valve actuation of internal combustion engines". *Applied Sciences (Switzerland)*, Vol. 10 n^o 4, 2020.

[195] Miller R. H. "Supercharging and Internal Coolimg Cycle for High Output". *Trans. ASME*, Vol. 69, 1947.

[196] Oh H., Lee J., Woo S. and Park H. "Effect of synergistic engine technologies for 48 V mild hybrid electric vehicles". *Energy Conversion and Management*, Vol. 244 n^o May, pp. 114515, 2021.

[197] Ebrahimi R. "Thermodynamic modeling of performance of a Miller cycle with engine speed and variable specific heat ratio of working fluid". *Computers and Mathematics with Applications*, Vol. 62 n^o 5, pp. 2169–2176, 2011.

[198] Miklanek L., Vitek O., Gotfryd O. and Klir V. "Study of Unconventional Cycles (Atkinson and Miller) with Mixture Heating as a Means for the Fuel Economy Improvement of a Throttled SI Engine at Part Load". *SAE International Journal of Engines*, Vol. 5 n^o 4, pp. 1624–1636, 2012.

[199] Hatamura K., Hayakawa T., Goto T. and Hitomi M. "A study of the improvement effect of Miller-cycle on mean effective pressure limit for high-pressure supercharged gasoline engines". *JSAE Review*, Vol. 18, pp. 101–106, 1997.

[200] Li Y., Zhao H., Stansfield P. and Freeland P. "Synergy between Boost and Valve Timings in a Highly Boosted Direct Injection Gasoline Engine Operating with Miller Cycle". *SAE Technical Paper*, 2015.

[201] Li T., Gao Y., Wang J. and Chen Z. "The Miller cycle effects on improvement of fuel economy in a highly boosted, high compression ratio, direct-injection gasoline engine: EIVC vs. LIVC". *Energy Conversion and Management*, Vol. 79, pp. 59–65, 2014.

[202] Kouba A., Hnilicka B. and Navratil J. "Downsized Gasoline Engine Cylinder Deactivation MiL Development and Validation Using Real-Time 1-D Gas Code". *SAE Technical Papers*, Vol. 2018-April, pp. 1–7, 2018.

[203] Parker M. C., Jiang C., Butcher D., Spencer A., Garner C. P. and Witt D. "Impact and observations of cylinder deactivation and reactivation in a downsized gasoline turbocharged direct injection engine". *International Journal of Engine Research*, Vol. 22 n^o 4, pp. 1367–1376, 2021.

[204] Zhao J. "Research and application of over-expansion cycle (Atkinson and Miller) engines - A review". *Applied Energy*, Vol. 185 n^o January 2017, pp. 300–319, 2017.

[205] Wang C., Daniel R. and Ma X. "Comparison of Gasoline (UGL), 2,5-Dimethylfuran (DMF) and Bio-Ethanol in a DISI Miller Cycle with Late Inlet Valve Closing Time". *SAE Technical Paper*, 2012.

[206] França O. "Impact of the Miller Cycle in the efficiency of an FVVT (Fully Variable Valve Train) Engine During Part Load Operation". *SAE Technical Paper*, 2009.

[207] Pešić R. B., Milojević S. T. and Veinović S. P. "Benefits and challenges of variable compression ratio at diesel engines". *Thermal Science*, Vol. 14 n^o 4, pp. 1063–1073, 2010.

[208] Khan I. R. "Study of Variable Compression Ratio Engine (VCR) and Different Innovations to Achieve VCR". *International Journal for Research in Applied Science and Engineering Technology*, Vol. V n^o XI, pp. 1473–1478, 2017.

[209] Schwaderlapp M., Habermann K. and Yapici K. "Variable Compression Ratio - A Design Solution for Fuel Economy Concepts". *SAE Technical Papers*, 2002.

[210] Roberts M. "Benefits and challenges of variable compression ratio (VCR)". *SAE Technical Papers*, n^o 724, 2003.

[211] Kleeberg H., Tomazic D., Dohmen J., Wittek K. and Balazs A. "Increasing efficiency in gasoline powertrains with a two-stage variable compression ratio (VCR) system". *SAE Technical Papers*, Vol. 2, 2013.

[212] De Bortoli M., Lucio M., Marco A. and Gradella S. "Variable Compression Ratio Engines". *SAE Technical Papers*, 2009.

[213] García A., Monsalve-Serrano J., Martínez-Boggio S. and Wittek K. "Potential of hybrid powertrains in a variable compression ratio downsized turbocharged VVA Spark Ignition engine". *Energy*, Vol. 195, pp. 117039, 2020.

[214] Zhao X., Zhu Z., Zheng Z., Yue Z., Wang H. and Yao M. "Effects of flame propagation speed on knocking and knock-limited combustion in a downsized spark ignition engine". *Fuel*, Vol. 293 n^o January, pp. 120407, 2021.

[215] Wang Y., Wei H., Zhou L., Zhang X. and Zhong L. "Effects of reactivity inhomogeneities on knock combustion in a downsized spark-ignition engine". *Fuel*, Vol. 278 n^o May, pp. 118317, 2020.

[216] Coltman D., Turner J. W. G., Curtis R., Blake D., Holland B., Pearson R. J., Arden A. and Nuglisch H. "Project Sabre: A close-spaced direct injection 3-cylinder engine with synergistic technologies to achieve low CO_2 output". *SAE Technical Paper n. 2008-01-0138*, 2009.

[217] Turner J. W. G., Popplewell A., Patel R., Johnson T. R., Darnton N. J., Richardson S., Bredda S. W., Tudor R. J., Bithell C. I., Jackson R., Remmert S. M., Cracknell R. F., Fernandes J. X., Lewis A. G. J., Akehurst S., Brace C. J., Copeland C., Martinez-Botas R., Romagnoli A. and Burluka A. A. "Ultra Boost for Economy: Extending the Limits of Extreme Engine Downsizing". *SAE Technical Paper n. 2014-01-1185*, 2014.

[218] Lumsden G., Oudenijeweme D., Fraser N. and Blaxill H. "Development of a turbocharged direct injection downsizing demonstrator engine". *SAE Technical Papers*, Vol. 2 n^o 1, pp. 1420–1432, 2009.

[219] Chen L., Li T., Yin T. and Zheng B. "A predictive model for knock onset in spark-ignition engines with cooled EGR". *Energy Conversion and Management*, Vol. 87, pp. 946–955, 2014.

[220] Andersen J., Karlsson E. and Gawell A. "Variable Turbine Geometry on SI Engines". *SAE Technical Paper n. 2006-01-0020*, 2006.

[221] Pallotti P., Torella E., New J., Criddle M. and Brown J. "Application of an Electric Boosting System to a Small, Four-Cylinder S.I. Engine". *SAE Technical Paper n. 2003-32-0039*, 2003.

[222] George S., Morris G., Dixon J., Pearce D. and Heslop G. "Optimal Boost Control for an Electrical Supercharging Application". *SAE Technical Paper n. 2004-01-0523*, 2004.

[223] Herbst F., Staber-Schmidt C., Eilts P., Sextro T., Kammeyer J., Natkaniec C., Seume J., Porzig D. and Schwarze H. "The Potential of Variable Compressor Geometry for Highly Boosted Gasoline Engines". *SAE Technical Paper n. 2011-01-0376*, 2011.

[224] Hacohen J., Ashcroft S. J. and Belmont M. R. "Lean burn versus EGR S.I. engine". *SAE Technical Paper n. 951902*, 1995.

[225] Roy M. M., Tomita E., Kawahara N., Harada Y. and Sakane A. "Comparison of performance and emissions of a supercharged dual-fuel engine fueled by hydrogen and hydrogen-containing gaseous fuels". *International Journal of Hydrogen Energy*, Vol. 36 n^o 12, pp. 7339–7352, 2011.

[226] Li T., Wu D. and Xu M. "Thermodynamic analysis of EGR effects on the first and second law efficiencies of a boosted spark-ignited direct-injection gasoline engine". *Energy Conversion and Management*, Vol. 70 n^o x, pp. 130–138, 2013.

[227] Caton J. A. "The thermodynamic characteristics of high efficiency, internal-combustion engines". *Energy Conversion and Management*, Vol. 58, pp. 84–93, 2012.

[228] Bozza F., De Bellis V. and Teodosio L. "Potentials of cooled EGR and water injection for knock resistance and fuel consumption improvements of gasoline engines". *Applied Energy*, Vol. 169, pp. 112–125, 2016.

[229] Duan X., Liu Y., Liu J., Lai M. C., Jansons M., Guo G., Zhang S. and Tang Q. "Experimental and numerical investigation of the effects of low-pressure, high-pressure and internal EGR configurations on the performance, combustion and emission characteristics in a hydrogen-enriched heavy-duty lean-burn natural gas SI engine". *Energy Conversion and Management*, Vol. 195 n^o March, pp. 1319–1333, 2019.

[230] Park Y. and Bae C. "Experimental study on the effects of high/low pressure EGR proportion in a passenger car diesel engine". *Applied Energy*, Vol. 133, pp. 308–316, 2014.

[231] Takaki D., Tsuchida H., Kobara T., Akagi M., Tsuyuki T. and Nagamine M. "Study of an EGR system for downsizing turbocharged gasoline engine to improve fuel economy". *SAE Technical Papers*, Vol. 1, 2014.

[232] Shen Kai, Xu Zishun, Chen Hong and Zhang Zhendong. "Investigation on the EGR effect to further improve fuel economy and emissions effect of Miller cycle turbocharged engine". *Energy*, Vol. 215, pp. 119116, 2021.

[233] Su J., Xu M., Li T., Gao Y. and Wang J. "Combined effects of cooled EGR and a higher geometric compression ratio on thermal efficiency improvement of a downsized boosted spark-ignition direct-injection engine". *Energy Conversion and Management*, Vol. 78, pp. 65–73, 2014.

[234] Sjerić M., Taritaš I., Tomić R., Blažić M., Kozarac D. and Lulić Z. "Efficiency improvement of a spark-ignition engine at full load conditions using exhaust gas recirculation and variable geometry turbocharger - Numerical study". *Energy Conversion and Management*, Vol. 125, pp. 26–39, 2016.

[235] Zhen X., Tian Z., Wang Y., Xu M., Liu D. and Li X. "Knock analysis of bio-butanol in TISI engine based on chemical reaction kinetics". *Energy*, Vol. 239, pp. 122190, 2022.

[236] Wang X., Zhang X., Wang M., Han Y. and Chen H. "Numerical Simulation of Knock Combustion in a Downsizing Turbocharged Gasoline Direct Injection Engine". *Applied Sciences*, Vol. 9 n^o 19, pp. 4133, oct 2019.

[237] Szybist James P, Wagnon Scott W, Splitter Derek, Pitz William J and Mehl Marco. "The Reduced Effectiveness of EGR to Mitigate Knock at High Loads in Boosted SI Engines". *SAE Technical Paper 2017-24-0061*, 2017.

[238] Parsons D., Orchard S., Evans N., Ozturk U., Burke R. and Brace C.s. "A comparative study into the effects of pre and post catalyst exhaust gas recirculation on the onset of knock". *International Journal of Engine Research*, 2020.

[239] Shen K., Li F., Zhang Z., Sun Y. and Yin C. "Effects of LP and HP cooled EGR on performance and emissions in turbocharged GDI engine". *Applied Thermal Engineering*, Vol. 125 n^o x, pp. 746–755, 2017.

[240] Zhang Z., Zhang H., Wang T. and Jia M. "Effects of tumble combined with EGR (exhaust gas recirculation) on the combustion and emissions in a spark ignition engine at part loads". *Energy*, Vol. 65 n^o x, pp. 18–24, 2014.

[241] Huang B., Hu E., Huang Z., Zheng J., Liu B. and Jiang D. "Cycle-by-cycle variations in a spark ignition engine fueled with natural gas-hydrogen blends combined with EGR". *International Journal of Hydrogen Energy*, Vol. 34 n^o 19, pp. 8405–8414, 2009.

[242] Zhang S., Li Y., Wang S., Zeng H., Liu J., Duan X. and Dong H. "Experimental and numerical study the effect of EGR strategies on in-cylinder flow, combustion and emissions characteristics in a heavy-duty higher CR lean-burn NGSI engine coupled with detail combustion mechanism". *Fuel*, Vol. 276 n^o February, pp. 118082, 2020.

[243] Yu X., Zhao Z., Huang Y., Shi W., Guo Z., Li Z., Du Y., Jin Z., Li D., Wang T. and Li Y. "Experimental study on the effects of EGR on combustion and emission of an SI engine with gasoline port injection plus ethanol direct injection". *Fuel*, Vol. 305 n^o August, pp. 121421, 2021.

[244] Zhou L., Dong K., Hua J., Wei H., Chen R. and Han Y. "Effects of applying EGR with split injection strategy on combustion performance and knock resistance in a spark assisted compression ignition (SACI) engine". *Applied Thermal Engineering*, Vol. 145 n^o 2011, pp. 98–109, 2018.

[245] Cairns A., Blaxill H. and Irlam G. "Exhaust gas recirculation for improved part and full load fuel economy in a turbocharged gasoline engine". *SAE Technical Papers*, n^o 724, 2006.

[246] Galloni E., Fontana G. and Palmaccio R. "Numerical analyses of EGR techniques in a turbocharged spark-ignition engine". *Applied Thermal Engineering*, Vol. 39, pp. 95–104, 2012.

[247] Galindo J., Climent H., De la Morena J., Pitarch R., Guilain S. and Besancon T. "A methodology to study the interaction between variable valve actuation and exhaust gas recirculation systems for spark-ignition engines from combustion perspective". *Energy, Conversion and Management*, Vol. 250, 2021.

[248] Li T., Yin T. and Wang B. "Anatomy of the cooled EGR effects on soot emission reduction in boosted spark-ignited direct-injection engines". *Applied Energy*, Vol. 190, pp. 43–56, 2017.

[249] Su J., Xu M., Zhang Y., Hung D. and Li T. "Soot emission reduction using cooled EGR for a boosted spark-ignition direct-injection (SIDI) engine". *Proceedings of the 8th International Conference on Modeling and Diagnostics for Advanced Engine Systems, COMODIA 2012*, pp. 98–103, 01 2012.

[250] Ivanič Ž., Ayala F., Goldwitz J. and Heywood J. B. "Effects of hydrogen enhancement on efficiency and NOx emissions of lean and EGR-diluted mixtures in a SI engine". *SAE Technical Papers*, n^o 724, 2005.

[251] Fontanesi S., Pecchia M. D., Pessina V., Sparacino S. and Iorio S. D. "Quantitative investigation on the impact of injection timing on soot formation in a GDI engine with a customized sectional method". *International Journal of Engine Research*, Vol. (in press), 2021.

[252] Cairns A., Fraser N. and Blaxill H. "Pre Versus Post Compressor Supply of Cooled EGR for Full Load Fuel Economy in Turbocharged Gasoline Engines". *SAE Technical Paper 2008-01-0425*, 2008.

[253] Potteau S., Lutz P., Leroux S., Moroz S. and Tomas E. "Cooled EGR for a Turbo SI Engine to Reduce Knocking and Fuel Consumption". *SAE Technical Papers*, 2007.

[254] Grandin B., Angstrom H. E., Stalhammar P. and Olofsson E. "Suppression in a Turbocharged SI Engine by Using Cooled EGR". *SAE Technical Papers*, 1998.

[255] Kumano K. and Yamaoka S. "Analysis of knocking suppression effect of cooled egr in turbo-charged gasoline engine". *SAE Technical Papers*, Vol. 1, 2014.

[256] Alger T., Chauvet T. and Dimitrova Z. "Synergies between high EGR operation and GDI systems". *SAE International Journal of Engines*, Vol. 1 n^o 1, pp. 101–114, 2009.

[257] Wheeler J., Polovina D., Ramanathan S., Roth K., Manning D. and Stein J. "Increasing EGR tolerance using high tumble in a modern GTDI engine for improved low-speed performance". *SAE Technical Papers*, Vol. 2, 2013.

[258] Tomazic D. and Pfeifer A. "Cooled EGR - A Must or an Option for 2002/04 Reprinted From: Compression Ignition Combustion and In-Cylinder Diesel Particulates and NOx Control". *SAE Technical Papers*, Vol. 2002-01-00962, 2002.

[259] Roth D. B., Gonzalez Tabares I. and Sotelo Álvarez A. "Condensing LPL EGR Mixer with Mid-Pressure Loop". *SAE International Journal of Engines*, Vol. 8 n^o 4, 2015.

[260] Gong Changming, Si Xiankai and Liu Fenghua. "Combustion and emissions behaviors of a stoichiometric GDI engine with simulated EGR (CO2) at low load and different spark timings". *Fuel*, Vol. 295 n^o December 2020, pp. 120614, 2021.

[261] "Dedicated EGR Vehicle Demonstration". *SAE International Journal of Engines*, Vol. 10 n^o 3, pp. 898–907, 2017.

[262] Chadwell C. J., Alger T., Zuehl J. and Gukelberger R. "A Demonstration of Dedicated EGR on a 2.0 L GDI Engine". *SAE International Journal of Engines*, Vol. 7 n^o 1, pp. 434–447, 2014.

[263] Jung D. and Lee S. "An investigation on the potential of dedicated exhaust gas recirculation for improving thermal efficiency of stoichiometric and lean spark ignition engine operation". *Applied Energy*, Vol. 228 n^o June, pp. 1754–1766, 2018.

[264] Alger T., Gingrich J. and Mangold B. "The effect of hydrogen enrichment on EGR tolerance in spark ignited engines". *SAE Technical Papers*, n^o 724, 2007.

[265] Gerty Michael D. and Heywood John B. "An investigation of gasoline engine knock limited performance and the effects of hydrogen enhancement". *SAE Technical Papers*, n^o 724, 2006.

[266] Alger T., Walls M., Chadwell C., Joo S., Denton B., Kleinow K. and Robertson D. "The Interaction between Fuel Anti-Knock Index and Reformation Ratio in an Engine Equipped with Dedicated EGR". *SAE International Journal of Engines*, Vol. 9 n^o 2, pp. 786–795, 2016.

[267] Malaquias A. C. T., Netto N. A. D., da Costa R. B. R. and Baêta J. G. C. "Combined effects of internal exhaust gas recirculation and tumble motion generation in a flex-fuel direct injection engine". *Energy Conversion and Management*, Vol. 217 n^o March, pp. 113007, 2020.

[268] Lanzanova T. D. M., Dalla Nora M., Martins M. E. S., Machado P. R. M., Pedrozo V. B. and Zhao H. "The effects of residual gas trapping on part load performance and emissions of a spark ignition direct injection engine fuelled with wet ethanol". *Applied Energy*, Vol. 253 n^o January, pp. 113508, 2019.

[269] Rodriguez J. F. and Cheng W. "Potential of Negative Valve Overlap for Part-Load Efficiency Improvement in Gasoline Engines". *SAE International Journal of Engines*, Vol. 11 n^o 6, pp. 657–668, 2018.

[270] Hunicz J., Mikulski M., Geca M. S. and Rybak A. "An applicable approach to mitigate pressure rise rate in an HCCI engine with negative valve overlap". *Applied Energy*, Vol. 257 n^o August 2019, pp. 114018, 2020.

[271] Puranam S. V. and Steeper R. R. "The Effect of Acetylene on Iso-octane Combustion in an HCCI Engine with NVO". *SAE International Journal of Engines*, Vol. 5 n^o 4, pp. 1551–1560, 2012.

[272] Mikulski M., Balakrishnan P. R. and Hunicz J. "Natural gas-diesel reactivity controlled compression ignition with negative valve overlap and in-cylinder fuel reforming". *Applied Energy*, Vol. 254 n^o July, pp. 113638, 2019.

[273] Szwaja S., Ansari E., Rao S., Szwaja M., Grab-Rogalinski K., Naber J. D. and Pyrc M. "Influence of exhaust residuals on combustion phases, exhaust toxic emission and fuel consumption from a natural gas fueled spark-ignition engine". *Energy Conversion and Management*, Vol. 165 n^o December 2017, pp. 440–446, 2018.

[274] Malaquias A. C. T., Netto N. A. D., da Costa R. B. R. and Baêta J. G. C. "Combined effects of internal exhaust gas recirculation and tumble motion generation in a flex-fuel direct injection engine". *Energy Conversion and Management*, Vol. 217 n^o March, pp. 113007, 2020.

[275] Khoa N. X., Quach Nhu Y. and Lim O. "Estimation of parameters affected in internal exhaust residual gases recirculation and the influence of exhaust residual gas on performance and emission of a spark ignition engine". *Applied Energy*, Vol. 278 n^o June, pp. 115699, 2020.

[276] Tang Q., Liu J., Zhan Z. and Hu T. "Influences on Combustion Characteristics and Performances of EGR vs. Lean Burn in a Gasoline Engine". *SAE Technical Papers*, Vol. 2013-April, 2013.

[277] Khosravi M., Harihar A., Pitsch H. and Weber C. "Modeling and Numerical Investigation of Auto-Ignition and Megaknock in Boosted Gasoline Engines". *SAE Technical Papers*, Vol. 2017-March n^o March, 2017.

[278] Guardiola C., Triantopoulos V., Bares P., Bohac S. and Stefanopoulou A. "Simultaneous Estimation of Intake and Residual Mass Using In-Cylinder Pressure in an Engine with Negative Valve Overlap". *IFAC-PapersOnLine*, Vol. 49 n^o 11, pp. 461–468, 2016.

[279] Ortiz-Soto E. A., Vavra J., and Babajimopoulos A. "Assessment of Residual Mass Estimation Methods for Cylinder Pressure Heat Release Analysis of HCCI Engines With Negative Valve Overlap". *J. Eng. Gas Turbines Power*, n^o 134, pp. 9, 2012.

[280] Bourhis G, Chauvin J, Gautrot X and de Francqueville L. "LP EGR and IGR compromise on a GDI engine at middle load". *SAE International Journal of Engines*, Vol. 6 n^o 1, pp. 67–77, 2013.

[281] Galindo J., Climent H., De la Morena J., González-Domínguez D., Guilain S. and Besançon T. "Experimental and modeling analysis on the optimization of combined

VVT and EGR strategies in turbocharged direct-injection gasoline engines with VNT". *Proceedings of the Institution of Mechanical Engineers, Part D: Journal of Automobile Engineering*, Vol. 235 n^o 10-11, pp. 2843–2856, 2021.

[282] Yu C., Zhao Z., Wang L., Cui H. and Zhang F. "The effect of cooled EGR on combustion and load extension in a kerosene spark-ignition engine". *Fuel*, Vol. 280 n^o March, pp. 118681, 2020.

[283] Galloni E., Fontana G. and Palmaccio R. "Effects of exhaust gas recycle in a downsized gasoline engine". *Applied Energy*, Vol. 105, pp. 99–107, 2013.

[284] Zamboni G. and Capobianco M. "Experimental study on the effects of HP and LP EGR in an automotive turbocharged diesel engine". *Applied Energy*, Vol. 94, pp. 117–128, 2012.

[285] Luján J. M., Guardiola C., Pla B. and Reig A. "Switching strategy between HP (high pressure)- and LPEGR (low pressure exhaust gas recirculation) systems for reduced fuel consumption and emissions". *Energy*, Vol. 90, pp. 1790–1798, 2015.

[286] Reihani A., Hoard J., Klinkert S., Kuan C. K., Styles D. and McConville G. "Experimental response surface study of the effects of low-pressure exhaust gas recirculation mixing on turbocharger compressor performance". *Applied Energy*, Vol. 261 n^o December 2019, pp. 114349, 2020.

[287] Franken T., Mauss F., Seidel L., Gern M. S., Kauf M., Matrisciano A. and Kulzer A. C. "Gasoline engine performance simulation of water injection and low-pressure exhaust gas recirculation using tabulated chemistry". *International Journal of Engine Research*, Vol. (in press), 2020.

[288] Zhao L., Su X. and Wang X. "Comparative study of exhaust gas recirculation (EGR) and hydrogen-enriched EGR employed in a SI engine fueled by biobutanol-gasoline". *Fuel*, Vol. 268 n^o October 2019, pp. 117194, 2020.

[289] Gainey B., Yan Z., Moser S. and Lawler B. "Lean flammability limit of high-dilution spark ignition with ethanol, propanol, and butanol". *International Journal of Engine Research*, pp. 1–11, 2021.

Chapter 3

Experimental and theoretical tools

Contents

3.1 Introduction

This chapter provides a detailed description and explanation of all the theoretical and experimental tools that have been used throughout this PhD-Thesis. All these tools are strictly necessary for the satisfactory fulfillment of the objectives set. The understanding of the peculiarities of the tools and their limitations is crucial for scientific dissemination.

Two main sections are distinguished in this chapter. First, all the tools that were used experimentally are explained, including the engine, the test bench and the experimental set-up together with all the instrumentation employed. Besides, a brief subsection about the climatic chamber is included since this engine was tested in two different benches. The second section is the theoretical tools. In this section, tests processing is explained together with all the calculations from the in-cylinder pressure: pumping mean effective pressure, maximum amplitude of pressure oscillations (MAPO) and the combustion analysis. Moreover, the different thermodynamic calculations such as specific heat values, mixing temperatures based on the conservation of enthalpy and compressor efficiency, are described.

3.2 Experimental tools

All the experimental tools that have been useful for the development of this PhD-Thesis are explained in this section of the chapter. First, the tested engine and the experimental set-up are detailed. Then, the test bench and instrumentation used for the main studies carried out are explained in detail. The last part of this section is dedicated to explaining the climate chamber, in which a series of tests were carried out to study the condensation of LP-EGR.

3.2.1 The engine and experimental set-up

The engine under study in this PhD-Thesis is a 4-stroke, four cylinder in line spark-ignited gasoline engine. The engine displacement is 1.3 liter and it equips a turbocharger with a VGT and a direct injection system. There is also a TWC and a GPF placed in the exhaust line, downstream the turbine, to comply with emission standards. The main engine characteristics are described in Table 3.1.

A VVT system based on cam phasing is used for both intake and exhaust valves independently. The system allows the intake and exhaust valve events to be varied linearly, maintaining lift and duration, from zero to forty, with zero being the minimum overlap condition and forty the maximum overlap condition.

Table 3.1. *Characteristics of the tested engine.*

Magnitude	**Units**	**Value**
Typology	[-]	GTDI 4-stroke
Cylinders	[-]	4
Valves	[-]	4
Bore	[mm]	72
Stroke	[mm]	81.2
Displaced volume	[cc]	1300
Compression ratio	[-]	10.6:1
Turbocharger	[-]	VGT

Following the widespread enrichment strategy in gasoline engines, the engine operates with lambda below one at high loads and several engine speeds for exhaust temperature control and protection of the main exhaust components, for example, the turbine. The lambda engine map is shown in Figure 3.1, where it is possible to see that enrichment starts from 2500 revolutions per minute (rpm) to full speed and from about 80% of engine load, achieving a bottom value of 0.86 at full load conditions.

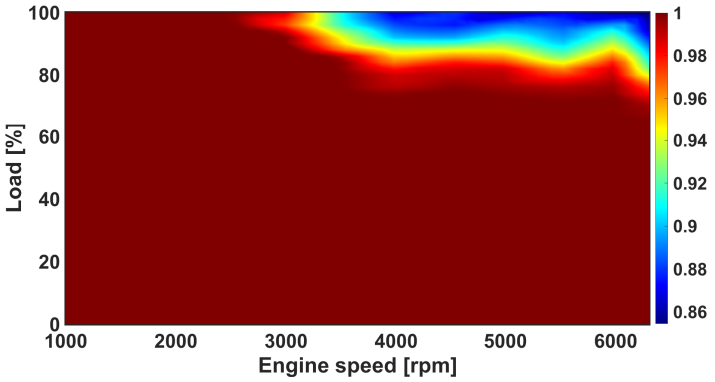

Figure 3.1. *Lambda engine map depending on speed and load.*

Custom made LP-EGR and HP-EGR lines were installed in the production engine, since these were not included. For the LP-EGR system, the exhaust

gas is extracted right after the TWC and passes through a cooler with at 90°C and the EGR valve. Another configuration of the LP-EGR was tested, in which the exhaust gas was extracted upstream the TWC, changing the composition of the gas to that expected from an HP system. This system will be called LP-EGR PRE, in reference to the extraction point of the exhaust gas upstream the TWC. The exhaust gas is then reintroduced with a T-joint before the compressor inlet and a choke valve is placed upstream the joint in order to cause further pressure difference and increase the recirculated rate, specially at low engine speeds. The mixture of fresh air and exhaust gases are compressed and cooled in a integrated WCAC, normally to 30°C. Note that the main throttle valve is placed between the compressor outlet and the WCAC inlet.

For the HP-EGR system, the exhaust gas is extracted with an elbow at the exhaust manifold, which is integrated with the turbine housig, and reintroduced at the WCAC outlet, pointing directly to the intake runners. Due to the high temperatures that may be found at the exhaust manifold, a cooled EGR valve is used followed by an EGR cooler. The nature of this system makes it impossible to obtain a reliable measure of the EGR rate given the difficulty of having a homogeneous mix and the little space available.

The engine set-up diagram is shown in Figure 3.2, with the WCAC, the turbocharger and the three EGR lines: LP-EGR, LP-EGR PRE and HP-EGR. Note that two water circuits for the WCAC were used, one that was fed from the ordinary water deposit available and the other that was fed from a chiller, in order to achieve lower intake temperatures at the WCAC outlet. The location of all temperature and pressure measures are also included in the diagram.

In terms of cooling circuits, the main cooling circuit of the engine is a high-temperature one, designed in order to keep the coolant temperature around 90°C at warmed-up conditions. This circuit is also used for the EGR coolers, both the low and the high pressure circuits. Another cooling circuit is used for the WCAC, since the high-temperature circuit would induce extremely high intake temperatures, damaging the perfomance of the engine given the lower density of the charge and the decreased knock resistance. This second circuit only feeds the WCAC, so that the charge temperatures in the intake runnners are at reasonable levels and below 50°C even at the higher load conditions.

All the experiments were carried out with a 98 octane gasoline, always obtained from the same source. A summary of characteristics from a fuel analysis is shown in Table 3.2.

In conclusion, the engine is framed in the current downsizing trend, with a direct injection system, variable valve actuation and EGR, making it a suitable

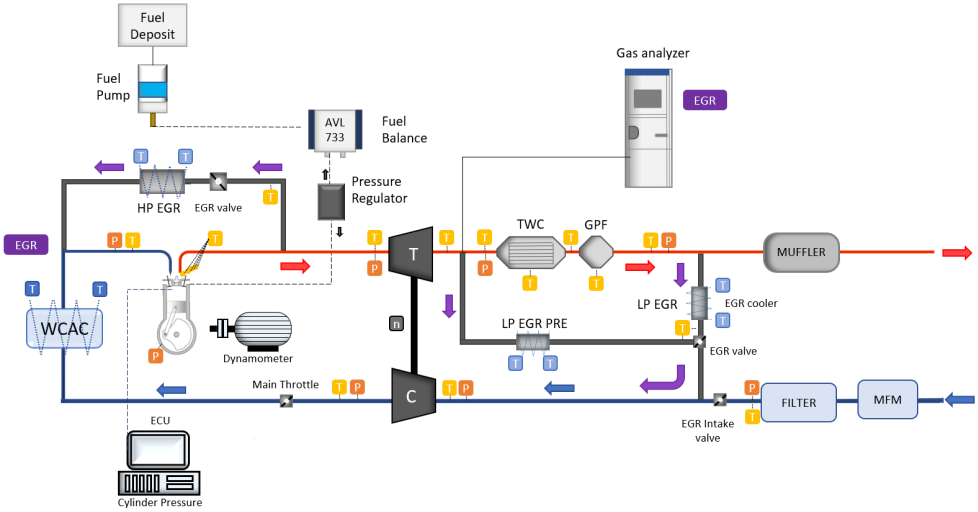

Figure 3.2. *Engine set-up diagram.*

Table 3.2. *Fuel analysis.*

Magnitude	**Units**	**Value**
Fuel	[-]	Gasoline
RON	[-]	98
Carbon content	[%]	85.98
Hydrogen content	[%]	12.09
Nitrogen content	[%]	<0.01
Sulfur content	[mg/kg]	7.83
Upper heating value	[MJ/kg]	45.31
Lower heating value	[MJ/kg]	42.82

aspirant to assess the impact of exhaust gases in gasoline engines. Besides, it is a good option to be combined in the future with hybrid techonologies.

3.2.2 Test bench and instrumentation

The test bench in CMT-Motores Térmicos consists basically on the engine dynamometer and the different auxiliar systems to feed and operate the engine, as the cooling system, the fuel supply, the instrumentation, the acquisition system and the ventilation of the room.

The dynamometric brake of the engine is an AVL-AFA 200/4-8EU which is easily adaptable to many types of engines. The dynamometer is controlled by a PUMA software that allows the engine speed and torque to be controlled in different modes and to accomplish steady and transient tests. Furthermore, there is the possibility to impose engine speed, pedal or torque profiles in order to implement homologation cycles, among others. The PID's of the dynamometric brake can be adjusted in order to control de dynamic response depending on the application. Besides, it includes control over the fuel, intercooler and engine coolant temperatures.

The variable valve timing system, the spark timing and the main throttle position could be adjusted through a partially open electronic control unit (ECU), which was operated and their variables saved via INCA v7.1. Besides, a bypass was activated in order to control several ECU variables with an external control system based on a National Instruments PXI software with the LabVIEW environment, as the one described and used in [1]. The conexion between PXI and the ECU was made with an ETAS ES910 configured with the environment INTECRIO. The control of all the EGR valves as well as the VGT was also made through this software, via DRIVVEN. Moreover, all high-frequency variables as the instantaenous in-cylinder, intake and exhaust manifold pressures or the pulse signal were recorded using PXI. In this way, it was possible to carry out online estimations, as the apparent heat release rate together with several CA's, the indicated mean effective pressure and its coefficient of variation (COV) and a knock calculation based on MAPO as in [1].

In terms of instrumentation, the in-cylinder pressure was measured with instrument spark-plugs AVL ZI33 and the instantaneous pressures at the manifolds were measured with piezorresistive sensors, specifically the Kistler 4007. Since it is a relative measurement, the in-cylinder pressure is adjusted with the instantaneous intake manifold pressure. The signal is then phased with respect to TDC and filtered. The treatment of the in-cylinder pressure measurements together with calculation of the MAPO and the apparent heat release rate will be explained in further sections. Many Kistler 4045A5 pressure sensors for mean measurements were also distributed along the lines

together with type K thermocouples for temperature measurement as shown in Figure 3.2.

A MICRO-EPSILON DS05 sensor was used to measure the turbocharger speed and an AVL-optical encoder was used for crank angle reference. This optical enconder could be changed to obtain with a resolution of 0.2 or 0.5 CAD. Besides, the air mass flow was obtained with an AVL-FLOWSONIX air flowmeter, and the fuel mass flow was measured with a gavimetric balance model AVL-733S. The mass flow of fuel is basically measured by weighing with a recipient and a capacitive displacement sensor. This recipient must be filled between tests, with a frequency that depends on its capacity. Otherwise, if the measure is done while refilling, it will not useful.

The specifications of the main sensors used are shown in Table 3.3:

Table 3.3. *Specifications of the main sensors used.*

Magnitude	**Sensor**	**Linearity**	**Range**
In-cylinder pressure	AVL-ZI33	$\pm$ 0.3%	0 - 200 bar
Instantaneous pressure	Kistler 4007	$\leqslant \pm$ 0.2%	0 - 5 bar
Mean pressure	Kistler 4045A5	$\leqslant \pm$ 0.2%	0 - 5 bar
Charge Amplifier	Kistler 5018A	$<\pm$ 0.3%	2 - 2.2·10^6 pC
Mean temperature	K Thermocouple	$\pm$ 0.35%	270 - 1260$^\circ C$
Air mass flow	AVL-FLOWSONIX	$\pm$ 0.25%	0 - 1400 kg/h
Fuel mass flow	AVL-733S	$\pm$ 0.12%	0 - 150 kg/h
Turbocharger speed	MICRO-EPSILON DS05	$\pm$ 0.2%	2·10^2 -4·10^5 rpm
Torquemeter	HBM T10F	$\pm$ 0.1%	0 - 10 kN·m
Optical encoder	AVL-364	$\pm$ 0.006%	2.5·10^{-2} - 2.8·10^4 rpm

On the emission side, an HORIBA MEXA-ONE was used in order to measure regulated gaseous emissions: NO_x, HC and CO. Note that this device does also account for CO_2, despite it is not considered a pollutant emission as explained in subsection 2.2.3. Other components such as methane (CH_4), NMHC (Non-Methane Hydrocarbons), oxygen (O_2), NO and NO_2 were also measured together with the air-to-fuel ratio and lambda. A summary of the HORIBA MEXA-ONE is shown in Table 3.4.

The concentration of CO and CO_2 was measured with a NDIR system (Non Dispersive Infrared Detector). The exhaust gas is introduced into a chamber where infrared light is passed at a given wavelength depending on the component that is intended to measure. The component absorbs the light and

Table 3.4. *Specifications of the HORIBA MEXA-ONE.*

Species	**Sensor & Principle**	**Linearity**	**Range**
CO(L)	AIA-11 - NDIR	$<\pm$ 1%	0-3000 ppm
CO(H)	AIA-33 - NDIR	$<\pm$ 1%	0-10 vol%
CO_2	AIA-33 - NDIR	$<\pm$ 1%	0-20 vol%
THC	FIA-02O-ND - H.FID	$<\pm$ 1%	0-25 K ppmC
NMHC, CH_4	FIA-02O-ND - H.FID+NMC	$<\pm$ 1%	0-25 K ppmC
NO, NO_2, NO_x	CLA-02OV-3 -H.CLD	$<\pm$ 1%	0-5000 ppm
O_2	MPA-01 - MPD	$<\pm$ 1%	0-25 vol%

this would decrease the intensity of the light that is leaving the chamber at the other end. The difference between this intensity and a reference one is then converted to concentration of the species. Note that there are two measures for CO, L (for Low) and H (for High), and the difference between them is the operation range. The total hydrocarbons (THC) concentration was measured with a FID system (Flame Ionization Detector). The measurement consists of passing a sample of the gas though a hydrogen flame. An ionization current is produced, which is proportional to the amount of carbons in the sample. In a very similar way, NMHC and CH_4 were measured with a FID system, in which there are two colums to separate methane. The first column retains the non-methane hydrocarbons, allowing oxygen and methane to go through a second column in which only the oxygen will be held, and the methane will go to an ionization flame. For NO, NO_2 and NO_x, a CLD system (Chemiluminescence Detector) was used. A photo-diode is used to observe the amount of photons emitted in the reaction between NO and ozone, which will be proportional to the amount of NO. For NO_x, there is a route to dissociate NO_x to NO in order to use the same principle. Lastly, the oxygen concentration was measured with a MPD (Magnetopneumatic Detector). In the end, all species are recorded in ppm as chosen by the operator in the HORIBA.

The HORIBA MEXA-ONE is connected at the turbine outlet, upstream the TWC in order to gauge raw engine-out emissions. At some point, several tests were made with the connection at the TWC outlet to assess the conversion efficiency of the aftertreatment system. Another measurement tap is connected to the WCAC inlet, shown in purple, in order to measure intake carbon dioxide concentration to calculate the EGR rate [2–5] as in Equation 3.1:

$$EGR_{rate} = \frac{[CO_2]_{int} - [CO_2]_{atm}}{[CO_2]_{exh} - [CO_2]_{atm}} \cdot 100 \tag{3.1}$$

where $[CO_2]$ is the concentration of carbon dioxide and the subscripts int, exh and atm represent intake, exhaust and atmospheric conditions, which is set to 400 ppm at the analyzer. To obtain the most accurate EGR rate possible, the carbon dioxide concentration at the exhaust should be monitored at the TWC outlet for the low-pressure EGR loop in order to account for the little amount of carbon dioxide that is formed from the conversion of hydrocarbons and carbon monoxides. In practice, this amount is negligible and the location of the measurement tap remains for simplicity. For the HP-EGR circuit and the LP-EGR PRE, the carbon dioxide concentration is exact since gases are extracted upstream the TWC. However, the EGR rate measurement for the HP circuit is not completely reliable since the mixture with air starts at the intake runners and other methods are used, as already explained in section 2.4.

To operate the engine, the same warm-up procedure was followed each testing day. Once fired-up, the engine was set to a low torque condition, specifically 1500 rpm and a 10% of pedal. This situation was stablished and maintained until the engine oil and coolant temperature reached and stabilized at approximately 90°C. When the engine reached an optimal condition for testing, some cheks were done in the test cell in order to ensure that no leakages or defects had appeared.

Some reference tests were regularly repeated in order to check and compare between days and confirm the correct functioning of the installation. The chosen checkpoints were at 1500 rpm at 6 bar BMEP without EGR and with a 10% rate. To achieve the desired conditions, slow ramps were introduced in the PUMA test bench control. The main cheked variables were the engine speed and torque, the brake specific fuel consumption, the spark timing, lambda, the variable valve timing, the position of the EGR valves and the mean intake and exhaust temperatures and pressures.

Once all the starting procedure was completed, the engine was set to the desired conditions of engine speed and torque (or any other parameter to control the load as the throttle, pedal or VGT position). The engine speed was again set with PUMA, and the load condition depended on the control that was implemented. Normally, the steady-state tests were done at constant torque condition, so the position of the throttle valve and the VGT position were adjusted via bypass with LabVIEW. The EGR rate was set by changing the position of the EGR valves with LabVIEW and the VVT system could be adjusted with INCA or via bypass, as well as the spark advance. Other

parameters as the WCAC temperature set point or lambda were also changed if needed. Once the engine was at the desired condition in all variables, a brief stabilization period was needed before the acquisition began. After the engine stabilized, the three acquisition systems, PUMA, INCA and LabVIEW start recording for 60 seconds and 300 cycles in the case of LabVIEW. The acquisition frequency of the PUMA variables is 0.1 seconds, whereas in the case of INCA it depends on each variable. The high-frequency variables were recorded in LabVIEW each 0.2 or 0.5 crank angle degree, depending on the engine point, and other variables were recorded with a one-per-cycle value.

3.2.3 Climatic chamber

During the course of this PhD-Thesis, the engine was also mounted in a climatic chamber in order to better control the temperature conditions for the condensation tests. The main difference of this room with respect to the previous one is the possibility to control the air, fuel and coolant temperatures easily, as explained in [6].

The only noticeable difference in terms of instrumentation is the use of an HORIBA 7100 D EGR instead of the MEXA-ONE for emissions measurement. The HORIBA 7100 D EGR, which specifications are shown in Table 3.5, is one of the predecessor of the MEXA-ONE and the main differences between them are due to the simplicity when operating with it and its efficiency in the use of consumables.

Table 3.5. *Specifications of the HORIBA 7100 D EGR.*

Species	**Sensor & Principle**	**Linearity**	**Range**
CO(L)	AIA-721 - NDIR	$<\pm$ 1%	50-2500 ppm
CO(H)	AIA-722 - NDIR	$<\pm$ 1%	0.5-10 vol%
CO_2	AIA-722 - NDIR	$<\pm$ 1%	0.5-20 vol%
THC	FIA-720 - FID	$<\pm$ 1%	10-20 K ppmC
NMHC, CH_4	GFA-720 - FID	$<\pm$ 1%	5-2500 ppm
NO, NO_2, NO_x	CLA-720 - CLD	$<\pm$ 1%	10-10K ppm
O_2	MPA-720 - MPD	$<\pm$ 1%	1-25 vol%

3.3 Data processing

All the data processing is explained in detail in this section. First, all the test processing is explained together with the calculations from the in-cylinder pressure signal: the IMEP, its coefficient of variation, the PMEP (Pumping Mean Effective Pressure), the knock indicator through MAPO and the combustion analysis. It must be noted that, since all tests analysed in this document are stationary, an average of the variables is done with a verification that there are no anomalous data. Second, the thermodynamic calculations to estimate the specific heat values, mixing temperature and the compressor efficiency are described.

3.3.1 In-cylinder pressure analysis and data processing

Since the in-cylinder pressure is measured with high frequency with respect to time and in relative values, some treatment to the signal has to be made in order to extract valuable information. First of all, the signal is filtered with two different criteria, one for knocking and another for all the cycle estimations. Depending on the operating condition, the enconder was set to a resolution of 0.2 or 0.5 CAD, giving 3600 and 1440 in-cylinder pressure values respectively per cycle. An example of raw in-cylinder pressure measurement for each cylinder is shown in Figure 3.3 with a resolution of 0.2 CAD. Note that the intake stroke is at negative conditions in cylinders 2 and 3, almost at zero bar in cylinder 1 and around 10 bars in cylinder 4.

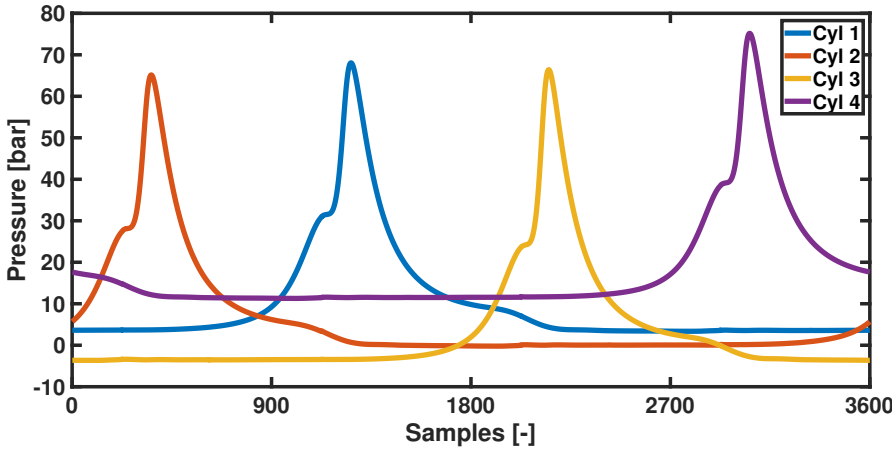

Figure 3.3. *Raw in-cylinder pressure measurement example.*

It is necessary to find the TDC of each cylinder with respect to the temporal measurement. To do this, there are several methods in the literature [7]. In this PhD-Thesis, the TDC was determined from motoring cycles in different conditions. It is worth mentioning that in order to phase the in-cylinder pressure with respect to its own TDC, some peculiarities must be taken into account. In the case of the cylinders 1 and 2 in Figure 3.3, the intake stroke that is plotted (values around 3600 and 2700 respectively) belong to the next cycle. A similar thing occurs with the exhaust stroke for cylinders 3 and 4 (values around 0 and 900 respectively). In this sense, the first and last cycles of the measurement for each cylinder are incomplete and need to be removed, losing in practice only one cycle. For this reason, at least 201 cycles were recorded in order to obtain 200. The result of the phasing process is shown in Figure 3.4.

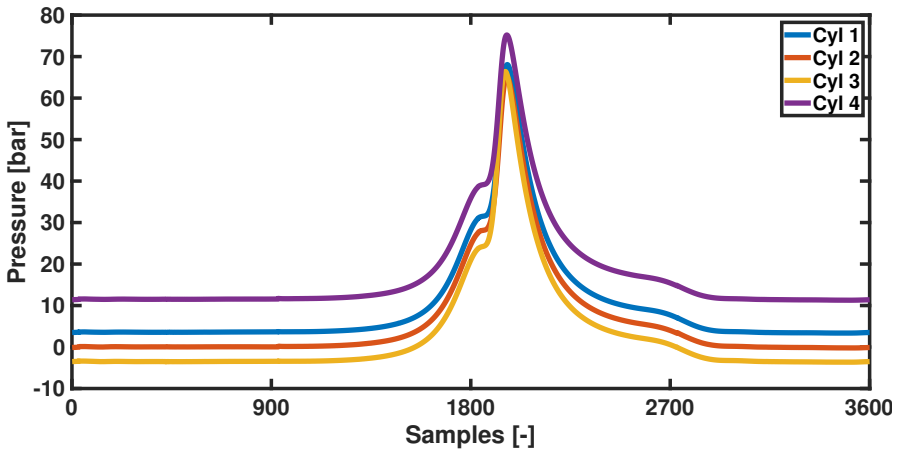

Figure 3.4. *Phased in-cylinder pressure example.*

The phasing of the in-cylinder pressure does also take into account possible missplacements of the recording signal thanks to the pulse signal. Note that the differences in the y-axis between cylinders in Figure 3.4 remain as in Figure 3.3. Any difference with respect to the x-axis could now be induced by cyclic dispersion. The process for referring the in-cylinder pressure to the intake pressure is called pegging [8]. The two processes explained, the phasing and the pegging of the in-cylinder pressure, are of vital importance, so that any little error can significantly change subsequent calculations. Once both are completed, the four curves should coincide in one if not for the small variations that may exist due to repeatability and cyclical dispersion. Due to the nature of a high-frequency experimental measure, it is mandatory to filter the signal.

In this case, the signal is filtered with two different criteria: with a band pass filter from 4-20 kHz for knock estimation and a low-pass filter with a cutting frequency of 4.5 kHz for the cycle calculations. The final result, with a phased, referenced and filtered in-cylinder pressure signal is showed in Figure 3.5

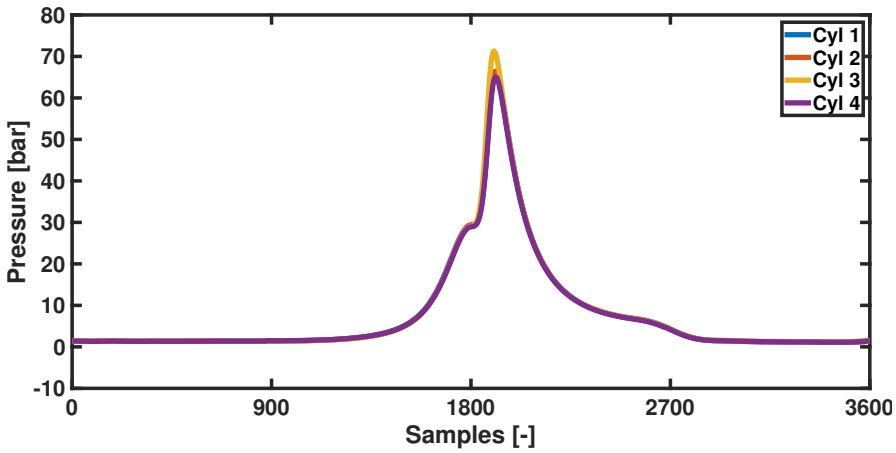

Figure 3.5. *Filtered in-cylinder pressure example.*

The displaced volume is calculated based on the connecting rod-crank mechanism, the diameter, stroke, compression ratio and radius of the crankshaft and connecting rod, assuming that there are no mechanical deformations.

The IMEP of each engine cycle is computed based on Equation 3.2.

$$IMEP = \frac{1}{V_{disp}} \cdot \oint P_{cyl} \cdot dV \tag{3.2}$$

With discrete data, the integral shown in Equation 3.2 becomes the sum of each in-cylinder pressure value multiplied by each delta volume. The coefficient of variation of the IMEP is then computed as the standard deviation of 200 cycles divided by the mean as in Equation 3.3:

$$COV_{IMEP} = \frac{std(IMEP)}{mean(IMEP)} \cdot 100 \tag{3.3}$$

The COV calculation is of vital importance since it gives an idea of the cyclic dispersion and several limits are set depending on the engine speed and load to ensure driveability and stability. For this PhD-Thesis, the COV limits

were set based on the BMEP: 3.33% for 6 bar or lower and 2% for higher loads except for the 19 bar BMEP cases. No tests were performed below 6 bar BMEP because the engine is designed to work in a hybrid configuration and it is assumed that this low-efficiency area is covered by the electric motor. Moreover, the IMEP and COV are displayed online during testing together with the knock indicator and the apparent heat release rate, which will be explained in following sections, in order to check the condition of the engine and the test in question.

Other calculations of great importance that are carried out in the processing are for example the effective, indicated and mechanical efficiency, the effective and indicated power and fuel consumption. Once the pumping losses are computed, all these parameters can be calculated with respect to the gross part of the cycle, so only compression, combustion and expansion affect.

3.3.1.1 Pumping mean effective pressure estimation

In order to decouple the effects coming from combustion side and from the air renewal process, the calculation of the pumping work is essential. Many studies include the calculation of the PMEP by taking into account the crank angle degrees at which intake and exhaust occur. However, the estimation of the PMEP in this PhD-Thesis is based on the P-V diagram to calculate the area enclosed by the intake and exhaust pressures.

During the course of this PhD-Thesis, three empirical-analytical methods to estimate the pumping losses have been used, obtaining very little differences between them. A fourth method, the use of a 1D engine model, has been used as a verification.

The first method used is the polynomial fit. Based on the P-V diagram, a part of the compression, expansion and exhaust strokes are identified in volume, specifically in the intersection area. Two polynomials are fitted, one for the compression stroke and the other for the expansion-exhaust part. The goal is to find the point in which both curves collide and give way to the negative part of the cycle. The solution of the system is a value of pressure and volume in which the pumping part of the cycle starts. Note the dificulty of the method since the code needs to be suitable for a wide range of operating conditions and the solver needs a square in which the solution is framed, so this square was changed often depending on the operating point.

For this reason, a second method was implemented. Once the the compression, expansion and exhaust strokes were identified in volume, two in-cylinder pressure vectors were obtained, one for the compression stroke and the other for the expansion and exhaust part. With these two vectors, it

is possible to find the smallest difference in pressure between them, so the intersection point is obtained. Note that since the in-cylinder pressure is a discrete variable, seldom is the intersection point actually going to be found in these vectors. When computing the difference in pressure between the vectors, there will be an aproach from the left and one from the right to the intersection point. The smallest of both differences in absolute value is chosen and the final result is the mean of the pressure values that have resulted in the smallest difference and the volume at which it is placed. Figure 3.6 shows an example of the PMEP calculation with this method with P-V diagrams. On the left hand side, the pumping area of a P-V diagram is depicted together with the full P-V diagram as an inset. In orange, there is a circle showing the calculation of the intersection point. On the right hand side, there is a zoom on the intersection area in which it is possible to appreciate that the circle is placed between the two pressure values which are the closest to the real intersection. Note that the accuracy of the method reaches the fourth decimal.

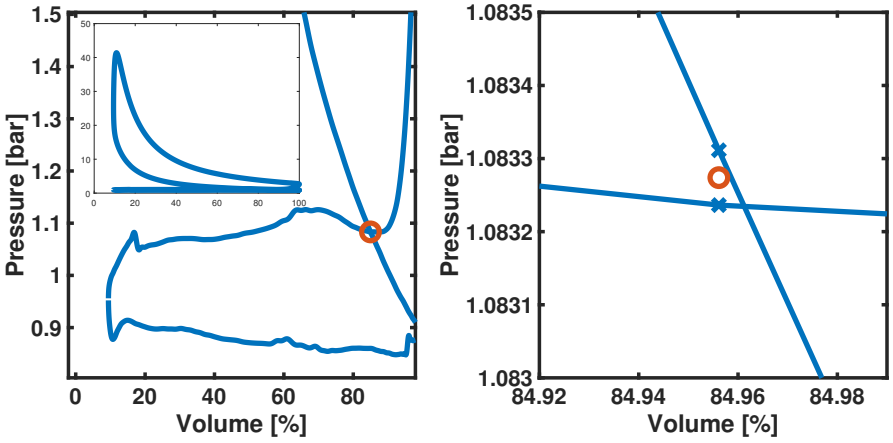

Figure 3.6. *P-V diagram and calculated intersection point for PMEP estimation with method 2.*

A third method is implemented as a mix of the previous two. When the smallest pressure differences are found on both sides of the intersection, left and right, a box is defined by the four P-V points inside which the intersection is framed. A first degree equation can be fitted for each reduced pressure vector resulting in a simple linear equation system with two variables and two equations. Figure 3.7 depicts the same information as in Figure 3.6 but with the third method, showing an improved accuracy. Despite this, the improvement in the final calculation of the PMEP is almost negligible. Once the intersection

point is estimated with any method, the PMEP is computed as in Equation 3.2 but only with the values that enclose the negative cycle.

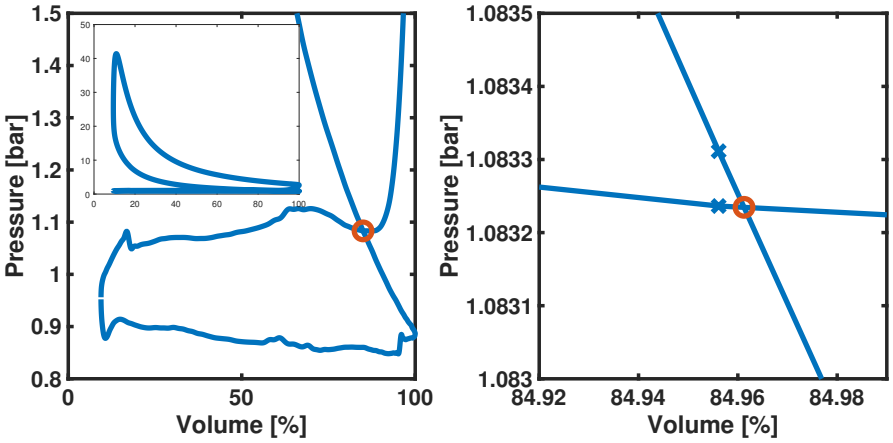

Figure 3.7. *P-V diagram and calculated intersection point for PMEP estimation with method 3.*

3.3.1.2 Knock indicator

One of the major restrictions on the efficiency of gasoline engines is the appearance of abnormal combustion or knock, as explained in subsubsection 2.2.2.5. In this sense, detecting this phenomenon is vital to be able to operate the engine safely and efficiently.

Many methods have been developed to detect knocking cycles in gasoline engines, divided into direct and indirect methods. The direct methods are based on the measurement and treatment of the in-cylinder pressure signal, whereas the indirect methods normally use external sensors to identify knock as in the case of engine block vibration sensors. These sensors are widely used today in gasoline engines due to its practicality, despite being highly affected by noise [9].

However, direct methods are the most accurate and trustworthy, thus the most used in engine testing and investigation [10]. The most employed direct methods to detect knock are based on filtering the in-cylinder pressure signal to detect pressure oscillations with a high or band-pass filter as the MAPO or the IMPO (Integral of Modulus of Pressure Oscillations). MAPO calculates the maximum value of the pressure oscillation for each cycle. Apart from in-cylinder pressure oscillations, knock can also be detected from the heat release

rate due to the increased burning speed that it induces, or from the cylinder resonance [1].

In the case of this PhD-Thesis, MAPO was computed online in the engine test bench for each cylinder ir order to adjust the parameters for safe and efficient operation. Different MAPO limits were set depending on the engine speed. Besides, an automatic control over the spark-timing was set in order to delay it if knock was over a certain limit.

3.3.1.3 Combustion analysis

The in-cylinder pressure signal and the displaced volumen along the engine cycle are very useful for the combustion diagnosis both online in the test bench and for postprocessing. The models used for combustion diagnosis from experimental data usually assume a homogeneous fluid field both in fuel and air distribution and in temperature, so the effect of air entrainment, oil or fuel droplets are not taken into account.

In this PhD-Thesis, a global combustion analysis is made directly linked to the pressure evolution, thus the energy released when the fuel is burned inside the chamber. A single-zone 0D combustion model as the one explained in [11, 12] is used to compute the apparent heat release rate with Equation 3.4. As stated by [13], the wall heat transfer is usually despised for simpleness, so the HRR computed is the net instead of the gross, achieving a typically lower value of around a 15%.

$$HRR = \frac{\gamma}{\gamma - 1} \cdot P_{cyl} \cdot dV + \frac{1}{\gamma - 1} \cdot V \cdot dP_{cyl} \tag{3.4}$$

where γ is the constant pressure to constant volume ratio of specific heats. The choice of this model instead of a complex multi-zone one is justified for simplicity and calculation efficiency, with a little penalty in accuracy. The model used in this PhD-Thesis does not account for spatial variations, so a uniform temperature and composition is assumed and it is expected that temperatures would be underestimated.

The mass fraction burnt (MFB) can be estimated for each crank angle degree as the cumulative sum of the HRR divided by its maximum. In this way, the mass fraction burn is in a range between zero and one. From the MFB profile, the following parameters can be estimated:

- **CA10, CA50 and CA90:** the crank angle degree at which the 10, 50 and 90% of the heat is released respecively. Note that the CA50 is

considered of vital importance for combustion centering since it is the center of gravity, and its value plays a fundamental role on efficiency as explained by [14]. In fact, any CA can be computed.

- **Induction time:** defined as the crank angle degrees from the spark event to the CA10. It represents the initial stages and the firts laminar phase of combustion.
- **TOC:** the time of combustion defined by the difference between CA90 and CA10.

An example of both the HRR (left) and MFB (right) is shown in Figure 3.8 for several engine cycles. Note that the crank angle degree for reference in the x-axis is in the range between negative and positive 360°, so zero is the combustion TDC. In this sense, negative CA values mean that a part of combustion is developed before TDC.

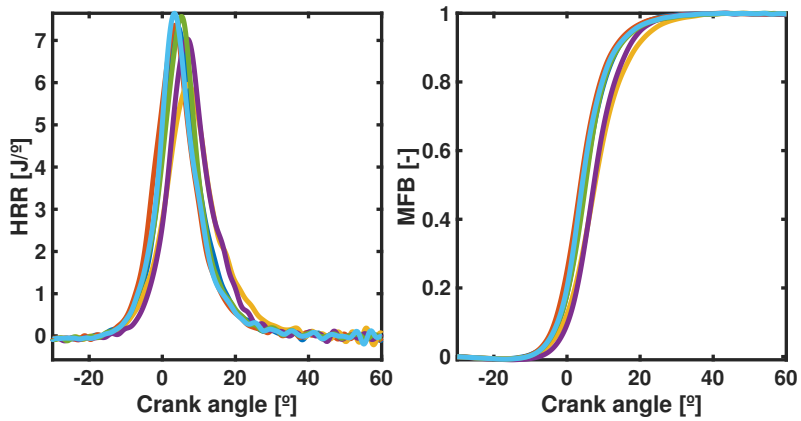

Figure 3.8. *HRR (left) and MFB (right) example for several engine cycles.*

This method was used online during the tests for monitoring of the CA50. During the course of the analysis, the combustion analysis performed based on Equation 3.4 were validated with a thermodynamic model for combustion diagnosis as the one used in [15].

3.3.2 Thermodynamic calculations

In this subsection, some of the thermodynamic based calculations are presented. This calculations were necessary to complete the analysis of the different studies in this PhD-Thesis. Among these calculations stand out: the

specific heat values and ratio of specific heats, the perfect mixing temperature between fresh air and EGR and the compressor efficiency.

The specific heat value at constant pressure, c_p, can be estimated for several species i with the NIST polynomials [16] as in Equation 3.5.

$$c_{p,i} = A + B \cdot t + C \cdot t^2 + D \cdot t^3 + E \cdot t^2 \tag{3.5}$$

where t is the temperature in K divided by one thousand, and the coefficients A-E vary depending on the species and the temperature. Table 3.6 shows the values of the coefficients for carbon dioxide, water, oxygen and nitrogen.

Table 3.6. *Coefficients for thermodynamic properties calculation for several species.*

Species [–]	**Temperature** [K]	**A** [–]	**B** [–]	**C** [–]	**D** [–]	**E** [–]
CO_2	T<1200	24.99735	55.18696	-33.69137	7.948387	-0.136638
	T>1200	58.16639	2.720074	-0.492289	0.038844	-6.447293
H_2O	T<1700	30.092	6.832514	6.793435	-2.53448	0.082139
	T>1700	41.96426	8.622053	-1.49978	0.098119	-11.15764
O_2	T<700	31.32234	-20.23531	57.86644	-36.50624	-0.007374
	700⩽T<2000	30.03235	8.772972	-3.988133	0.788313	-0.741599
	T>2000	20.91111	10.72071	-2.020498	0.146449	9.245722
N_2	T<500	28.98641	1.853978	-9.647459	16.63537	0.000117
	500⩽T<2000	19.50583	19.88705	-8.598535	1.369784	0.527601
	T>2000	35.51872	1.128728	-0.196103	0.014662	-4.553760

The specific heat value of the fluid in question is calculated based on its composition and the specific heats of each species at the fluid temperature. For the air, a composition of 21% of oxygen and 79% of nitrogen is assumed and for the exhaust gas the composition is that of a one step stoichiometric oxidation reaction. Of course, the calculation for the air-EGR mixture will depend strongly on the EGR rate.

To estimate the specific heat value at constant volume, c_v, the Mayer relationship between specific heats and the universal gas constant Ru for ideal gases is used, and the ratio of specific heats, γ, is calculated.

For some studies in this PhD-Thesis, the compressor inlet temperature, T_1, has been computed as a perfect mixture between the fresh air and the EGR mass flow by enthalpy conservation as in Equation 3.6. This calculation was necessary since the mixture between air and EGR was very close to the compressor inlet and the measure was not completely reliable.

$$T_1 = \frac{c_{p,amb} \cdot T_{amb} \cdot \dot{m}_{air} + c_{p,EGR} \cdot T_{EGR} \cdot \dot{m}_{EGR}}{c_{p,1} \cdot (\dot{m}_{air} + \dot{m}_{EGR})} \tag{3.6}$$

where the subscripts amb, air and EGR refer to ambient, air and EGR conditions respectively, T is the temperature of the gas, $\dot{m}$ is the air mass flow and c_p is the specific heat capacity at constant pressure computed depending on the composition and temperature from Equation 3.5. This is an iterative process since $c_{p,1}$ and T_1 are unknown and depend on each other. To initialize the calculation, the experimental measure of T_1 is used. For these studies, the apparent compressor efficiency, η_c, was estimated with Equation 3.7 and using the estimation of T_1.

$$\eta_c = \frac{W_{isen}}{W_{real}} \cdot 100 = \frac{\dot{m} \cdot (c_{p,2isen} \cdot T_{2isen} - c_{p,1} \cdot T_1)}{\dot{m} \cdot (c_{p,2} \cdot T_2 - c_{p,1} \cdot T_1)} \cdot 100 \tag{3.7}$$

where W_{isen} and W_{real} are the isentropic and real compressor work respectively, $\dot{m}_T$ is the total mass flow going through the compressor (sum of air and exhaust gases) and the subscripts 1 and 2 refer to the conditions upstream and downstrem the compressor. T_{2isen} is the isentropic temperature after compression and it is calculated with the isentropic equation.

In addition, for the LP-EGR condensation model explained in subsection 3.4.2, estimations of saturation pressures and temperatures have been used, as well as gas-vapor partial pressures and relative and specific humidities. Equation 3.8 was used to calculate the saturation pressure at a given temperature, T.

$$P_{sat} = 10^{4.6543 - \frac{1435.264}{T + 273.15 - 64.848}} \tag{3.8}$$

From this equation, the saturation temperature at vapor pressure can also be estimated. The partial pressure of vapor at a given pressure, P, was estimated with Equation 3.9.

$$P_{vap} = \frac{P}{1 + 1000 \cdot \frac{MW_{H_2O}}{w \cdot MW_{dry,air}}} \tag{3.9}$$

where w is the specific humidity of the flow, MW_{H_2O} is the molecular weight of water and $MW_{dry,air}$ is the molecular weight of dry air. The relative humidity is obtained with Equation 3.10.

$$RH = \frac{P_{vap}}{P_{sat}} \cdot 100 \tag{3.10}$$

3.4 Modelling tools

In this section, the two modelling tools used for the analysis in this PhD-Thesis are described. First, the 1D engine model used mainly to estimate IGR and the HP-EGR rate is detailed. Second, the model used to assess the problem of sudden dilution due to water condensation is explained.

3.4.1 1D engine model

An engine model has been built and calibrated in the commercial software GT-Power, from Gamma Technologies, in order to predict the behaviour and performance of the engine in several conditions. For this PhD-Thesis, the greatest utility of this model has been to estimate different parameters that are experimentally difficult to obtain, such as the IGR concentration and the HP-EGR rate, as well as to validate and understand different experimental results.

The model is built as closely as possible to the real engine, taking into account the particularities of the systems that it includes, like the EGR lines and VVT system, and respecting the characteristic lengths, diameters and volumes. The compressor and turbine maps are included, particularly the manufacturers maps and the extrapolated and adiabatized ones with the methodology detailed in [17].

Based on the calibration process explained in detail in [18], the model has been used in two different ways, which will be named from now on as fitting and fitted. The fitting model is used in the first steps of calibration. In this model, several parts of the engine are decoupled, the compressor and turbine are unlinked, and the boundary conditions in terms of pressure and temperature are imposed or achieved with PI controllers in the dominant parameter of each. In this way, a faster procedure is obtained and there is no error communication between parts.

The strategy followed with the fitting model can be summarized in six bulletpoints:

- The valve timings are impossed as in the experimental test with the ECU values.
- Pressure at the compressor outlet and exhaust manifold (P_2 and P_3) are impossed independently and the turbocharger is decoupled. The intake manifold pressure (P_2') is controlled by the main engine throttle. With this procedure, all pressures controlling the air renewal process and the trapping ratio are matched. Besides, the pressure downstream the turbine, P_4, is refined with a discharge coefficient.
- The overall heat transfer multiplier inside the cylinder, also known as overall convection multiplier (OCM), is used to refine the final air mass flow through the engine. The same procedure is followed with temperatures and pressures by adjusting the heat transfer multipliers (HTM) and friction multipliers (FM) respectively. Lastly, the FMEP (Friction Mean Effective Pressure) from the experimental side is needed to obtain the engine torque. The FMEP is computed from the IMEP and the BMEP.
- The LP-EGR rate of the test is obtained by changing the position of the main EGR valve and the one located at the intake for choking.
- The fuel injected is computed through the lambda measurement and the air mass flow.
- A Wiebe function [19] reproduces the combustion process by using the spark advance value, the angle at which the 50% of the heat release and the time of combustion, already defined with the CA90 and CA10. These combustion timings are obtained as aforexplained from the in-cylinder pressure recording and the apparent heat release rate calculation with Equation 3.4.

When using the high-pressure EGR, the line is added to the model as in the test bench, with an EGR valve and cooler. Since the injection of the HP-EGR flow is carried out at the WCAC outlet, there is not such a distance that allows a homogeneous mixture and therefore a reliable measure of the rate. For this reason, when there is HP-EGR, the model is adapted so that the position of the HP-EGR valve is set to match the air mass flow, and so the HP-EGR rate is obtained.

All results obtained with the fitting model need to be validated with the experimental test that is reproduced, mainly on air mass flow, intake, exhaust and in-cylinder pressures. A validation of the fitting model is shown in [18].

With the calibration outputs from the fitting model (FM, HTM, OCM, discharge coefficient and FMEP) correlations capable of predicting the dependent variables under different operating conditions are built. For combustion prediction, two strategies have been followed throughout this PhD-Thesis. The first one is the implementation of an artificial neural network (ANN) trained with the fitting tests and introduced in the fitted model. The second is the use of the Wiebe function as in the fitting model but fed with experimental data similar to those that are intended to simulate. Naturally, the accuracy of the fitted model at a given engine point will depend strongly on the points that have been calculated with the fitting model.

Compared to the validation process of the fitting model, the fitted model does not need to be validated for each simulated point, since a general validation is made for several operating conditions. In this sense, a validation of the fitted model is performed in [20] and [21] and shown in Figure 3.9 for the air mass flow (AMF) at the left hand side and IMEP at the right hand side. In this validation, 25 experimental tests were simulated in order to compare the AMF and IMEP for each engine operating condition. A 5% error threshold was set as the maximum acceptable. In Figure 3.9, different errors are considered: the mean percentage error (MPE), the mean absolute percentage error (MAPE) and the maximum error (EMAX).

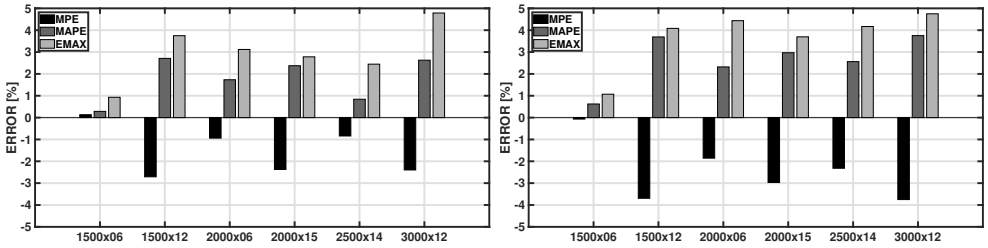

(a) AMF (b) IMEP

Figure 3.9. *AMF (left) and IMEP (right) fitted model validation. Source: Adapted from [21].*

The fitting model is probably the best option to obtain information from experimental tests that have already been performed, since it ensures the obtaining of the parameters in the different parts of the engine and therefore represents the test in a faithful way. For this reason, and the lower computational cost, this model has been used to obtain the IGR concentration and the HP-EGR rate from the steady-state experimental tests. In the case of the fitted model, it is very interesting to predict the behavior of different

parameters when changes are introduced, prior to engine testing. For this reason, in this PhD-Thesis the fitted model was used to predict the pumping losses and IGR concentration depending on the VVT system for several steady-state engine speed and load conditions.

3.4.2 Condensation model

In this section, the psychrometric model developed and validated by Galindo et al. in [22] and [23] is explained, as it will be used to evaluate the problem of dilution induced by water droplets from LP-EGR (section 4.3). This model computes the condensation coming from three different sources in a LP-EGR setup: EGR cooler, EGR mixing with fresh air and the charge cooler, in this case, the WCAC. This worst-case scenario model takes into account an infinite residence time, so it predicts a condensation normally greater than the real one and allows to operate on the safe side. The model can be used to represent real tests or to perform parametric studies, giving a range of values to different variables such as ambient conditions, cooling temperatures, lambda or EGR rates, among others.

To assess condensation, the model computes the specific humidity of ambient conditions in the first place. Then, taking into account the fuel formulation and the fuel to air ratio, the amount of water present in the exhaust gases and the specific humidity of the EGR are calculated taking into account the water present in the air and the one produced during the combustion process. Having these two different streams, the initial conditions of each cooling process are computed. In the case of the EGR cooler, only the exhaust gas coming from combustion is considered. For the mixture of air and EGR, both streams are mixed, taking into account the conditions at the outlet of the EGR cooler previously calculated. In the same way, the result obtained after mixing both flows is taken into account at the WCAC inlet.

From that point on, condensation is computed based on the change of the specific humidity in the different cooling processes. The specific humidity changes depending on the ratio of vapor to gas partial pressures, while the relative humidity depends on the ratio of vapor partial pressure to saturation pressure.

For the EGR cooler, the partial pressure of vapor and the saturation temperature at that conditions are estimated. The saturation temperature is compared to the temperature at the EGR cooler outlet, leading to condensation if the outlet temperature is lower. In general terms, the saturation temperature is around 50°C for normal operating conditions, so condensation does not appear since the EGR cooler is fed by the main engine cooling circuit, at about

90°C, keeping the relative humidity constant. In the event that the outlet temperature is lower, the saturation pressure is obtained at this temperature together with the vapor and gas pressures, taking into account that the total pressure is kept constant. In this way, the relative humidity is reduced due to condensation. The total flow of EGR is reduced since part of the vapor has condensed, while the gas side remains constant. From the change in specific humidity and the EGR gas flow, the amount of condensed water is calculated with Equation 3.11:

$$\dot{m}_{cond,cooler} = \dot{m}_{dry,EGR} \cdot \frac{w_{in,cooler} - w_{out,cooler}}{1000} \tag{3.11}$$

where $\dot{m}_{dry,EGR}$ is the amount of dry mass flow in the exhaust gas and $w_{in,cooler}$ and $w_{out,cooler}$ are the specific humidities at the inlet and outlet of the EGR cooler respectively.

After the EGR cooler, the two flows are mixed upstream the compressor and condensation can occur by mixing. Considering the composition of the EGR downstream the cooler, the composition of the mixture between both flows is calculated taking into account the gas and vapor parts of each. In the same way, the specific humidity of the mixture is calculated with the proportion of mass flow and humidity of air and EGR. The temperature and enthalpy of mixture are also calculated. From this point, the saturation pressure at the mixture temperature and the relative humidity are estimated. If the relative humidity is 100% or higher, saturation occurs.

If the water vapor present in the mixture condenses, heat is released, changing the temperature of the mixture and therefore affecting the condensation process itself. For this reason, the specific humidity of the mixture, w_{mix}, is calculated with an iterative process taking into account that the enthalpy of the mixture remains constant. In this way, the amount of condensed water due to mixing is computed with Equation 3.12:

$$\dot{m}_{cond,mix} = \frac{\dot{m}_{dry,EGR} \cdot w_{out,cooler} + \dot{m}_{dry,air} \cdot w_{air} - \dot{m}_{dry,mix} \cdot w_{mix}}{1000} \tag{3.12}$$

where the subscript EGR refers to exhaust gas, air to air and mix to mixture. Note that $\dot{m}_{dry,mix}$ is the sum of the dry mass flow of EGR and air.

In the case of the WCAC, the problem is approached very similarly to the EGR cooler. It is assumed that all the water condensed first in the EGR cooler and then by mixing has evaporated due to the compression process that

the mixture undergoes in the compressor. Then, the specific humidity of the mixture at the WCAC inlet is estimated taking into account the relationship between partial pressures of vapor and gas. Then, the saturation pressure and temperature are estimated and the latter is compared with the outlet temperature of the WCAC, so that if the WCAC outlet temperature is lower than the saturation limit, there is condensation.

If there is condensation, the saturation and partial pressures are calculated at the outlet temperature of the WCAC to obtain the specific humidity. The amount of condensed water is determined with Equation 3.13:

$$\dot{m}_{cond,WCAC} = \dot{m}_{dry,WCAC} \cdot \frac{w_{in,WCAC} - w_{out,WCAC}}{1000} \tag{3.13}$$

Bibliography

[1] Pla B., De la Morena J., Bares P. and Jiménez I. "Knock Analysis in the Crank Angle Domain for Low-Knocking Cycles Detection". *SAE Technical Papers*, Vol. 2020-April n^o April, pp. 1–11, 2020.

[2] Piqueras P., De la Morena J., Sanchis E. J. and Pitarch R. "Impact of Exhaust Gas Recirculation on Gaseous Emissions of Turbocharged Spark-Ignition Engines". *Applied Sciences*, pp. 1–17, 2020.

[3] Zhang Z., Wang T., Jia M., Wei Q., Meng X. and Shu G. "Combustion and particle number emissions of a direct injection spark ignition engine operating on ethanol/gasoline and n-butanol/gasoline blends with exhaust gas recirculation". *Fuel*, Vol. 130, pp. 177–188, 2014.

[4] Randolph E., Fieseler K., Conway G., Alger T. and Chadwell C. "The Effects of EGR Composition on Combustion Performance and Efficiency". *SAE Technical Papers*, n^o 2020, pp. 1–12, 2020.

[5] Vianna J. N. De S., Reis A. Do V., Oliveira A. B. De S., Fraga A. G. and De Sousa M. T. "Reduction of pollutants emissions on SI engines - Accomplishments with efficiency increase". *Journal of the Brazilian Society of Mechanical Sciences and Engineering*, Vol. 27 n^o 3, pp. 217–222, 2005.

[6] Galindo J., Dolz V., Monsalve-Serrano J., Bernal Maldonado M. A. and Odillard L. "Advantages of using a cooler bypass in the low-pressure exhaust gas recirculation line of a compression ignition diesel engine operating at cold conditions". *International Journal of Engine Research*, Vol. 22 n^o 5, pp. 1624–1635, 2021.

[7] Benajes J., Olmeda P., Martín J. and Carreño R. "A new methodology for uncertainties characterization in combustion diagnosis and thermodynamic modelling". *Applied Thermal Engineering*, Vol. 71 n^o 1, pp. 389–399, 2014.

[8] Gopujkar S., Worm J., and Robinette D. "Methods of Pegging Cylinder Pressure to Maximize Data Quality". *SAE Technical Papers*, 2019.

[9] Zhen X., Wang Y., Xu S., Zhu Y., Tao C., Xu T. and Song M. "The engine knock analysis - An overview". *Applied Energy*, Vol. 92, pp. 628–636, 2012.

[10] Shu G., Pan J. and Wei H. "Analysis of onset and severity of knock in SI engine based on in-cylinder pressure oscillations". *Applied Thermal Engineering*, Vol. 51 n^o 1-2, pp. 1297–1306, 2013.

[11] Shiao Y. and Moskwa J. J. "Cylinder Pressure and Combustion Heat Release Estimation for SI Engine Diagnostics Using Nonlinear Sliding Observers". *IEEE Transactions on Control Systems Technology*, Vol. 3 n^o 1, pp. 70–78, 1995.

[12] Mauro S., cSener R., Gül M. Z., Lanzafame R., Messina M. and Brusca S. "Internal combustion engine heat release calculation using single-zone and CFD 3D numerical models". *International Journal of Energy and Environmental Engineering*, Vol. 9 n^o 2, pp. 215–226, 2018.

[13] Brunt M. F. J. and Platts K. C. "Calculation of heat release in direct injection diesel engines". *SAE Technical Papers*, n^o 724, 1999.

[14] Lavoie G. A., Ortiz-soto E., Babajimopoulos A., Martz J. B. and Assanis D. N. "Thermodynamic sweet spot for high- efficiency , dilute , boosted gasoline engines". *International Journal of Engine Research*, Vol. 14 n^o 3, pp. 260–278, 2012.

[15] Martín J. *Aportación al diagnóstico de la combustión en motores Diesel de inyección directa*. 2007.

[16] Eric W. L., Mark O. M. and F. Daniel G. "Thermophysical Properties of Fluid Systems". *NIST Chemistry WebBook, NIST Standard Reference Database Number 69*, 2021.

[17] Serrano J. R., Arnau F. J., García-Cuevas L. M., Gómez-Vilanova A., Guilain S. and Batard S. "A Methodology for Measuring Turbocharger Adiabatic Maps in a Gas-Stand and Its Usage for Calibrating Control Oriented and One-Dimensional Models at Early ICE Design Stages". *Journal of Energy Resources Technology*, Vol. 143 n^o 4, pp. 1–11, 2021.

[18] Serrano J., Climent H., Navarro R. and González-Domínguez D. "Methodology to Standardize and Improve the Calibration Process of a 1D Model of a GTDI Engine". *SAE Technical Papers*, Vol. 2020-April n^o April, pp. 1–13, 2020.

[19] Ghojel J. I. "Review of the development and applications of the Wiebe function: A tribute to the contribution of Ivan Wiebe to engine research". *International Journal of Engine Research*, Vol. 11 n^o 4, pp. 297–312, 2010.

[20] Galindo J., Climent H., De la Morena J., González-Domínguez D., Guilain S. and Besançon T. "Experimental and modeling analysis on the optimization of combined VVT and EGR strategies in turbocharged direct-injection gasoline engines with VNT". *Proceedings of the Institution of Mechanical Engineers, Part D: Journal of Automobile Engineering*, Vol. 235 n^o 10-11, pp. 2843–2856, 2021.

[21] Climent H., Dolz V., Pla B. and González-Domínguez D. "Analysis on the potential of EGR strategy to reduce fuel consumption in hybrid powertrains based on advanced gasoline engines under simulated driving cycle conditions". *Energy Conversion and Management*, Vol. 266 n^o June, pp. 115830, 2022.

[22] Galindo J., Navarro R., Tari D. and Moya F. "Development of an experimental test bench and a psychrometric model for assessing condensation on a low-pressure exhaust gas recirculation cooler". *International Journal of Engine Research*, Vol. 22 n^o 5, pp. 1540–1550, 2021.

[23] Galindo J., Gil A., Navarro R. and García-Olivas G. "Numerical assessment of mixing of humid air streams in three-way junctions and impact on volume condensation". *Applied Thermal Engineering*, Vol. 201, 2022.

Chapter 4

Cooled low-pressure EGR system impact on engine operation

Contents

In the present chapter, the effects of a cooled low-pressure EGR system on engine operation is studied. First, the tolerance to EGR addition and the influence of calibration of different parameters is assessed in section 4.1. Two different operating conditions are studied in depth to analyse the effect of EGR on emissions and catalyst operation. In a second step, the effects of LP-EGR and IGR on emissions and efficiency are decoupled in section 4.2, with special attention to emissions, pumping work, combustion and heat transfer losses. Lastly, the problem of water condensation is studied in section 4.3. The water content in recirculated exhaust gases can condense when these gases undergo a cooling process, either in the EGR cooler, when mixed with fresh air or in the intercooler, in this case a WCAC. This condensation can cause a sudden dilution inside the cylinder which can result in combustion instability, altering emissions, efficiency and drivability.

4.1 EGR tolerance and influence of calibration

The main goal of this experimental campaign is to assess the impact and effects of EGR addition on a direct injection spark-ignition engine, its tolerance and influence on the optimal calibration depending on the operating conditions. To perform this analysis, a design of experiments for the spark timing, intake and exhaust VVT system was implemented experimentally at several levels of EGR in the search for the optimal calibrations for fuel consumption. The air-to-fuel ratio was kept constant for every test at stoichiometic conditions according to probe upstream of the aftertreatment, previously calibrated in the ECU for operation without EGR. Several steady-state points were tested, defined by the engine speed and BMEP. The results of this study were useful to understand the interaction between EGR and IGR, the tolerance to EGR inclusion and the influence of the calibration of the VVT system and the spark timing.

Besides, the results of this study in terms of emissions are also included in subsection 4.1.2 in order to assess the direct impact of exhaust recycle on emissions and oxygen concentration in the exhaust. Given the composition of the gases that result from combustion with EGR addition, with lower NO_x and O_2 concentrations and higher hydrocarbons compared to no EGR operation, the capability of the aftertreatment system to oxidize hydrocarbons and carbon monoxide is studied in subsection 4.1.3.

The engine operation in this DoE methodology is not only affected by exhaust recirculation, but by the VVT settings, affecting the air renewal process and pumping work but also changing the concentration of IGR, even more at low loads, and by the spark activation, due to the in-cylinder

temperature and combustion speed. Due to the number of parameters of the DoE, a high number of tests is needed in order to have sufficient and representative combinations of the parameters and to develop a meaningful appraisal. Figure 4.1 shows the tested points for 1500 rpm at 6 bar BMEP as an example of the DoE.

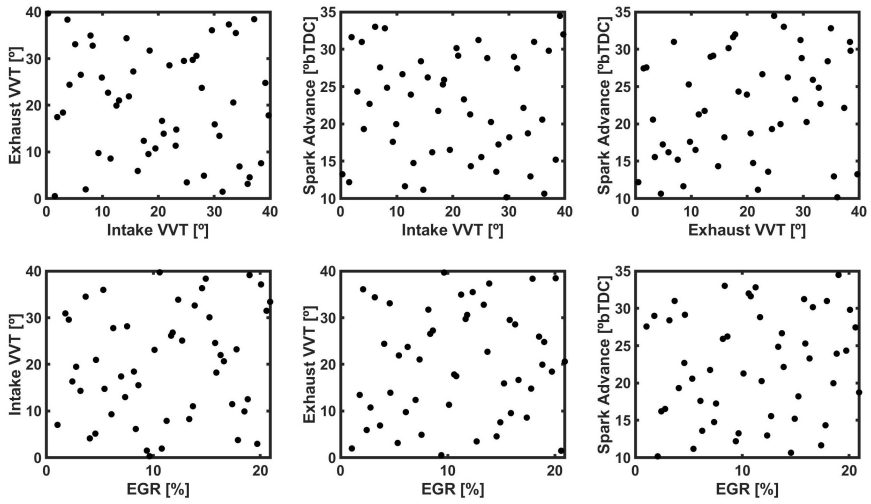

Figure 4.1. *Example of 1500 rpm at 6 bar BMEP DoE combination of parameters.*

This DoE is performed at several operating conditions, from 6 to 15 bar BMEP and from 1500 to 3000 rpm. With this DoE, the optimal calibration for fuel consumption of the aforementioned parameters is obtained for several EGR rates, from zero to maximum recirculating rate possible. In order to perform the DoE, the boundaries for each parameter need to be set both in the high and the low limit. For the VVT system, the boundaries are set for safety reasons, avoiding contact between piston and valves. The limits for the EGR and the spark timings are based on previous experience. At low loads, high EGR rates and low spark advance are excluded to avoid misfires and excessive instabilities. For high load operation, low recirculation rates and great spark advances were avoided for knock. From a functional approach, the throttle and VGT positions were changed individually for each test in order to keep the given load with the other parameters already set. Table 4.1 shows the upper and lower boundaries tested in the DoE for each engine condition.

Table 4.1. *Definition of the DoE parameters for each engine point.*

Engine Point rpm - bar	**VVT Intake & Exhaust** [º]	**Spark Advance** [º bTDC]	**EGR rate** [%]
1500 - 6	0 - 40	10 - 35	0 - 28
1500 - 12	0 - 40	0 - 20	0 - 33
2000 - 6	0 - 40	5 - 35	0 - 28
2000 - 15	0 - 40	-5 - 25	0 - 32
2500 - 14	0 - 40	0 - 35	0 - 35
3000 - 12	0 - 40	3 - 32	0 - 25

When the tests are completed and data processed as explained in subsection 3.3.1, if a test does not comply with both the stability and knock criteria, it is removed from the study. The stability criterion depends on the COV of the IMEP computed with Equation 3.3 with 200 cycles for each cylinder, with limit values depending on the engine BMEP. A limit of 3.33% was set for 6 bar BMEP tests and 2% for any higher load. For knock assessment, the MAPO parameter is computed as explained in subsubsection 3.3.1.2. With 200 cycles acquired for each cylinder, the limit was set at a maximum of 3% of the cycles over a 0.5 bar limit, based on previous tests for knock characterization.

With the DoE performed, surface response models are built in order to analyse the effect of the VVT settings, the spark timing and the EGR rate on efficiency. In this way, the best calibrations with the models are obtained and reduced DoEs in the areas of interest are performed, following the same methodology. At this stage, the optimization is done considering only the specific fuel consumption, since regulated emissions are assumed to be abatable by the aftertreatment system.

The 1-D model explained in subsection 3.4.1 in its fitting configuration was used in order to represent the tests and compute the IGR rate in the low load tests due to its higher concentration, thus interaction with EGR and importance for the analysis.

A deep analysis of the results is performed for two keypoints in terms of engine operation which are also representative of medium and low load operation. This selection is also made due to the different behaviour in terms of IGR and turbocharging. For this engine, and in general terms since it greatly

depends on the engine speed, the throttling area is up to approximately 10 bar BMEP. In this area, the variation of IGR with the VVT system is notably higher than that from the turbocharger area, beyond 10 bar BMEP. The two conditions need to be analysed separately due to the different implication of EGR and IGR on emissions and calibration as well as EGR tolerance.

4.1.1 Optimal calibration analysis

The optimal calibration for each EGR rate in terms of VVT settings and spark timing is depicted in Figure 4.2 for a medium load condition, 3000 rpm at 12 bar BMEP. As previously stated, 0-0 values on the VVT settings represent the minimum possible overlap for security. This configuration is the optimal found for operation without EGR. However, for greater EGR rates, the exhaust setting is fixed at zero, but an anticipation in the intake valve is observed. Besides, the spark timing is, as expected, advanced significantly with EGR in order to compensate the lower combustion speed and with the increased margin as the knock probability is reduced.

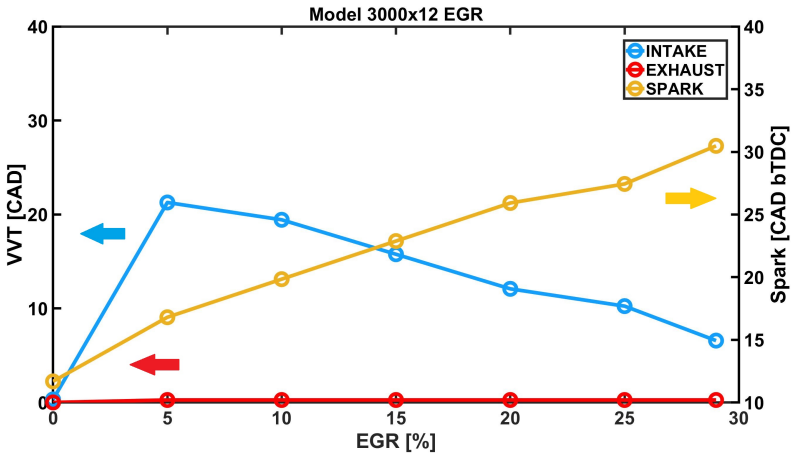

Figure 4.2. *Optimal calibration for fuel consumption achieved with DoE methodology for 3000 rpm at 12 bar BMEP.*

The recirculability limits at this engine speed and load are around a 30%. This rate is in the range of the expected since there is still margin from boosting side and the main limits are found on the peak pressures inside the cylinder and the combustion stability. The BSFC and pumping losses for this EGR sweep are depicted in Figure 4.3 as a variation with respect to no EGR operation. Results show a reduction in both parameters with the limit of stable operation

for BSFC and the greater VGT settings needed from 15% EGR, increasing PMEP.

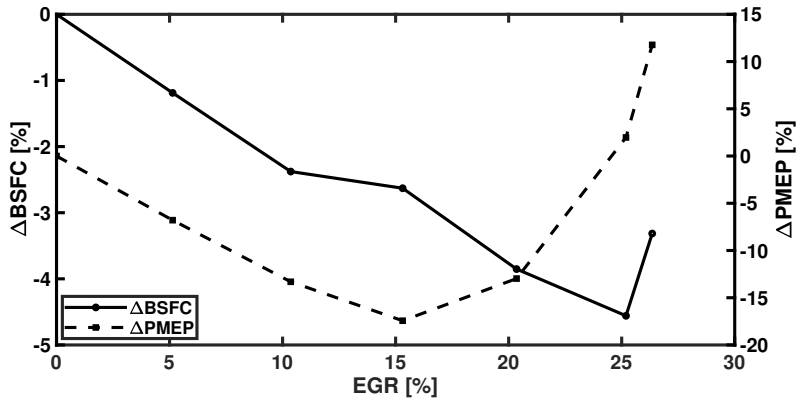

Figure 4.3. *$\Delta BSFC$ (left axis) and $\Delta PMEP$ (right axis) evolution with EGR for 3000 rpm at 12 bar BMEP.*

The condition of 1500 rpm at 6 bar BMEP is also studied in this section. For this conditions, the load is fully controlled by the main throttle position. For this reason, if the DoE methodology is followed, the results tend to produce calibrations with high overlap and the VVT settings at 40. This is explained by the fact that greater overlaps lead to lower volumetric efficiencies, which are desired at low loads to operate with higher intake pressures, thus higher throttle openings to reduce pumping work. Despite the higher intake pressure and the similar level of exhaust pressure, the longer period of opened cycle is translated into higher IGR rates due to the huge pressure differential at this load. This condition is observed in Figure 4.4, where the IGR concentration computed with the 1-D model is shown for 0 and 20% EGR.

The maximum IGR concentration, up to 25% is achieved at this condition, with great overlaps, compared to values of 5% for minimum overlap. For greater EGR percentages, the trend with the VVT system is maintained but achieving lower concentrations since a higher intake pressure is needed for the same load, and a lower pressure differential across the intake and exhaust valves is obtained, which can promote a more efficient scavenging process. This great variation of the residuals with the VVT is not observed in the case of 3000 rpm, where also lower residuals are obtained given the higher engine load.

The lower IGR concentration found with lower overlap, at 0-0 condition of the VVT, is translated into the chance to recirculate greater EGR rates compared to a great overlap condition. This is explained by the fact that

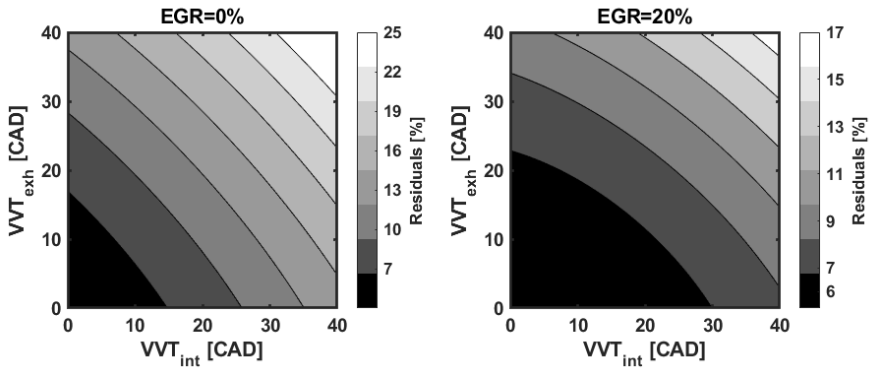

Figure 4.4. *IGR concentration depending on the VVT settings for 1500 rpm at 6 bar BMEP for 0% (left) and 20% EGR (right).*

combustion stability is mostly affected by the total concentration of residuals, or the RGF, computed as the sum of IGR and EGR. In this sense, there could be an interest to increase the EGR rate by reducing the IGR to keep the RGF, observing a gross indicated efficiency increase due to lower heat transfer losses compared to more IGR concentration. This is shown in Figure 4.5, where an EGR sweep at minimum overlap (orange) and another at maximum overlap (blue) are displayed. Note that the pumping losses are represented taking as reference the value at 0% of EGR with maximum overlap.

Indeed, results show the higher EGR rate achieved with low overlap compared to high overlap. This is translated into higher gross indicated efficiencies despite pumping work is deteriorated with lower throttle openings. Again, the maximum recirculable rate is around 30% as explained for medium load conditions, but in this case it is highly dependent on the IGR concentration and the VVT system for stability reasons. The BSFC evolution with EGR for both configurations is shown in Figure 4.6, showing that the higher IGR concentration brings dilution benefits for the greatest overlap condition at low EGR rates. Besides, as EGR is introduced and the total RGF equalizes between settings, fuel efficiency reach similar levels.

Table 4.2 shows the best VVT settings found for each operating condition, together with the maximum amount of EGR achieved and the main limit to increase the rate. Note that, out of the seven conditions tested, three were limited by combustion instabilities (COV). Another condition was limited by boosting, being unable to maintain the engine load if more EGR was introduced (VGT) and another condition was limited by the delta pressure between the

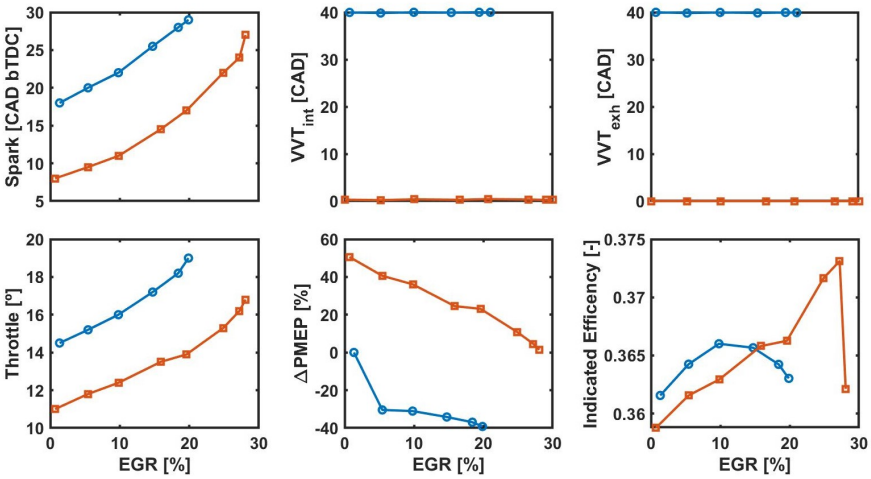

Figure 4.5. *EGR sweep with minimum (orange) and maximum (blue) overlap for 1500 rpm at 6 bar BMEP.*

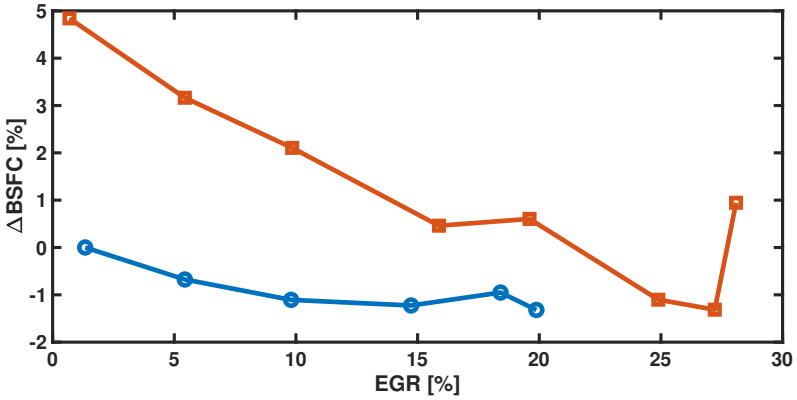

Figure 4.6. *ΔBSFC evolution with EGR for minimum (orange) and maximum (blue) overlap for 1500 rpm at 6 bar BMEP.*

ends of the circuit (ΔP).The in-cylinder pressure limit was only reached in one operating condition (P MAX) and the maximum power output condition was limited by the increase in the compressor outlet temperature (T2).

Table 4.2. *LP-EGR VVT settings and recirculability limits for each operating condition.*

Engine	**VVT**	**LP-EGR**	
Point	Int - Exh	Max EGR rate	Limit
rpm - bar	[º]	[%]	[-]
1500 - 6	0 - 0	30	COV
1500 - 12	14 - 3	30	VGT
2000 - 6	0 - 0	26	COV
2000 - 15	17 - 8	29	P MAX
2500 - 14	29 - 2	29	COV
3000 - 12	18 - 2	25.5	ΔP
4500 - 19	40 - 0	19	T2

4.1.2 EGR effects on engine-out emissions

Following the methodology and the study presented in section 4.1, this section includes the emission analysis from the corresponding tests, and it is divided following the same structure. The main objective of the study was to analyse the EGR recirculability limits and the influence on the optimal calibration for fuel economy. However, a deep analysis of the emissions with EGR was also carried out in order to understand the impact of EGR on gaseous emissions.

4.1.2.1 Medium load operation

The results of the optimal EGR sweep in emissions is shown in Figure 4.7 in variation respect with the calibration without EGR, so that values for 0% EGR is always 0. The most obvious result is, as expected, the evolution of NO_x emissions on the top left part of the figure. The lower concentration of oxygen together with the lower temperatures obtained due to the increased heat capacity of the mix between fresh air and EGR are the main factors on reducing NO_x formation as stated by the Zeldovich mechanism in Equation 2.12. For hydrocarbon emissions, shown in the bottom left of the figure with solid line, the results are mainly affected by quenching and the lower temperatures inside the cylinder, following the opposite trend to NO_x. For higher EGR rates, the flame speed is decreased, mainly in the laminar section, as can be observed

in the graph with the induction time, in dashed lines in the right axis. The induction time is the time that elapses between the spark timing and the release of 10% of the cumulative heat. This part of the process is mainly the initial kernel formation and development, which is very influenced by laminar conditions and the flow structure around the spark plug [1]. For the oxygen content, on the top right side of the figure with solid line, the oxygen concentration is mainly influenced by quenching, since operation is always around lambda equal to one. In this sense, for higher quenching distance, higher oxygen levels should be obtained since there is a higher volume of the mixture unburned going through the exhaust valves. However, the oxygen concentration is naturally reduced with the EGR rate, which is the main result obtained being this the dominant factor. The COV is also displayed in this figure with dashed lines in the right axis, showing a general trend to increase with EGR, as expected.

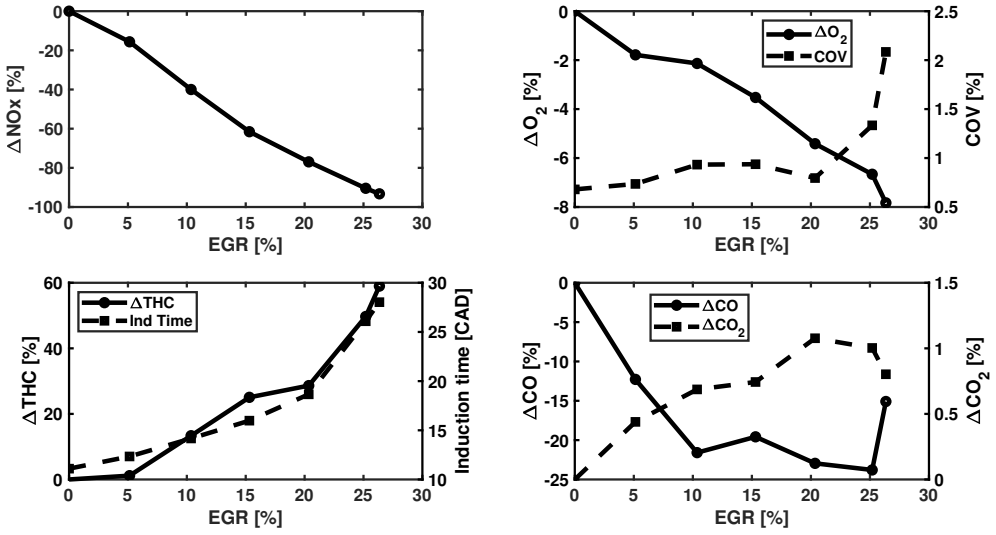

Figure 4.7. *Main exhaust emissions evolution with EGR rate for 3000 rpm at 12 bar BMEP.*

For carbon monoxides, in the bottom right part of the figure, the evolution is more complex and affected by several opposing factors. The concentration of carbon monoxides is mainly dependent on the oxidation reaction of carbon monoxide to carbon dioxides and its kinetics, as reflected by the opposite trends of both species in the figure. As the EGR rate increases and the oxygen concentration is reduced, the equilibrium of the oxidation reaction

would change to a greater carbon monoxide concentration due to the lack of oxygen to fully oxidize carbon. Nonetheless, two factors are contrary to this one. The dissociation of carbon dioxides is reduced with reduced combustion temperatures, thus greater EGR rates promote that the CO_2 formed remains unchanged. Moreover, the kinetics of the oxidation reaction are also reduced with lower temperatures. These two effects, oxygen concentration and temperature, are reduced with EGR and govern the final concentration of CO with opposite results. However, it must be taken into account that the interaction of these effects with the temperature evolution due to the combustion development has also an impact on CO formation, so that spark timing and VVT variations may also affect.

4.1.2.2 Low load operation

For the lower load and engine speed, the EGR sweep with the highest possible overlap is studied and the emissions are shown in Figure 4.8 with the same structure as in Figure 4.7.

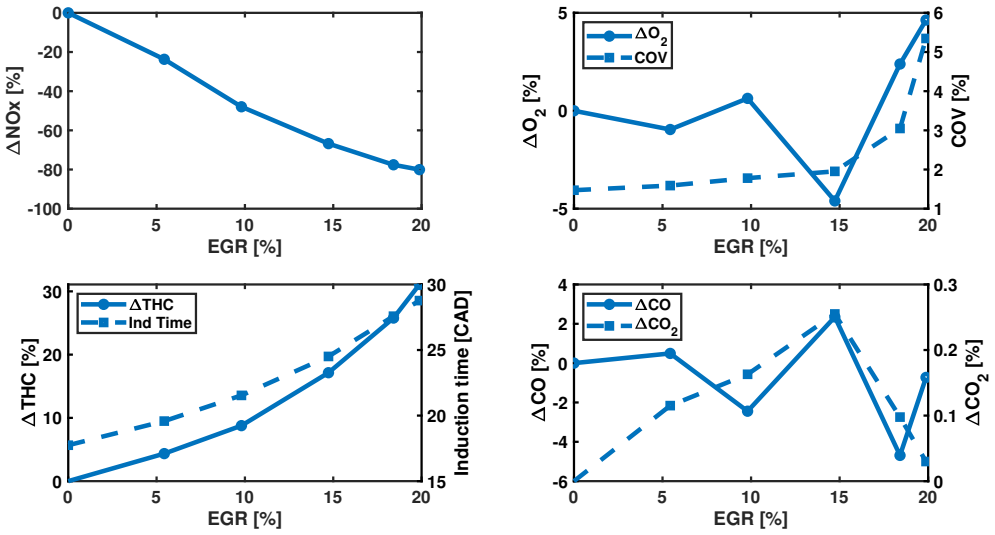

Figure 4.8. *Main exhaust emissions evolution with EGR rate for 1500 rpm at 6 bar BMEP and maximum overlap.*

As expected, NO_x emissions are linked to the in-cylinder temperature evolution and the oxygen available in the unburned zone. With the reduction of both with the EGR, the nitrogen oxides are monotonously reduced. Hydrocarbon concentration is again the result of the impact of EGR on

reducing flame propagation speed and increasing quenching, lengthening the time needed to develop the flame kernel as seen on the induction time and increasing HC emissions. For the oxygen content, different trends can be observed at several ranges of exhaust recycle. For low to mid EGR rates, the oxygen concentration is almost constant and does not depend on the exhaust recycle. This trend is opposite to that observed at medium load in the figure Figure 4.7. The explanation for this is the huge effect of IGR at low load, which was almost negligible at medium load. As already explained and seen in Figure 4.4, IGR concentration is reduced at a constant VVT setting when the rate of exhaust recycle is increased due to a higher intake pressure and the reduced pressure differential between intake and exhaust, so the oxygen content trend is compensated. For EGR rates beyond 10%, the oxygen concentration is reduced. Moreover, the combustion stability is highly affected by the amount of residuals inside the chamber for greater EGR rates, leading to a higher increase in the COV than the one seen at medium load and increasing the oxygen content due to incomplete combustion. All this changes highly affect the equilibrium of carbon monoxide to carbon dioxides, as aforexplained.

The fact that IGR concentration is a dominant factor in emissions for maximum overlap, it is interesting to study the opposite configuration, minimum overlap and a lower concentration of IGR. The minimum overlap EGR sweep is shown in solid lines and compared to the previous one in dashed lines in Figure 4.9. The 0% EGR test of the maximum overlap is the one used as the datum for all data shown in percentage.

The first difference between both EGR sweeps that draws attention is the amount of EGR that is recirculated with an stable condition. With a lower IGR concentration in the minimum overlap sweep, the EGR rate can be increased to 25% within stability limits, whereas the interaction with residuals in the maximum overlap sweep shows stability problems around 15%. This is observed in the COV of the IMEP. For NO_x emissions, a clear increase is observed as the IGR concentration is reduced with minimum overlap due to the lower amount of total residuals. This trend is reversed when the EGR rate reaches 25%, so that the amount of EGR and IGR is similar to that of 20% EGR with maximum overlap. This explanation fits with the IGR prediction in Figure 4.4. For HC concentration, the lower IGR concentration is translated into a faster propagation of the flame kernel, thus a faster combustion and lower emissions. However, as EGR is introduced, the emissions are increased for both sweeps with a similar growth and the same level is finally achieved when the RGF reaches its maximum. Besides, the lower IGR concentration leads to a CO reduction and the increase of CO_2 with EGR, whereas lower levels of of both are obtained in the end. These results conclude that the

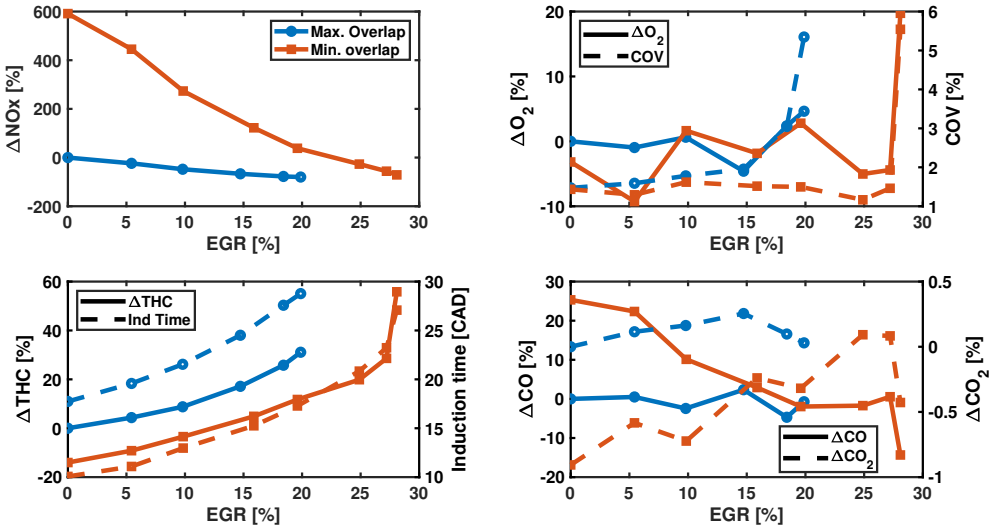

Figure 4.9. *Main exhaust emissions evolution with EGR rate for 1500 rpm at 6 bar BMEP. Solid line: minimum overlap; Dashed line: maximum overlap.*

emissions obtained with exhaust recycle are much affected by the IGR rate and the total RGF than the operating point.

4.1.2.3 Other operating conditions

In this section, other operating conditions apart from the low and medium load are assessed in terms of emissions following the methodology and study explained in section 4.1. Table 4.3 summarizes the impact of EGR addition on NO_x, HC and CO emissions by comparing operation without EGR and with the maximum rate obtained for all operating conditions tested in the study. Note that for low load operation at 1500 rpm, the two sweeps studied in subsubsection 4.1.2.2 are included.

Table 4.3. *Comparison of emissions for different operating conditions with 0% and maximum EGR.*

Engine Point rpm - bar	**EGR** [%]	**NO_x** [ppm]	**HC** [ppm]	**CO** [ppm]
1500 - 6 bar (max. overlap)	0	401	2306	5938
	19.9	80	3023	5895
1500 - 6 bar (min. overlap)	0	2777	1982	7442
	28.0	116	2965	5087
2000 - 6 bar	0	1006	1926	6988
	27.7	155	2687	5171
1500 - 12 bar	0	2645	1366	6306
	24.6	392	1987	5162
2000 - 15 bar	0	2764	1230	8158
	27.4	185	1700	7592
2500 - 14 bar	0	3359	1138	5271
	28.8	187	1821	5200
3000 - 12 bar	0	3240	1196	6310
	26.3	218	1902	5358

The three engine points at the top of Table 4.3 are the low engine and load points tested. For the 2000 rpm tests, the optimization process achieved the optimal calibration at a high overlap condition for without exhaust recycle, whereas the overlap was reduced for the maximum EGR rate, as expected due to the similarity with the 1500 rpm studied in the previous section. This also explains the maximum EGR rate achieved with minimum overlap for both engine points. With this conditions, the IGR rate maintains NO_x emissions at a low level without EGR, and this emission is further reduce with the addition of external EGR owing to lower temperatures at combustion start and during the cycle. The increase of hydrocarbons and the reduction of carbon monoxides with EGR is similar to that explained for 1500 rpm.

The remaining four rows are higher loads, 12 bar for 1500 and 3000 rpm, 14 bar for 2500 rpm and 15 bar for 2000 rpm. The IGR concentration is directly reduced as the load increases, and there is less sensitivity to control them with the VVT settings. For this reason, the results shown are similar to those from minimum overlap in the low bar of BMEP cases. The effect of EGR on NO_x is more important, achieving a significant rate of emission reduction around

one order of magnitude. Moreover, EGR addition is also capable of reducing carbon monoxides in a lower to a lesser degree than nitrogen oxides and to increase the hydrocarbons formation.

4.1.3 Impact on catalyst performance

Based on the results obtained in subsubsection 4.1.2.2 and subsubsection 4.1.2.1, there is a growing need to study the remaining potential of the catalyst to fulfil its function of almost completely oxidizing hydrocarbons and carbon monoxides due to the change in the composition of the exhaust gases caused by EGR addition. These exhaust gases have a lower concentration of nitrogen oxides and pure oxygen together with lower temperatures compared to the normal exhaust gas expected from a gasoline engine due to the effects previously studied, difficulting the oxidation process.

With this aim, the theoretical capability of the catalyst to oxidize carbon monoxides and hydrocarbons under these new conditions of NO_x, O_2 and temperature reduction was assessed with an stoichiometric calculation of the required oxygen mass flow in Equation 4.1.

$$\dot{m}_{O_2,req} = \left[\frac{1}{2}\frac{\dot{m}_{CO}}{MW_{CO}} + \left(n + \frac{m}{4}\right)\frac{\dot{m}_{HC}}{MW_{HC}} - \frac{1}{2}\frac{\dot{m}_{NO}}{MW_{NO}}\right] MW_{O_2} \tag{4.1}$$

In Equation 4.1, $\dot{m}_{O_2,req}$ is the oxygen mass flow needed to completely oxidize carbon monoxides and hydrocarbons. The main assumption is that all NO is converted into NO_2 and then reduced to pure nitrogen during the oxidation of hydrocarbons and carbon monoxides. Following with the equation, $\dot{m}_i$ is the mass flow rate and MW_i is the molecular weight respectively of species i. The composition of the unburned hydrocarbons is determined by n and m, being these the number of atoms of carbon and hydrogen respectively. For the study, it is assumed that hydrocarbons are dimethylbutadiene based on previous studies, so that the composition is C_6H_{10}.

As stated, the lower concentration of NO_x and O_2 together with the lower temperatures at the exhaust achieved with EGR and the increased hydrocarbons could suppose a great difficulty for the catalyst to fulfill its function. Moreover, computing the conversion efficiency of the catalyst would not be realistic since its principles of operation are changed and a new catalyst, more focused or similar to a DOC should be implemented.

Figure 4.10 shows the analysis of the catalyst performance on the 3000 rpm at 12 bar BMEP EGR sweep in subsubsection 4.1.2.1. In this figure,

the oxygen mass accumulated during 60 seconds in the test (dashed line) is compared to the oxygen mass flow needed in order to fully oxidize hydrocarbons and carbon monoxides (solid line) computed with Equation 4.1. Besides, the lambda measured experimentally is included in green.

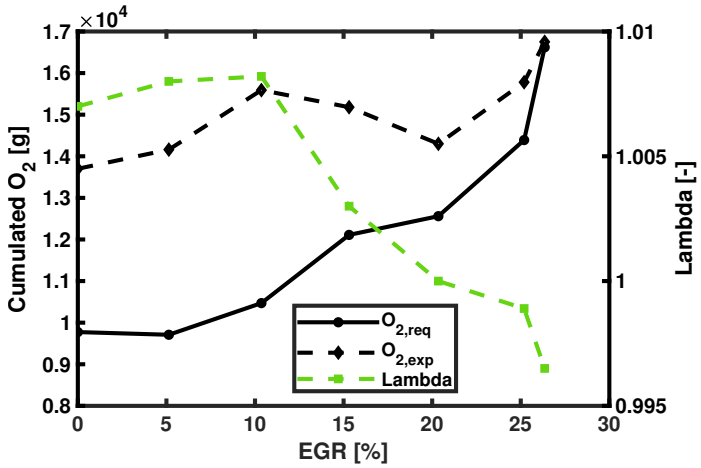

Figure 4.10. *Catalyst performance for 3000 rpm at 12 bar BMEP EGR sweep.*

For lower EGR rates, the difference between the oxygen available and the needed is very high, so that there should be no problem at all in the catalyst. As the EGR rate is increased, the difference is notably reduced due to the increase in hydrocarbons and the reduced NO_x emissions, so a reduced margin is obtained. The reduction of carbon monoxides that is observed up to this point is also playing an important role since it is a compensating factor for the lack of oxygen in the exhaust, so full oxidation is still possible. When EGR reaches its maximum and carbon monoxides increase, the oxygen required and available are almost equal. This is translated into the recommendation to have a slightly lean operation for high EGR rates, even more if the huge reduction in nitrogen oxides with EGR is considered. It must be said that the small margin found in the maximum EGR rate may be also influenced by the slight rich lambda found in this test.

The same study repeated for the 1500 rpm at 6 bar BMEP EGR sweeps in subsubsection 4.1.2.2. Following the structure in Figure 4.10, Figure 4.11 shows the oxygen available, the oxygen required for full oxidation of hydrocarbons and carbon monoxides and the lambda value for maximum (left) and minimum (right) valve overlap.

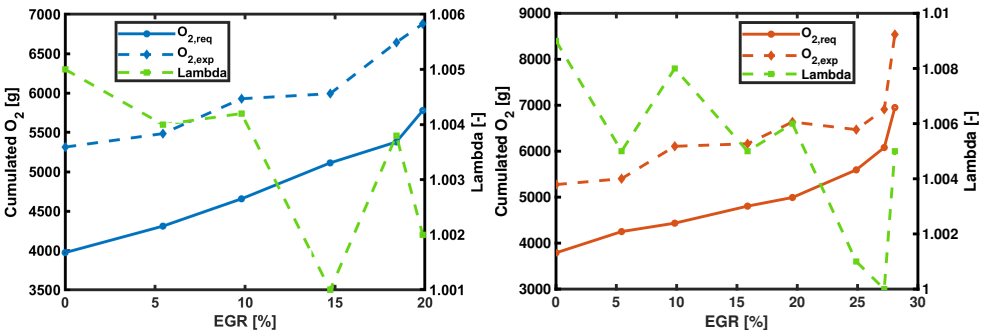

Figure 4.11. *Catalyst performance for 1500 rpm at 6 bar BMEP EGR sweep for: a) maximum overlap; b) minimum overlap.*

The available oxygen is enough to oxidize carbonaceous emissions for both EGR sweeps, despite the margin is reduced with EGR. This same trend was observed in Figure 4.10. However, in this two EGR sweeps a slight lean condition is found due to ECU control, whereas in the case of 3000 rpm the control at the highest EGR rate was a bit rich.

4.2 Decoupling of IGR and LP-EGR effects

In the previous study, it was found that there is a great influence on the concentration of IGR with the VVT at low loads, and this translates into different effects, especially when adding EGR. To further decouple the effects coming from IGR and EGR individually and delve into the interaction between both systems in greater detail, a methodology is developed to identify the impact of each on engine operation, combustion, emissions and efficiency.

4.2.1 Methodology

In order to select the exact operating conditions at which to perform the study, the IGR concentration of the tests on the DoE methodology explained in section 4.1 and other conditions were computed with the 1D engine model in its fitting configuration. The results are displayed in Figure 4.12.

As depicted in Figure 4.12, minimum variations of IGR are found for most tested conditions. For turbocharged tests, with BMEP beyond 10 bar, the pressure differential across the engine is reduced compared to throtlling operation. Moreover, at high engine load and low speed, several combinations

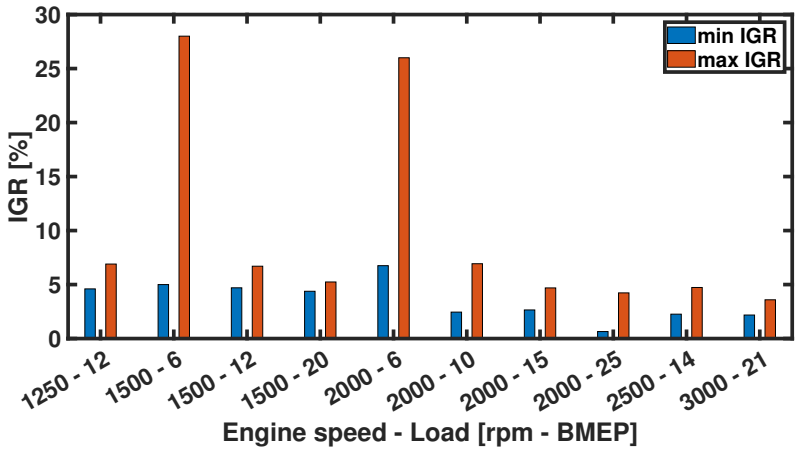

Figure 4.12. *IGR concentrations computed with a 1D model for several engine conditions based on the DoE methodology. Blue: minimum; Orange: maximum.*

of VVT are limited by scavenging and can affect lambda control. Since the intention of the study was to decouple the effects of IGR and EGR, conditions of maximum sensitivity of internal residuals with VVT were required, so the tests at 1500 rpm at 6 bar BMEP in section 4.1 with the DoE methodology were chosen.

From the DoE tests, three different levels of RGF, the sum of EGR rate and IGR, are searched with an equal separation between them, in this case 13, 20 and 27 % of RGF. Note that the IGR concentration is computed through the fitting model explained in subsection 3.4.1. A visual scheme of the RGF concentration sought is shown in Figure 4.13.

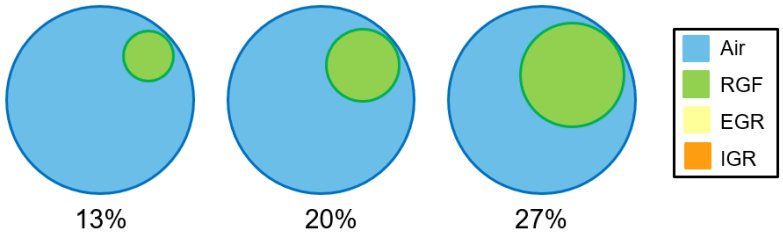

Figure 4.13. *Scheme of the RGF levels (green) sought inside the cylinder.*

For each of the RGF levels presented above, four combinations of VVT and EGR are used so that the RGF is achieved with different EGR and IGR rates

in order to decouple temperature and composition effects. The combinations of EGR-IGR for the three RGF levels are shown in Figure 4.14, achieving a total of 12 tests. Note that the combination of 100% of EGR and 0% of IGR is unreachable at this engine load for the three RGF levels.

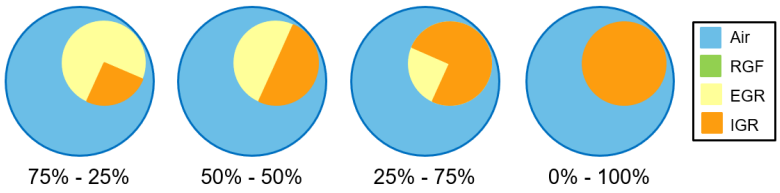

Figure 4.14. *Scheme of the EGR (yellow) and IGR (orange) combinations for each RGF level.*

If there is no combination of VVT and EGR in the DoE to meet an specific distribution of EGR, IGR and RGF, the 1D model in its fitted configuration is used in order to be predictive. For a given EGR rate, the model operates to search for the VVT combination that fulfils the desired IGR and RGF concentration. Once the model finds the combination, the test is reproduced experimentally and reprocessed in the fitting configuration of the model following the methodology already explained.

Table 4.4 is a summary of the experiments used for the study, with its VVT combinations at intake and exhaust, the RGF, EGR rate and concentration of internal residuals. The IGR and EGR is also shown in brackets as a percentage of the RGF. Note that the combinations of EGR and IGR sought in principle are approximated due to the complexity of obtaining exact values.

Table 4.4. *Definition of testing parameters.*

RGF [%]	**Point** [−]	**Int - Exh VVT** [°]	**EGR [% in RGF]** [%]	**IGR [% in RGF]** [%]
13	1	1 - 0	9 [65]	5 [35]
	2	9 - 10	6 [47]	7 [53]
	3	20 - 10	3 [25]	9 [75]
	4	0 - 35	0 [0]	13 [100]
20	1	18 - 9	15 [71]	6 [29]
	2	15 - 21	10 [53]	9 [47]
	3	16 - 33	5 [25]	15 [75]
	4	24 - 29	0 [0]	19 [100]
27	1	30 - 2	22 [78]	6 [22]
	2	24 - 32	13 [48]	14 [52]
	3	37 - 33	5 [20]	20 [80]
	4	37 - 33	0 [0]	23 [100]

Spark actuation is a key point in the study since if a constant timing was set, there would be two factors at play. First, higher temperatures would be expected at combustion start with higher IGR concentrations, achieving faster combustions especially at laminar stages. However, the composition of the exhaust gases has an important impact on combustion since the gases have already been treated at the aftertreatment system. For this reason, three strategies are defined for the spark timing. First of all, the same spark is set for each RGF levels. This tests are named as Isospark. In a second approach, the spark timing is adjusted so that the temperature at combustion start is almost constant. In this Isotemperature tests, the effect of temperature can be better understood. For this purpose, late spark tests are carried out in order to analyse the temperature evolution without combustion impact with the 1D model. Then, a temperature of 760 K is targeted and the crank angle at which it is achieved, thus the spark timing, is obtained for each test. Lastly, the spark activation is adjusted in order to achieve the highest possible efficiency (Optimal spark) so that both systems can be compared under design conditions. The criterion for maximum efficiency is centering the combustion with the parameter of CA50 between 7 and 10 degrees aTDC, as explained

Table 4.5. *Spark timing calibration strategies.*

RGF	**IGR**	**Spark Advance**		
	Value [% in RGF]	**Isospark**	**Isotemperature**	**Optimal**
[%]	[%]	[°bTDC]	[°bTDC]	[°bTDC]
13	5 [35]	6	9	11
	7 [53]	6	14	11
	9 [75]	6	18	10
	13 [100]	6	17	11
20	6 [29]	10	15	16
	9 [47]	10	18	15
	15 [75]	10	20	14
	19 [100]	10	22	13
27	6 [22]	15	17	21
	14 [52]	15	20.5	19.5
	20 [80]	15	24.5	19
	23 [100]	15	24.2	17

in [2]. The spark timings used for each batch of tests are summarized in Table 4.5.

In the Isospark tests, greater spark advance are needed as the RGF increases in order to obtain stable conditions due to reduced oxygen concentrations. In the case of Isotemperature tests, the spark is advanced with the IGR and RGF concentration, meaning that the target temperature is achieved earlier as expected with IGR. In the Optimal tests, the spark is notably advanced with respect to Isospark tests, around 5 CAD. This reveals the need to advance spark for efficiency in order to center combustion. In terms of IGR concentration, the optimal spark is almost constant for low RGF levels and there is a delaying trend for higher RGF. This is seen as a positive effect of IGR compared to EGR in the first stages of combustion development since less CAD are needed to reach the same CA50.

With the final tests carried out experimentally, a total of 36 since there are 3 RGF levels with 4 combinations of EGR-IGR and 3 spark strategies, the

Table 4.6. *Main engine throttle position used for each test.*

RGF	**IGR**	**Main Engine Throttle**		
	Value [% in RGF]	**Isospark**	**Isotemperature**	**Optimal**
[%]	[%]	[°]	[°]	[°]
13	5 [35]	12.2	12.3	12.2
	7 [53]	11.8	11.8	11.8
	9 [75]	11.6	11.8	11.6
	13 [100]	11.2	11.7	11.1
20	6 [29]	13.3	13.2	13.0
	9 [47]	12.5	12.8	12.5
	15 [75]	12.1	12.7	12.0
	19 [100]	11.4	12.1	11.4
27	6 [22]	14.9	14.8	14.4
	14 [52]	13.8	14.0	13.7
	20 [80]	13.6	14.2	13.6
	23 [100]	12.8	13.6	12.8

model is used again to simulate them in order to ensure that the conditions in the initial tests of the DoE and those computed with the fitted model remain within a deviation of 0.5% between batches. The 6 bar of engine load in the tests was kept with the main throttle, which was adjusted individually due to the changes in volumetric efficiency with EGR and VVT to control IGR. Table 4.6 shows the throttle values needed for each case in order to maintain the load. Moreover, the injection parameter was set at 82 crank angle degree after the beginning of the intake phase.

4.2.2 Model validation

All final tests used in this study followed a validation process as the one presented in this section for the Optimal spark batch. As explained in subsection 3.4.1, tests simulated with the fitting model need to be validated in order to corroborate its trustworthiness.

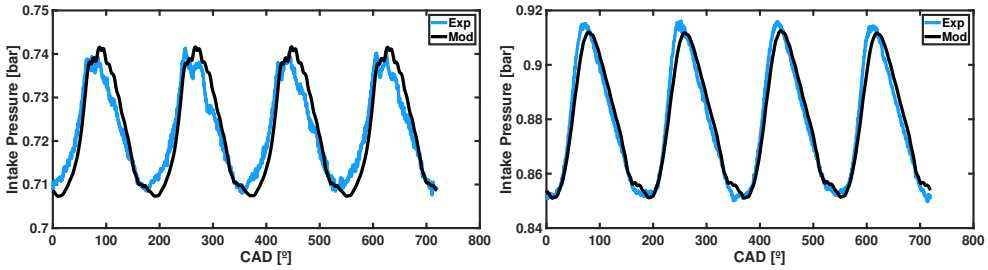

Figure 4.15. *Evolution of the intake manifold pressure for point 2 of 13% RGF (a) and point 4 of 27% RGF (b). Blue: experimental; Black: simulated.*

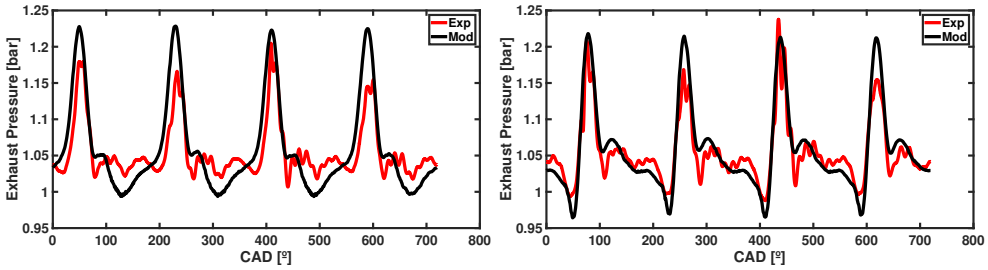

Figure 4.16. *Evolution of the intake manifold pressure for point 2 of 13% RGF (a) and point 4 of 27% RGF (b). Red: experimental; Black: simulated.*

To validate the results of the model in terms of instantaneous pressures at the intake and exhaust manifolds, these are compared with the experimental evolution for two different settings of the VVT, in this case, point 2 of 13% RGF and point 4 of 27% RGF. This is shown for the intake manifold in Figure 4.15 and for the exhaust manifold in Figure 4.16.

4.2.3 Decoupling temperature and composition

First of all, a comparison between the Isotemperature and the constant spark tests is done so that the effects of composition and temperature can be better identified. In this sense, a comparison of the temperature at the spark event between both batches of tests is shown in Figure 4.17 with respect to IGR concentration in RGF. Note that the remaining residuals are achieved with EGR, so that a 0% IGR would mean a complementary 100% EGR. From

this point, the RGF level is identified with the colour of the line and the symbol (green squares for 27%, blue diamonds for 20% and orange circles for 13%). Besides, in this section the Isospark tests and the Isotemperature tests are represented by solid and dashed lines respectively.

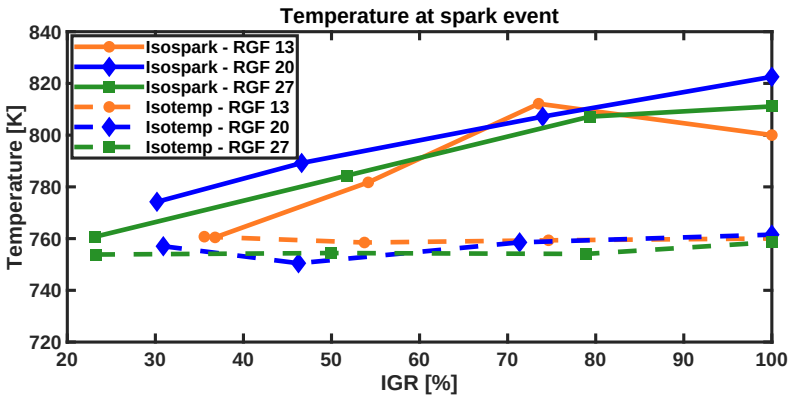

Figure 4.17. *Temperature at spark event with respect to IGR concentration in RGF for Isospark (solid lines) and Isotemperature (dashed lines) tests.*

As observed, the temperature goal was achieved for the Isotemperature tests with a deviation within 10 K, whereas a general increase in temperature with IGR concentration is observed for the Isospark tests, as expected. However, the variation with the RGF level is not significant despite a different total amount of IGR is found because there is a more advanced spark timing with RGF.

For combustion analysis, the induction time and the time of combustion are shown in Figure 4.18 and Figure 4.19 for 13% and 27% RGF. Note that the induction time is defined as the difference in crank angle degrees between the 10% of heat release and the spark activation, whereas the time of combustion is the crank angle degree elapsed between the 90% and the 10% of the heat released.

For the Isospark analysis, the more advanced spark that is used for higher RGF levels results in shorter CA10 than the Isotemperature tests. This is explained by the influence of temperature effect on laminar combustion speed in Equation 4.2.

$$S_L(\phi, T_u, p_u) = S_{L0} \left(\frac{T_u}{T_0}\right)^{\alpha} \left(\frac{p_u}{p_0}\right)^{\beta} \tag{4.2}$$

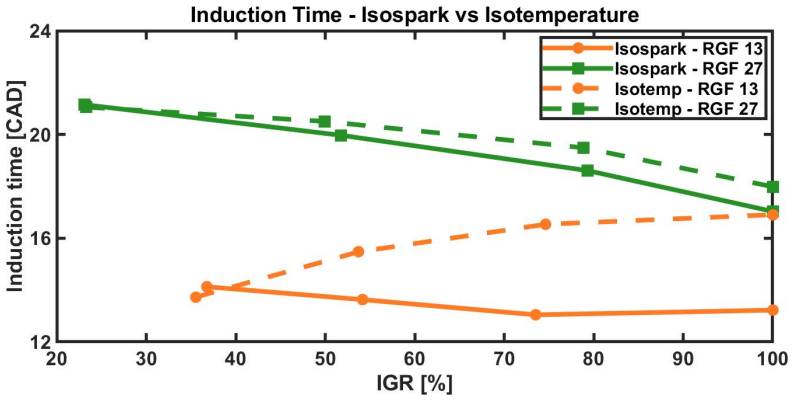

Figure 4.18. *Induction time with respect to IGR concentration in RGF comparison between Isospark (solid lines) and Isotemperature (dashed lines) tests.*

Equation 4.2 is used for laminar flame speed prediction, and it is defined by S_{L0}, the standard laminar speed (at $p_0 = 0.1MPa$ and $T_0 = 298K$), p_u and T_u, the conditions of pressure and temperature respectively in the unburned area. α and β are the coefficients of dependence on pressure and temperature. These coefficients are very dependent on the fuel, composition and lambda. At stoichiometric conditions and without residuals, α 1.69 and β -0.278 are the values found in the literature [3]. For the Isospark tests, the same pressure is expected at combustion start for each RGF level, so the factors that most affect combustion development are temperature and residuals. Given the conditions of temperature observed in Figure 4.17, a maximum increase of around 11% can be awaited in the laminar flame speed when increasing IGR due to temperature effects. This would be translated into shorter times of induction around 1.5 CAD and 2.3 CAD for 13% and 27% RGF levels when comparing maximum to minimum IGR concentration.

For 13% RGF level, if this result is compared with the values in Figure 4.18, the variation in induction time can be completely explained by the change in temperature at combustion start affecting laminar development. For the Isotemperature tests, the trend is reversed at 13% RGF level and a deterioration is found for greater concentrations of IGR. This can be partially explained by changes in the conditions of the spark plug surroundings as stated in [1]. For the 27% RGF level, the variation observed in the Isospark tests is around 4 CAD, notably higher than the expected 2.3 CAD. Therefore, an effect from composition is observed, increasing laminar flame speed with IGR concentration since EGR has a lower reactivity induced by the lower

concentration of unburned compounds. In fact, for the Isotemperature tests, lower sensitivity with IGR is found, around 3 CAD. This is closer to the prediction with Equation 4.2.

With the same structure, a TOC comparison between these tests is depicted in Figure 4.19.

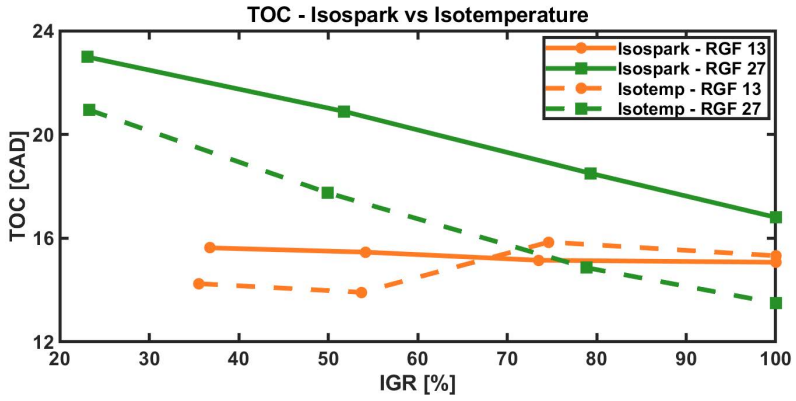

Figure 4.19. *Time of combustion with respect to IGR concentration in RGF comparison between Isospark (solid lines) and Isotemperature (dashed lines) tests.*

For the 13% RGF level, very little sensitivity is found with different compositions of the total residuals, so an almost flat trend is obtained for both conditions. This clearly demonstrates that the composition of residuals has no effect when its concentration is relatively low. However, for the 27% RGF level, a clear decrease in the total time of combustion is obtained as the IGR concentration increases with both conditions. Besides, when the IGR concentration is low and the RGF level is obtained with cooled EGR, longer combustions are obtained when comparing 27% to 13% RGF. This is explained by the higher dilution obtained with higher RGF levels. However, as the share of IGR concentration is increased, this effect diminishes, from what can be deduced that addition of IGR could compenste the negative effects of EGR on combustion.

Table 4.7 shows the variability analysis of the combustion parameters shown in Figure 4.18 and Figure 4.19. A reduction of standard deviation is observed as IGR concentration increases, especially for high RGF levels, so for higher total amount of IGR. This is explained by the greater temperature at the spark event and the residence of unburned from the previous cycle that help the flame development.

Table 4.7. *Variability analysis of the combustion parameters for the Isospark and Isotemperature tests.*

RGF	**IGR**	**Std Induction Time - Std TOC**	
	Value [% in RGF]	**Isospark**	**Isotemperature**
[%]	[%]	[°]	[°]
13	5 [35]	1.96 - 2.74	1.86 - 2.32
	7 [53]	1.83 - 3.08	1.43 - 1.47
	9 [75]	1.41 - 2.53	1.24 - 0.83
	13 [100]	1.84 - 2.97	1.20 - 0.83
20	6 [29]	2.17 - 4.42	1.26 - 2.79
	9 [47]	1.96 - 3.63	1.72 - 2.12
	15 [75]	1.92 - 3.42	1.24 - 0.95
	19 [100]	1.73 - 2.59	1.20 - 1.00
27	6 [22]	2.87 - 6.48	2.55 - 4.97
	14 [52]	2.44 - 5.09	2.20 - 3.35
	20 [80]	2.19 - 3.56	1.66 - 1.40
	23 [100]	2.19 - 3.02	1.59 - 1.06

4.2.4 Empirical correlations

The results presented up to this point have demonstrated the direct impact of composition, merely the share of internal and external residuals, on combustion development. The information depicted can be used in order to build empirical correlations that could predict the behaviour and results of a given test and account for the different effects coming from both composition and temperature, decoupling IGR and EGR. Note that this correlations would be useful for the engine under study due to its characteristics as well as the fuel used, but the methodology is extensible to others.

In this sense, the value of the coefficients would shed light on the weight and relative impact of IGR and EGR respectively in combustion. Moreover, 1D engine models based on fluid-dynamics as the one used along the study use

Table 4.8. *Induction time empirical correlation.*

Parameter	w/ IGR		w/o IGR	
	Value	**Interval 95%**	**Value**	**Interval 95%**
a	1.98	[1.5, 2.4]	0.94	[0.6, 1.3]
b	0.12	[0.08, 0.16]	0.23	[0.09, 0.37]
c	-0.15	[-0.19, -0.11]	-	-
d	0.3	[0.24, 0.36]	0.23	[0.13,0.33]
R^2	92.15		77.3	
$R^2 - adj$	90.97		75.2	

empirical correlations for combustion predictions due to the lack of a predictive model. A proper correlation that include these efects individually is mandatory for predictive purposes. The Equation 4.3 is proposed for the induction time correlation.

$$\tau_{ind} \quad [CAD] = (a \cdot RGF^b \cdot IGR^c \cdot \tau_{Spark}^d) \left(\frac{T_{Spark}}{T_0}\right)^{-1.67} \left(\frac{p_{Spark}}{p_0}\right)^{0.278} \tag{4.3}$$

where t_{Spark} is the spark setting in crank angle degrees before top dead center (bTDC), whereas p_{Spark} and T_{Spark} are the conditions of pressure and temperature at the spark activation. These are obtained with the GT-Power model. The coefficiencts $a - d$ are the ones to adjust in the correlation. Naturally, the exponents for the pressure and temperature ratios are the ones found for gasoline in the literature [3] and the ones used in Equation 4.2 but with the opposite sign since a faster development means shorter times. The inclusion of the spark timing is justified due to the inclusion of turbulence effects around the spark plug depending on the position of the piston.

Two different configurations of the correlations are fitted, depending on the inclusion of the IGR concentration. The goal of developing two correlations was to assess the need to differentiate between EGR and IGR. The main coefficients and parameters of the statistical analysis are shown in Table 4.8.

As can be observed, the correlation is capable of reproducing the data to a greater extent if the IGR concentration is considered, with 15% increased R-squared value. This is a clear indicator of the importance to decouple IGR and EGR.

A comparison between both correlations is shown in Figure 4.20, with blue dots for the correlation with IGR and orange diamonds for the correlation without IGR. For the correlation with IGR, all predictions fall within ±1 CAD and a deviation of 0.6 CAD is obtained. On the other hand, a higher mean and maximum deviation of 1.1 and 3 CAD respectively is obtained for the correlation without IGR.

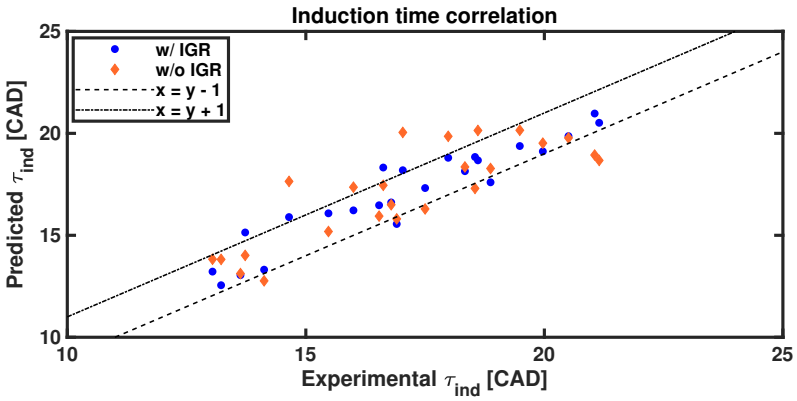

Figure 4.20. *Correlations prediction vs experimental induction time with and without the effect of IGR concentration.*

For the combustion duration, Equation 4.2.4 is adjusted.

$$TOC \quad [CAD] = a \cdot \tau_{ind}^{b} \cdot \tau_{Spark}^{c} \tag{4.4}$$

where τ_{ind} is the induction time and τ_{Spark} is again the spark timing. Coefficients $a - c$ are the ones to adjust for the correlation. The inclusion of the induction time is to include all the effects from laminar flame development together with composition and temperature. However, it has to be stated that the great dependence of combustion development on turbulent kinetic energy and fluid flow might not be fully reflected with this correlation, so a more detailed one should be implemented for future works to account for this effect. Nonetheless, results with a high correlation are obtained with this approximation as can be seen in Table 4.9 and Figure 4.21.

Table 4.9. *Results of the empirical correlations for the combustion duration.*

Parameter	Value	Interval 95%
a	0.63	[0.46, 0.80]
b	1.48	[1.22, 1.73]
c	-0.35	[-0.44, -0.26]
R^2	86.85	
$R^2 - adj$	85.60	

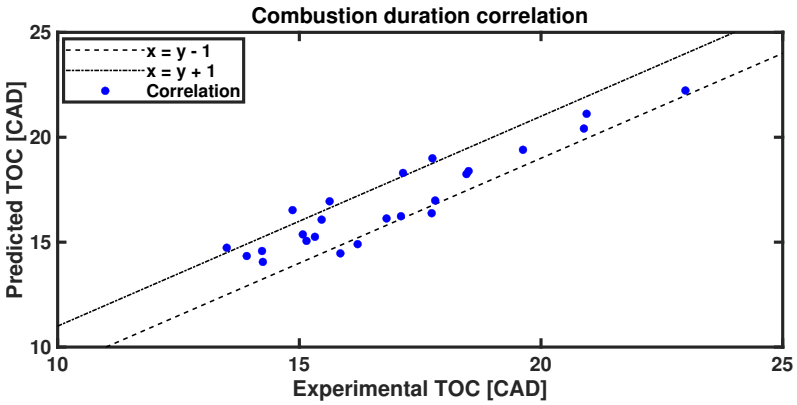

Figure 4.21. *Experimental vs. predicted combustion duration.*

A general increased deviation and a lower R-squared value is obtained compared to the induction time correlation, around a 6%. This is an expected result due to the dependence between these. However, the maximum deviation is 1.66 CAD and the average is 0.7, so an acceptable and adequate prediction is obtained for 1-D simulation.

Results show the possibility to predict induction and combustion time as already defined taking into account IGR and EGR concentrations. However, the prediction capability of these correlations is severely deteriorated when these two are not decoupled and just the total RGF is taken into account. This is seen as a powerful argument to consider composition when developing semiempirical models in this field.

4.2.5 Optimal spark timing

After setting the spark at a constant value for each RGF level (Isospark tests) and to obtain 760 K at the spark event (Isotemperature tests), the spark was set in order to obtain maximum efficiency, thus the minimum fuel consumption, within stability and knock limits already defined. To do so, the spark was set based on the CA50 value seen online on the test bench, trying to set this value between 7 and 10 CAD aTDC as stated in [2].

The induction time for the Optimal spark calibration is displayed in Figure 4.22. As in the previous graphs, the colour and symbol are used to differentiate the RGF level. In this sense, orange circles are used for 13%, blue diamonds for 20% and green squares for the 27% RGF level. Moreover, solid lines are used to show the experimental values and the dashed lines are used for predictions with the correlations previously presented in subsection 4.2.4.

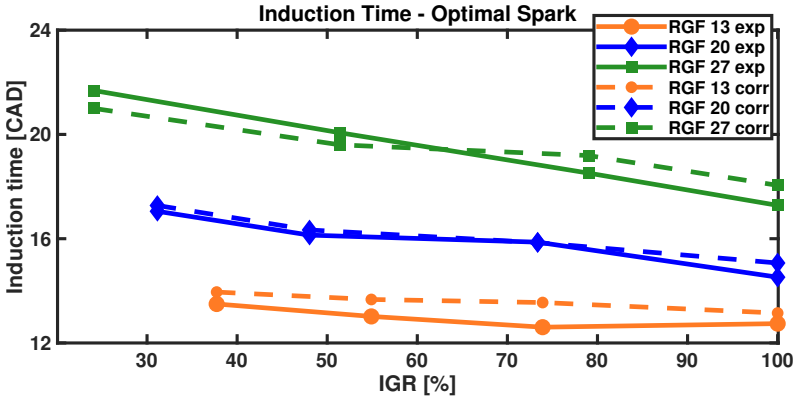

Figure 4.22. *Induction time comparison between experimental (solid line) and correlation prediction (dashed line) for Optimal spark tests with respect to IGR concentration in RGF.*

A longer induction time is obtained as the RGF level increases as previously discussed. However, as the share of IGR increases, a faster initial stage of combustion is achieved owing to a higher level of reactivity in the mixture compared to EGR addition. The trends are well predicted in general with the correlation, with a slight overprediction for all cases except the highest RGF level and lowest IGR share. With a similar structure, Figure 4.23 displays the combustion duration.

The same trends as in the induction time are obtained for the combustion duration, with an increasing trend with the RGF level and decreasing with IGR concentration due to higher temperatures and mixture reactivity.

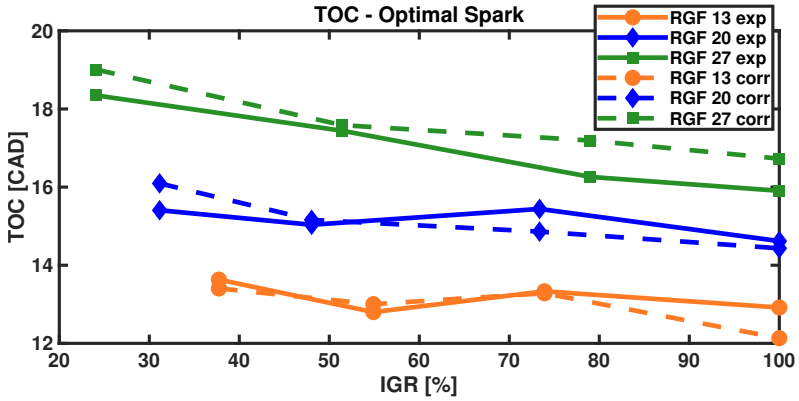

Figure 4.23. *Time of combustion comparison between experimental (solid line) and correlation prediction (dashed line) for Optimal spark tests with respect to IGR concentration in RGF.*

In comparison with the prediction from the correlation, again a slight overprediction is found for almost all cases, with a maximum difference of around 1 CAD.

The direct influence of the residuals is thus demonstrated, which when increasing in the absence of EGR cause an elongation of the combustion process. This fact can be observed in both graphs, with a bigger effect on the induction time as demonstrated in [4]. This effect of internal residuals was studied in depth in [5], showing a 5 CAD increase in TOC with higher IGR concentrations.

The variability analysis of the combustion parameters for the Optimal spark tests is shown in Table 4.10.

Following the trends observed in the Isospark and Isotemperature comparison, the variability analysis for the Optimal spark tests shows in general lower deviations for both combustion parameters when the share of IGR increases. Moreover, higher deviations are obtained with greater RGF levels as expected.

With the optimal spark set for each RGF level, a fair comparison between the IGR trapped with the VVT system and LP-EGR can be performed in terms of efficiency and emissions so that the interaction between systems can be better understood. To do so, the energy balance of each test is computed with the 1D model, namely the indicated efficiency (IND), the in-cylinder heat transfer losses (HT) and the exhaust enthalpy (EXH). The heat transfer losses are calculated with an adapted Woschni model, which coefficients were tuned

Table 4.10. *Variability analysis of the combustion parameters for the Optimal spark tests.*

RGF	**IGR Value [% in RGF]**	**Std Induction Time**	**Std TOC**
[%]	[%]	[°]	[°]
13	5 [35]	1.73	1.91
	7 [53]	1.70	2.32
	9 [75]	1.48	2.16
	13 [100]	1.66	2.09
20	6 [29]	2.01	3.07
	9 [47]	1.85	2.58
	15 [75]	1.76	2.51
	19 [100]	1.68	2.29
27	6 [22]	2.27	3.80
	14 [52]	2.32	3.22
	20 [80]	2.21	2.75
	23 [100]	2.14	2.61

based on motoring conditions under different conditions of engine speed and intake pressure, thus air mass flow. Values of 3.24 and 1.91 for constants C1 and C2 were used. The final analysis of the energy balance is shown in Figure 4.24, with the x-axis representing the IGR concentration in RGF (orange for 13% and green for 27%), and the color transparency is used determines the contributor to the energy balance. The darker color is used for the indicated efficiency, the intermediate is for losses coming from in-cylinder heat transfer and the lighter for the exhaust enthalpy.

The indicated efficiency is almost constant with IGR with a clear advantage with higher RGF levels, whereas the higher temperature that is obtained with greater IGR concentrations during intake and compression is increasing heat transfer losses. This, together with the lower exhaust temperatures derived

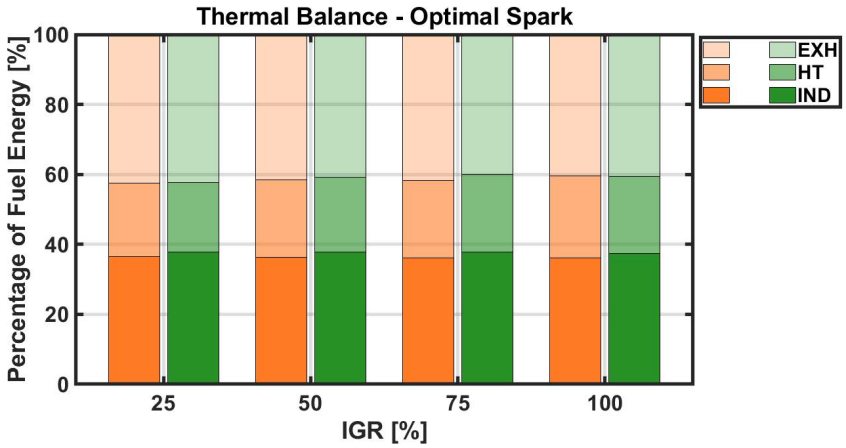

Figure 4.24. *Thermal balance comparison between 13% (orange) and 27% (green) RGF level for Optimal spark tests with respect to IGR concentration in RGF.*

from shorter combustions is the main responsible for the reduced exhaust enthalpy with higher IGR.

Since the thermal balance includes the gross indicated efficiency computed during the 720 CAD of the cycle, a part of the indicated cycle that is not displayed: the mechanical and pumping losses. Given the similarity of the operating conditions, very little discrepancies are expected in terms of friction and mechanical losses, being the main impact the differences in pumping losses induced by the LP-EGR and VVT settings. This information is shown in Figure 4.25, taking as a reference the value of 27% RGF without EGR.

When increasing the RGF level, pumping losses are always reduced, whereas the only clear trend with the IGR concentration is found for 27% RGF. When the RGF is obtained only through IGR, increasing the RGF level is translated into reduced pumping losses. These results are in agreement with those found by [5], with a reduction between 14 to 10% in pumping losses when increasing residuals.

As with the pumping losses, the BSFC variation with respect to 27% RGF level without EGR is displayed in Figure 4.26.

An important fuel economy benefit is found as the RGF level is increased. For the low and medium RGF levels, an improvement in BSFC is found for high EGR rates. This may be explained due to the effect of heat transfer losses, whereas the pumping losses achieved with only IGR at 27% RGF compensates this effect, so the trend with IGR is merely flat.

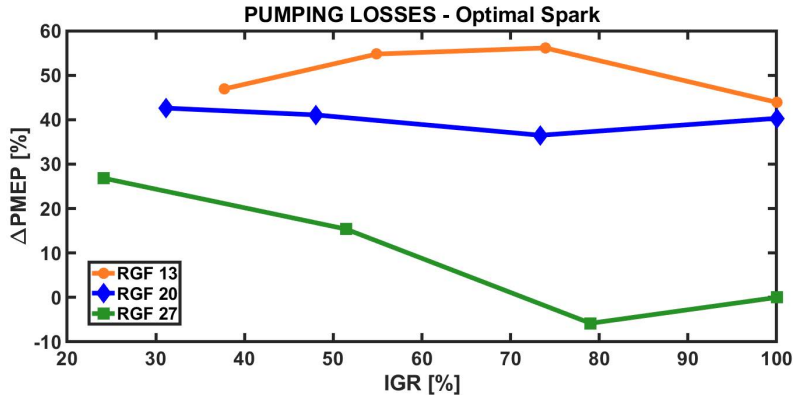

Figure 4.25. *Pumping losses comparison between RGF levels for Optimal spark tests with respect to IGR concentration in RGF.*

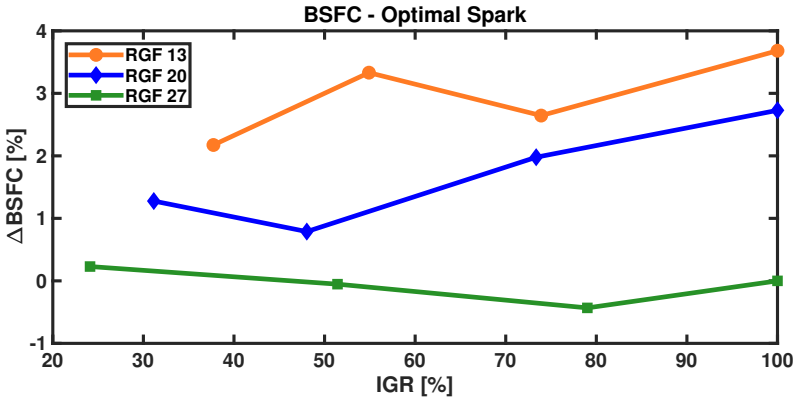

Figure 4.26. *BSFC comparison between RGF levels for Optimal spark tests with respect to IGR concentration in RGF.*

For the emissions analysis, Figure 4.27 shows the reduction trend of hydrocarbons when increasing the share of IGR. Besides, the amount of hydrocarbons increase for the highest RGF level, as expected. It seems interesting, however, the fact that 13% and 20% RGF levels are almost overlapped even though combustion speed was reduced when increasing the RGF level as shown in Figure 4.22 and Figure 4.23. This could be explained by different conditions of temperature in the walls of the combustion chamber.

For spark-ignited engines, the main sources of hydrocarbon emissions are two [6]: the flame termination as it reaches small volumes, the spark or

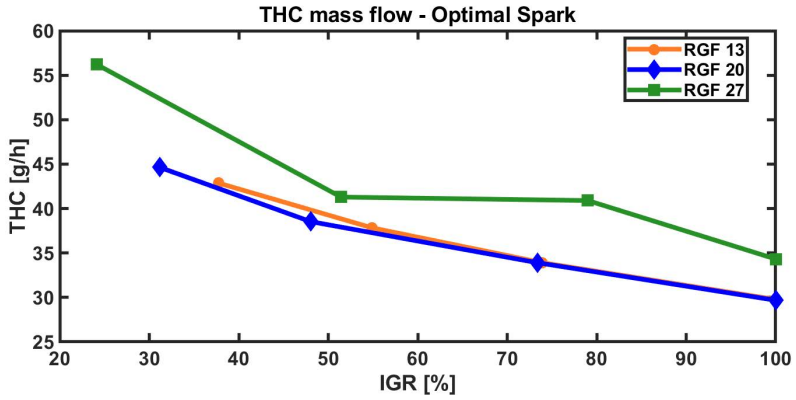

Figure 4.27. *HC mass flow comparison between RGF levels for Optimal spark tests with respect to IGR concentration in RGF.*

valve seats, among others, and the flame quenching when the front reaches the surface of the wall in different parts of the engine. The both sources of hydrocarbon formation are dominated by heat transfer and are normally important with low speed flames [7].

The NO_x mass flow is displayed with respect to the peak combustion temperature in Figure 4.28, since it is the main contributor to NO_x formation together with oxygen concentration [8, 9]. As it could be expected, the peak temperature and oxygen concentration reduction obtained with greater RGF levels results in less NO_x formated.

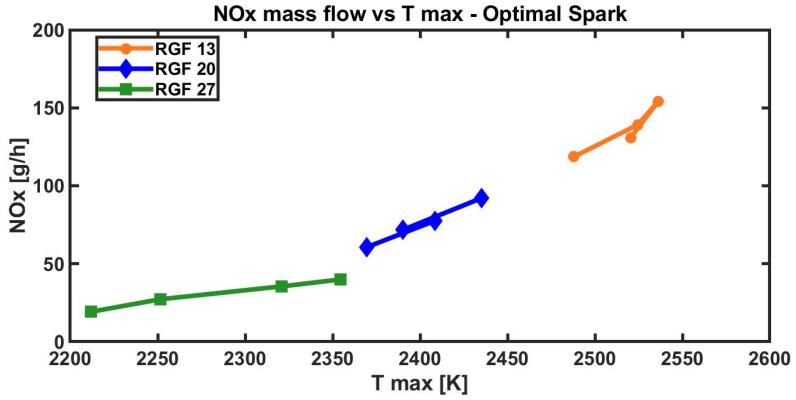

Figure 4.28. *NO_x mass flow comparison between RGF levels for Optimal spark tests with respect to peak combustion temperature.*

For the CO formation, it is mainly dependent on the oxidation reaction to carbon dioxide. As the oxygen concentration is reduced with higher RGF levels, the thermal equilibrium of the reaction is shifted to higher CO_2 production. Nonetheless, as the combustion temperature is reduced, a slower dissociation of carbon dioxide to monoxide is obtained. The result of these two opposite effects is a general trend to reduce carbon monoxides with RGF as displayed in Figure 4.29.

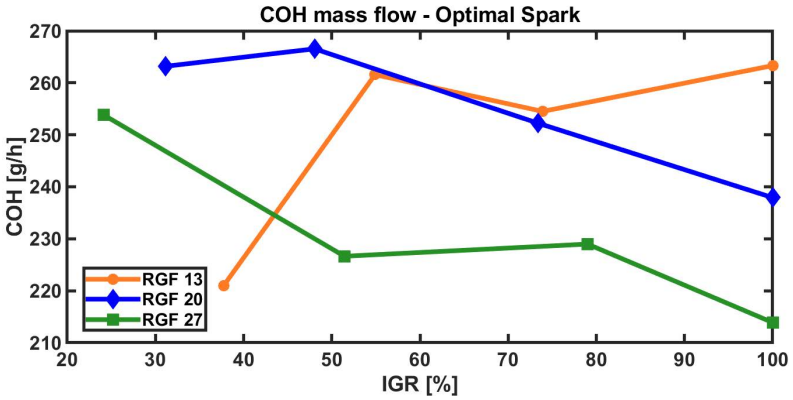

Figure 4.29. *CO mass flow comparison between RGF levels for Optimal spark tests with respect to IGR concentration in RGF.*

When the engine is running only with IGR, the emission of NO_x is reduced together with carbon monoxides and hydrocarbons are increased with increasing RGF levels. This is in line with what was reported by [4] except for carbon monoxides, which is very variant. Around a 30 to 40% of NO_x and carbon monoxides reduction was also found by [5], together with an increase in hydrocarbons.

4.3 Combustion instability induced by condensation

The water content present in the exhaust gases of a low-pressure EGR system is susceptible to condensation from various sources when the gases undergo a cooling process or at cold starts [10]. This is explained by the high concentration of water and specific humidity of the exhaust gases. Condensation and its negative impact on components life is a well-known and studied problem, especially in the case of water droplets that reach the compressor and erode it [11, 12]. The damage produced to the compressor wheel can be controlled in 3 main ways, all of them normally impairing the efficiency. The first one is with a proper design of the junction between

fresh air and EGR gases [13, 14]. The second would be suppressing EGR operation during cold starts or warm-ups [12]. The last one is the introduction of water separators, directly preventing contact between water droplets and the compressor [15].

Moreover, different elements of the engine can be affected by corrosion due to acidic compositions. Garcia [16] established the risk of disintegration of components on account of sour solutions and demonstrated the opposition to corrosion of various materials, allowing a good disintegration prognosis. In the case of SI engines with TWC, secondary reactions in the aftertreatment can produce ammonia, resulting in a very different acidity compared to diesel or non-TWC SI engines [17], with a more neutral to alkaline gases (pH-values from 7 to 9) [18–21].

Despite there is a vast knowledge about condensation in EGR circuits, most studies have been performed on compression engines, with much lower specific humidities than SI engines due to lean operation. In the case of spark ignition engines, water represents a 10% in weight or a 14% molar fraction concentration in the exhaust gases for stoichiometric operation. In this way, the problem of water condensation can be more significant in SI engines, even more with fuels that are currently being investigated for decarbonization as ammonia [22], methanol [23], natural gas [24, 25] or hydrogen [26]. Besides, previous condensation studies base their analysis on corrosion, compressor damage and icing, but do not account for the effect of the water droplets reaching the intake runners and the cylinders spontaneously, being this problem yet to be deeply understood.

Condensation of water suddenly reaching the cylinders is a different problem than the dilution by water injection, since the latter is a well controlled and intentional dilution technique that has proven its potential on increasing efficiency in several studies [27–29]. However, the similarity between both phenomena is undeniable, so the knowledge acquired about this dilution technique is applicable to the condensation problem. Vaudrey [30] stated that when water is injected and evaporates, it blends with the air, absorbing the enthalpy of vaporisation and thus cooling the charge. The drop in temperature has several consequences from an operational point of view:

- Reduced autoignition and combustion temperatures, thus reduced knock tendency and a potential benefit in centering combustion and increasing compression ratio.
- Increased air density, increasing the volumetric efficiency and so the amount of air aspirated.

- Reduced mechanichal work needed to compress, given the lower temperature at the start. Some water may remain liquid and evaporate later, adding some cooling effect.
- Better expansion work due to increased amount of gas in the process.

The same increase in volumetric efficiency that is obtained with water injection is observed when the condensed water in the WCAC accumulates and is released into the cylinders. However, in the case of the condensation problem, it is a sudden, uncontrollable and undesired phenomenon.

In this study, several engine conditions of speed and load are tested in a climatic chamber with high LP-EGR rates under conditions conductive to water condensation in the WCAC, and the effects of water condensation on combustion, emissions and efficiency are assessed. The three main sources of condensation found in the current experimental set-up are: the EGR cooler, the mixing of EGR and fresh air upstream the compressor and the WCAC. Given that the first two sources could affect the compressor wheel operation, a psychrometric analysis is performed with a validated 0D condensation model, explained in subsection 3.4.2, in order to avoid condensation in the EGR cooler nor the mixing with fresh air by selecting the ambient and WCAC coolant temperature (both set equal). In this sense, all water condensation in this study is located in the WCAC. Three different engine operating points are chosen, 1500 rpm at 6 and 12 bar BMEP, and 3000 rpm at 12 bar BMEP. Each condition is tested under high EGR rates and condensing conditions in the WCAC, acquiring during 20 minutes so that the effect of accumulation of water in the WCAC can be studied. The combustion process and the cyclic dispersion are discussed based on the in-cylinder pressure acquisition, and the fuel consumption and emissions are analysed. To conclude, a preliminary evaluation of the condensation problem with different fuels that are being investigated with a view to decarbonization is carried out. With the aforementioned psychrometric model, the limit temperature for the appearance of condensates is studied for ammonia, methanol, natural gas and hydrogen.

4.3.1 Methodology

Any cooling process that exhaust gases undergo is prone to condensation of water from the EGR. In this way, three condensation sources are found in the current engine set-up:

- **EGR cooler:** the exhaust gases extracted for recirculation are cooled in a heat exchanger before being reintroduced. The low temperature of the coolant during the engine warm-up can lead to condesation.

- **Mix with fresh air:** in the joint upstream the turbocharger due to low ambient temperatures.
- **Charge cooler:** either air o water coolers. In this case, a WCAC is implemented with a separate coolant circuit as in transportation applications.

In this experimental campaign, two different cooling circuits are used. The main high-temperature cooling circuit is used for the engine and its coolant temperature is set to 90°C in order to operate at warm conditions. The second one is a low-temperature circuit used for the WCAC, designed to operate below 50°C, since using the main cooling circuit would induce extremely high temperatures at the intake, with significant damage to performance due to reduced densities and higher knock tendency. Given that the main objective in this research is to evaluate the effects of sudden dilution through water droplets on combustion, the experimental campaign is designed in order to obtain condensation only and exclusively in the WCAC. Any condensation upstream the compressor is prevented for security and to avoid compressor wheel damage. In this sense, condensation in the LP-EGR cooler is avoided by connecting it to the main high-temperature cooling circuit, since saturation temperatures at the EGR cooler are around 50°C in these conditions. Then, the ambient and WCAC coolant temperature are chosen with the model explained in subsection 3.4.2, taking into account that it must be high enough to avoid condensation from mixing EGR with fresh air, but allowing the coolant to reach the WCAC at a temperature that can induce condensation in the charge cooler. Since the WCAC coolant and ambient temperatures can be very similar in real conditions, both are always considered the same for simplification in the model. Experimentally, both are controlled to be the same in the climatic chamber.

In order to obtain a WCAC coolant and ambient temperature that can promote this situation, the psychrometric model explained in subsection 3.4.2, developed and validated in [13, 31] is used, performing a sweep of both temperatures from -15 at 30°C for the engine operating conditions to be experimentally tested. These conditions are 1500 rpm with two engine loads, 6 and 12 bar BMEP, and 3000 rpm at 12 bar BMEP. In this model, the condensation of water in the mixture between EGR and fresh air and in the WCAC are estimated. The results of the model are depicted in Figure 4.30, with dashed lines for the T-joint and solid lines for the WCAC, and different colors for each operating conditions. Note that the temperature in the x-axis are both the ambient and WCAC coolant temperatures.

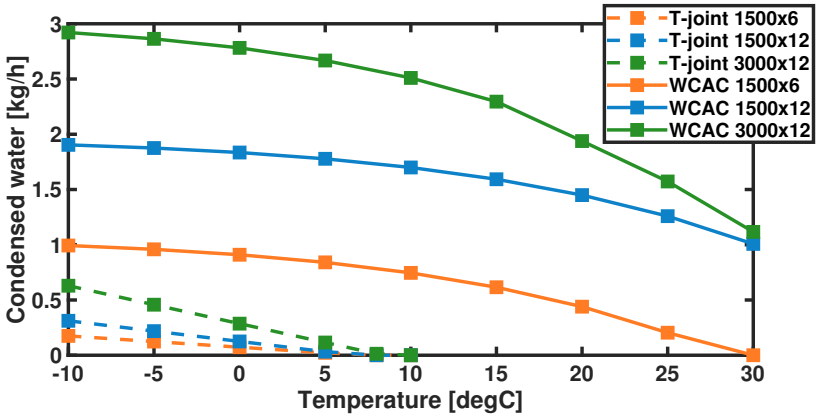

Figure 4.30. *Modeled condensation in the T-joint (dashed lines) and in the WCAC (solid lines) for several operating conditions.*

The information extracted from the model shows that condensation due to mixture between EGR and fresh air occur for ambient temperatures below 10°C, whereas condensation in the WCAC can occur from 30°C. This restricts the area in which only condensation in the WCAC is obtained to a range between 10 and 30°C of ambient and coolant temperature. For this reason, and to ensure a considerable condensation condition, 15°C is chosen as the WCAC coolant and the room temperature in the climatic chamber.

The three engine points aforementioned are calibrated in terms of VVT, throttle, VGT, spark and EGR following the methodology explained in [32], achieving the Optimal settings for fuel economy with combustion stability and knock limits. Table 4.11 shows a summary of the calibration used for each engine condition tested.

Table 4.11. *Main engine parameters for condensation tests.*

Speed [*rpm*]	**BMEP** [*bar*]	**Int - Exh VVT** [°]	**LP EGR** [%]	**Spark Timing** [°bTDC]	**Throttle** [°]	**VGT** [%]
1500	6	0 - 0	25	32	16.4	0
1500	12	14 - 3	25	17	WOT	84
3000	12	18 - 2	22	24	WOT	36

The calibration presented for each engine point serves as a starting point for the two experimental procedures that are proposed. In a first step, the engine is tested with the calibration at lambda equal to one, acquiring every 5 minutes and for as long as 20 minutes, starting at time 0. The main goal of this procedure is to assess the build-up effect of condensation with time. The second procedure consists of a lambda sweep at an equivalent time 0, for which the EGR valves are closed between tests and the WCAC coolant temperature increased to 40°C so that all condensed water is consumed, maintaining these conditions during 3 minutes. The lambda sweeps are performed in order to compare the dilution level induced by condensation with that of different air to fuel ratios.

4.3.2 Results

In this section, both testing procedures are discuted and analysed in terms of combustion, stability, emissions and efficiency. From this point on, the color scheme is kept constant, with orange used for 1500 rpm at 6 bar BMEP, blue for the same regime at 12 bar BMEP and green for 3000 rpm at 12 bar BMEP.

First of all, in order to confirm the results predicted with the model and to ensure that there is an accumulation effect, an endoscope is placed at the WCAC outlet and some images are extracted for 0, 10, 15 and 20 minutes as shown in Figure 4.31.

The images confirm the results of the model, showing an evolution from the start at time 0, without any remarkable drop, to 10 and 15 minutes time, with some drops appearing and growing at the left side of the image. For 10 minutes, a red circle is used to highlight the location of the drop that subsequently grows. At 20 minutes, the entire image is distorted due to the growth of the drop, which has occupied completely the width of the lens.

Once condensation and water accumulation has been confirmed through the endoscope, two different analysis are proposed: one from combustion and stability and other from efficiency and emissions analysis.

The combustion stability is analysed through the combustion timings from the apparent heat release rate computed from the 800 in-cylinder pressure recordings per test. The difference between CA90 and CA10, from this point on called time of combustion or TOC, and the CA50 are the parameters considered for the analysis. An statistical analysis is performed on these two combustion parameters, TOC and CA50, dividing the individual values of each cycle into two groups depending on the dispersion level: normal (in black) and abnormal (in red) dispersion. The first group is made up of the values that are within 10% of the reference IMEP of the test, representing approximately the standard

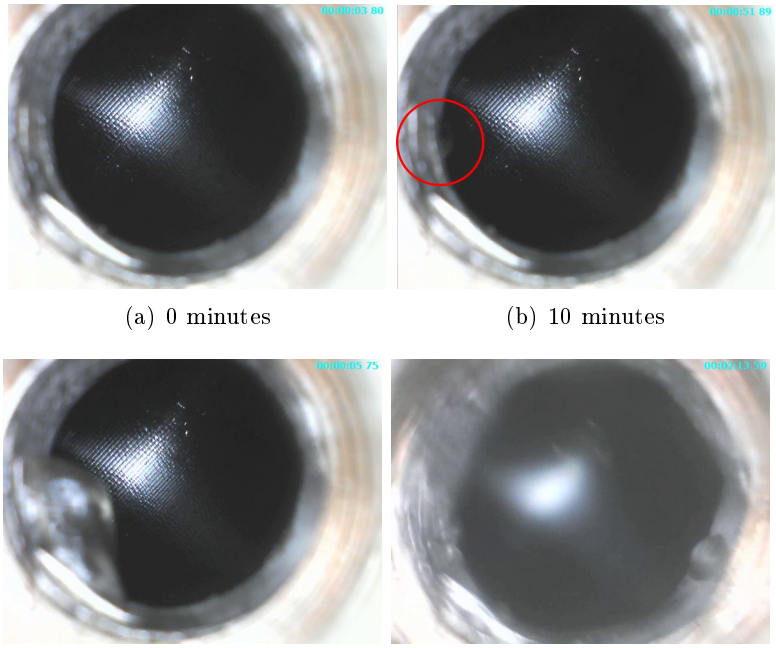

(a) 0 minutes (b) 10 minutes

(c) 15 minutes (d) 20 minutes

Figure 4.31. *Images acquired with the endoscope at the WCAC for different accumulation times.*

instabilities induced by EGR operation without condensation. Those cycles with IMEP below this threshold are grouped in abnormal dispersion, excluding those with IMEP below 1 bar. This exclusion is made since these cycles are considered misfires or non-representative combustion. The horizontal lines are included to show the maximum and minimum values of each dispersion group. The mean value of the cycles in normal dispersion is shown with a solid line in the colour chosen for the engine operating condition. Besides, a second stability analysis is performed to further assess the effect of condensation in combustion. This second analysis is made through the coefficient of variation of the IMEP, as typically done in combustion engines, along with the percentage distribution of cycles based on the CA50 value.

The global effect of condensation on engine operation is assessed through fuel economy and emissions. For pollutant emissions, data is represented as a percentual variation with respect to the best engine point found without EGR. In this sense, the viability of the EGR is called into question due to

condensation. In the charts, delta positive mean that operation without EGR is the better strategy due to the negative effects of EGR condensation.

Finally, a preliminary analysis of condensation in different fuels is performed with the model with a view to the new fuels that are being investigated for decarbonization. The lower content of carbon in these fuels result in a increased specific humidity in the exhaust compared to a typical gasoline. In this sense, the limit temperature at which condensation occurs is higher, showing that the condensation problem may be even greater.

4.3.2.1 Combustion and stability

The in-cylinder pressure evolution is displayed in Figure 4.32 for two accumulation times, 0 minutes in the left hand side and 20 minutes in the right hand side. The grey colour is used to plot all recorded cycles and the orange color is used for the mean cycle at 1500 rpm at 6 bar BMEP. The comparison of both situations reflects a clear decrease in mean pressure with time, which is explained by the dispersion produced by water dilution. With similar peak pressures for the unaffected cycles, there are more low power or misfiring cycles at 20 minutes.

From combustion perspective, CA50 (left) and TOC (right) are displayed in Figure 4.33 together with the two dispersion criteria aforexplained. Normal dispersion, in black, shows those cycle with an IMEP within a 10% of the reference value, whereas abnormal dispersion, in red, is for those cycles below this threshold excluding cycles below 1 bar IMEP.

At this operating condition, combustion can be phased with the spark timing without any concern about knock, so normally a combustion close to TDC is desired, even more with EGR in order to improve flame development and maintain stable conditions. At the beginning of the test, a mean value of 2 CAD aTDC is observed for the combustion centering, whereas very short combustion durations are obtained for all cycles, below 25 CAD. These mean values are obtained from the cycles in normal dispersion. As this condition is maintained with time and condensed water accumulates, the combustion process is deteriorated with increased CA50 and TOC. Moreover, the number of cycles in abnormal dispersion and the magnitude of these cycles is also increased with time, from no representation at 0 minutes to a huge increase at 10 minutes on, also reflecting combustion deterioration.

This deterioration is mainly reflected by abnormal dispersion, since the increase in the mean value computed from the first dispersion criteria is very slight. This behaviour could be explained by the hypothesis of sudden dilution. The water condensed at the WCAC reaches the cylinder suddenly as a result

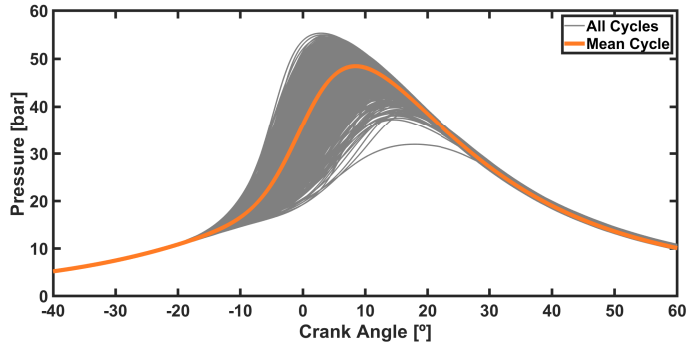

(a) 0 minutes

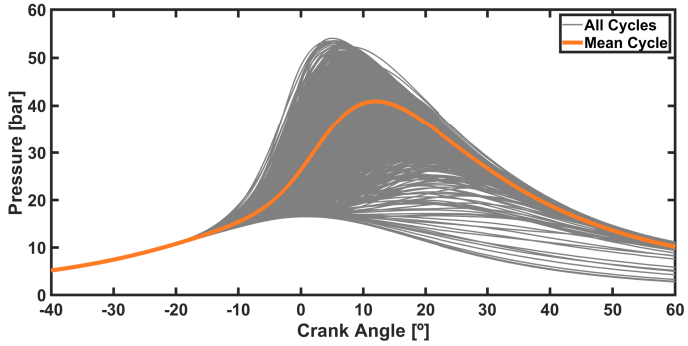

(b) 20 minutes

Figure 4.32. *Recorded in-cylinder pressure for 1500 rpm at 6 bar BMEP: a) 0 minutes; b) 20 minutes. All cycles in grey, mean cycle in orange.*

of the accumulation and the release of water drops, as already observed with the endoscope. The evaporation of water droplets inside the cylinder promotes a cooling effect that increases volumetric efficiency for that particular cycle, diluting the mixture given the fact that fuel injection is constant according to the average engine operation. The lean condition achieved together with high EGR rates slows down combustion, specially at initial stages, elongating combustion and affecting stability.

The same analysis is performed for 1500 rpm at 12 bar BMEP in Figure 4.34 and for 3000 rpm at 12 bar BMEP in Figure 4.35. Very similar trends are observed for the new operating conditions. At time 0, all cycles are within the limits of a 10% IMEP. However, several cycles with longer combustions and lower mean pressures start appearing as time elapses, specially from 10 minutes on, when almost equilibrium is reached.

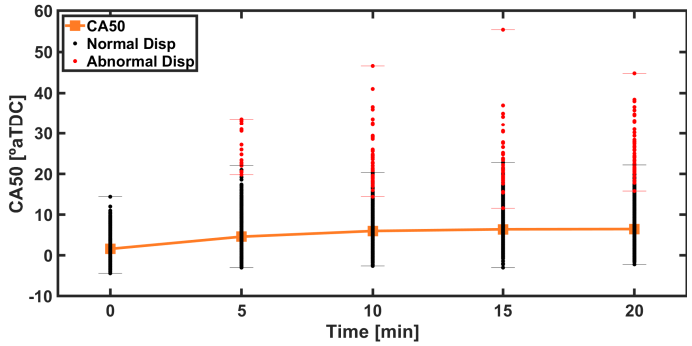

(a) CA50

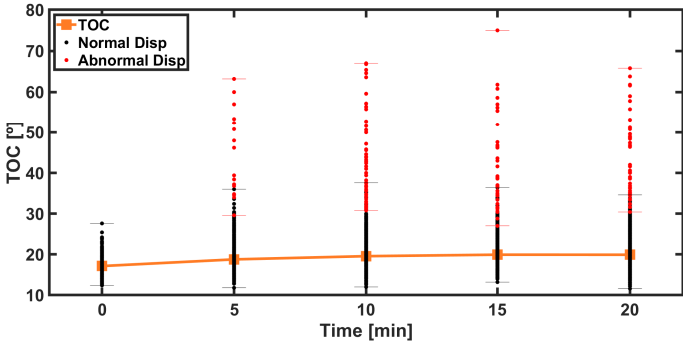

(b) TOC

Figure 4.33. *Combustion analysis evolution with time for 1500 rpm at 6 bar BMEP: a) CA50; b) TOC. Normal (black) and abnormal (red) dispersion criteria.*

When comparing the effect of dilution in the different operating conditions, it is noticeable that the 1500 rpm at 12 bar BMEP is the least affected point in terms of cyclic variability. The greater stability when facing the sudden dilution promoted by water condensation is explained by the higher engine load for the regime and the lower spark advance level, resulting in a comparatively higher combustion start temperature. Higher engine loads mean higher in-cylinder temperatures and faster combustions, thus more stable conditions despite the higher pressure that exists in the WCAC, lowering the dew point, increasing the rate of condensates.

For 3000 rpm, the same benefit from stability perspective seen in 1500 rpm at 12 bar BMEP is observed due to a higher load operation compared to 6 bar BMEP conditions. However, as seen in Figure 4.30, greater condensation rates

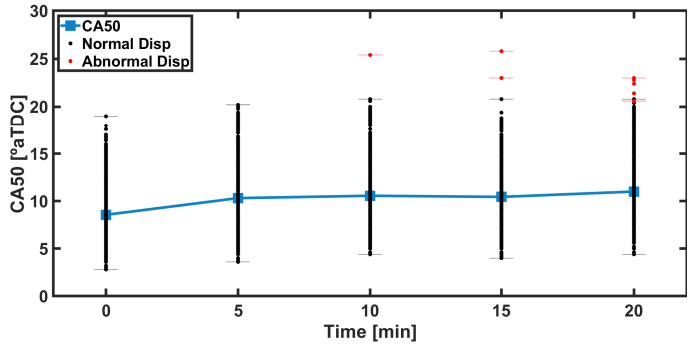

(a) CA50

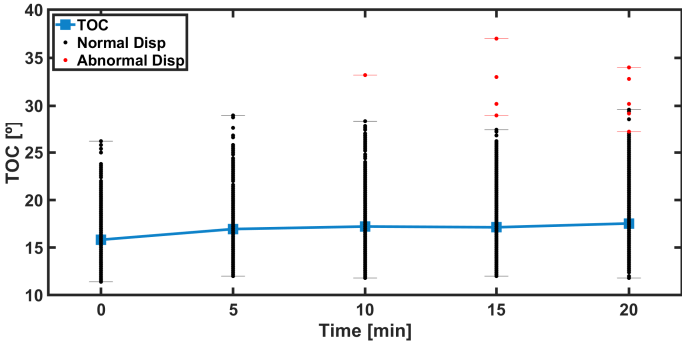

(b) TOC

Figure 4.34. *Combustion analysis evolution with time for 1500 rpm at 12 bar BMEP: a) CA50; b) TOC. Normal (black) and abnormal (red) dispersion criteria.*

are expected for this regime, deteriorating combustion more than in the case of 1500 rpm, partially overcoming these benefits.

A more detailed analysis of the cyclic variability is done by classifying individually the 800 cycles recorded per test at each time slot in different groups depending on the computed CA50. The different CA50 groups are defined depending on the engine load, with different levels for 6 and 12 bar BMEP. Besides, the coefficient of variation of the IMEP is displayed in black in the right y-axis. The COV limits stand for stability and driveability and are set at 3.33% and 2% for 6 and 12 bar BMEP respectively, based on previous experience.

The evolution over time of the distribution of cycles in each CA50 group is shown as a percentage for 1500 rpm at 6 bar BMEP in Figure 4.36. As time elapses, the share of cycles with higher CA50 is clearly increased, representing

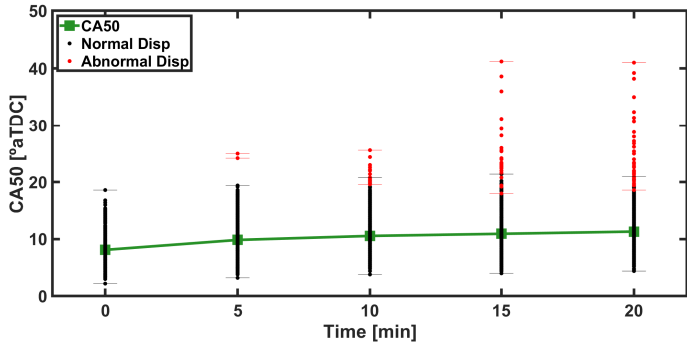

(a) CA50

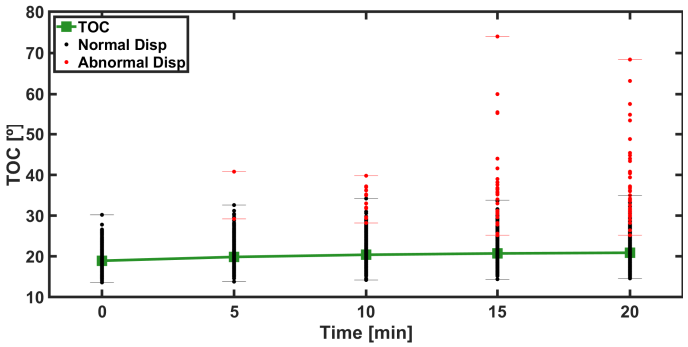

(b) TOC

Figure 4.35. *Combustion analysis evolution with time for 3000 rpm at 12 bar BMEP: a) CA50; b) TOC. Normal (black) and abnormal (red) dispersion criteria.*

longer combustions due to water accumulation and dilution effects. After 5 minutes, the test is not acceptable from stability perspective following the COV indicator.

In order to assess the dilution level achieved with water condensation, a lambda sweep is performed from reach to lean conditions at an equivalent time 0. To do so, EGR valves are closed between tests so that all water condensation is consumed and suppressed. The analysis on CA50 groups is also performed for the lambda sweep and the last time condition, in this case 20 minutes, is included. Figure 4.37 shows the distribution of cycles in each CA50 group as a percentage with lambda for 1500 rpm at 6 bar BMEP.

It is clear that with fuel enrichment, with lambdas 0.94 and 0.96, there are no cycles with CA50 beyond 10 CAD. This trend confirms that the poor combustion performance found with water condensation can be explained by

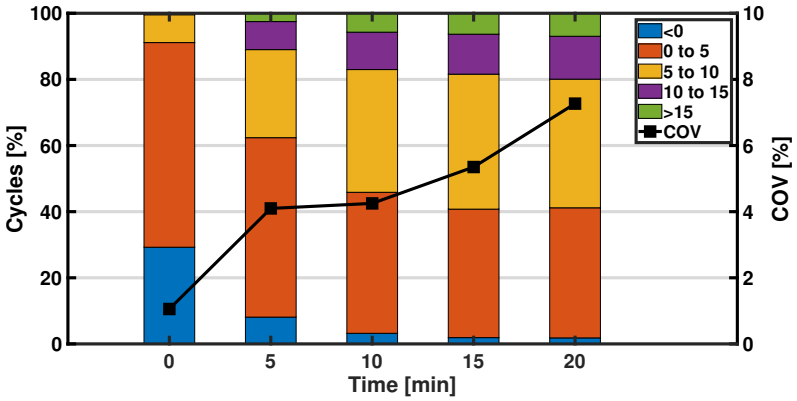

Figure 4.36. *Evolution with time of the distribution of cycles in each CA50 group and the IMEP COV for 1500 rpm at 6 bar BMEP.*

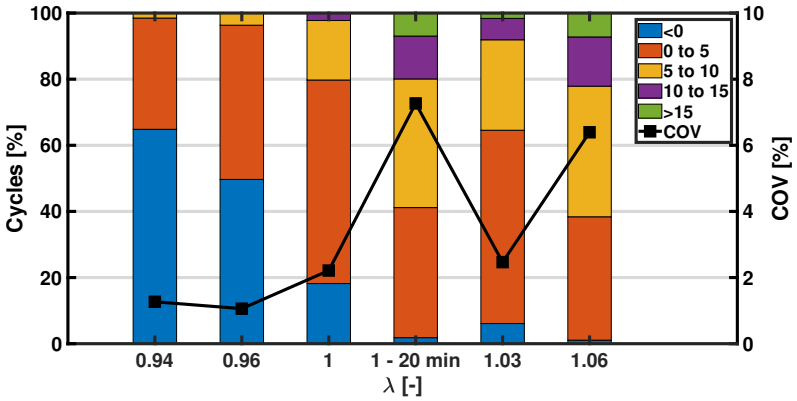

Figure 4.37. *Evolution with lambda of the distribution of cycles in each CA50 group and the IMEP COV for 1500 rpm at 6 bar BMEP.*

overleaning, which in these cases is grossly compensated for all cycles with more fuel. Since the problem of condensation is presented suddenly and unpredictably for individual cycles, an overall enrichment strategy cannot be chosen given the efficiency and hydrocarbon emissions penalty. The deterioration with time is again evident when comparing both stoichiometric conditions, since the cycles distribution achieved at 20 minutes time is comparable to that of lambda 1.06, being a clear indicator of the similar dilution levels.

For 12 bar BMEP, the analysis is performed with different CA50 groups for 1500 rpm in Figure 4.38 and Figure 4.39, and for 3000 rpm in Figure 4.40 and Figure 4.41. The evolution of COV with time is very similar for all conditions tested, clearly increasing between 5 and 10 minutes. Something similar occurs with the share of cycles within each group, increasing the number of cycles that have longer combustions with time. In the case of 1500 rpm, the COV of the IMEP limit is only reached at 20 minutes, confirming a more stable condition due to higher load operation as observed in Figure 4.34. In terms of dilution level, the 20 minutes condition seems to fit with a dilution between lambda 1 and 1.04, which is a noticeably lower lean condition than at 6 bar BMEP.

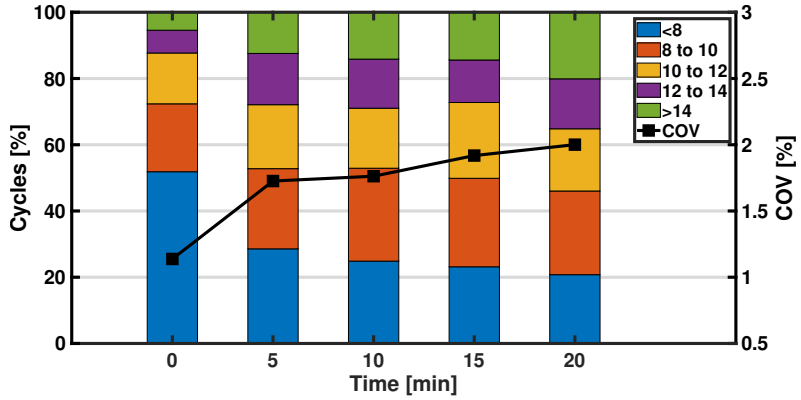

Figure 4.38. *Evolution with time of the distribution of cycles in each CA50 group and the IMEP COV for 1500 rpm at 12 bar BMEP.*

For 3000 rpm, the same trends are obtained with time and the results of IMEP COV lead to the same conclusions, despite not exceeding the limit set for this operating point due to greater stability conditions. When assessing the level of dilution reached at 20 minutes, the conclusion is that the situation is comparable to that reached with lambdas between 1.03 and 1.07. This is in accordance with what was expected compared to the other operating conditions, since it is a lower dilution level than at 6 bar but higher than 1500 rpm at the same engine load.

4.3.2.2 Fuel economy and emissions

This section focuses on discussing the impact of EGR water condensation on fuel economy and emissions measured upstream the aftertreatment. The data in the charts is presented as a percentage variation with respect to the same engine operating conditions but without EGR. The reference point is

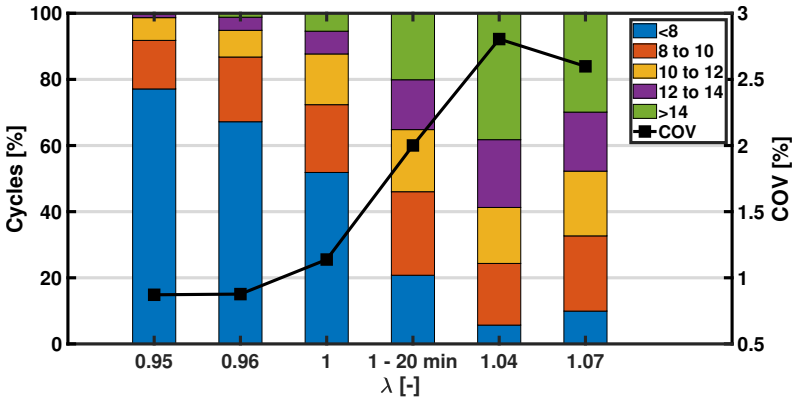

Figure 4.39. *Evolution with lambda of the distribution of cycles in each CA50 group and the IMEP COV for 1500 rpm at 12 bar BMEP.*

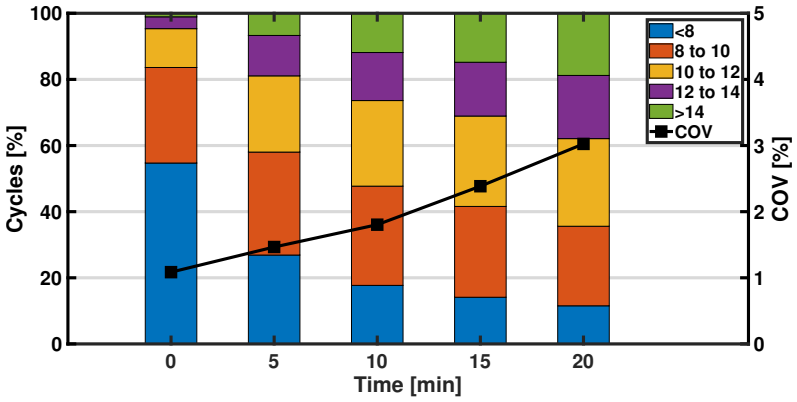

Figure 4.40. *Evolution with time of the distribution of cycles in each CA50 group and the IMEP COV for 3000 rpm at 12 bar BMEP.*

the best one obtained in previous studies in terms of calibration from fuel consumption perspective. In this way, all positive values mean a negative effect for EGR operation due to the effect of water condensation.

The BSFC evolution with time is shown in Figure 4.42. A clear increase with time is found for all operating conditions, following the combustion analysis. In addition, the 6 bar BMEP operating condition is the only one that reported a negative effect of the EGR operation due to water condensation, obtaining worse consumption than in the case of the same engine point without EGR. In this sense, EGR would not be beneficial in this low load condition.

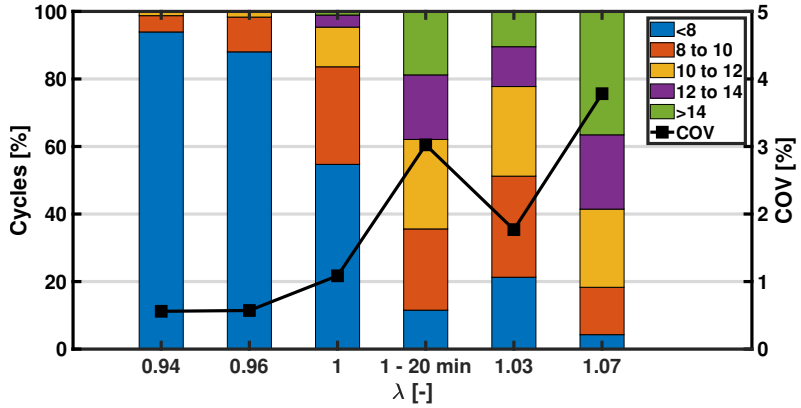

Figure 4.41. *Evolution with lambda of the distribution of cycles in each CA50 group and the IMEP COV for 3000 rpm at 12 bar BMEP.*

For higher loads, the EGR strategy is still better than operation without exhaust recycle even though the deterioration found with time due to water accumulation. The better combustion centering obtained with EGR due to knock mitigation at this engine load could be the biggest responsible for this trend.

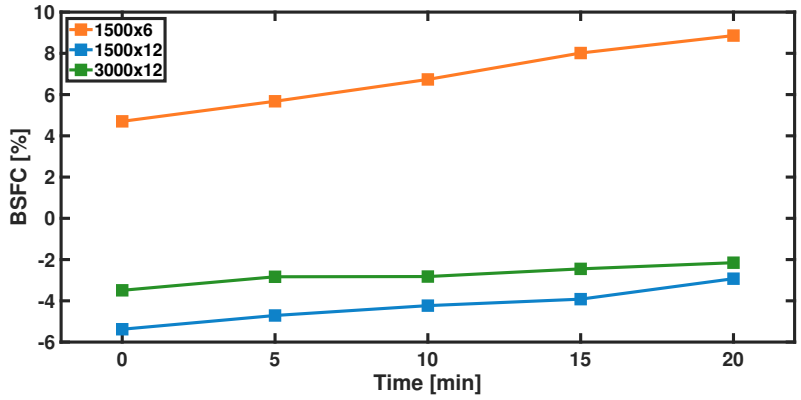

Figure 4.42. *Effect of condensation accumulation on percentual BSFC with respect to no EGR operation.*

For NO_x emissions, depicted in Figure 4.43, reduced nitrogen oxides are found with time due to reduced in-cylinder temperatures promoted by the sudden dilution effect. This effect is combined with the one from EGR operation, with lower temperatures during the combustion process, so all cases

produce lower NO_x emissions, achieving a reduction close to 90% for the high load cases.

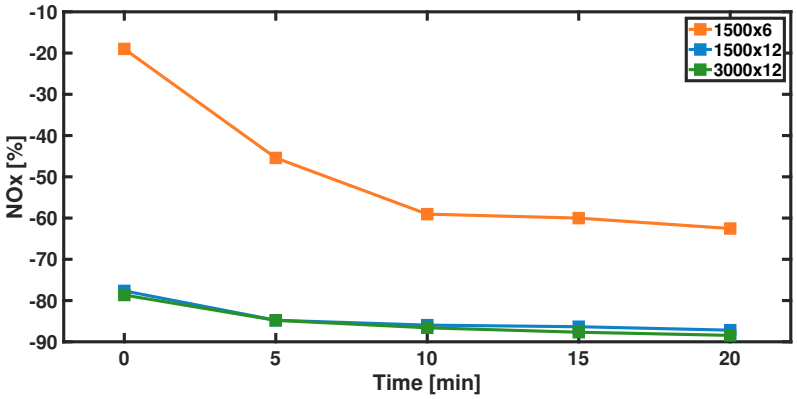

Figure 4.43. *Effect of condensation accumulation on percentual NO_x with respect to no EGR operation.*

Following the opposite trend to NO_x, total hydrocarbons are generally increased as the water condensation effect builds up over time, as shown in Figure 4.44. Longer combustions and reduced temperatures leading to an increase in quenching effects, together with misfiring at several cycles are translated into increased HC emissions. When comparing with the reference point, EGR dilution promotes a higher level of hydrocarbons per se, except for the high load 1500 rpm case at 0 minutes, which curiously experiences a reduction of about 5%, probably due to repetitiveness.

4.3.2.3 Preliminary assessment of condensation with different fuels

The instability induced by water dilucion from condensation and its effects on combustion, efficiency and emissions have been explained in the previous sections for a typical gasoline engine. In order to obtain condensing conditions, the ambient and WCAC coolant temperature had to be relatively low, around 15°C. The limit temperature at which condensation occurs is calculated with the psychrometric model and depends largely on the specific humidity in the exhaust, which in turn depends directly on the fuel formulation, in particular the hydrogen content.

In this section, the psychrometric model explained in subsection 3.4.2 is used as a preliminary approach to assess the impact of fuel formulation on condensation. With a view to decarbonization, five different fuels have been simulated with the model, being four of these low-carbon fuels with a potential

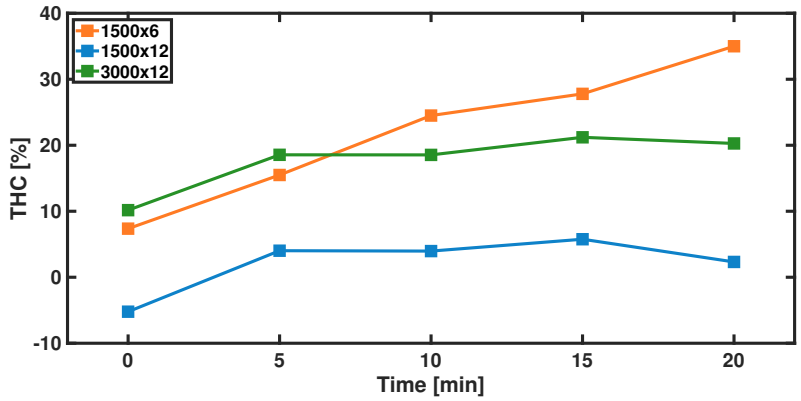

Figure 4.44. *Effect of condensation accumulation on percentual THC with respect to no EGR operation.*

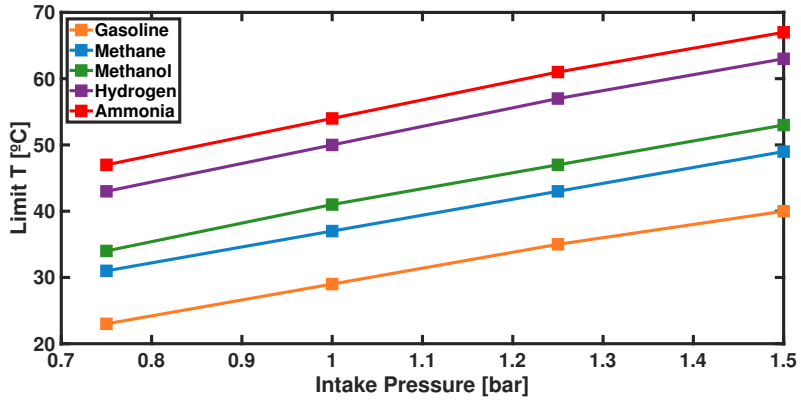

Figure 4.45. *Critical temperature for condensation formation as a function of the intake pressure and fuel formulation.*

application in SI engines in the future. The fuels in question are: gasoline (same fuel as the rest of the study), methane, methanol, hydrogen and ammonia. A constant EGR rate of 25% is set for all simulations and fuels, and the intake manifold pressure is changed from 0.75 to 1.5 bar in order to represent a wide range of conditions at stoichiometric operation. Then, the limit ambient and WCAC coolant temperature at which condensation occurs in the WCAC is obtained and depicted in Figure 4.45.

As observed, condensation in the WCAC is induced between 20 to 40°C with a traditional gasoline used in the tests. This result is in line with what has been analysed so far, with 15°C as the temperature chosen for the activity. As the ratio of hydrogen to carbon is increased with methane and methanol, the limit temperature increases 5 to 10°C at a given intake pressure and the same EGR level. This means that to avoid condensation, the WCAC coolant and ambient temperatures must be increased, so there is a greater limitation with these fuels. For zero-carbon fuels as ammonia and hydrogen, the limit temperatures are above 40°C in the best case of the study at low intake pressures, reaching values between 60 and 70°C in the worst cases. In the case of these fuels, water condensation would occur even at temperatures much higher than normal ambient temperatures, promoting condensation also in the EGR cooler and by mixing with air. This would force the WCAC to operate at outlet temperatures much higher than usual nowadays, limiting the power output of the engine given the reduced amount of charge introduced at the same volumetric efficiency. The results obtained for the limit temperature are justified by the specific humidity in the exhaust gases of each fuel, from 81.9 grams of water per kilogram of dry air in gasoline, to 140.9 and 177.6 grams of water per kilogram of dry air for methane and methanol respectively and 339.5 and 458.7 grams of water per kilogram of dry air for hydrogen and ammonia respectively.

However, the direct effect of condensation on combustion, efficiency and emissions due to sudden dilution could be very different for each fuel. Moreover, the current study was performed at stoichiometric conditions, which for these fuels, especially hydrogen and ammonia, may not be fully representative given the reactivity, knock resistance, variability and the concern of each fuel with emissions [26, 33–35]. For this reason, a second study is performed with the model for these fuels at a constant intake pressure of 1 bar in order to see the effect of lambda, since leaner operation than with gasoline is expected. Figure 4.46 shows the evolution of the limit temperature for condensation with lambda from 1 to 1.5.

As lambda increases, less water is produced in the combustion process, reducing the specific humidity at the exhaust and the critical temperature for condensation. However, there is only a few degrees reduction, around 5 and 7°C for ammonia and hydrogen respectively. The critical temperature level is still above typical ambient values, beyond 40°C, so high intake temperatures should be induced in order to avoid this problem, reducing the engine power output and knock resistance.

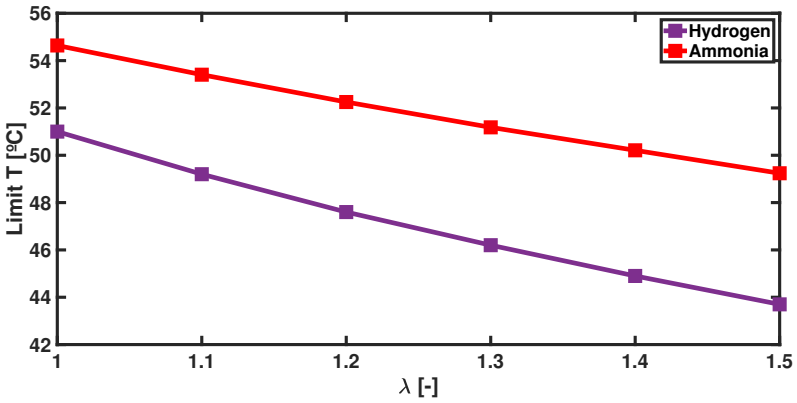

Figure 4.46. *Critical temperature for condensation formation as a function of lambda and fuel formulation.*

In order to completely assess the phenomenon, specific studies on EGR water condensation with different fuels would be required in order to quantify the possible effect of sudden dilution on stability, efficiency and emissions.

4.4 Summary and findings

This chapter has presented a deep analysis of a cooled low-pressure EGR system in a gasoline engine from several points of view. The influence of the engine calibration and the tolerance to EGR inclusion was studied in section 4.1 with a view to the effect on emissions and catalyst operation. A methodology to deocuple the effects coming from IGR and EGR was presented in section 4.2 from emissions, combustion and efficiency perspective. Finally, the problem of water condensation of a low-pressure EGR circuit was assessed in section 4.3, analysing the sudden dilution that can occur when water droplets appear in the WCAC and enter the cylinders, resulting in combustion instabilities, altered emissions and efficiency. Moreover, a preliminary analysis of this problem was performed for several fuels that are being implemented nowadays with a view to decarbonization.

An experimental campaign based on a design of experiments was performed in section 4.1, in order to assess the impact of EGR addition and influence on optimal calibration in a gasoline engine. The main variables of the DoE were the spark advance, the VVT at intake and exhaust and the LP-EGR rate. The following conclusions were extracted from the study:

- EGR addition has an impact on the optimal calibration of the spark timing, advancing it as dilution increases due to improved knock resistance and lower flame speed. Similarly, the VVT settings need to be adjusted, especially at low loads, the interaction with internal residuals being crucial.
- A linear decay of NO_x is obtained with EGR addition, together with an increase in HC, as expected given the lower in-cylinder temperatures and oxygen concentration. Carbon monoxides are generally reduced with EGR, but the trend is almost flat with great concentrations of internal residuals given the nearly constant amount of total residuals as EGR is introduced.
- The ideal catalyst operation can be affected by the change in composition of the exhaust gases, reducing the difference between oxygen available and required for HC and CO abatement. This could imply the need to operate at slightly lean conditions for high EGR rates.

In section 4.2, a methodology was developed in order to further decouple the effects coming from EGR and IGR at a low load condition, given the higher sensitivity of IGR with VVT. From the DoE tests and with the fitting

model, three equally spaced levels of RGF were obtained, with different shares of EGR-IGR at each.

First, two spark strategies are defined in order to decouple temperature and composition effects. The spark is set constant for each RGF level in the Isospark strategy, whereas the spark is adjusted in order to achieve the same temperature at combustion start in the Isotemperature strategy. The conclusions from this part were:

- In general, the induction time and the time of combustion are both increased with RGF, being reduced as the share of IGR increases probably due to higher temperatures compared to EGR.

- For the Isospark tests, a maximum decrease in induction time with IGR of 1.5 CAD for 13% and 2.3 CAD for 27% could be expected from the laminar flame speed rate correlation. This prediction is suitable for 13%, but falls short for 27%, with a reduction of 4 CAD. This is a clear indicator of the composition effect.

- Similarly, in the case of Isotemperature tests, the induction time is also reduced with IGR at 27% RGF despite the same temperature at the start is forced, confirming the composition effect.

Finally, the spark is optimized in the Optimal strategy, obtaining the following findings:

- Increased induction times and TOC are obtained with RGF and EGR compared to IGR, with flatter trends for low RGF levels. The correlations for both combustion parameters slightly overpredict the experimental value, at most 1 CAD.

- Greater RGF levels would reduce both PMEP and BSFC, with an advantage for EGR in terms of efficiency given the lower heat transfer losses. The exception is found at 27%, where greater IGR concentrations result in better BSFC driven by the PMEP improvement due to the high overlap condition.

- In terms of emissions, hydrocarbons are increased both with RGF and EGR. For nitrogen oxides, the opposite trend is observed, being increased with IGR given the higher temperatures.

The problem of sudden dilution induced by LP-EGR condensation has been explained in section 4.3, basing the analysis on the publication by Galindo et al. [36]. The problem of EGR condensation has been deeply studied for compression ignition engines, specially from corrosion, compressor damage and icing. However, this problem can be more severe for spark-ignited engines given the higher specific humidities in the exhaust, even more in the case of alternative fuels in the search for decarbonization as hydrogen, ammonia, natural gas or methanol. Besides, the problem of water droplets reaching the cylinders is yet to be completely studied.

In this sense, the analysis presented in section 4.3 focuses on the sudden dilution induced by water droplets evaporating in the cylinder, increasing the air density and the volumetric efficiency. This phenomenon, very similar to the principle of operation of the water injection technique, is unwanted because, unlike this technique, it cannot be controlled as it appears suddenly.

Three different condensation sources can be found in the experimental set-up: the LP-EGR cooler, mixing EGR gases with fresh air at low ambient temperatures and the WCAC. Since the intention of the study was to explore the effect of water droplets inside the cylinder, the first two condensation sources are supressed in order to protect the compressor wheel. Condensation in the LP-EGR cooler is prevented by connecting it to a high-temperature cooling circuit at 90°C, whereas mixing condensation is prevented by using the psychrometric model explained in subsection 3.4.2 in order to choose an ambient and WCAC coolant temperature (set equal) that allow condensation only to occur in the WCAC. Finally, the temperature for the activity was 15°C.

Condensing conditions, confirmed via endoscope, were tested during 20 minutes at 1500 rpm at two load conditions, 6 and 12 bar BMEP, and at 3000 rpm at 12 bar BMEP. Besides, a lambda sweep was performed at each operating condition in order to compare dilution levels. The analysis was performed based on combustion stability, efficiency and emissions compared to optimal strategies without EGR. Finally, a prelimanry assessment of this problem was performed with the condensation model for new fuels with a view to decarbonization. The main conclusions extracted from this study were the following:

- At the beginning of the test, all cases fell within an acceptable variation of IMEP. As time elapsed, water droplets accumulated and released, deteriorating combustion in specific cycles and reaching a steady situation beyond 10 minutes.

- The instability observed is directly related to more individual cycles with longer combustions, since the mean CA50 and TOC based on the cycles within a 10% variation of the IMEP remained very similar, with a slight decay in combustion speed. In this sense, the instability is caused by the sudden arrival of water and the dilution caused.

- Applying fuel enrichment solved instabilities, proving the charge dilution effect in individual cycles. The dilution level is estimated around 5% by comparing the share of cycles within groups of CA50 with a lambda sweep. However, fuel enrichment cannot be proposed as a suitable solution as the problem only affects specific cycles, thus considerable damage to efficiency and hydrocarbon emissions would occur.

- Not all operating conditions were affected to the same extent. At higher engine loads, higher in-cylinder temperatures are expected, so faster and more stable combustions are obtained, making these conditions less susceptible to instabilities even with greater rates of condensed water. Following this explanation, 1500 rpm at 12 bar BMEP shows the greatest stability given the highest relative load and the lowest spark advance level, promoting higher temperatures at combustion start.

- The increased variability in combustion produced an spoilage in fuel consumption between 3 to 5% depending on the operating condition. However, better fuel efficiencies are obtained even in the worst condensation case compared to the best strategy without EGR except for 1500 rpm at 6 bar BMEP.

- NO_x emissions decreased between 10 and 40% with time whereas HC increased between 10 and 30% due to worse combustions and reduced temperatures, specially at low engine loads with more frequent misfires. For this reason, an iso-NO_x strategy could be proposed in order to keep nitrogen oxides low, reducing the EGR rate with time in order to mantain HC and BSFC to the lowest possible.

- The greater specific humidity in the exhaust for the fuels that are being investigated for decarbonization increases the problem of WCAC condensation compared to traditional gasolines. In this way, the limit temperature for condensation appearance is increased beyond normal ambient temperatures, increasing around 10 degrees for methane and methanol, and 20 degrees for ammonia and hydrogen compared to gasoline. This could extend the problem to the EGR cooler and mixing with air, with a potential damage to the compressor.

The arrival of drops of water in the cylinder from EGR condensation has been shown to be a non-negligible phenomenon and must be studied and avoided. In this sense, a simple psychrometric model depending on EGR rate, intake pressure and temperature should be included in the engine controller to detect condensation. In this way, condensation can be reduced or suppressed changing the EGR rate or the WCAC coolant temperature. If no control is applied, there is a risk to operate under non-optimal conditions of fuel efficiency and emissions, especially hydrocarbons that may not be fully oxidized by the aftertreatment. Future low and zero-carbon fuels could present this problem to a higher extent, given its higher hydrogen-to-carbon ratio compared to a traditional gasoline. In order to avoid this, a simple psychrometric model should be included in the engine controllers so that condensation could be quickly evaluated based on EGR, intake pressure and temperature and mitigated. Alternatively, highly unstable conditions could appear in combustion, affecting fuel consumption and emissions.

Bibliography

[1] Nishiyama A., Le M. K., Furui T. and Ikeda Y. "The Relationship between In-Cylinder Flow-Field near Spark Plug Areas, the Spark Behavior, and the Combustion Performance inside an Optical S.I. Engine". *Applied Sciences*, Vol. 9 n^o 8, pp. 1545, apr 2019.

[2] Lavoie G. A., Ortiz-soto E., Babajimopoulos A., Martz J. B. and Assanis D. N. "Thermodynamic sweet spot for high- efficiency , dilute , boosted gasoline engines". *International Journal of Engine Research*, Vol. 14 n^o 3, pp. 260–278, 2012.

[3] Amirante R., Distaso E., Tamburrano P. and Reitz R. D. "Laminar flame speed correlations for methane, ethane, propane and their mixtures, and natural gas and gasoline for spark-ignition engine simulations". *International Journal of Engine Research*, Vol. 18 n^o 9, pp. 951–970, 2017.

[4] Szwaja S., Ansari E., Rao S., Szwaja M., Grab-Rogalinski K., Naber J. D. and Pyrc M. "Influence of exhaust residuals on combustion phases, exhaust toxic emission and fuel consumption from a natural gas fueled spark-ignition engine". *Energy Conversion and Management*, Vol. 165 n^o December 2017, pp. 440–446, 2018.

[5] Malaquias A. C. T., Netto N. A. D., da Costa R. B. R. and Baêta J. G. C. "Combined effects of internal exhaust gas recirculation and tumble motion generation in a flex-fuel direct injection engine". *Energy Conversion and Management*, Vol. 217 n^o March, pp. 113007, 2020.

[6] Dorsch M, Neumann J and Hasse C. "Application of a Phenomenological Model for the Engine-Out Emissions of Unburned Hydrocarbons in Driving Cycles". *Journal of Energy Resources Technology*, Vol. 138 n^o 2, pp. 22201, 2016.

[7] Esposito S, Diekhoff L and Pischinger S. "Prediction of gaseous pollutant emissions from a spark-ignition direct-injection engine with gas-exchange simulation". In *THIESEL 2020 Conference on Thermo- and Fluid Dynamic Processes in Direct Injection Engines*, pp. 1–20, 2020.

[8] Wei H., Zhu T., Shu G., Tan L. and Wang Y. "Gasoline engine exhaust gas recirculation - A review". *Applied Energy*, Vol. 99, pp. 534–544, 2012.

[9] Xie F., Li X., Su Y., Hong W., Jiang B. and Han L. "Influence of air and EGR dilutions on improving performance of a high compression ratio spark-ignition engine fueled with methanol at light load". *Applied Thermal Engineering*, Vol. 94, pp. 559–567, 2016.

[10] LujÃ¡n J. M., Dolz V., Monsalve-Serrano J. and Bernal Maldonado M. A. "High-pressure exhaust gas recirculation line condensation model of an internal combustion diesel engine operating at cold conditions". *International Journal of Engine Research*, 2019.

[11] Galindo J., Piqueras P., Navarro R., Tarí D. and Meano C. M. "Validation and sensitivity analysis of an in-flow water condensation model for 3D-CFD simulations of humid air streams mixing". *International Journal of Thermal Sciences*, Vol. 136 n^o November 2018, pp. 410–419, 2019.

[12] Song H. and Song S. "Numerical investigation on a dual loop EGR optimization of a light duty diesel engine based on water condensation analysis". *Applied Thermal Engineering*, Vol. 182, pp. 116064, 2021.

[13] Galindo J., Gil A., Navarro R. and García-Olivas G. "Numerical assessment of mixing of humid air streams in three-way junctions and impact on volume condensation". *Applied Thermal Engineering*, Vol. 201, 2022.

[14] Galindo J., Navarro R., Tarí D. and Moya F. "Quantitative validation of an in-flow water condensation model for 3D-CFD simulations of three-way junctions using indirect condensation measurements". *International Journal of Thermal Sciences*, Vol. 172 n^o PB, pp. 107303, 2022.

[15] Choi J., Satpathy S., Hoard J., Styles D. and Kuan C. "An Experimental and Computational Analysis of Water Condensation Separator Within a Charge Air Cooler". *ASME*, n^o October 2017, 2017.

[16] Garcia J. J. "Exhaust gas condensate corrosion test on low pressure cooling system of aluminum brazed EGR, ACAC and WCAC". *SAE Technical Papers*, Vol. 8, 2012.

[17] Bielaczyc P., Szczotka A., Swiatek A. and Woodburn J. "A Comparison of Ammonia Emission Factors from Light-Duty Vehicles Operating on Gasoline, Liquefied Petroleum Gas (LPG) and Compressed Natural Gas (CNG)". *SAE International Journal of Fuels and Lubricants*, Vol. 5 n^o 2, pp. 751–759, 2012.

[18] Weltens H., Garcia P. and Walther H. "Internal and External corrosion of exhaust systems for passenger vehicles - test procedures, laoratory and field results". *Materials and Corrosion*, pp. 31–42, 1999.

[19] Stephanie, M. Bourgoin G., Lujan J. and Pla B. "Acidic Condensation in Low Pressure EGR Systems using Diesel and Biodiesel Fuels". *SAE Technical Papers*, 2009.

[20] Chance R. and Ceselli R. "Corrosiveness of Exhaust Gas Condensates". *SAE Technical Papers*, 1983.

[21] Garrido N., Baar R., Drueckhammer J. and Kaeppner C. "The Thermodynamics of Exhaust Gas Condensation". *SAE International Journal of Engines*, Vol. 10 n^o 4, pp. 1411–1421, 2017.

[22] Cardoso J. S., Silva V., Rocha R. C., Hall M. J., Costa M. and Eusébio D. "Ammonia as an energy vector: Current and future prospects for low-carbon fuel applications in internal combustion engines". *Journal of Cleaner Production*, Vol. 296, 2021.

[23] Zhu Z., Wei Y., Mu Z., Du R., Guan W. and Liu S. "Cylinder-to-cylinder variation of knock and effects of mixture formation on knock tendency for a heavy-duty spark ignition methanol engine". *Energy*, Vol. 254, pp. 124197, 2022.

[24] Li Y., Zhang X., Wang Y., Sun J. and Fan X. "Experimental study on premixed combustion characteristics of methane-air under dual spark plug ignition strategy in a closed spherical chamber". *Fuel*, Vol. 314 n^o January, pp. 123093, 2022.

[25] Ortiz-Imedio R., Ortiz A. and Ortiz I. "Comprehensive analysis of the combustion of low carbon fuels (hydrogen, methane and coke oven gas) in a spark ignition engine through CFD modeling". *Energy Conversion and Management*, Vol. 251, pp. 114918, 2022.

[26] Salvi B. L. and Subramanian K. A. "A novel approach for experimental study and numerical modeling of combustion characteristics of a hydrogen fuelled spark ignition engine". *Sustainable Energy Technologies and Assessments*, Vol. 51 n^o January, pp. 101972, 2022.

[27] Franken T., Mauss F., Seidel L., Gern M. S., Kauf M., Matrisciano A. and Kulzer A. C. "Gasoline engine performance simulation of water injection and low-pressure exhaust gas recirculation using tabulated chemistry". *International Journal of Engine Research*, Vol. (in press), 2020.

[28] Bozza F., De Bellis V. and Teodosio L. "Potentials of cooled EGR and water injection for knock resistance and fuel consumption improvements of gasoline engines". *Applied Energy*, Vol. 169, pp. 112–125, 2016.

[29] da Rocha D. D., de Castro Radicchi F., Lopes G. S., Brunocilla M. F., Gomes P. C., Santos N., Malaquias A. C. T., Rodrigues Filho F. A. and Baêta J. G. C. "Study of the water injection control parameters on combustion performance of a spark-ignition engine". *Energy*, Vol. 217, 2021.

[30] Vaudrey Alexandre. "Thermodynamics of indirect water injection in internal combustion engines: Analysis of the fresh mixture cooling effect". *International Journal of Engine Research*, Vol. 20 n^o 5, pp. 527–539, 2019.

[31] Galindo J., Navarro R., Tari D. and Moya F. "Development of an experimental test bench and a psychrometric model for assessing condensation on a low-pressure exhaust gas recirculation cooler". *International Journal of Engine Research*, Vol. 22 n^o 5, pp. 1540–1550, 2021.

[32] Piqueras P., De la Morena J., Sanchis E. J. and Pitarch R. "Impact of Exhaust Gas Recirculation on Gaseous Emissions of Turbocharged Spark-Ignition Engines". *Applied Sciences*, pp. 1–17, 2020.

[33] Elyanov A., Golub V. and Volodin V. "Premixed hydrogen-air flame front dynamics in channels with central and peripheral ignition". *International Journal of Hydrogen Energy*, Vol. 47 n^o 53, pp. 22602–22615, 2022.

[34] Qu W., Fang Y., Wang Z., Sun H. and Feng L. "Optimization of injection system for a medium-speed four-stroke spark-ignition marine hydrogen engine". *International Journal of Hydrogen Energy*, Vol. 47 n^o 44, pp. 19289–19297, 2022.

[35] Lhuillier C., Brequigny P., Contino F. and Mounaïm-Rousselle C. "Experimental study on ammonia/hydrogen/air combustion in spark ignition engine conditions". *Fuel*, Vol. 269 n^o September 2019, pp. 117448, 2020.

[36] Galindo J., Navarro R., De la Morena J., Pitarch R. and Guilain S. "On combustion instability induced by water condensation in a low-pressure exhaust gas recirculation system for spark-ignition engines". *Energy*, Vol. 261, pp. 125122, 2022.

Chapter 5

Alternative EGR architectures

Contents

Once the baseline low-pressure EGR system has been reviewed in depth together with its interaction with internal residuals and its implications on engine operation, other alternative architectures for EGR operation are studied in this chapter. First, this LP-EGR system is compared to a high-pressure one from recirculability limits, combustion, pumping work, heat losses, efficiency and emissions perspective. An overall assessment of all conditions tested is also performed, comparing these two EGR circuits with the only IGR optimal strategy.

Besides, another low-pressure EGR structure is implemented in the engine, called pre-catalyst, since the extraction of the exhaust gas is upstream the TWC. A comparison between this system and the normative one presented in chapter 4 is performed in section 5.2. This pre-catalyst system has several implications on the composition and temperature of the exhaust recycle, making it more similar to a high-pressure one.

5.1 Comparative analysis of LP and HP-EGR

With a deep review of the low-pressure EGR system in chapter 4, a comparison with a custom made high-pressure system is performed in this section. First, the recirculability limits of each circuit are studied in subsection 5.1.1. Then, two different operating conditions are compared in subsection 5.1.2 from combustion, pumping and efficiency perspective. The conditions are chosen in order to represent throttling area (1500 rpm at 6 bar BMEP) and the transition to turbocharging area (3000 rpm at 12 bar BMEP). Lastly, an overall assessment of all operating conditions tested is performed in subsection 5.1.3, by comparing the effects of the optimal conditions found with each EGR circuit and the only IGR optimal calibration.

Following the DoE methodology described in section 4.1, the optimal calibration for efficiency in terms of VVT settings is obtained with and without EGR for different operating points. To compare both EGR systems, an EGR sweep is performed on each circuit at the same VVT setting, the optimal found for the best fuel consumption with LP-EGR within stable limits. In this sense, the throttle and VGT positions are adjusted to maintain the engine load of the test, and different EGR rates are obtained with the valves of each EGR circuit. In the case of HP-EGR, throttling and the VGT rack position may also be used to increase the pressure differential between intake and exhaust manifolds, thus the rate of recycled gas. The spark advance is set based on the efficiency criterion explained in [1], centering combustion with a CA50 value between 7 and 10 CAD aTDC. This criterion can be limited by knock at some operating conditions, specially at high loads, low engine speed and low EGR

rates. A summary of the optimal VVT settings, spark timings and EGR rates used for all tested operating conditions is shown in Table 5.1.

Table 5.1. *Operating conditions tested for LP and HP comparison.*

Engine	**VVT**	**LP-EGR**		**HP-EGR**	
Point	**Int - Exh**	**EGR rate**	**Spark Advance**	**EGR rate**	**Spark Advance**
rpm - bar	[º]	[%]	[º bTDC]	[%]	[º bTDC]
1500 - 6	0 - 0	0 - 30	7 - 27	0 - 25	7 - 27
1500 - 12	14 - 3	0 - 30	1.5 - 22	0	0 - 1.5
2000 - 6	0 - 0	0 - 26	9.5 - 35	0 - 29	9.5 - 35
2000 - 15	17 - 8	0 - 29	0 - 21	0	-1 - 0
2500 - 14	29 - 2	0 - 29	4 - 27	0 - 5	4 - 5.5
3000 - 12	18 - 2	0 - 25.5	7.5 - 30	0 - 19	8 - 17
4500 - 19	40 - 0	0 - 19	-3 - 14	0 - 9	-3 - 6

All high-pressure EGR tests are simulated with the 1D engine model explained in subsection 3.4.1 in its fitting configuration in order to obtain the HP-EGR rate, given the complexity to obtain it experimentally due to the compactness of the line and the little space available for the mixture between recycled and fresh gas. Note that at 1500 rpm and 12 bar BMEP and at 2000 rpm and 15 bar BMEP no EGR could be recirculated with the high pressure circuit given the pressure differential. This phenomenon will be explained in detail in subsection 5.1.1.

5.1.1 Recirculability limits

In this section, the capability of each system to recirculate exhaust gas is assessed, with particular attention to HP-EGR cases where it was impossible to recirculate any exhaust gas, at 1500 rpm at 12 bar BMEP and 2000 rpm at 15 bar BMEP. A summary of the maximum EGR rate and the main limit for recirculability is shown in Table 5.2. In general, greater EGR rates can be recirculated with the LP system except for the low load condition at 2000 rpm, in which throttling was used for HP.

Table 5.2. *Recirculability limits for each operating condition and EGR circuit.*

Engine	**VVT**	**LP-EGR**		**HP-EGR**	
Point	Int - Exh	Max EGR rate	Limit	Max EGR rate	Limit
rpm - bar	[º]	[%]	[-]	[%]	[-]
1500 - 6	0 - 0	30	COV	26	COV
1500 - 12	14 - 3	30	VGT	0	ΔP
2000 - 6	0 - 0	26	COV	28	COV
2000 - 15	17 - 8	29	P MAX	0	ΔP
2500 - 14	29 - 2	29	COV	4	ΔP
3000 - 12	18 - 2	25.5	ΔP	18	ΔP
4500 - 19	40 - 0	19	T2	14	COV

In the case of the LP-EGR system, the main restrictions were due to stable operation. In the case of 12 bar BMEP, both 1500 and 3000 rpm, tests are limited by the pressures at the ends of the EGR circuit. In the case of 1500 rpm, the VGT is fully closed and no more choking can be performed at the injection point to increase the rate. For 3000 rpm, although there is room to close the VGT, any further choking position that was attempted led to the loss of engine load. In the case of 2000 rpm at 15 bar BMEP, the maximum in-cylinder pressure for this regime was achieved so recirculation was limited for safety reasons. In the maximum power output condition, at 4500 rpm, the need for boosting led to the compressor outlet temperature limit at 170°C.

For the HP-EGR, only low load points and the maximum power output condition were limited by stability. Although the average of the four cylinders was within acceptable ranges, some cylinders significantly exceeded them. All other operating conditions were limited by the difference between intake and exhaust pressure manifolds once the EGR valve was fully open. The mid load points at 1500 and 2000 rpm were studied in depth, since no combination of EGR valve, VGT or throttle resulted in a minimum of recirculated exhaust gas. Figure 5.1 shows the pressure evolution at the intake (blue) and exhaust (red) manifold along the cycle together with the instantaneous EGR mass flow (green) for two cases of each sweep with maximum EGR valve opening, at 1500 rpm at 12 bar BMEP at the top and at 2000 rpm at 15 bar BMEP on the bottom. Note that the black line marks the change from positive to negative EGR flow.

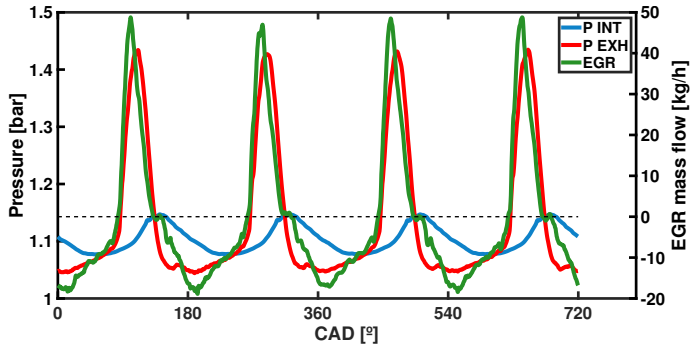

(a) 1500 rpm - 12 bar BMEP

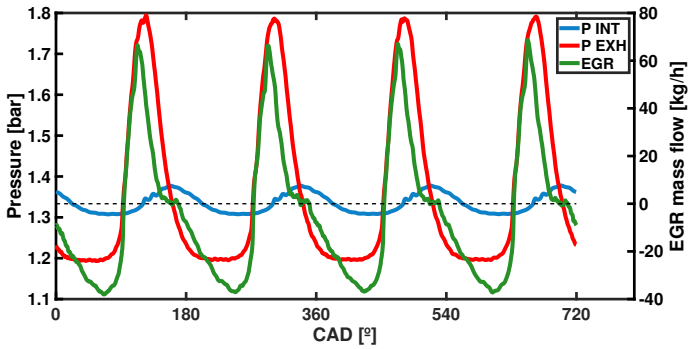

(b) 2000 rpm - 15 bar BMEP

Figure 5.1. *Evolution of intake manifold pressure (blue), exhaust manifold pressure (red) and EGR mass flow (green) for 1500x12 (top) and 2000x15 (bottom).*

As expected, the pressure pulses in the manifolds generate situations in which the ΔP is positive and negative depending on the valve events, despite the mean value of exhaust pressure being 0.03 bar higher than the intake one for both cases. As soon as the exhaust pressure pulse is slightly higher than that of the intake manifold, positive EGR flow is observed. However, when the intake pressure overcomes the exhaust pressure, reverse EGR occurs owing to the negative values of the EGR flow. In the end, the net EGR flow for all tested conditions at these operating conditions are negative and close to zero, corresponding to reverse EGR.

In these two operating conditions, some simulations were run with the fitted model in order to investigate if any HP-EGR could be recirculated with different calibrations, even though these would imply a deterioration in efficiency. With this aim, two approaches were made:

- **VVT settings:** the first approach consisted of changing the evolution of the ΔP with the VVT, so that the EGR mass flow could be increased and the reverse flow reduced or supressed. To do so, a DoE covering 25 combinations of intake and exhaust VVT was simulated.

- **Combustion:** the second approach was to change the combustion centering with the spark timing. Different combustion centerings and duration around the experimental value were simulated, promoting higher exhaust temperatures and pressures.

The two proposed strategies would mean a reduction in efficiency with respect to the reference test that should be offset by the effects of the addition of EGR. This also means that in some way, the comparison with respect to operation without EGR would start at a disadvantage. However, none of the proposed strategies resulted in a significant HP-EGR rate.

5.1.2 Low and mid load operation

As already mentioned, in this section the low load condition of 1500 rpm at 6 bar BMEP (top graphs) and the mid load condition of 3000 rpm at 12 bar BMEP (bottom graphs) are studied. The blue color and squares are used for LP-EGR and the red color with diamonds are used for HP-EGR in all charts. Since part of the analysis is based on the fitting model results, a brief validation of the results is shown in Figure 5.2 in terms of air mass flow, intake and exhaust pressures, displayed with solid, dashed and dotted line respectively.

A 5% error with respect to the test is set as the limit for each of the variables displayed. Note that the instantaneous pressure pulses in the manifolds are also verified. Since the EGR rate is unknown, the valve of the EGR circuit is used to obtain the experimental air mass flow, giving the EGR rate as a result.

In Figure 5.3, the mean pressure evolution with EGR at the intake manifold (solid line), exhaust manifold (dashed line) and turbine outlet (dotted line) are displayed. Note that in the case of 1500 rpm, the intake pressure is shown on the left axis, whereas the exhaust manifold and turbine outlet pressures are shown on the right axis due to different scaling. In the case of 3000 rpm, a dotted vertical black line is used in order to differentiate between throttling (left) and boosting (right) areas.

As explained, a higher intake pressure is needed in order to move an increased mass flow running towards the cylinders due to the addition of EGR. The intake pressures, obtained in the case of 1500 rpm with greater throttle positions, are slightly higher for the HP-EGR system in both conditions.

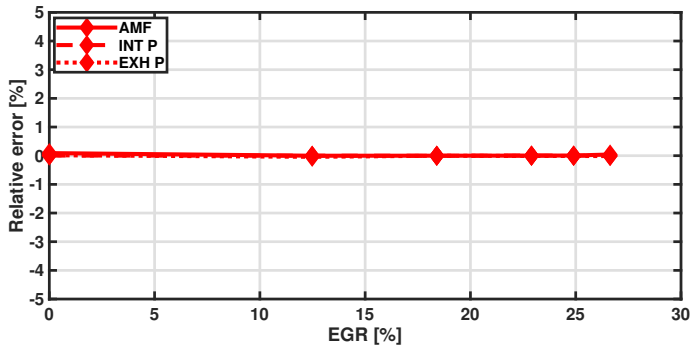

(a) 1500 rpm - 6 bar BMEP

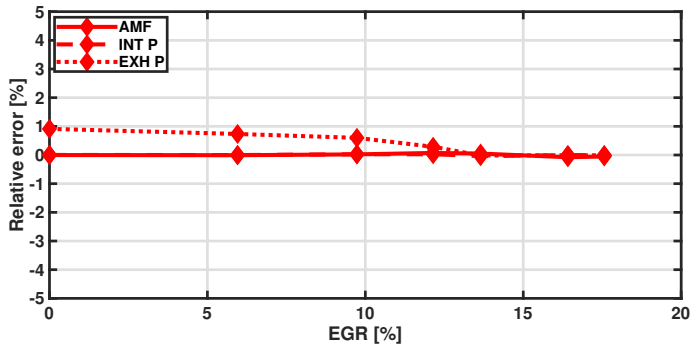

(b) 3000 rpm - 12 bar BMEP

Figure 5.2. *1D model validation for 1500x6 (top) and 3000x12 (bottom). Solid line: Air mass flow; Dashed line: Intake pressure; Dotted line: Exhaust pressure.*

Despite achieving higher rates with the LP-EGR system, the intake pressure level of the HP-EGR is not reached at 1500 rpm. When comparing the exhaust pressure at 1500 rpm, it can be seen that there is a clear pressure reduction in the HP-EGR system promoted by the extraction of the exhaust gas before its arrival at the turbine. Besides, the difference in exhaust pressure between systems increases as more EGR is recycled as for the LP system the trend is increasing and for the HP system is decreasing. The same trend is obtained at 3000 rpm up to 10% EGR. From this point on, the usage of the VGT is needed to maintain the engine load, promoting a change in the P3 trend.

One of the dominant factors when recirculating exhaust gas with HP is the pressure difference between manifolds, thus the ends of the EGR circuit. This difference is clearly reduced with EGR, despite having a notable margin at 1500 rpm. Moreover, the recirculability limits are also very marked by

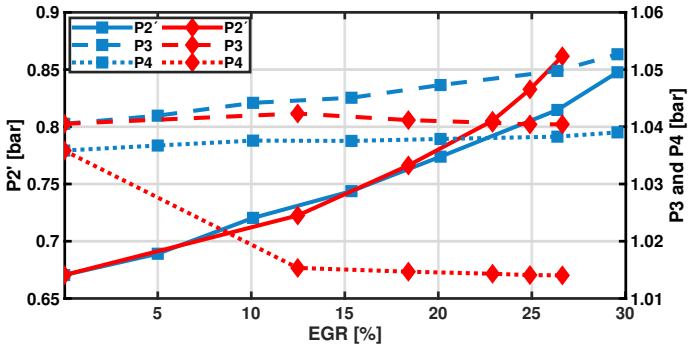

(a) 1500 rpm - 6 bar BMEP

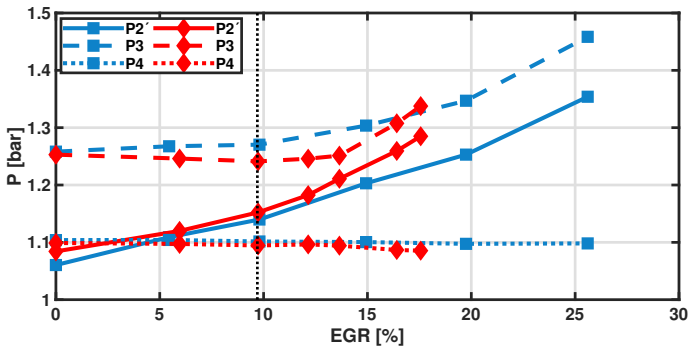

(b) 3000 rpm - 12 bar BMEP

Figure 5.3. *Pressures comparison between LP-EGR (blue) and HP-EGR (red) for 1500x6 (top) and 3000x12 (bottom). Solid line: P2; Dashed line: P3; Dotted line: P4.*

the pressure pulses that directly influence the instantaneous flow that passes through the valve, causing reverse EGR at certain moments of the cycle. This effect is diluted in the low-pressure system due to the nature of the circuit, which attenuates the pulses, in addition to the possibility of regulating the pressure in the EGR injection area with a choke valve. In the end, the similar pressure levels of the manifolds is the main limiting to recirculate greater EGR rates at 3000 rpm.

In terms of spark advance in Figure 5.4, greater advances are used since the level of dilution with EGR is increased, obtaining longer combustions. Spark is advanced based on the CA50 computed online, with the goal of centering it around 7 to 10 CAD aTDC [1]. At 3000 rpm, the spark level of the LP circuit is slightly higher than the HP circuit. This could be an indicator of a

slower combustion with LP when the CA50 is constant due to lower in-cylinder temperatures, or an indicator of a greater knock resistance for tests with CA50 beyond 10.

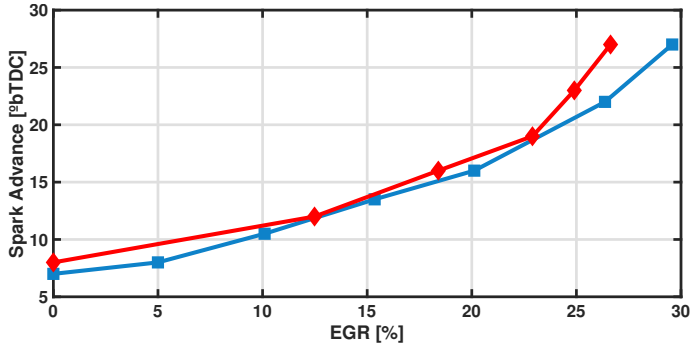

(a) 1500 rpm - 6 bar BMEP

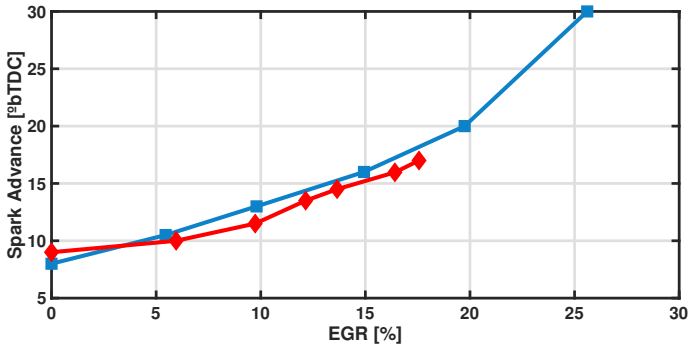

(b) 3000 rpm - 12 bar BMEP

Figure 5.4. *Spark advance comparison between LP-EGR (blue) and HP-EGR (red) for 3000x12 (top) and 2000x6 (bottom).*

The mean coefficient of variation of the IMEP is displayed in Figure 5.5. Increased dilution with EGR leads to more unstable combustions that affect the IMEP stability of the test, being this fact the limiting factor for EGR recirculation at low loads, at which the in-cylinder temperatures are relative low. Despite the mean COV not reaching the limit set for this load at 3.33%, at least one cylinder exceeded it. In the case of 3000 rpm, COV limit at 2% is not exceeded and the main limit for EGR operation is the pressure difference between manifolds.

The effects of the EGR systems on combustion timings are shown in Figure 5.6. Since the spark advance is monotonically increasing with EGR,

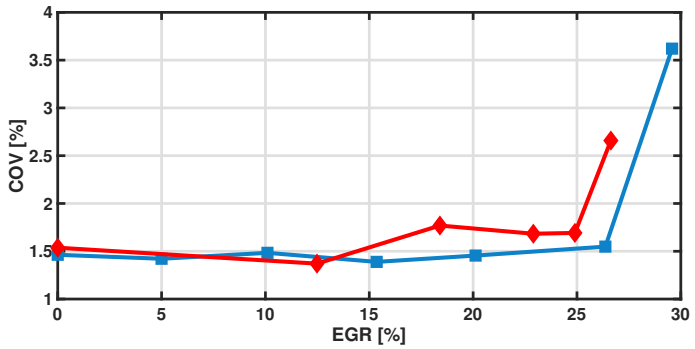

(a) 1500 rpm - 6 bar BMEP

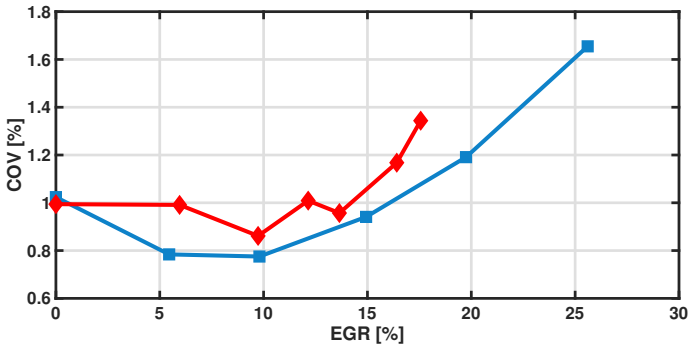

(b) 3000 rpm - 12 bar BMEP

Figure 5.5. *COV of the IMEP comparison between LP-EGR (blue) and HP-EGR (red) for 1500x6 (top) and 3000x12 (bottom).*

and the CA10 is almost kept constant with a slight reduction trend, it can be stated that the induction time is naturally increased with EGR for both conditions, as expected due to reduced laminar combustion propagation. In this sense, the first phase of combustion development is slowed with lower oxygen concentrations. Since the spark advance is set to obtain an almost constant CA50 value between 7 and 10 CAD aTDC, the greater spark advances needed to achieve a similar CA50 indicates a slower combustion from spark event to CA50, also from CA10. Knock events did not limit the spark setting at 3000 rpm since the CA50 target was easily obtained. As expected, the time of combustion obtained is increased with EGR. However, an almost flat trend is obtained for low to medium EGR rates at medium load, whereas a clear increase is obtained beyond 15%. This trend was also obtained at other medium load conditions.

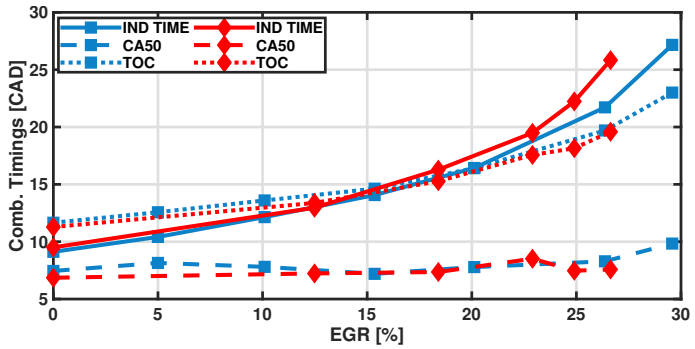

(a) 1500 rpm - 6 bar BMEP

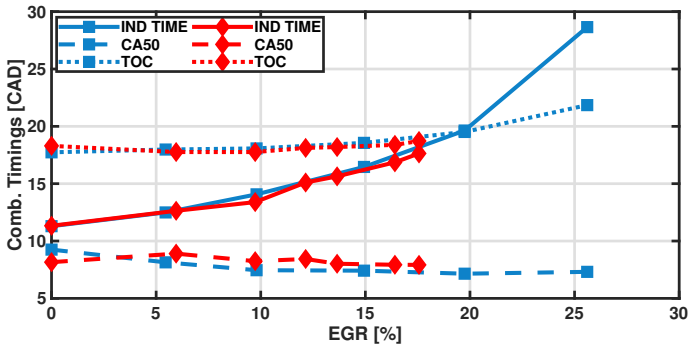

(b) 3000 rpm - 12 bar BMEP

Figure 5.6. *Combustion timings comparison between LP-EGR (blue) and HP-EGR (red) for 1500x6 (top) and 3000x12 (bottom). Solid line: Induction Time; Dashed line: CA50; Dotted line: TOC.*

The intake pressure increase is directly translated into reduced pumping losses for both systems as depicted in Figure 5.7. The pumping losses are displayed in percentage with respect to the 0% EGR case, so that only the effect of EGR addition is accounted. The reduction effect is amplified in the case of the HP system due to the exhaust pressure reduction, achieving even lower pumping levels for both regimes. A reduction of around 30% is obtained with the LP system at 1500 rpm, whereas the HP system achieves a further reduction of almost 50%. In the case of 3000 rpm, the increase in P3 promoted by the VGT position beyond 10% EGR reduces the benefit in pumping losses. However, a benefit is always obtained with respect to LP and to the reference point and.

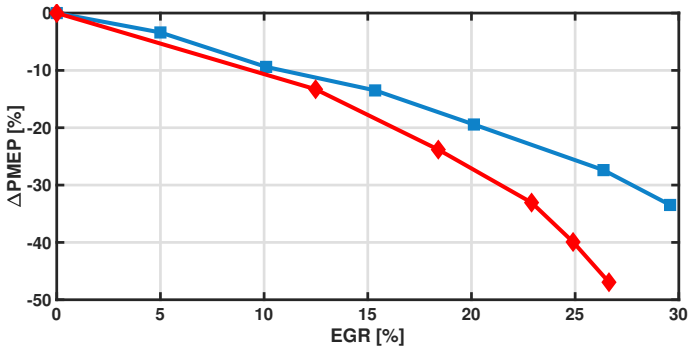

(a) 1500 rpm - 6 bar BMEP

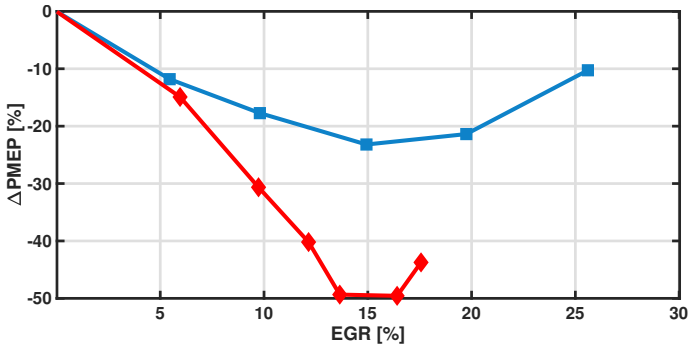

(b) 3000 rpm - 12 bar BMEP

Figure 5.7. *ΔPMEP comparison between LP-EGR (blue) and HP-EGR (red) for 1500x6 (top) and 3000x12 (bottom) with respect to 0% EGR.*

The energy balance is shown in Figure 5.8, with the top row for net indicated efficiency, the middle row for in-cylinder heat transfer and the bottom row for the energy at the exhaust. Note that the sum of these three is equal to 100% for each and every test, as expected, but results are showed as a percentual variation with respect to the first case (0% EGR) in order to assess the effect of EGR addition. Despite longer combustions and lower temperatures are obtained due to EGR dilution, benefits are observed on indicated efficiency due to pumping and better combustion phasing. A noticeable increase in the indicated efficiency is observed for both EGR systems and conditions. However, the slope of the curve flattens for greater EGR rates, the main reason for this being the appearance of more unstable cycles. At 3000 rpm, the deterioration in pumping losses already explained also is also affecting. This was also observed in other conditions, even causing the trend to reverse.

In terms of in-cylinder heat transfer, a reduction is observed with respect to operation without exhaust gases due to the temperature reduction associated with a lower reactivity and the greater ratio of specific heats for the two systems tested. Comparing EGR circuits, the higher temperatures of the HP system given the extraction of the gases upstream the turbine would induce more heat transfer than in the case of LP. The remaining energy is expelled to the exhaust, with an increase in this term for both operating conditions but with a very flat trend in HP-EGR at 1500 rpm. This is explained by the greater total flow, which increases with the EGR rate, despite the lower exhaust temperatures.

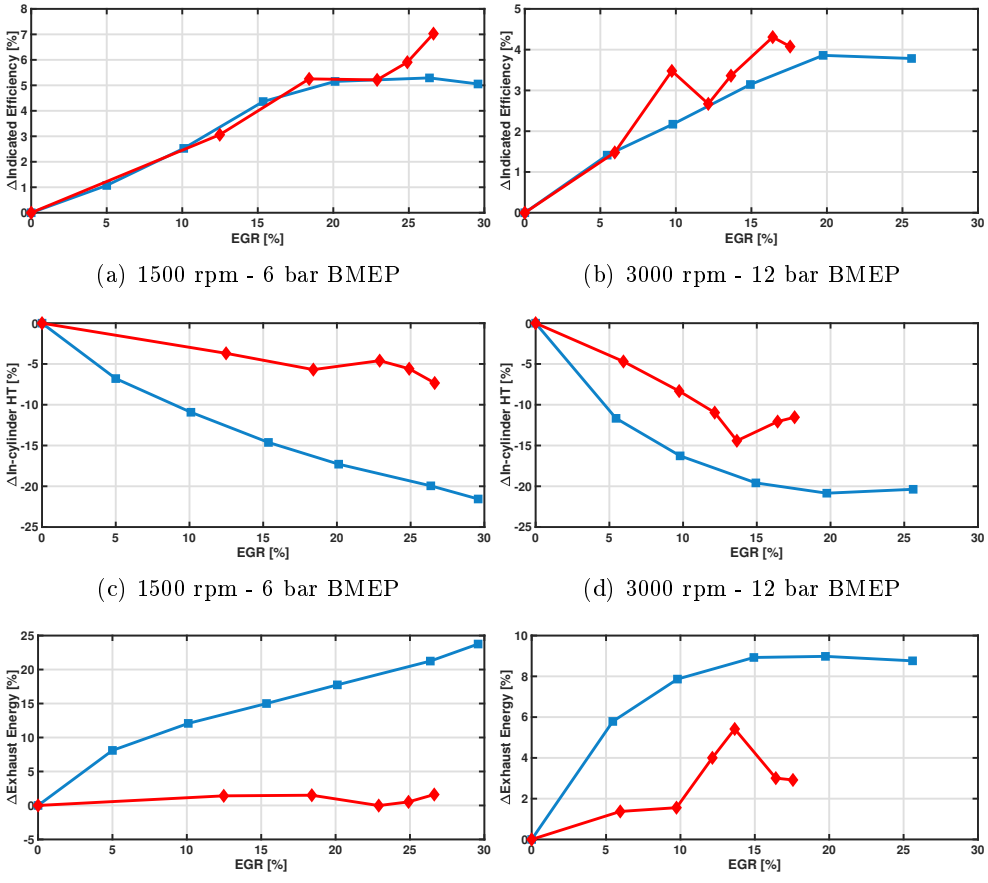

(a) 1500 rpm - 6 bar BMEP (b) 3000 rpm - 12 bar BMEP

(c) 1500 rpm - 6 bar BMEP (d) 3000 rpm - 12 bar BMEP

(e) 1500 rpm - 6 bar BMEP (f) 3000 rpm - 12 bar BMEP

Figure 5.8. *Energy balance comparison between LP-EGR (blue) and HP-EGR (red) for 1500x6 (left) and 3000x12 (right) with respect to 0% EGR. Top row: Indicated efficiency; Mid row: In-cylinder heat transfer; Bottom row: Exhaust energy.*

The sum of all the aforementioned effects is the result of the break specific fuel consumption shown in Figure 5.9, depicted as a percentual variation with respect to no EGR operation. The addition of exhaust gases increases the break efficiency for both systems. A very similar fuel consumption reduction is obtained for both circuits at 1500 rpm, with a slight advantage for the HP circuit. The main difference is found for the points at maximum EGR rate, outside stable operation. In the case of 3000 rpm, EGR addition seems more benefitial for the HP circuit at all rates, but since the LP circuit is capable of recirculating more EGR, it achieves a small advantage in consumption.

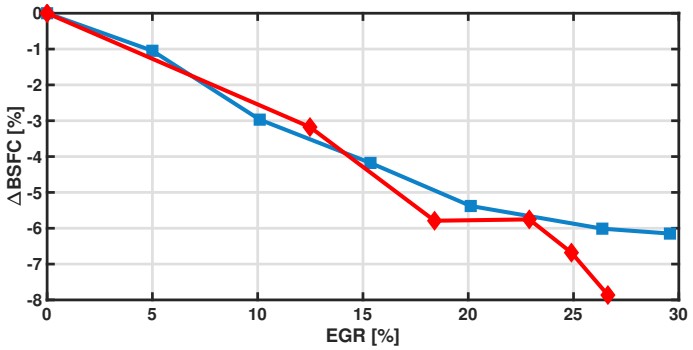

(a) 1500 rpm - 6 bar BMEP

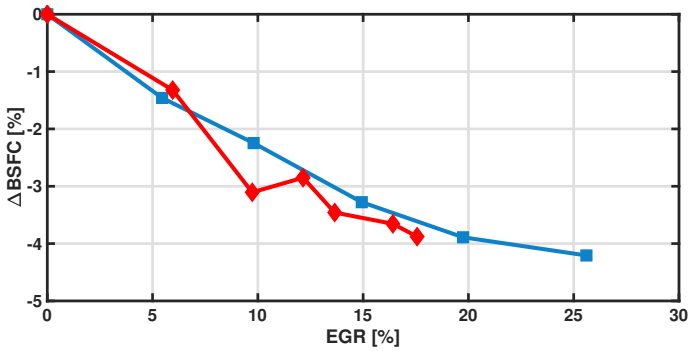

(b) 3000 rpm - 12 bar BMEP

Figure 5.9. *ΔBSFC comparison between LP-EGR (blue) and HP-EGR (red) for 1500x6 (top) and 3000x12 (bottom) with respect to 0% EGR.*

5.1.3 Overall assessment

The optimal EGR rate for fuel consumption is shown in Figure 5.10 for all conditions tested. This EGR rate is the one that provides the best efficiency

within stable limits of COV. In general, higher EGR rates are recirculated with the low pressure circuit, especially at medium load, given the greater pressure differences that exists between the ends of the circuit compared to the high pressure one. It is noteworthy the case of 2500 rpm and 14 bar BMEP, where very low EGR rates were recirculated with the high-pressure circuit, following the problem explained in subsection 5.1.1. In this sense, not much benefit could be obtained with HP-EGR in this operating condition.

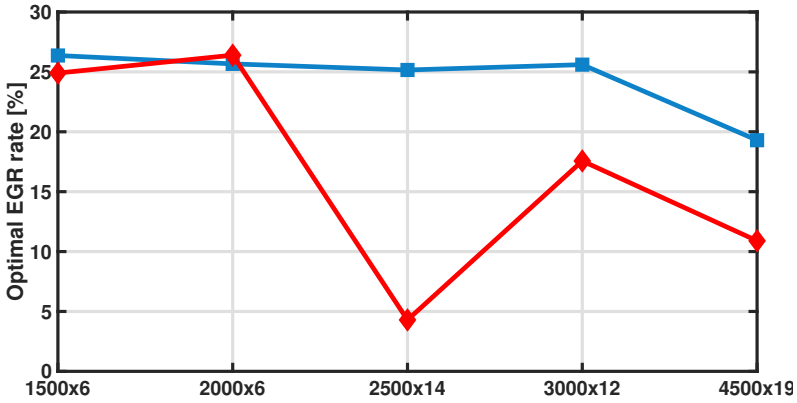

Figure 5.10. *Comparison of optimal EGR rate obtained for best BSFC within stable limits between LP-EGR (blue) and HP-EGR (red) for all tested conditions.*

The net variation in PMEP and the percentual variation in BSFC achieved with the optimal EGR rate for efficiency are depicted in Figure 5.11 and Figure 5.12 respectively for all tested conditions. These variations have been calculated with respect to two different conditions without EGR. First, the variation with respect to 0% EGR at a constant VVT calibration, thus the first point in each EGR sweep performed, is shown with solid lines. Second, the variations are computed with respect to the optimal conditions found with the only IGR strategy, and are shown with dashed lines. In this sense, any negative value would mean a benefit of EGR addition with respect to the reference point, whereas positive values would mean a benefit for the corresponding no EGR strategy. In this sense, and since the dashed lines are computed based on the best possible strategy without EGR, these lines should always be above the solid ones in terms of BSFC.

The HP circuit is always a better pumping loss reducer than the LP-circuit. This is easily explained by the extraction of the exhaust gas upstream the turbine, which reduces the total amount of flow and the back pressure. Besides, the intake pressure is further increased in some cases compared to the LP-EGR

circuit, specially at low loads. In the case of 2500 and 4500 rpm, these are the only conditions in which LP-EGR addition turns out not to be beneficial for pumping losses due to the usage of the VGT. This trend does not appear with HP-EGR, which always reduces PMEP compared to normal operation. This is expected to occur at any other high load condition with the low-pressure circuit, more the lower the regime is. It must be noted that the only IGR strategy provides better pumping losses at low loads than the LP circuit owing to a LIVC strategy. However, this advantage fades compared to the high-pressure circuit, making the HP-EGR strategy slightly better from pumping perspective.

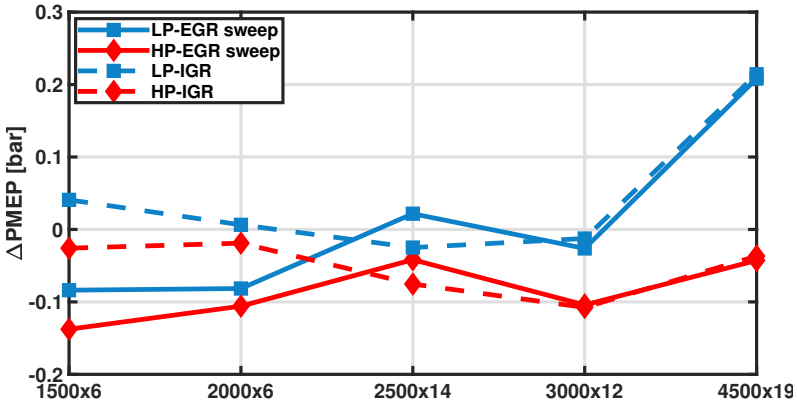

Figure 5.11. *Optimal ΔPMEP comparison for all tested conditions between LP-EGR (blue) and HP-EGR (red) with respect to 0% EGR at same calibration (solid line) and optimal IGR calibration (dashed line).*

For fuel consumption, EGR strategies are in general benefitial compared to both non-EGR strategies. Moreover, the only IGR strategy is always better than the 0% EGR case of the sweep, as expected, including at 3000 rpm, being this one the case with the least difference. It is noteworthy that the only condition in which EGR addition with the high-pressure circuit achieves a better fuel consumption than the low-pressure one is at 1500 rpm. Apart from this point, all LP-EGR sweeps reduced fuel consumption to a greater extent than HP-EGR, despite the pumping losses. This is explained by the lower heat transfer losses of the LP-circuit, both at equal and optimal EGR rates. It must be stated that better efficiencies could be obtained with the only IGR strategies at 1500 rpm compared to the LP circuit and at 2500 rpm compared to the HP circuit. In this way, if only one of these EGR circuits were mounted on the engine, the best consumption strategy would be not to use EGR at the point in question. In the case of mounting both circuits, the only IGR strategy

would never be the best one for consumption, and a transition between circuits should be made. The usage of both circuits at the same time should be further explored and it is proposed as future works.

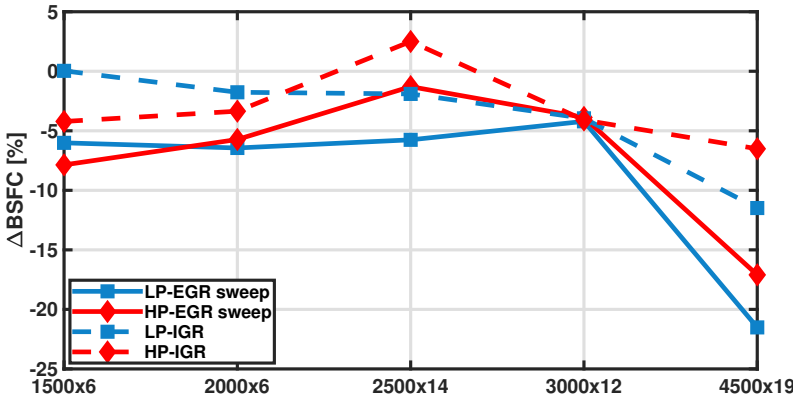

Figure 5.12. *Optimal ΔBSFC comparison for all tested conditions between LP-EGR (blue) and HP-EGR (red) with respect to 0% EGR at same calibration (solid line) and optimal IGR calibration (dashed line).*

The emissions analysis is shown in Figure 5.13, with the percentual variation of NO_x in the top row, HC in the middle row and CO in the bottom row. In terms of nitrogen oxides, the addition of EGR is proven as a good reduction technique with both circuits, with a slight advantage for LP due to the lower temperatures. However, there are some exceptions worth mentioning. In the case of 2500 rpm with HP-EGR, the low rate achieved does not provide a great reducing effect on nitrogen oxides, as expected. Moreover, at 4500 rpm, enrichment suppression results in a greater production of nitrogen oxides with HP-EGR addition. With the LP circuit, NO_x is still reduced in this condition given the lower temperatures. Comparing with the IGR only strategy, it is notable that the reduction produced in NO_x is less at low loads. This is explained by the fact that at low loads, the optimal strategy with only IGR is achieved with high overlap conditions, reaching very high levels of dilution through residuals, so the nitrogen oxides level in this tests were much lower than that of the 0% EGR cases in the sweeps. For HC, the totally opposite trend is observed, increasing as EGR is introduced, especially with the low-pressure circuit, given the lower temperatures. The only case close to a 0% variation in hydrocarbons is again at 2500 rpm with HP-EGR, due to the low rate achieved. Moreover, the high dilution achieved with only IGR at low loads is confirmed since the variation in hydrocarbons is lower compared to the first case of the EGR sweep. Again, the high temperatures of the HP-circuit

combined with enrichment suppression results in reduced HC at 4500 rpm. In general, EGR usage reduces carbon monoxide production, especially when the low-pressure circuit is used. In this sense, it seems that the fact of slowing down the dissociation of CO_2 formed during combustion is a factor of greater weight than the fact of freezing the carbon monoxide oxidation reaction, since the result in CO is a balance between these two factos. It should be noted that with the only IGR strategy, the same CO levels are achieved as with EGR for low loads and at 2500 rpm.

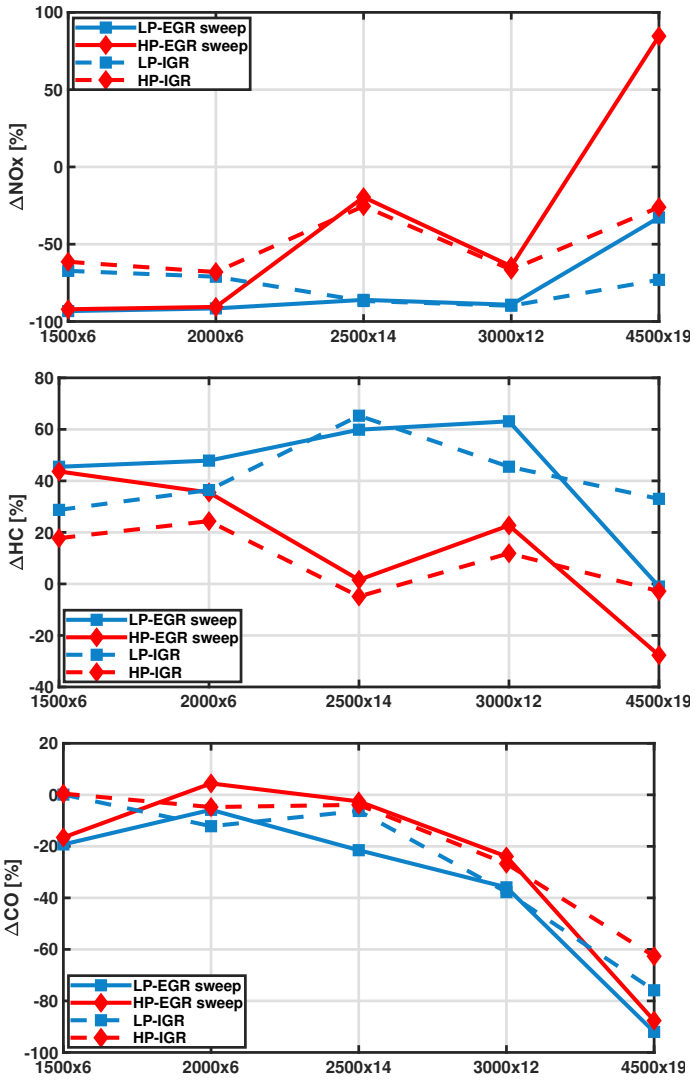

Figure 5.13. *Emissions comparison for all tested conditions between LP-EGR (blue) and HP-EGR (red) with respect to 0% EGR at same calibration (solid line) and optimal IGR calibration (dashed line). Top row: NO_x; Mid row: HC; Bottom row: CO.*

5.2 Effects of recirculated gas composition (pre-post catalyst)

In this section, two LP-EGR configurations are tested and compared. The first one, which is always shown in blue, is called POST and it is the same configuration used to compare with the HP-EGR circuit in section 5.1. The second one, shown in orange, is called PRE. The difference between the two systems lies in the extraction point of the EGR with respect to the aftertreatment system, in this case a TWC. For the LP-EGR POST, the extraction point remains downstream the TWC as in the case of the LP sweeps in section 5.1, whereas in the case of LP-EGR PRE, the extraction point is moved upstream the TWC. This change in exhaust gas extraction has several implications in combustion, since the composition of the gas is very different, with more fuel traces in the form of HC and CO, as well as NO_x, for the PRE configuration. Besides, the extraction point will change the back pressure downstream the turbine and the temperature of the exhaust gas running towards the intake line.

The two LP-EGR configurations were tested in the same seven engine operating conditions of speed and load as the comparison between HP and LP and with the same VVT configuration. In this sense, the LP-EGR sweep in section 5.1 is the same as in this section, but was repeated due to changes in the hardware and to eliminate any variable that may have changed due to wear associated with time and that may distort the comparison between systems. A comparison of the two LP-EGR sweeps was performed in order to ensure that the observed trends hold.

The tests are carried out by achieving the engine load with the throttle or the VGT position with the optimal VVT calibration found for EGR and at stoichiometric conditions except for the highest load case. The EGR rates are achieved with the combination of the LP-EGR and the choke valves, the latter being placed upstream the compressor. For the spark timing, two different strategies have been followed. The first one, called Isospark, is keeping the same spark timing as in the LP-EGR sweeps in section 5.1 and it is shown in lighter colours. With this spark strategy, the implications of each system on combustion speed can be better assessed. The second strategy aims for the best efficiency of each sweep, following the criteria of CA50 between 7 and 10 CAD as in [1] when possible, since there is still a limitation with knock and exhaust temperature in some cases. With this spark strategy, the feasibility of the systems is better compared in terms of emissions and efficiency.

Following the structure presented in the comparison between LP and HP-EGR circuits, the comparison is divided into two parts. First of all, both EGR configurations are compared for two different operating conditions in subsection 5.2.1: 1500 rpm at 6 bar BMEP on the left hand side and 2500 rpm at 14 bar BMEP on the right hand side. These operating conditions are representative of the throttling and boosting area respectively. The comparison is made based on combustion, stability, intake pressure, pumping losses and fuel efficiency. In subsection 5.2.2, all operating conditions are assessed in order to observe general trends in terms of compressor operation, optimal EGR rates, fuel efficiency, PMEP, energy balance and emissions.

5.2.1 Low and mid load operation

Figure 5.14 shows the comparison between EGR systems for spark timing (top row) and CA50 (bottom row) for the two operating conditions aforementioned, 1500 rpm at 6 bar BMEP (left) and 2500 rpm at 14 bar BMEP (right). Note than the lighter colors are for the Isospark strategy, whereas the darker colors are for the optimal one, with more advanced spark levels, keeping orange for PRE and blue for POST.

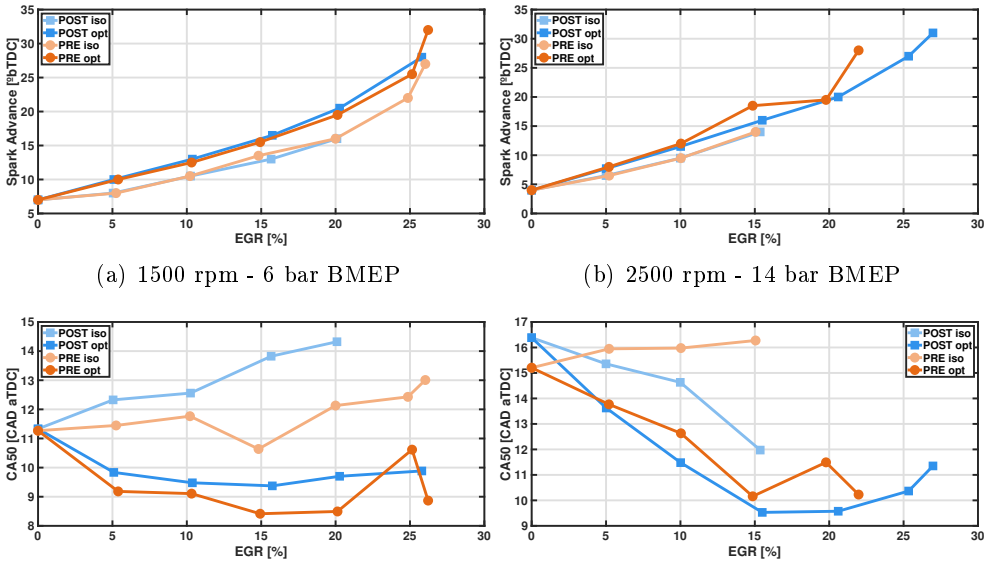

(a) 1500 rpm - 6 bar BMEP

(b) 2500 rpm - 14 bar BMEP

(c) 1500 rpm - 6 bar BMEP

(d) 2500 rpm - 14 bar BMEP

Figure 5.14. *Spark timing (top row) and CA50 (bottom row) comparison between POST (blue) and PRE (orange) for 1500x6 (left) and 2500x14 (right).*

For both operating conditions, advanced spark levels are needed for stability as EGR is introduced, reaching very similar levels between systems. Note that for 2500 rpm, the recirculability of the PRE system is reduced at optimal conditions compared to POST. This is also observed when comparing between spark strategies. Naturally, increased CA50 values are obtained with the Isospark strategy, denoting slower combustions. It is noteworthy that with the PRE system, faster combustion is obtained at 1500 rpm, contrary to what is observed at 2500 rpm, demonstrating the advantage that fuel traces and increased temperatures can have at low loads and speeds. Note that the optimal spark at 2500 rpm is limited by knock probability at low EGR rates. the remaining parameters used for the combustion analysis are shown in Figure 5.15, with the induction time in the top row and the TOC in the bottom row.

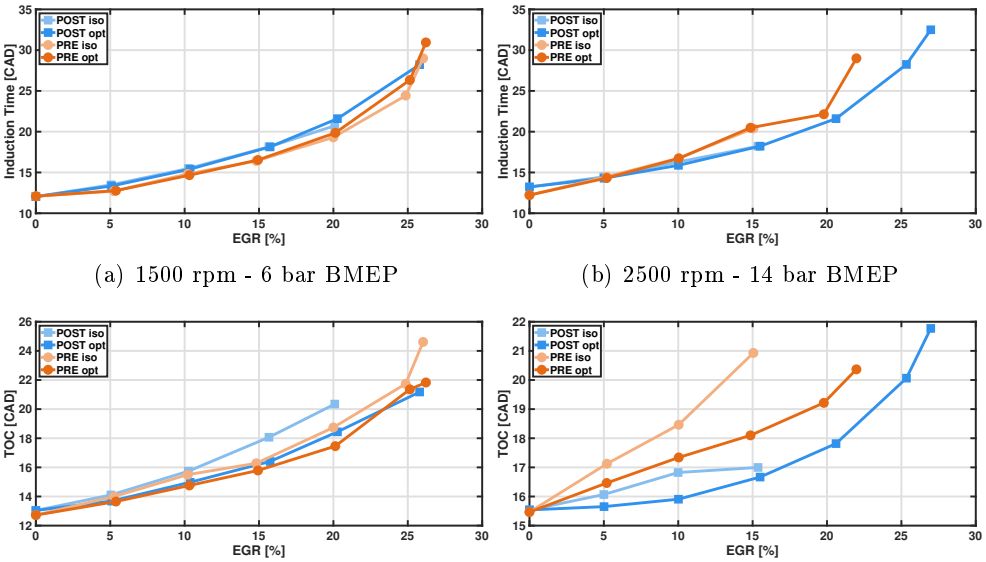

(a) 1500 rpm - 6 bar BMEP

(b) 2500 rpm - 14 bar BMEP

(c) 1500 rpm - 6 bar BMEP

(d) 2500 rpm - 14 bar BMEP

Figure 5.15. *Induction time (top row) and TOC (bottom row) comparison between POST (blue) and PRE (orange) for 1500x6 (left) and 2500x14 (right).*

As expected, increased times are obtained as EGR is introduced with both circuits, with reduced differences for the induction time than for TOC. The time of combustion confirms that flame propagation is enhanced with the PRE system at 1500 rpm, while it is slower at 2500 rpm. Longer combustions are obtained at this regime even with the optimal spark strategy for the PRE

circuit. This combustion deterioration with the PRE circuit is observed for all conditions tested except 1500 rpm at low load.

Combustion stability is evaluated based on the COV of the IMEP in Figure 5.16. Very stable combustions are observed, specially for the optimal spark strategy, until the behaviour reaches a cliff, in a non-progressive way especially at 1500 rpm, demonstrating the high sensitivity to the limit EGR rate. In this sense, stable operation is obtained up to 25% EGR for both circuits at 1500 rpm, being the limit at 3.33% for this engine load and discarding the last EGR rate achieved for the PRE circuit. In a similar way, the last EGR rate achieved with both circuits is discarded in the case of 2500 rpm, with a the limit set at 2%.

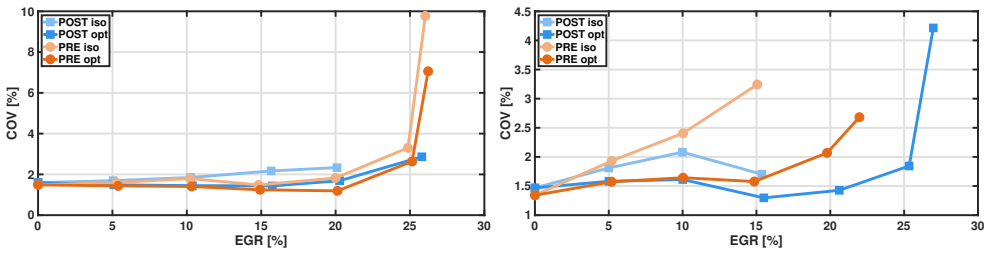

(a) 1500 rpm - 6 bar BMEP (b) 2500 rpm - 14 bar BMEP

Figure 5.16. *COV comparison between POST (blue) and PRE (orange) for 1500x6 (left) and 2500x14 (right).*

Increased intake pressure is needed in order to introduce EGR in the cylinders for both systems, as depicted in Figure 5.17. The higher temperature of the gases in the intake line for the PRE system promote higher intake pressures compared to the POST system in order to compensate for the lower volumetric efficiency. This is observed in all the conditions tested, being 1500 rpm at 6 bar BMEP the point in which there is less difference between systems. In this sense, the combustion deterioration with the PRE system was also observed in the in-cylinder pressure evolution, with a slowdown close to TDC. This deterioration in combustion due to the different composition could be aggravated by a change in the flow field in the surroundings of the spark plug, given the higher pressure level, which in turn is compensated by further increasing the intake pressure. However, a CFD study would be necessary to confirm this hypothesis and is proposed for future studies.

Figure 5.18 shows the variation in pumping losses (top row) and BSFC (bottom row) obtained with EGR addition as a percentual difference with

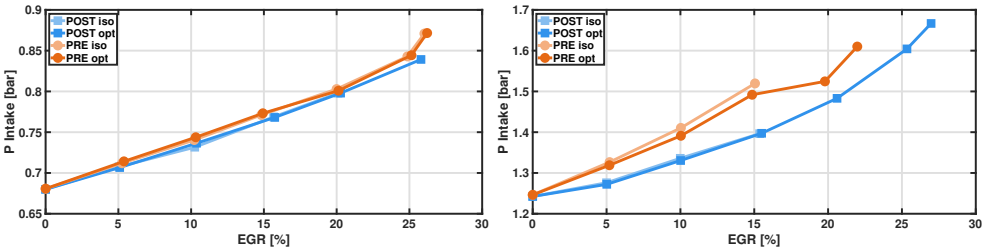

(a) 1500 rpm - 6 bar BMEP (b) 2500 rpm - 14 bar BMEP

Figure 5.17. *Intake pressure comparison between POST (blue) and PRE (orange) for 1500x6 (left) and 2500x14 (right).*

respect to 0%. Note that the Isospark tests have been removed in order to only assess the optimal strategy. The reduced back pressure obtained with the extraction of the exhaust gases upstream the TWC is translated into reduced pumping losses for the PRE system at both regimes, as expected. However, bigger differences are observed at 2500 rpm, where pumping losses tend to be reduced up to 15%, moment in which the greater position of the turbine causes an increase in the back pressure that leads to greater pumping losses. It should be noted that for the PRE system, all the conditions produce an improvement with respect to the case without EGR, while from 20% of EGR for the POST system there is a net deterioration. In terms of BSFC, pumping losses reduction with the PRE system drives the improvement in fuel efficiency, obtaining reduced consumptions for the PRE system. This difference is enlarged for the case of 1500 rpm given the better combustions obtained with the PRE circuit. At both regimes, the best BSFC within stability limits are obtained at 20 and 25% EGR for the PRE and POST system respectively. In this sense, if the optimal values are compared, the POST system achieves better pumping levels than the PRE system.

5.2.2 Overall assessment

The temperature (left) and pressure (right) at the compressor inlet are shown in Figure 5.19 with respect to the EGR flow for all tests conducted, keeping the colour scheme for each circuit. As EGR is introduced, the higher temperature of the exhaust gas for the PRE circuit induced greater temperatures at the compressor inlet. However, the increased pressure level at the extraction point of the PRE circuit, since the gases have not passed through the catalyst, is translated into increased pressures at the compressor

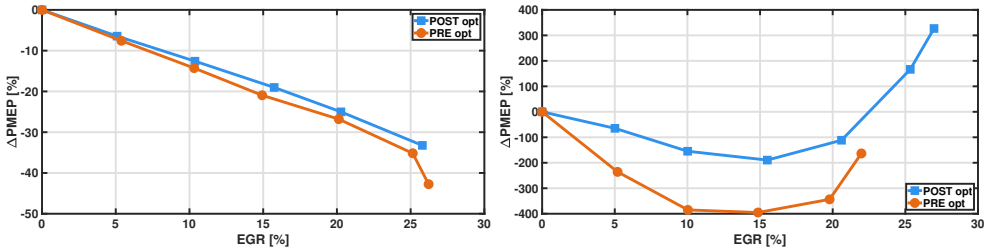

(a) 1500 rpm - 6 bar BMEP

(b) 2500 rpm - 14 bar BMEP

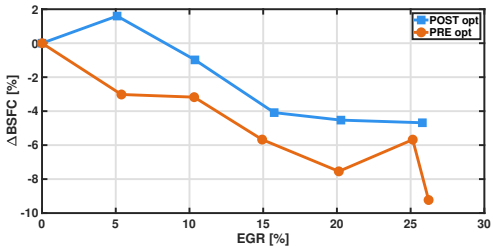

(c) 1500 rpm - 6 bar BMEP

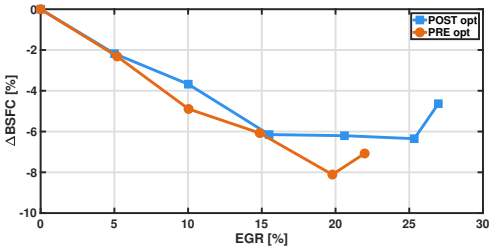

(d) 2500 rpm - 14 bar BMEP

Figure 5.18. *ΔPMEP (top row) and ΔBSFC (bottom row) comparison between POST (blue) and PRE (orange) for 1500x6 (left) and 2500x14 (right).*

inlet compared to the POST circuit. The difference in compressor inlet pressure is increased with the EGR flow.

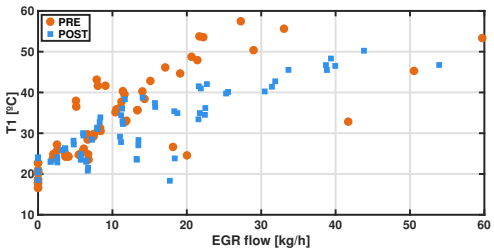

(a) Compressor inlet temperature

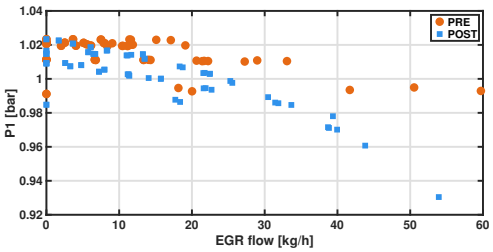

(b) Compressor inlet pressure

Figure 5.19. *Compressor inlet temperature (left) and pressure (right) with respect to EGR flow comparison between POST (blue) and PRE (orange) for all tested conditions.*

Despite the higher inlet temperature of the PRE circuit, the difference found in compressor inlet pressure results in no bigger differences in the

compressor efficiency, shown in Figure 5.20. The compressor efficiency is not negatively affected for the PRE circuit, being roughly equivalent to or better than the POST circuit except at some mid turbocharger speed points.

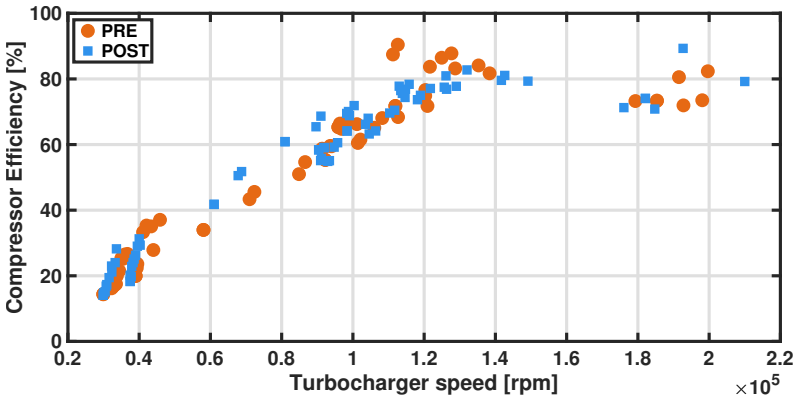

Figure 5.20. *Compressor efficiency with respect to EGR flow comparison between POST (blue) and PRE (orange) for all tested conditions.*

The optimal EGR rate for fuel efficiency within stable operation is depicted in Figure 5.21 for all operating conditions tested. Results show that the optimal consumption is obtained with between 5 and 10% less EGR with the PRE circuit, so less EGR flow is needed to obtain similar or improved levels of BSFC. The only condition tested in which similar optimal EGR rates were obtained is 4500 rpm at 19 bar BMEP, whereas the greatest difference is found in 2000 rpm at 15 bar BMEP, with very low EGR rates for the PRE systems due to combustion instabilities. In this condition, the PRE system reached the same BSFC level as the POST circuit with a 10% EGR rate, but COV was beyond 2%.

The net variation in PMEP achieved with the optimal EGR rate is shown in Figure 5.22 with respect to no EGR operation for both circuits. At low loads, it is expected that greater EGR rates induce lower pumping losses. Despite the lower EGR rates achieved with the PRE system, greater PMEP reductions are obtained except for the 1500 rpm at 6 bar BMEP condition. In the case of mid and high engine loads, the use of VGT means that after a certain point, adding EGR can be harmful, so recirculating less EGR with the PRE system is beneficial.

The fuel consumption obtained with the optimal EGR rate is shown in Figure 5.23 as a percentual variation with respect to no EGR operation.

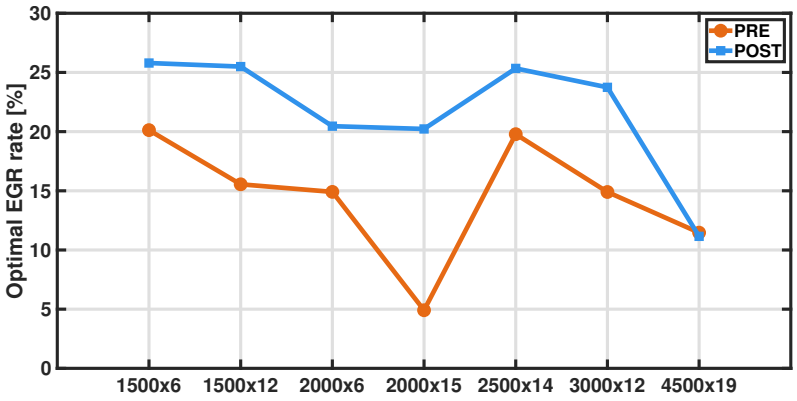

Figure 5.21. *Comparison of optimal EGR rate obtained for best BSFC within stable limits between POST (blue) and PRE (orange) for all tested conditions.*

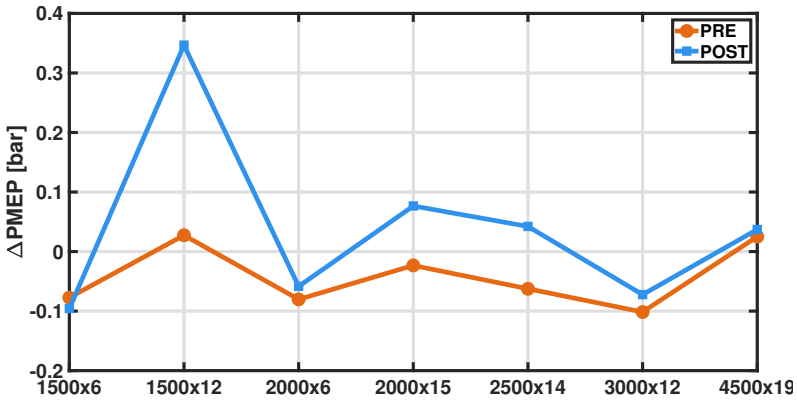

Figure 5.22. *Comparison of optimal $\Delta PMEP$ with respect to 0% EGR between POST (blue) and PRE (orange) for all tested conditions.*

The PRE system achieves better BSFC reductions with respect to operation without EGR except for the following conditions:

- 2000 rpm at 15 bar BMEP: due to the low EGR rate achieved with the PRE circuit and the difference in heat transfer losses.
- 3000 rpm at 12 bar BMEP: due to the reduced advantage in PMEP compared to other conditions, the combustion deterioration and reduced heat transfer for the POST circuit.

- 4500 rpm at 19 bar BMEP: due to similar pumping losses and reduced heat transfer for the POST circuit. The great BSFC reduction in this condition is due to enrichment suppression.

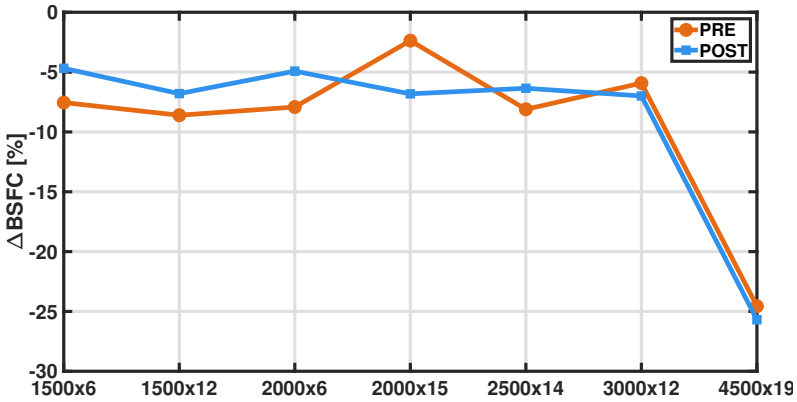

Figure 5.23. *Comparison of optimal ΔBSFC with respect to 0% EGR between POST (blue) and PRE (orange) for all tested conditions.*

The energy balance is shown for all operating conditions in Figure 5.24, with the percentual variation of indicated efficiency in the top row, in-cylinder heat transfer in the middle row and exhaust energy in the bottom row. In general, the indicated efficiency is positive, following the trends observed in optimal consumption and resulting in the PRE system being more efficient except in the conditions listed above. In terms of heat losses, the PRE system is a better reducer at the same EGR rate than the POST system. However, since the POST system achieves higher EGR rates at its optimum, heat losses are lower for this system. The only conditions in which better heat transfer losses are obtained are the ones explained in subsection 5.2.1, being these operating conditions the ones with the lower difference in the optimal EGR rate after 4500 rpm. It should be noted that the low load condition at 2000 rpm shows a similar difference between optimal EGR rates, but the POST circuit still achieves better heat losses, as at 4500 rpm. For the exhaust energy, an increase compared to no EGR operation is always obtained due to greater total flow and despite the exhaust temperature reduction. Besides, the POST circuit presents greater exhaust energies due to the higher EGR rates and exhaust temperatures achieved compared to the PRE circuit.

The percentual variation of emissions is shown in Figure 5.25, with NO_x in the top row, HC in the middle row and CO in the bottom row. For nitrogen oxides, both EGR strategies achieve a great reduction effect given

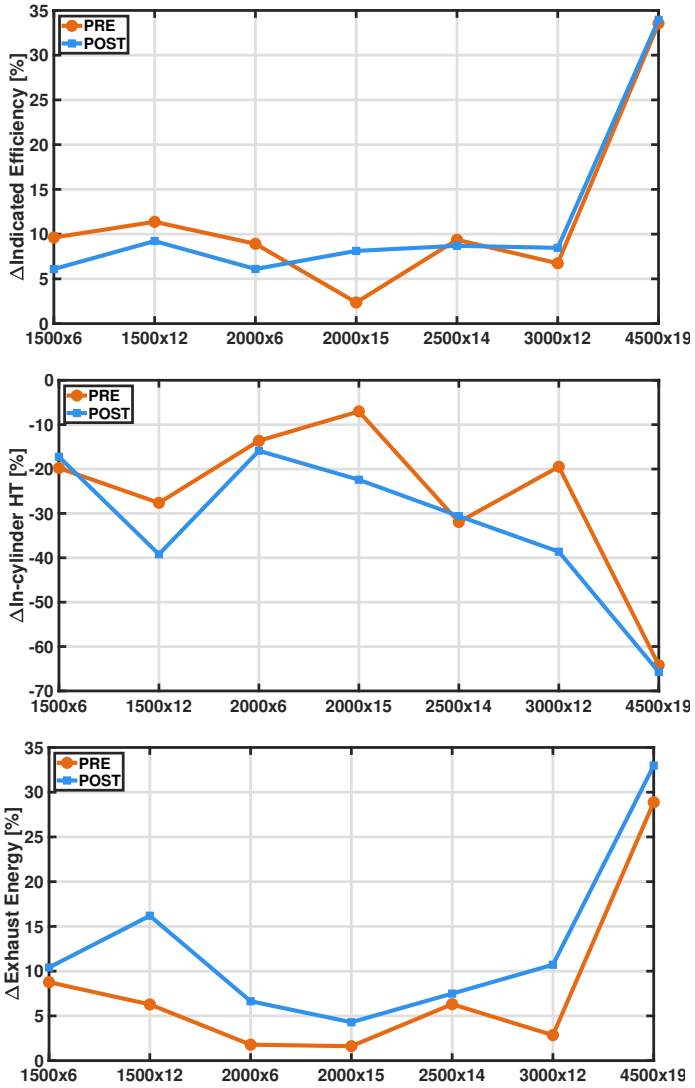

Figure 5.24. *Comparison of optimal energy balance variation with respect to 0% EGR between POST (blue) and PRE (orange) for all tested conditions. Top row: Indicated efficiency; Mid row: In-cylinder heat transfer; Bottom row: Exhaust energy.*

the oxygen concentration and temperature reduction. Moreover, the POST circuit is generally reducing to a greater extent this pollutant, probably due to the lower temperatures. It is worth noting the low load case at 2000 rpm, in which combustion deterioration with the PRE circuit results in lower combustion temperatures and therefore lower NO_x production. Besides, the

low EGR rate achieved with the PRE circuit at 2000 rpm with a higher engine load means a lower nitrogen oxides reducing effect. In the case of 4500 rpm, EGR addition produces an huge increase in nitrogen oxides due to the enrichment suppression. For hydrocarbons, the opposite trend to nitrogen oxides is observed, increasing with EGR. This increase in hydrocarbons is seen to a lesser degree for the PRE circuit due to the greater temperatures inside the cylinders. The exception is found in the low load cases at 1500 and 2000 rpm. Following the previous explanation, the suppression of enrichment at 4500 rpm supposes an increase in HC despite the addition of EGR with both systems. In general, CO emissions are reduced with EGR addition, especially with the POST circuit. The temperature reduction produced by the addition of EGR paralyses both the oxidation of the fuel to CO_2 and the dissociation of the one that has already been formed. In this sense, and given the reduction effect that EGR has on carbon monoxides, the dissociation of carbon dioxides formed could have a greater weight in the final phases of combustion, so that the greater the reduction in temperature, the lower the amount of CO is finally obtained. In this way, the POST circuit is a greater reducer of CO.

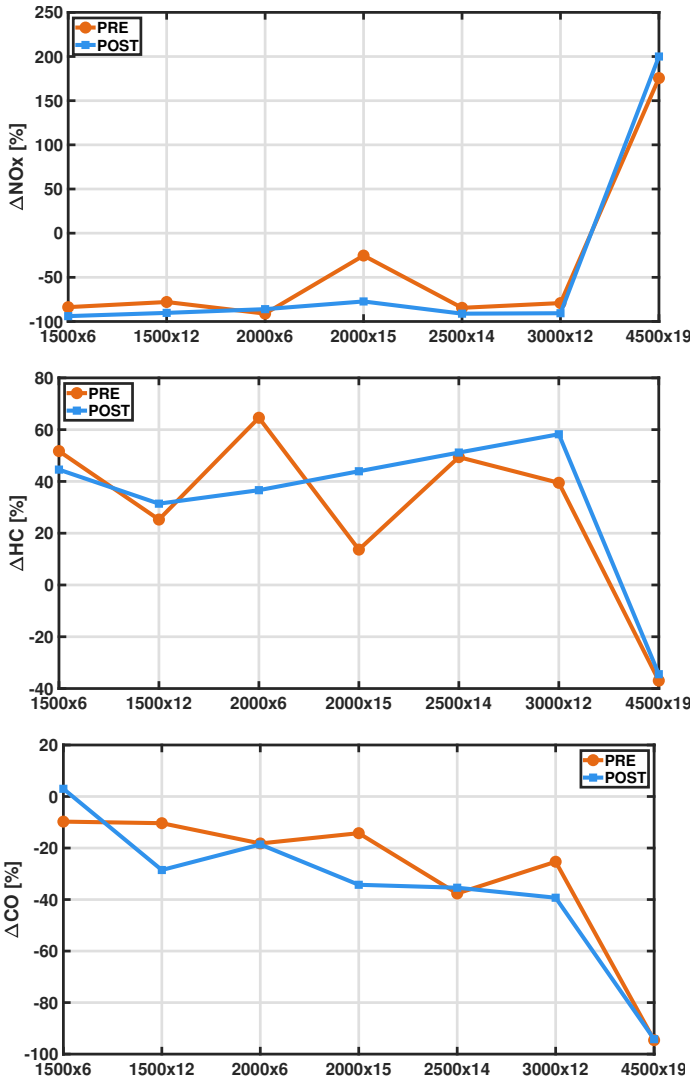

Figure 5.25. *Comparison of optimal emissions variation with respect to 0% EGR between POST (blue) and PRE (orange) for all tested conditions. Top row: NO_x; Mid row: HC; Bottom row: CO.*

5.3 Summary and findings

In this chapter, the low-pressure EGR circuit reviewed in chapter 4 has been compared to a high-pressure one in section 5.1 and to another low-pressure

circuit in section 5.2, the latter being called PRE due to the extraction of the exhaust gas upstream the TWC.

In the comparison with HP-EGR, it is noteworthy that the majority of the limits for HP-EGR were the pressure difference between the ends of the circuit, with the COV being the limiting factor in only 3 cases. In addition, no HP rates could be recirculated at two operating conditions given this limitation, not even changing the calibration in spark nor valve timings.

Regarding the comparison in two operating conditions, the intake pressure increases with both systems, although to a greater extent for the HP circuit. A lower exhaust pressure is observed for the HP system than for the LP due to the extraction of the exhaust gases upstream the turbine. However, when the use of the VGT becomes necessary to mantain the load, the trend changes and the back pressure begins to increase, exceeding the level reached with the LP. In this sense, pumping losses are reduced by adding EGR with both systems, with an advantage for the HP circuit, even when the use of the VGT becomes necessary.

Combustion deterioration is observed as EGR is added both at induction time and at TOC, with no major differences between the two systems. The indicated efficiency increases with the EGR rate for both systems with a slight advantage for HP, likely due to further pumping losses reduction. However, the higher temperature inside the cylinder obtained with the high-pressure circuit causes greater heat losses than the LP system, despite the fact that with both systems these are reduced with respect to operation without EGR. Regarding the BSFC, the reduction observed with respect to the case without EGR is greater for HP at constant rate, but the greater recirculation of the low-pressure system makes it possible to increase the EGR rate and further reduce consumption.

In a general comparison, the optimal EGR rate for fuel consumption is always greater for the LP circuit except in the case of 2000 rpm at 6 bar BMEP, highlighting the case of 2500 rpm, in which it was only possible to recirculate around a 5% with HP. In this way, the low-pressure system is capable of obtaining lower consumptions reaching higher rates. Comparing with the case without EGR at constant calibration and the optimal case with only IGR, it is observed that the addition of EGR is always beneficial from the point of view of consumption, even more so if it is done with the low-pressure system except at 1500 rpm at 6 bar BMEP, the only point where HP shows better efficiencies than LP.

Regarding emissions, NO_x is clearly reduced with both circuits, especially with LP due to the lower temperatures. The opposite trend is obtained for the

HC, with increases with respect to operation without EGR, especially for LP. In general, CO is also greatly reduced by using both EGR circuits.

Both EGR systems are presented as better alternatives to the two IGR strategies both from the point of view of fuel consumption and for emissions, except hydrocarbons. In the event of having to choose between one circuit and another, the greater versatility of the low-pressure system would be key in the decision, since it allows higher EGR rates to be recirculated and covers practically the entire map, unlike the high-pressure system, with which there are recirculation problems at medium-to-high loads and low-to-medium engine speeds. This is the main factor that makes the low-pressure system more suitable to install on the engine, winning over the high-pressure system. In addition, the low-pressure system is better overall in terms of fuel consumption, NO_x and CO emissions.

In the comparison between low-pressure circuits, it is observed how the higher temperature on the intake side for the PRE circuit promotes higher intake pressures than in the POST system to maintain the engine load. In addition, there is a combustion deterioration with the PRE circuit that was even observed in the in-cylinder pressure evolution and that promoted lower optimal EGR rates due to instabilities. The higher intake pressures, together with the gas extraction closer to the turbine, made the PRE circuit a better pumping losses reducer at equal EGR rates.

However, since the optimum EGR rates for consumption with the PRE system are significantly lower than those of the POST system, the PMEP advantage of the PRE system is not as great as at constant rate, although it is still better.

A similar trend is observed for fuel consumption and in-cylinder heat losses. In this sense, the PRE circuit is a better heat losses reducer, but since these are highly dependent on the recirculated rate, the POST system achieves in general better heat losses at its best consumption. For BSFC, the advantage of the PRE system is mantained in most of the conditions tested despite the lower optimal EGR rates.

In terms of emissions, both systems are great reducers of NO_x and CO in general. However, the lower temperatures of the POST system result in a greater reduction of both emissions compared to the PRE circuit, with the corresponding penalty in hydrocarbons.

In the end, the PRE system shows that it can achieve the same or better performance in most conditions with a lower EGR rate. This would mean that the PRE circuit could be implemented in a vehicle in a more compact and

reduced line than the POST circuit, in addition to not needing the choke valve on the intake side.

Bibliography

[1] Lavoie G. A., Ortiz-soto E., Babajimopoulos A., Martz J. B. and Assanis D. N. "Thermodynamic sweet spot for high- efficiency , dilute , boosted gasoline engines". *International Journal of Engine Research*, Vol. 14 n^o 3, pp. 260–278, 2012.

Chapter 6

Conclusions and findings

Contents

6.1 Introduction

Finally, this chapter is dedicated to compiling the most outstanding contributions of the work developed throughout the PhD-Thesis. In this sense, a review of all the results and conclusions shown and discussed in the previous chapters is presented.

Along with this compilation, a section of future works proposed is added. These future works are in line with the studies presented in this document and are the result of different suggestions, proposals for improvement and complementary studies that have emerged throughout it.

6.2 Conclusions and findings

The studies presented in chapter 4 and chapter 5 have been proposed and developed to meet the objectives described in chapter 1 of this PhD-Thesis. In this sense, chapter 4 is conceived as a deep analysis of a low-pressure EGR system, studying the tolerance that the engine has to EGR addition and its influence on the optimal calibration. In order to achieve this aim, it has been essential to know the effects of recirculated gases based on their composition and temperature, as well as an analysis from efficiency, energy balance, pumping and emissions perspective. In addition, one of the potential problems of the low-pressure EGR system, the condensation of the water present in the exhaust gas, has been analysed in detail from the point of view of combustion, efficiency and emissions. From the analysis of the low-pressure system, the following findings stand out:

- Dilution with low-pressure EGR directly affects the optimum engine calibration. These effects are reflected both in the spark timing, due to slower combustion and greater knock tolerance, and in the variable valve timing, due to the EGR-IGR interaction and the intake and exhaust pressure changes.

- The ideal operation of the three-way catalyst can be affected by the change in the composition of the exhaust gases, reducing the oxygen available to reduce hydrocarbon and carbon monoxide emissions.

- The EGR-IGR interaction is fundamental for the optimization of the calibration from the point of view of efficiency. As the total recirculated rate increases, the combustion times lengthen, with a smaller effect the higher the IGR share is. In this sense, for a constant rate of total residuals, an improvement in the induction time is obtained as the

total rate is obtained with IGR and not with EGR. Said improvement is fully explained by the difference in temperature of the recirculated gases for low total residual rates, as indicated by the estimation with a laminar combustion velocity correlation. However, with a higher total residual rate, the prediction is not enough, since experimentally a greater improvement is obtained that could be explained by the differences in composition, thus demonstrating its effect.

- As the dilution with exhaust gases increases, pumping losses and consumption are reduced at the operating condition of the study, proving to be a beneficial technique from the point of view of efficiency. This advantage is greater for the EGR in general compared to IGR, given the lower heat losses obtained.

- For emissions, as the total rate of residuals and EGR share increases, nitrogen oxides are reduced and hydrocarbons are increased. The higher temperatures obtained with IGR result in opposite tendencies with respect to EGR for both emissions.

- The cooling that occurs in the WCAC, which in the case of the low-pressure EGR affects both the fresh air and the recirculated exhaust gases, can result in the condensation of part of the water vapour present in the mixture. The water droplets generated in this process can accumulate and suddenly enter the cylinders, reducing the temperature of the intake gas. This effect is translated into a spontaneous improvement in volumetric efficiency that cannot be corrected with fuel injection given its nature. In this way, an uncontrolled dilution with air is obtained, affecting stability, efficiency and emissions.

- The problem of sporadic dilution due to water condensation is reflected in an increase in combustion times and is highly dependent on the water accumulation time, obtaining practically stationary states beyond 10 minutes. In addition, it does not affect all operating conditions in to the same extent, the relative load of the engine being a key factor given the higher temperatures and the resistance to dilution that is obtained.

- The increase in variability that occurs when admitting the condensed water increases the specific consumption between 3 and 5%, depending on the operating condition. However, in some operating conditions the specific consumption is still better than that obtained without EGR, so the dilution technique may continue to be of interest. Similarly, NO_x emissions are reduced by between 10 and 40%, whereas HC emissions are increased between 10 and 30%.

- The use of new fuels with lower carbon content for decarbonization could significantly worsen this problem given the higher specific humidity of the exhaust gases. While for conventional gasoline the refrigeration temperatures at which this phenomenon occurs are relatively low, the condensation limits for these fuels increase beyond normal ambient temperatures, especially for hydrogen and ammonia. In this way, the problem of water vapour condensation from the exhaust gases could not only be present throughout the normal operating range, but also extend to the EGR cooler and the mixture between exhaust gases and fresh air, notably affecting the wear of components such as the compressor.

In chapter 5, the low-pressure system presented in the previous chapter is compared under different operating conditions first with a high-pressure circuit and then with another low-pressure circuit, the main difference of the latter compared to the traditional one being the extraction of the exhaust gas upstream of the three-way catalyst. From the comparisons between EGR systems, the following findings should be highlighted:

- The high-pressure EGR system is very limited by recirculation given the lower pressure difference between the ends of the circuit, in this case, the intake and exhaust manifolds. These recirculation limits mean lower EGR rates compared to the low-pressure circuit at most of the operating points tested, and even the impossibility of recirculating exhaust gases at two operating points. On the other hand, the limits in the case of low-pressure EGR are very varied: combustion instability, pressure difference, maximum temperature at the compressor outlet or impossibility of maintaining the load due to turbocharging.

- In general, the intake pressure increases when adding EGR with both systems, with a greater increase for the high-pressure circuit. For the exhaust pressure, lower values are in general obtained with this system given the extraction of gases before the turbine. These variations in intake and exhaust pressures mean a reduction in pumping losses with both EGR systems, with an advantage for the high-pressure circuit.

- Combustion slows down with both systems to a very similar level given the dilution obtained, as can be seen in the induction and total combustion times. The high-pressure circuit is shown to be a better reducer of pumping losses, while the lower temperature of the EGR with the low-pressure circuit positions this circuit as a better heat losses reducer. Both effects compensate for the slower combustion from the

point of view of efficiency. In this sense, the reduction in specific consumption obtained with respect to operation without EGR is greater for the high-pressure circuit than for the low-pressure circuit at a constant EGR rate. However, the higher rates that can be recirculated with the low-pressure circuit result in better optimum consumption reductions.

- Regarding emissions, nitrogen oxides are reduced compared to operation without EGR with both circuits, especially with the low-pressure circuit due to lower temperatures. As for hydrocarbons, the opposite trend is obtained both with the addition of EGR and with both systems, increasing especially in the case of low-pressure. Both circuits are capable of reducing carbon monoxide emissions compared to operation without EGR.

- The extraction of the exhaust gas upstream of the three-way catalyst with the new low-pressure circuit supposes a higher temperature of the gases, which in turn requires a higher intake pressure compared to the traditional circuit. This, together with a reduction in the exhaust pressure that is produced by the extraction of the gas closer to the turbine, results in a better reduction in pumping losses for this system than for the traditional one.

- A deterioration in combustion is observed in the PRE circuit, probably due to the higher intake pressure levels that change the flow structure and flame propagation. This effect results in a limitation of the maximum recirculation rate with this system.

- In this way, the optimal EGR rates of the traditional system are much higher than those of the new system, reducing the advantage observed for the PRE system at a constant rate in pumping losses and specific consumption. Despite this, the PRE system generally keeps the advantage, obtaining lower fuel consumptions than the traditional low-pressure circuit.

- The traditional low-pressure system is also presented as a better reducer of nitrogen oxides and carbon monoxide given the lower operating temperatures, while the PRE system is better in terms of hydrocarbons reduction.

- The PRE system proves to be able to obtain better efficiencies in most of the operating conditions analysed than the traditional circuit with lower EGR rates, which means that it could be implemented in a vehicle in a

more compact way and without the need to use a choke valve as in the case of the traditional low-pressure system.

6.3 Further works

During the course of this PhD-Thesis, a series of proposals, suggestions and improvements related to the work developed have emerged, not being included in the present document given the limitations of time and budget. This future works could complement the studies presented, as well as increase the current knowledge about the techniques for reducing consumption and emissions of ICEs, which will play an important role in the future for sustainable mobility. The most important future works proposed are the following:

- Study the impact of EGR condensation with different fuels. The decarbonization of transport is one of the biggest challenges the sector is facing today and in the future. The use of new fuels with lower carbon content will be of vital importance to reduce the carbon footprint and make this a sustainable sector. In this PhD-Thesis, the potential impact of EGR condensation on engine operation with fuels for decarbonization has been preliminarily analysed. However, this study should be extended to deeply analyze the real impact that this phenomenon may have given the different deterioration of combustion that may exist, reactivity, resistance to cyclic variation and the effect of dilution in other fuels.

- In line with the previous study, it is proposed to understand the impact of dilution with EGR in engines with fuels for decarbonization. Dilution with EGR has been proven as a beneficial technique for increasing efficiency, but it needs be studied for new fuels and analyse whether all the current information and studies are applicable to new fuels.

- Comparative study between EGR systems with the optimal timing settings. In the case of this PhD-Thesis, the comparison has been made with the optimal variable valve timing settings for the traditional low-pressure system for all architectures. However, it is expected that this optimum calibration will differ, even slightly, for the different EGR systems and especially for the high-pressure one.

- High-pressure EGR recirculability study. In this document, seven operating conditions have been selected, showing that the high-pressure system was not capable of recirculating exhaust gases in two of them, in addition to a very important limitation in another. Therefore, it

is proposed to study the ability to recirculate exhaust gases with the high-pressure circuit depending on the operating condition. In order to perform this study, a greater discretization of the engine map is necessary, choosing a greater number of speed and load conditions that allows identifying from which engine load the system reduces its capacities and if it is possible to solve the problem by calibrating the variable valve timing system, for example.

- For the low-pressure EGR circuit with gas extraction upstream the catalyst, a study of the deterioration in combustion observed and the intake pressure increase is proposed. Combustion deterioration with the PRE system is attributed to an intake pressure increase that results to be counterproductive due to the movement of air in the cylinder. A study based on CFD techniques could shed light on the problem, showing the weaknesses of this EGR circuit and proposing improvements that reduce combustion deterioration, increase the recirculated rate and extend the benefits of this system.

- To assess the influence of injection parameters on the mixture formation with EGR dilution. The injection timing, duration and pressure can play a fundamental role in mixture formation and exploring these parameters could lead to an improvement in the operational range of exhaust gas recirculation, allowing more EGR to be introduced in the engine without stability penalties. This potential study could be performed with a design of experiments methodology as the one presented in this document in order to find the best strategy. Multi-injection and stratification strategies could also be taken into consideration to optimize the mixing process.

- In order to extend the range of EGR operation, it could also be interesting to design a piston and cylinder geometry focused on improving mixture formation and ignitability under high dilution conditions. This could be very interesting especially in the case of the PRE circuit. This improved design, together with a proper matching of the injector, spark plug and ignition power could extend the operational range of EGR dilution, thus its benefits from efficiency and emissions perspective.

- To explore the possibilities of EGR and air dilution together. The penalty in fuel consumption of SI engines compared to CI engines could be reduced by combining these two techniques. With lean operation, the three-way catalyst should be capable of abating hydrocarbon and carbon monoxides emissions, whereas nitrogen oxides could be reduced

with EGR. This strategy could be complemented with an SCR or NO_x trap as aftertreatment systems for NO_x abatement together with a TWC or oxidation catalyst.

- The development of control strategies for EGR operation in steady and transient conditions. This is one of the main challenges of EGR implementation in mass production SI vehicles. Estimating the instantaneous EGR rate and adapting the calibration both in variable valve and spark timing depending on the dilution level could lead not only to improved efficiency and emission throughout the hole operation of the engine, but also to avoid instabilities and emissions related to excessive dilution or non-optimal calibration strategies. This could also be applied to the water condensation problem, that could be mitigated with an EGR strategy depending on the cooling temperatures.

- Implementation of several EGR strategies together with high and low-pressure circuits. Combining both typologies could result in synergies that would complement the individual contributions of each circuit from emissions, efficiency and recirculability.

- Variable compression engines in combination with EGR strategies for high engine performance and efficiency. Increased compression ratio at low loads could significantly impact the engine efficiency with a proper control strategy that could be combined with the benefits from EGR dilution.

With the aim of finding the best possible synergy between the systems developed to improve engine efficiency, the list of future works can become endless. The interaction between the different systems and the optimal control strategy, as well as the development of new technologies, is a very complex problem that requires the contribution of the scientific community to continue progressing. Internal combustion engines have a long way to go and will play a fundamental role in the decarbonization and sustainability of the transport sector, whether with SI, CI, with alternative fuels such as ammonia or hydrogen, or with renewable and e-fuels.

Chapter 7

Appendix

Engine model IGR maps

In this section, the IGR maps obtained with the 1D engine model are shown for three operating conditions (1500 and 2000 rpm at 6 bar BMEP and 3000 rpm at 12 bar BMEP). These maps are displayed depending on the intake (x-axis) and exhaust VVT settings, and several EGR rates have been taken into account. As explained during the document, the change in the VVT settings or in the EGR rate suppose a change in the intake and exhaust pressures that modify the residuals concentration. The idea of ??these maps is to easily obtain an approximate IGR concentration for the desired condition without the need to use the model for specific cases, as well as to analyze the main trends of IGR with the aforementioned parameters.

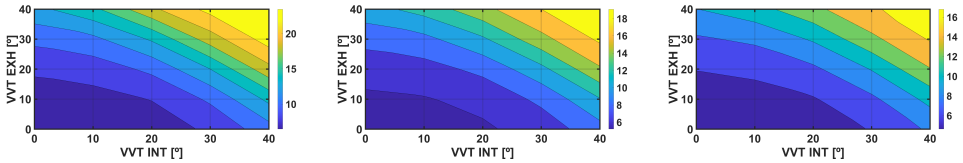

(a) 1500x6 0% EGR (b) 1500x6 10% EGR (c) 1500x6 15% EGR

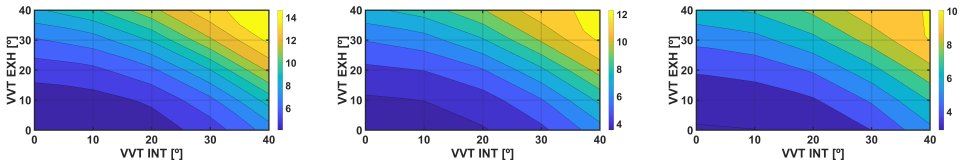

(d) 1500x6 20% EGR (e) 1500x6 25% EGR (f) 1500x6 30% EGR

Figure 7.1. *IGR concentration depending on EGR rate, intake and exhaust VVT settings for 1500 rpm at 6 bar BMEP.*

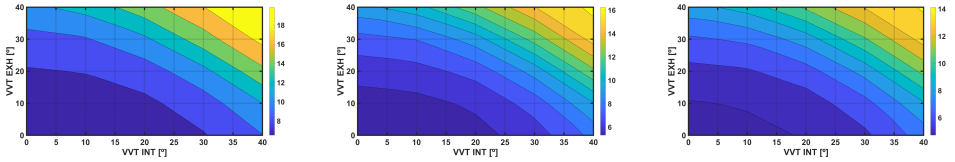

(a) 2000x6 0% EGR (b) 2000x6 10% EGR (c) 2000x6 15% EGR

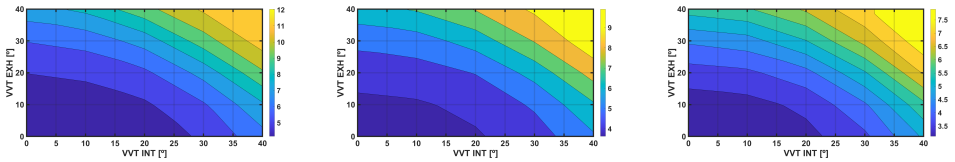

(d) 2000x6 20% EGR (e) 2000x6 25% EGR (f) 2000x6 30% EGR

Figure 7.2. *IGR concentration depending on EGR rate, intake and exhaust VVT settings for 2000 rpm at 6 bar BMEP.*

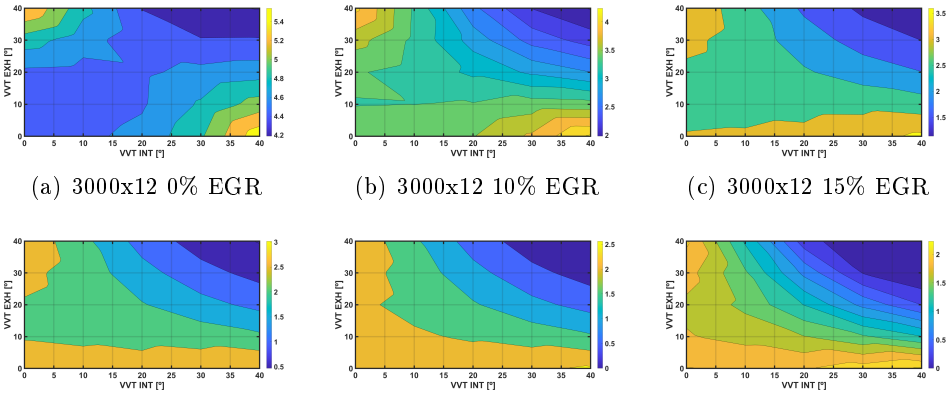

(a) 3000x12 0% EGR (b) 3000x12 10% EGR (c) 3000x12 15% EGR

(d) 3000x12 20% EGR (e) 3000x12 25% EGR (f) 3000x12 30% EGR

Figure 7.3. *IGR concentration depending on EGR rate, intake and exhaust VVT settings for 3000 rpm at 12 bar BMEP.*

Bibliography

The contribution of transport to air quality - TERM 2012: Transport indicators tracking progress towards environmental targets in Europe.
Number 10. 2012. (cited in p. 19)

-.
Dedicated EGR Vehicle Demonstration.
SAE International Journal of Engines, Vol. 10 n^o 3, pp. 898–907, 2017. (cited in p. 84)

-.
Suicidal Carbon Monoxide Poisoning Using Motor Vehicle Exhaust in an Open Space.
Medical Principles and Practice, Vol. 28 n^o 5, pp. 490–492, 2019. (cited in p. 58)

Aakko P. and Nylund N.
Particle emissions at moderate and cold temperatures using different fuels.
SAE Technical Paper n. 2003-01-3285, 2003. (cited in p. 65)

Abd Aziz A. R., Anbese Y. T., Hagos F. Y., Heikal M. R. and Firmansyah.
Characteristics of early flame development in a direct-injection spark-ignition CNG engine fitted with a variable swirl control valve.
Energies, Vol. 10 n^o 7, 2017. (cited in p. 46)

Abe S., Sasaki K., Baika T., Nakashima T. and Fujishiro O.
Combustion analysis on piston cavity shape of a gasoline direct injection engine.
SAE Technical Papers, n^o 724, 2001. (cited in p. 71)

Abraham J., Williams F. A. and Bracco F. V.
A discussion of turbulent flame structure in premixed charges.
SAE Paper 850345, 1985. (cited in p. 48)

Agarwal11 D., Singh S. K. and Agarwal A. K.
Effect of Exhaust Gas Recirculation (EGR) on performance, emissions, deposits and durability of a constant speed compression ignition engine.
Applied Energy, Vol. 88 n^o 8, pp. 2900–2907, 2011. (cited in pp. 21, 58)

Akihisa D. and Daisaku S.
Research on Improving Thermal Effiiency through Variable Super-High Expansion Ratio Cycle.
SAE Technical Paper n. 2003-32-0039, 2010. (cited in p. 68)

Al-Qurashi K., Lueking A. D. and Boehman A. L.
The deconvolution of the thermal, dilution, and chemical effects of exhaust gas recirculation (EGR) on the reactivity of engine and flame soot.
Combustion and Flame, Vol. 158 n^o 9, pp. 1696–1704, 2011. (cited in pp. 62, 81)

Alagumalai A.
Internal combustion engines: Progress and prospects.
Renewable and Sustainable Energy Reviews, Vol. 38, pp. 561–571, 2014. (cited in p. 68)

Alger T., Chauvet T. and Dimitrova Z.
Synergies between high EGR operation and GDI systems.
SAE International Journal of Engines, Vol. 1 n^o 1, pp. 101–114, 2009. (cited in p. 82)

Alger T., Gingrich J., Khalek I. A. and Mangold B.
The role of EGR in PM emissions from gasoline engines.
SAE Technical Papers, Vol. 3 n^o 1, pp. 85–98, 2010. (cited in pp. 66, 82, 83)

Alger T., Gingrich J. and Mangold B.
The effect of hydrogen enrichment on EGR tolerance in spark ignited engines.
SAE Technical Papers, n^o 724, 2007. (cited in p. 84)

Alger T., Walls M., Chadwell C., Joo S., Denton B., Kleinow K. and Robertson D.
The Interaction between Fuel Anti-Knock Index and Reformation Ratio in an Engine Equipped with Dedicated EGR.
SAE International Journal of Engines, Vol. 9 n^o 2, pp. 786–795, 2016. (cited in p. 84)

Alkidas A. C.
Combustion advancements in gasoline engines.
Energy Conversion and Management, Vol. 48 n^o 11, pp. 2751–2761, 2007.
(cited in p. 68)

Alkidas A. C. and El Tahry S. H.
Contributors to the fuel economy advantage of DISI engines over PFI engines.
SAE Technical Papers, n^o 724, 2003. (cited in p. 69)

Allen J. and Law D.
Production electro-hydraulic variable valve-train for a new generation of I.C. Engines.
SAE Technical Paper n. 2002-01-1109, 2002. (cited in p. 73)

Alvarez Carlos Eduardo Castilla, Couto Giselle Elias, Roso VinÃcius RÃ¼ckert, Thiriet Arthur Braga and Valle Ramon Molina.
A review of prechamber ignition systems as lean combustion technology for SI engines.
Applied Thermal Engineering, Vol. 128, pp. 107–120, 2018. (cited in p. 72)

Amann M., Alger T. and Mehta D.
The Effect of EGR on Low-Speed Pre-Ignition in Boosted SI Engines.
SAE International Journal of Engines, Vol. 4 n^o 1, pp. 235–245, 2011. (cited in p. 54)

Amirante R., Distaso E., Tamburrano P. and Reitz R. D.
Laminar flame speed correlations for methane, ethane, propane and their mixtures, and natural gas and gasoline for spark-ignition engine simulations.
International Journal of Engine Research, Vol. 18 n^o 9, pp. 951–970, 2017.
(cited in pp. 166, 169)

Andersen J., Karlsson E. and Gawell A.
Variable Turbine Geometry on SI Engines.
SAE Technical Paper n. 2006-01-0020, 2006. (cited in p. 79)

Angiolini E.
Contribution to the understanding of filtration and pressure drop phenomena in wall-flow DPFs.
PhD-Thesis. Universitat Politècnica de València, Departamento de Máquinas y Motores Térmicos, n^o June, 2017. (cited in p. 40)

Barone T. L., Storey J. M. E., Youngquist A. D. and Szybist J. P.
An analysis of direct-injection spark-ignition (DISI) soot morphology.
Atmospheric Environment, Vol. 49, pp. 268–274, 2012. (cited in p. 69)

Barron M. B. and Powers W. F.
The role of electronic controls for future automotive mechatronic systems.
IEEE/ASME Transactions on Mechatronics, Vol. 1 n^o 1, pp. 80–88, 1996. (cited in p. 8)

Battistoni M., Foschini L., Postrioti, L. and Cristiani M.
Development of an Electro-Hydraulic Camless VVA System.
SAE Technical Paper, 2007. (cited in p. 74)

Benajes J., Olmeda P., Martín J. and Carreño R.
A new methodology for uncertainties characterization in combustion diagnosis and thermodynamic modelling.
Applied Thermal Engineering, Vol. 71 n^o 1, pp. 389–399, 2014. (cited in p. 123)

Beretta G. P., Rashidi M. and Keck J. C.
Turbulent flame propagation and combustion in spark ignition engines.
Combustion and Flame, Vol. 52 n^o C, pp. 217–245, 1983. (cited in p. 49)

Bermúdez V., Lujan J. M., Climent H. and Campos D.
Assessment of pollutants emission and aftertreatment efficiency in a GTDi engine including cooled LP-EGR system under different steady-state operating conditions.
Applied Energy, Vol. 158, pp. 459–473, 2015. (cited in pp. 65, 81, 89)

Bernstein L., Bosch P., Canziani O., Chen Z., Christ R. and Riahi K.
Synthesis Report. Intergovernmental Panel on Climate Change 2007.
2007. (cited in p. 9)

Bielaczyc P., Szczotka A., Swiatek A. and Woodburn J.
A Comparison of Ammonia Emission Factors from Light-Duty Vehicles Operating on Gasoline, Liquefied Petroleum Gas (LPG) and Compressed Natural Gas (CNG).
SAE International Journal of Fuels and Lubricants, Vol. 5 n^o 2, pp. 751–759, 2012.
(cited in p. 179)

Bird G. L.
Ford 2.5 liter direct injection naturally aspirated diesel engine.
Proceedings of the Institution of Mechanical Engineers. Part D, Transport engineering, Vol. 199 n^o 2, pp. 113–122, 1985. (cited in p. 8)

Boccardi S., Catapano F., Costa M., Sementa P., Sorge U. and Vaglieco B. M.
Optimization of a GDI engine operation in the absence of knocking through numerical 1D and 3D modeling.
Advances in Engineering Software, Vol. 95, pp. 38–58, 2016. (cited in pp. 21, 69)

Boretti A.
Use of Variable Valve Actuation to Control the Load in a Direct Injection, Turbocharged, Spark-Ignition Engine.
SAE Technical Paper 2010-01-2225, 2010. (cited in pp. 73, 78)

Borghi R.
Turbulent combustion modelling.
Progress in Energy and Combustion Science, Vol. 14 n^o 1, pp. 245–292, 1988. (cited in p. 48)

Bourhis G, Chauvin J, Gautrot X and de Francqueville L.
LP EGR and IGR compromise on a GDI engine at middle load.
SAE International Journal of Engines, Vol. 6 n^o 1, pp. 67–77, 2013. (cited in pp. 21, 86)

Bozza F., De Bellis V. and Teodosio L.
Potentials of cooled EGR and water injection for knock resistance and fuel consumption improvements of gasoline engines.
Applied Energy, Vol. 169, pp. 112–125, 2016. (cited in pp. 80, 179)

Bradley D. and Kalghatgi G. T.
Influence of autoignition delay time characteristics of different fuels on pressure waves and knock in reciprocating engines.
Combustion and Flame, Vol. 156 n^o 12, pp. 2307–2318, 2009. (cited in p. 51)

Braisher M., Stone R. and Price P.
Particle number emissions from a range of European vehicles.
SAE Technical Paper n. 2010-01-0786, 2010. (cited in pp. 65, 70)

Brandi F. K., Wünsche P. and Gschweltl E.
Design strategies for low noise engine concepts.
SAE Technical Paper n. 911070, 1991. (cited in p. 8)

Brunt M. F. J. and Platts K. C.
Calculation of heat release in direct injection diesel engines.
SAE Technical Papers, n^o 724, 1999. (cited in p. 128)

Bybee K.
Reliable electronics for high-temperature downhole applications.
JPT, Journal of Petroleum Technology, Vol. 52 n^o 7, pp. 56–57, 2000. (cited in p. 8)

Cairns A., Blaxill H. and Irlam G.
Exhaust gas recirculation for improved part and full load fuel economy in a turbocharged gasoline engine.
SAE Technical Papers, n^o 724, 2006. (cited in p. 81)

Cairns A., Fraser N. and Blaxill H.
Pre Versus Post Compressor Supply of Cooled EGR for Full Load Fuel Economy in Turbocharged Gasoline Engines.
SAE Technical Paper 2008-01-0425, 2008. (cited in p. 82)

Cames M. and Helmers E.
Critical evaluation of the European diesel car boom - Global comparison, environmental effects and various national strategies.
Environmental Sciences Europe, Vol. 25 n^o 1, pp. 1–22, 2013. (cited in pp. 11, 31)

Cardoso J. S., Silva V., Rocha R. C., Hall M. J., Costa M. and Eusébio D.
Ammonia as an energy vector: Current and future prospects for low-carbon fuel applications in internal combustion engines.
Journal of Cleaner Production, Vol. 296, 2021. (cited in p. 179)

Carnot S.
Réflexions sur la puissance motrice du feu et sur les machines propres à développer cette puissance.
Bachelier, 1824. (cited in p. 3)

Castro A., Götschi T., Achermann B., Baltensperger U., Buchmann B., Felber Dietrich D., Flückiger A., Geiser M., Gälli Purghart B., Gygax H., Kutlar Joss M., Lüthi L. M., Probst-Hensch N., Strähl P. and Künzli N.
Comparing the lung cancer burden of ambient particulate matter using scenarios of air quality standards versus acceptable risk levels.
International Journal of Public Health, Vol. 65 n^o 2, pp. 139–148, 2020. (cited in p. 66)

Catapano F., Di Iorio S., Sementa P. and Vaglieco B. M.
Characterization of ethanol-gasoline blends combustion processes and particle emissions in a GDI/PFI small engine.
SAE Technical Papers, Vol. 1, 2014. (cited in p. 65)

Caton J. A.
The thermodynamic characteristics of high efficiency, internal-combustion engines.
Energy Conversion and Management, Vol. 58, pp. 84–93, 2012. (cited in p. 80)

Chadwell C. J., Alger T., Zuehl J. and Gukelberger R.
A Demonstration of Dedicated EGR on a 2.0 L GDI Engine.
SAE International Journal of Engines, Vol. 7 n^o 1, pp. 434–447, 2014.
(cited in pp. 84, 85)

Chala G. T., Abd Aziz A. R. and Hagos F. Y.
Natural Gas Engine Technologies: Challenges and Energy Sustainability Issue.
Energies, Vol. 11 n^o 11, 2018. (cited in p. 44)

Chan T., Meloche E., Kubsh J., Rosenblatt D., Brezny R. and Rideout G.
Evaluation of a Gasoline Particulate Filter to Reduce Particle Emissions from a Gasoline Direct Injection Vehicles.
SAE Int. J. Fuels Lubr., Vol. 5 n^o 3, pp. 1277–1290, 2012. (cited in p. 40)

Chance R. and Ceselli R.
Corrosiveness of Exhaust Gas Condensates.
SAE Technical Papers, 1983. (cited in p. 179)

Chen L., Li T., Yin T. and Zheng B.
A predictive model for knock onset in spark-ignition engines with cooled EGR.
Energy Conversion and Management, Vol. 87, pp. 946–955, 2014. (cited in p. 78)

Choi J., Satpathy S., Hoard J., Styles D. and Kuan C.
An Experimental and Computational Analysis of Water Condensation Separator Within a Charge Air Cooler.
ASME, n^o October 2017, 2017. (cited in p. 179)

Climent H., Dolz V., Pla B. and González-Domínguez D.
Analysis on the potential of EGR strategy to reduce fuel consumption in hybrid powertrains based on advanced gasoline engines under simulated driving cycle conditions.
Energy Conversion and Management, Vol. 266 n^o June, pp. 115830, 2022.
(cited in p. 134)

Coltman D., Turner J. W. G., Curtis R., Blake D., Holland B., Pearson R. J., Arden A. and Nuglisch H.
Project Sabre: A close-spaced direct injection 3-cylinder engine with synergistic technologies to achieve low CO_2 output.
SAE Technical Paper n. 2008-01-0138, 2009. (cited in p. 78)

Costa M., Catapano F., Sementa P., Sorge U. and Vaglieco B. M.
Mixture preparation and combustion in a GDI engine under stoichiometric or lean charge: an experimental and numerical study on an optically accessible engine.
Applied Energy, Vol. 180, pp. 86–103, 2016. (cited in p. 68)

da Rocha D. D., de Castro Radicchi F., Lopes G. S., Brunocilla M. F., Gomes P. C., Santos N., Malaquias A. C. T., Rodrigues Filho F. A. and Baêta J. G. C.
Study of the water injection control parameters on combustion performance of a spark-ignition engine.
Energy, Vol. 217, 2021. (cited in p. 179)

Davidson C. I., Phalen R. F. and Solomon P. A.
Airborne particulate matter and human health: A review.
Aerosol Science and Technology, Vol. 39 n^o 8, pp. 737–749, 2005. (cited in pp. 9, 66)

De Bellis V.
Performance optimization of a spark-ignition turbocharged VVA engine under knock limited operation.
Applied Energy, Vol. 164, pp. 162–174, 2016. (cited in p. 69)

De Bortoli M., Lucio M., Marco A. and Gradella S.
Variable Compression Ratio Engines.
SAE Technical Papers, 2009. (cited in p. 77)

Delphi Technologies.
Worldwide emissions standards, Passenger cars and light duty vehicles.
Delphi informative booklet, 2019/2020. (cited in p. 10)

Dong X., Wang B., Yip H. L. and Chan Q. N.
CO_2 Emission of Electric and Gasoline Vehicles under Various Road Conditions for China, Japan, Europe and World Average - Prediction through Year 2040.
Applied Sciences, Vol. 9 n^o 11, pp. 2295, Jun 2019. (cited in p. 16)

Dorsch M, Neumann J and Hasse C.
Application of a Phenomenological Model for the Engine-Out Emissions of Unburned Hydrocarbons in Driving Cycles.
Journal of Energy Resources Technology, Vol. 138 n^o 2, pp. 22201, 2016. (cited in p. 176)

Douaud A. M. and Eyzat P.
Four-octane-number method for predicting the anti-knock behavior of fuels and engines.
SAE Technical Paper n. 780080, 1978. (cited in p. 52)

Dresner T. and Barkan P.
A review of variable valve timing benefits and modes of operation.
SAE Technical Paper n. 891676, 1989. (cited in p. 73)

Duan X., Liu Y., Liu J., Lai M. C., Jansons M., Guo G., Zhang S. and Tang Q.
Experimental and numerical investigation of the effects of low-pressure, high-pressure and internal EGR configurations on the performance, combustion and emission characteristics in a hydrogen-enriched heavy-duty lean-burn natural gas SI engine.
Energy Conversion and Management, Vol. 195 n^o March, pp. 1319–1333, 2019. (cited in p. 80)

Duchaussoy Y., Lefebvre A. and Bonetto R.
Dilution interest on turbocharged SI engine combustion.
SAE Technical Papers, n^o 724, 2003. (cited in pp. 61, 81)

Eakle S., Avery S., Weber P. and Henry C.
Comparison of Accelerated Ash Loading Methods for Gasoline Particulate Filters.
SAE Technical Papers, Vol. 2018-September, pp. 1–14, 2018. (cited in p. 40)

Easter J., Fiano A., Bohac S., Premchand K. and Hoard J.
Evaluation of low mileage GPF filtration and regeneration as influenced by soot morphology, reactivity, and GPF loading.
SAE Technical Papers, Vol. 2019-April n^o April, pp. 1–9, 2019. (cited in p. 40)

Ebrahimi R.
Thermodynamic modeling of performance of a Miller cycle with engine speed and variable specific heat ratio of working fluid.
Computers and Mathematics with Applications, Vol. 62 n^o 5, pp. 2169–2176, 2011. (cited in p. 75)

Eichenberger D. A. and Roberts W. L.
Effect of unsteady stretch on spark-ignited flame kernel survival.
Combustion and Flame, Vol. 118 n^o 3, pp. 469–478, 1999. (cited in p. 46)

Elyanov A., Golub V. and Volodin V.
Premixed hydrogen-air flame front dynamics in channels with central and peripheral ignition.
International Journal of Hydrogen Energy, Vol. 47 n^o 53, pp. 22602–22615, 2022. (cited in p. 196)

EPA U.S.
The benefits and costs of the clean air act from 1990-2010.
1999. (cited in p. 9)

Eric W. L., Mark O. M. and F. Daniel G.
Thermophysical Properties of Fluid Systems.
NIST Chemistry WebBook, NIST Standard Reference Database Number 69, 2021. (cited in p. 130)

Esposito S, Diekhoff L and Pischinger S.
Prediction of gaseous pollutant emissions from a spark-ignition direct-injection engine with gas-exchange simulation.
In *THIESEL 2020 Conference on Thermo- and Fluid Dynamic Processes in Direct Injection Engines*, pp. 1–20, 2020. (cited in p. 177)

European Environment Agency.
Contribution of different greenhouse gases to the overall greenhouse gas concentration.
Data and Maps, 2017. (cited in p. 14)

European Environment Agency.
The European environment - state and outlook 2020. Knowledge for transition to a sustainable Europe, volume 60.
2020. (cited in p. 18)

Fansler T. D., Reuss David L., Sick V. and Dahms R. N.
Combustion instability in spray-guided stratified-charge engines: A review.
International Journal of Engine Research, Vol. 16 n^o 3, pp. 260–305, 2015.
(cited in p. 46)

Fayad M. A., Fernàndez-Rodríguez D., Herreros J. M., Lapuerta M. and Tsolakis A.
Interactions between aftertreatment systems architecture and combustion of oxygenated fuels for improved low temperature catalysts activity.
Fuel, Vol. 229 n^o October 2017, pp. 189–197, 2018. (cited in p. 68)

Fayad M. A., Tsolakis A., Fernández-Rodríguez D., Herreros J. M., Martos F. J. and Lapuerta M.
Manipulating modern diesel engine particulate emission characteristics through butanol fuel blending and fuel injection strategies for efficient diesel oxidation catalysts.
Applied Energy, Vol. 190, pp. 490–500, 2017. (cited in p. 65)

Fernández-Yáñez P., Soriano J. A., Soto F., Armas O., Pla B. and Bermúdez V.
Pollutant emissions from Euro 6 light duty vehicle tested under steady state and transient operation on a roller test bench with hydrogenated paraffinic and biodiesel fuels.
Fuel, Vol. 323 n^o March, 2022. (cited in pp. 56, 68)

Fitton, J. Nates R.
Knock erosion in spark-ignition engines.
SAE Technical Paper n. 962102, 1996. (cited in p. 51)

Flierl R. and Klüting M.
The third generation of valvetrains - New fully variable valvetrains for throttle-free load control.
SAE Technical Papers, Vol. 2000 n^o 724, 2000. (cited in p. 74)

Fontana G. and Galloni E.
Variable valve timing for fuel economy improvement in a small spark-ignition engine.
Applied Energy, Vol. 86, pp. 96–105, 2009. (cited in pp. 73, 86)

Fontanesi S., Pecchia M. D., Pessina V., Sparacino S. and Iorio S. D.
Quantitative investigation on the impact of injection timing on soot formation in a GDI engine with a customized sectional method.
International Journal of Engine Research, Vol. (in press), 2021. (cited in pp. 82, 90)

Fraidl G. K., Piock W. F. and Wirth M.
Gasoline Direct Injection: Actual Trends and Future Strategies for Injection and Combustion Systems.
SAE 960465, 1996. (cited in p. 71)

França O.
Impact of the Miller Cycle in the efficiency of an FVVT (Fully Variable Valve Train) Engine During Part Load Operation.
SAE Technical Paper, 2009. (cited in p. 76)

Francqueville L. and Michel J. B.
On the Effects of EGR on Spark-Ignited Gasoline Combustion at High Load.
SAE International Journal of Engines, Vol. 7 n^o 4, pp. 1808–1823, 2014.

Franken T., Mauss F., Seidel L., Gern M. S., Kauf M., Matrisciano A. and Kulzer A. C.
Gasoline engine performance simulation of water injection and low-pressure exhaust gas recirculation using tabulated chemistry.
International Journal of Engine Research, Vol. (in press), 2020. (cited in pp. 90, 179)

Fuquan Z., Lai M. C. and Harrington D. L.
Automotive spark-ignited direct-injection gasoline engines.
Prog Energy Combust Sci 25, pp. 437–562, 1999. (cited in p. 69)

Fushimi16 A., Kondo Y., Kobayashi S., Fujitani Y., Saitoh K., Takami A. and Tanabe K.
Chemical composition and source of fine and nanoparticles from recent direct injection gasoline passenger cars: effects of fuel and ambient temperature.
Atmospheric Environment, Vol. 124, pp. 77–84, 2016. (cited in p. 69)

Gainey B., Yan Z., Moser S. and Lawler B.
Lean flammability limit of high-dilution spark ignition with ethanol, propanol, and butanol.
International Journal of Engine Research, pp. 1–11, 2021. (cited in p. 90)

Galindo J., Climent H., De la Morena J., González-Domínguez D., Guilain S. and Besançon T.
Experimental and modeling analysis on the optimization of combined VVT and EGR strategies in turbocharged direct-injection gasoline engines with VNT.
Proceedings of the Institution of Mechanical Engineers, Part D: Journal of Automobile Engineering, Vol. 235 n^o 10-11, pp. 2843–2856, 2021. (cited in pp. 86, 134)

Galindo J., Climent H., De la Morena J., Pitarch R., Guilain S. and Besancon T.
A methodology to study the interaction between variable valve actuation and exhaust gas recirculation systems for spark-ignition engines from combustion perspective.
Energy, Conversion and Management, Vol. 250, 2021. (cited in pp. 21, 22, 81)

Galindo J., Dolz V., Monsalve-Serrano J., Bernal Maldonado M. A. and Odillard L.
Advantages of using a cooler bypass in the low-pressure exhaust gas recirculation line of a compression ignition diesel engine operating at cold conditions.
International Journal of Engine Research, Vol. 22 n^o 5, pp. 1624–1635, 2021.
(cited in p. 121)

Galindo J., Gil A., Navarro R. and García-Olivas G.
Numerical assessment of mixing of humid air streams in three-way junctions and impact on volume condensation.
Applied Thermal Engineering, Vol. 201, 2022. (cited in pp. 135, 179, 181)

Galindo J., Navarro R., De la Morena J., Pitarch R. and Guilain S.
On combustion instability induced by water condensation in a low-pressure exhaust gas recirculation system for spark-ignition engines.
Energy, Vol. 261, pp. 125122, 2022. (cited in pp. 21, 200)

Galindo J., Navarro R., Tari D. and Moya F.
Development of an experimental test bench and a psychrometric model for assessing condensation on a low-pressure exhaust gas recirculation cooler.
International Journal of Engine Research, Vol. 22 n^o 5, pp. 1540–1550, 2021.
(cited in pp. 135, 181)

Galindo J., Navarro R., Tarí D. and Moya F.
Quantitative validation of an in-flow water condensation model for 3D-CFD simulations of three-way junctions using indirect condensation measurements.
International Journal of Thermal Sciences, Vol. 172 n^o PB, pp. 107303, 2022.
(cited in p. 179)

Galindo J., Piqueras P., Navarro R., Tarí D. and Meano C. M.
Validation and sensitivity analysis of an in-flow water condensation model for 3D-CFD simulations of humid air streams mixing.
International Journal of Thermal Sciences, Vol. 136 n^o November 2018, pp. 410–419, 2019.
(cited in p. 178)

Galloni E.
Analyses about parameters that affect cyclic variation in a spark ignition engine.
Applied Thermal Engineering, Vol. 29 n^o 5-6, pp. 1131–1137, 2009.
(cited in pp. 46, 58, 62, 83)

Galloni E., Fontana G. and Palmaccio R.
Numerical analyses of EGR techniques in a turbocharged spark-ignition engine.
Applied Thermal Engineering, Vol. 39, pp. 95–104, 2012. (cited in p. 81)

Galloni E., Fontana G. and Palmaccio R.
Effects of exhaust gas recycle in a downsized gasoline engine.
Applied Energy, Vol. 105, pp. 99–107, 2013. (cited in p. 88)

García A., Monsalve-Serrano J., Martínez-Boggio S. and Wittek K.
Potential of hybrid powertrains in a variable compression ratio downsized turbocharged VVA Spark Ignition engine.
Energy, Vol. 195, pp. 117039, 2020. (cited in p. 77)

Garcia J. J.
Exhaust gas condensate corrosion test on low pressure cooling system of aluminum brazed EGR, ACAC and WCAC.
SAE Technical Papers, Vol. 8, 2012. (cited in pp. 34, 179)

García-Afonso O.
Análisis teórico-experimental de la arquitectura pre-turbo de sistemas de post-tratamiento en MCIA.
2013. (cited in p. 40)

Garrido N., Baar R., Drueckhammer J. and Kaeppner C.
The Thermodynamics of Exhaust Gas Condensation.
SAE International Journal of Engines, Vol. 10 n^o 4, pp. 1411–1421, 2017.
(cited in p. 179)

Gentz Gerald, Thelen Bryce, Gholamisheeri Masumeh, Litke Paul, Brown Adam, Hoke John and Toulson Elisa.
A study of the influence of orifice diameter on a turbulent jet ignition system through combustion visualization and performance characterization in a rapid compression machine.
Applied Thermal Engineering, Vol. 81, pp. 399–411, 4 2015. (cited in p. 73)

George S., Morris G., Dixon J., Pearce D. and Heslop G.
Optimal Boost Control for an Electrical Supercharging Application.
SAE Technical Paper n. 2004-01-0523, 2004. (cited in p. 79)

Gerty Michael D. and Heywood John B.
An investigation of gasoline engine knock limited performance and the effects of hydrogen enhancement.
SAE Technical Papers, n^o 724, 2006. (cited in p. 84)

Ghazikhani M., Feyz M. E. and Joharchi A.
Experimental investigation of the Exhaust Gas Recirculation effects on irreversibility and Brake Specific Fuel Consumption of indirect injection diesel engines.
Applied Thermal Engineering, Vol. 30 n^o 13, pp. 1711–1718, 2010. (cited in pp. 62, 81)

Ghojel J. I.
Review of the development and applications of the Wiebe function: A tribute to the contribution of Ivan Wiebe to engine research.
International Journal of Engine Research, Vol. 11 n^o 4, pp. 297–312, 2010.
(cited in p. 133)

Giechaskiel B., Dilara P. and Andersson J.
Particle Measurement Programme (PMP) light-duty inter-laboratory exercise: Repeatability and reproducibility of the particle number method.
Aerosol Science and Technology, Vol. 42 n^o 7, pp. 528–543, 2008. (cited in p. 70)

Glahn C., Kluin M., Konigstein A. and Cloos L. K.
Cooled External EGR - System Optimization of the Cooling and Charging System on a 3-Cylinder Gasoline DI T/C Engine.
In 24th Aachen Colloquium Automobile and Engine Technology, pp. 189–204, 2015.
(cited in pp. 34, 79, 87, 91)

Goering C. E. and Fry B.
Engine durability screening test of a diesel oil/soy oil/alcohol microemulsion fuel.
Journal of the American Oil Chemists Society, Vol. 61 n^o 10, pp. 1627–1632, 1984.
(cited in p. 8)

Gong Changming, Si Xiankai and Liu Fenghua.
Combustion and emissions behaviors of a stoichiometric GDI engine with simulated EGR (CO2) at low load and different spark timings.
Fuel, Vol. 295 n^o December 2020, pp. 120614, 2021. (cited in p. 83)

Gong J., Stewart M. L., Zelenyuk A., Strzelec A., Viswanathan S., Rothamer D. A., Foster D. E. and Rutland C. J.
Importance of filter's microstructure in dynamic filtration modeling of gasoline particulate filters (GPFs): Inhomogeneous porosity and pore size distribution.
Chemical Engineering Journal, Vol. 338 n^o November 2017, pp. 15–26, 2018.
(cited in p. 40)

Gopujkar S., Worm J., and Robinette D.
Methods of Pegging Cylinder Pressure to Maximize Data Quality.
SAE Technical Papers, 2019. (cited in p. 123)

Gould L. A., Richeson W. E. and Erickson F. L.
Performance evaluation of a camless engine using valve actuators with programmable timing.
SAE Technical Paper n. 910450, 1991. (cited in p. 73)

Grandin B. and Angstrom H.
Replacing Fuel Enrichment in a Turbo Charged SI Engine: Lean Burn or Cooled EGR.
SAE Technical Paper, 1999. (cited in pp. 68, 71)

Grandin B., Angstrom H. E., Stalhammar P. and Olofsson E.
Suppression in a Turbocharged SI Engine by Using Cooled EGR.
SAE Technical Papers, 1998. (cited in p. 82)

Grover, Jr. Ronald O. and Cleary David.
Correlating Measured Combustion Performance with CFD Predicted In-Cylinder Flows for a Spark-Ignition Direct-Injection (SIDI) Engine with Enhanced Charge Motion.
SAE Technical Papers, Vol. 2013-01-1090, 2013. (cited in p. 68)

Gu X., Huang Z., Cai J., Gong J., Wu X. and Lee C. F.
Emission characteristics of a spark-ignition engine fuelled with gasoline-n-butanol blends in combination with EGR.
Fuel, Vol. 93 n^o x, pp. 611–617, 2012. (cited in p. 58)

Guardiola C., Triantopoulos V., Bares P., Bohac S. and Stefanopoulou A.
Simultaneous Estimation of Intake and Residual Mass Using In-Cylinder Pressure in an Engine with Negative Valve Overlap.
IFAC-PapersOnLine, Vol. 49 n^o 11, pp. 461–468, 2016. (cited in p. 86)

Guillemot P.
Les émissions de polluants des moteurs á allumage commandé.
Ecole du Petrole et des Moteurs, 2008. (cited in p. 57)

Hacohen J., Ashcroft S. J. and Belmont M. R.
Lean burn versus EGR S.I. engine.
SAE Technical Paper n. 951902, 1995. (cited in p. 80)

Hagos F.
Combustion, Performance and Emissions Characteristics of Imitated Syngases in Direct-Injection Sparkigntion Engine.
PhD-Thesis. Universiti Teknologi Petronas, Seri Iskandar, Malaysia, 2013.
(cited in p. 43)

Hall D. and Dickens C.
Measurement of the number and size distribution of particles emitted from a gasoline direct injection vehicle.
SAE Technical Papers, 2009. (cited in p. 69)

Happer W.
The Truth About Greenhouse Gasses.
The Global Warming Policy Foundation, n^o 3, pp. 2–6, 2011. (cited in p. 13)

Harada J., Tomita T., Mizuno H., Mashiki Z. and Ito Y.
Development of Direct Injection Gasoline Engine.
SAE 970540, 1997. (cited in p. 71)

Hatamura K., Hayakawa T., Goto T. and Hitomi M.
A study of the improvement effect of Miller-cycle on mean effective pressure limit for high-pressure supercharged gasoline engines.
JSAE Review, Vol. 18, pp. 101–106, 1997. (cited in p. 75)

Hatano K., Lida K., Higashi H. and Murata S.
Development of a New Multi-Mode Variable Valve Timing Engine.
SAE Technical Papers, 1993. (cited in p. 74)

Herbst F., Staber-Schmidt C., Eilts P., Sextro T., Kammeyer J., Natkaniec C., Seume J., Porzig D. and Schwarze H.
The Potential of Variable Compressor Geometry for Highly Boosted Gasoline Engines.
SAE Technical Paper n. 2011-01-0376, 2011. (cited in p. 79)

Hess D. R.
Inhaled carbon monoxide: From toxin to therapy.
Respiratory Care, Vol. 62 n^o 10, pp. 1333–1342, 2017. (cited in p. 59)

Heywood J. B.
Internal combustion engine fundamentals.
McGraw-Hill, 1988. (cited in pp. 45, 65)

Hill J., Polasky S., Nelson E., Tilman D., Huo H., Ludwig L., Neumann J., Zheng H. and Bonta D.
Climate change and health costs of air emissions from biofuels and gasoline.
Proceedings of the National Academy of Sciences of the United States of America, Vol. 106 n^o 6, pp. 2077–2082, 2009. (cited in p. 9)

Hill P. G. and Zhang D.
The effects of swirl and tumble on combustion in spark-ignition engines.
Progress in Energy and Combustion Science, Vol. 20 n^o 5, pp. 373–429, 1994.
(cited in p. 49)

Hiroyuki O., Yasuyuki M., Toshimitsu F. and Masashi M.
Investigation of High-Compression Lean Burn Engine.
SAE Technical Paper n. 871215, 1987. (cited in p. 70)

Hirst, S. L. Kirsch L. J.
The application of a hydrocarbon auto-ignition model in simulating knock and other engine combustion phenomena, in: Combustion modeling in reciprocating engines.
New York: Plenum, 1980. (cited in p. 51)

Hoepke B., Jannsen S., Kasseris E. and Cheng W. K.
EGR Effects on Boosted SI Engine Operation and Knock Integral Correlation.
SAE International Journal of Engines, Vol. 5 n^o 2, pp. 547–559, 2012. (cited in p. 52)

Hosaka T. and Hamazaki M.
Development of the Variable Valve Timing and Lift (VTEC) Engine for the Honda NSX.
SAE Technical Papers, 1991. (cited in p. 74)

Hua Jianxiong, Zhou Lei, Gao Qiang, Feng Zhonghui and Wei Haiqiao.
Influence of pre-chamber structure and injection parameters on engine performance and combustion characteristics in a turbulent jet ignition (TJI) engine.
Fuel, Vol. 283, 1 2021. (cited in p. 72)

Huang B., Hu E., Huang Z., Zheng J., Liu B. and Jiang D.
Cycle-by-cycle variations in a spark ignition engine fueled with natural gas-hydrogen blends combined with EGR.
International Journal of Hydrogen Energy, Vol. 34 n^o 19, pp. 8405–8414, 2009.
(cited in p. 80)

Huang Z., Zhang Y., Wang Q., Wang J., Jiang D. and Miao H.
Study on flame propagation characteristics of natural gas-hydrogen-air mixtures.
Energy and Fuels, Vol. 20 n^o 6, pp. 2385–2390, 2006. (cited in pp. 46, 47)

Hunicz J., Mikulski M., Geca M. S. and Rybak A.
An applicable approach to mitigate pressure rise rate in an HCCI engine with negative valve overlap.
Applied Energy, Vol. 257 n^o August 2019, pp. 114018, 2020. (cited in p. 86)

Ibrahim A. and Bari S.
A comparison between EGR and lean-burn strategies employed in a natural gas SI engine using a two-zone combustion model.
Energy Conversion and Management, Vol. 50 n^o 12, pp. 3129–3139, 2009.
(cited in pp. 70, 80)

International Energy Agency.
Energy Technology Perspectives 2012: Pathways to a Clean Energy System.
2012. (cited in p. 31)

Ivanič Ž., Ayala F., Goldwitz J. and Heywood J. B.
Effects of hydrogen enhancement on efficiency and NOx emissions of lean and EGR-diluted mixtures in a SI engine.
SAE Technical Papers, n^o 724, 2005. (cited in p. 81)

Joshi A.
Review of Vehicle Engine Efficiency and Emissions.
SAE Technical Papers, Vol. 2, pp. 2479–2507, 2021. (cited in p. 68)

Jung D. and Lee S.
An investigation on the potential of dedicated exhaust gas recirculation for improving thermal efficiency of stoichiometric and lean spark ignition engine operation.
Applied Energy, Vol. 228 n^o June, pp. 1754–1766, 2018. (cited in p. 84)

Kakaee A. H., Shojaeefard M. H. and Zareei J.
Sensitivity and effect of ignition timing on the performance of a spark ignition engine: An experimental and modeling study.
Journal of Combustion, Vol. 2011, 2011. (cited in pp. 53, 80)

Kalghatgi G. T.
Spark ignition, early flame development and cyclic variation in I.C. engines.
SAE Technical Papers, n^o January, 1987. (cited in p. 45)

Kalghatgi G. T.
The outlook for fuels for internal combustion engines.
International Journal of Engine Research, Vol. 15 n^o 4, pp. 383–398, 2014.
(cited in p. 64)

Kamo R., Bryzik W. and Glance P.
Adiabatic engine trends-worldwide.
SAE Technical Paper n. 870018, 1987. (cited in p. 8)

Kanda M., Baika T., Kato S., Iwamuro M., Koike M. and Saito A.
Application of a new combustion concept to direct injection gasoline engine.
SAE Technical Papers, Vol. 2000 n^o 724, 2000. (cited in p. 71)

Karajalainen P., Pirjola L., Heikkila J., Lahde T., Tzamkiozis T., Ntziachristos L., Keskinen J. and Ronkko T.
Exhaust particles of modern gasoline vehicles: a laboratory and an on-road study.
Atmospheric Environment, Vol. 97, pp. 262–270, 2014. (cited in p. 69)

Karavalakis G., Short D., Vu D., Russell R., Hajbabaei M., Asa-Awuku A. and Durbin T. D.
Evaluating the effects of aromatics content in gasoline on gaseous and particulate matter emissions from SI-PFI and SIDI vehicles.
Environmental Science Technology, Vol. 49, pp. 7021–7031, 2015. (cited in p. 69)

Kawamoto M., Honda T., Katashiba H., Sumida M., Fukutomi N. and Kawajiri K.
A Study of Center and Side Injection in Spray Guided DISI Concept.
SAE Technical Papers, n^o 724, 2005. (cited in p. 65)

Kayes D. and Hochgreb S.
Mechanisms of particulate matter formation in spark-ignition engines. 1. Effect of engine operating conditions.
Environmental Science and Technology, Vol. 33 n^o 22, pp. 3957–3967, 1999. (cited in p. 65)

Khaled F., Badra J. and Farooq A.
Ignition delay time correlation of fuel blends based on Livengood-Wu description.
Fuel, Vol. 209 n^o August, pp. 776–786, 2017. (cited in p. 52)

Khan I. R.
Study of Variable Compression Ratio Engine (VCR) and Different Innovations to Achieve VCR.
International Journal for Research in Applied Science and Engineering Technology, Vol. V n^o XI, pp. 1473–1478, 2017. (cited in p. 77)

Khoa N. X., Quach Nhu Y. and Lim O.
Estimation of parameters affected in internal exhaust residual gases recirculation and the influence of exhaust residual gas on performance and emission of a spark ignition engine.
Applied Energy, Vol. 278 n^o June, pp. 115699, 2020. (cited in p. 86)

Khosravi M., Harihar A., Pitsch H. and Weber C.
Modeling and Numerical Investigation of Auto-Ignition and Megaknock in Boosted Gasoline Engines.
SAE Technical Papers, Vol. 2017-March n^o March, 2017. (cited in p. 86)

Kiga S., Mae Y., Akasaka Y. and Tomogane K.
Development of Innovative Variable Valve Event and Lift (VVEL) System.
SAE Technical Paper, 2007. (cited in p. 74)

Kim K. H., Kabir E. and Kabir S.
A review on the human health impact of airborne particulate matter.
Environment International, Vol. 74, pp. 136–143, 2015. (cited in pp. 9, 66)

Kinoshita K., Ueda K., Ito F., Shinojima Y., Yanagizawa T., Sakaguchi T. and Yamazaki T.
Development of a Custom Integrated Circuit for Continuously Variable Valve Lift Mechanism System Control.
SAE Technical Paper, 2008. (cited in p. 74)

Kleeberg H., Tomazic D., Dohmen J., Wittek K. and Balazs A.
Increasing efficiency in gasoline powertrains with a two-stage variable compression ratio (VCR) system.
SAE Technical Papers, Vol. 2, 2013. (cited in p. 77)

Kleinschmidt P. and Schmidt F.
How many sensors does a car need?
Sensors and Actuators: A. Physical, Vol. 31 n^o 1-3, pp. 35–45, 1992. (cited in p. 8)

Knop V. and Essayem E.
Comparison of PFI and DI operation in a downsized gasoline engine.
SAE Technical Paper n. 2013-01-1103, 2013. (cited in pp. 69, 71)

Knorr T., Ellmer D., Baensch S. and Schatz A.
"Optimization of the 48 V Hybrid Technology to Minimize Local Emissions in the RDE".
In *27th Aachen Colloquium Automobile and Engine Technology*, October 2018.
(cited in p. 16)

Ko J., Kim K., Chung W., Myung C. L. and Park S.
Characteristics of on-road particle number (PN) emissions from a GDI vehicle depending on a catalytic stripper (CS) and a metal-foam gasoline particulate filter (GPF).
Fuel, Vol. 238 n^o October 2018, pp. 363–374, 2019. (cited in p. 40)

Ko Y., Arpaci V. S. and Anderson R. W.
Spark ignition of propane-air mixtures near the minimum ignition energy: Part II. A model development.
Combustion and Flame, Vol. 83 n^o 1-2, pp. 88–105, 1991. (cited in p. 46)

Kohany T. and Sher E.
Using the 2nd law of thermodynamics to optimize variable valve timing for maximizing torque in a throttled SI engine.
SAE Technical Paper n. 1999-01-0328, 1999. (cited in p. 8)

Kojima S.
Development of high-performance and low-emission gasoline engine.
SAE Technical Papers, Vol. 2008 n^o 724, 2008. (cited in p. 74)

Kolodziej C. P., Pamminger M., Sevik J., Wallner T., Wagnon S. W. and Pitz W. J.
Effects of Fuel Laminar Flame Speed Compared to Engine Tumble Ratio, Ignition Energy, and Injection Strategy on Lean and EGR Dilute Spark Ignition Combustion.
SAE International Journal of Fuels and Lubricants, Vol. 10 n^o 1, pp. 82–94, 2017.
(cited in pp. 21, 68)

Konig, G. Maly R. R. Bradley D. Lau A. K. C. Sheppard C. G. W.
Role of exothermic centres on knock initiation and knock damage.
SAE Technical Paper n. 902136, 1990. (cited in p. 51)

Konig, G. Sheppard C. G. W.
End gas auto-ignition and knock in a spark ignition engine.
SAE Technical Paper n. 902135, 1990. (cited in p. 51)

Kouba A., Hnilicka B. and Navratil J.
Downsized Gasoline Engine Cylinder Deactivation MiL Development and Validation Using Real-Time 1-D Gas Code.
SAE Technical Papers, Vol. 2018-April, pp. 1–7, 2018. (cited in p. 75)

Kreuter P., Heuser P., and Schebitz M.
Strategies to Improve SIEngine Performance by Means of Variable Intake Lift, Timing and Duration.
SAE Technical Paper, 1992. (cited in p. 73)

Kumano K. and Yamaoka S.
Analysis of knocking suppression effect of cooled egr in turbo-charged gasoline engine.
SAE Technical Papers, Vol. 1, 2014. (cited in p. 82)

Kume T., Iwamoto Y., Lida K., Murakami M., Akishino K. and Ando H.
Combustion Control Technologies for Direct Injection SI Engine.
SAE 960600, 1996. (cited in p. 71)

Ladommatos N., Abdelhalim S. and Zhao H.
Control of oxides of nitrogen from diesel engines using diluents while minimising the impact on particulate pollutants.
Applied Thermal Engineering, Vol. 18 n^o 11, pp. 963–980, 1998. (cited in p. 64)

Ladommatos N., Abdelhalim S. M., Zhao H. and Hu Z.
Effects of EGR on heat release in diesel combustion.
SAE Technical Papers, Vol. 980184, 1998. (cited in pp. 62, 81)

Lanzanova T. D. M., Dalla Nora M., Martins M. E. S., Machado P. R. M., Pedrozo V. B. and Zhao H.
The effects of residual gas trapping on part load performance and emissions of a spark ignition direct injection engine fuelled with wet ethanol.
Applied Energy, Vol. 253 n^o January, pp. 113508, 2019. (cited in p. 86)

Lattimore T., Wang C., Xu H., Wyszynski M. L. and Shuai S.
Investigation of EGR Effect on Combustion and PM Emissions in a DISI Engine.
Applied Energy, Vol. 161 n^o x, pp. 256–267, 2016. (cited in pp. 66, 82, 90)

Lavoie G. A., Ortiz-soto E., Babajimopoulos A., Martz J. B. and Assanis D. N.
Thermodynamic sweet spot for high- efficiency , dilute , boosted gasoline engines.
International Journal of Engine Research, Vol. 14 n^o 3, pp. 260–278, 2012.
(cited in pp. 22, 129, 162, 172, 209, 215, 227)

Leduc P., Dubar B., Ranini A. and Monnier G.
Downsizing of Gasoline Engine: an Efficient Way to Reduce CO_2 Emissions.
Oil & Gas Science and Technology, Vol. 58 n^o 1, pp. 115–127, 2003.

Leiva-Candia D. E., García I. L., Lopez I., Serrano-Herrador J. A. and Dorado M. P.
Descriptive and inferential statistics as an exhaust emission comparative tool between different engine operating conditions and fuels. Application to highly oxidized biodiesel blended with primary alcohols.
Fuel, Vol. 324 n^o PA, pp. 124453, 2022. (cited in p. 56)

Lhuillier C., Brequigny P., Contino F. and Mounaïm-Rousselle C.
Experimental study on ammonia/hydrogen/air combustion in spark ignition engine conditions.
Fuel, Vol. 269 n^o September 2019, pp. 117448, 2020. (cited in p. 196)

Li T., Gao Y., Wang J. and Chen Z.
The Miller cycle effects on improvement of fuel economy in a highly boosted, high compression ratio, direct-injection gasoline engine: EIVC vs. LIVC.
Energy Conversion and Management, Vol. 79, pp. 59–65, 2014. (cited in p. 75)

Li T., Wu D. and Xu M.
Thermodynamic analysis of EGR effects on the first and second law efficiencies of a boosted spark-ignited direct-injection gasoline engine.
Energy Conversion and Management, Vol. 70 n^o x, pp. 130–138, 2013. (cited in p. 80)

Li T., Yin T. and Wang B.
Anatomy of the cooled EGR effects on soot emission reduction in boosted spark-ignited direct-injection engines.
Applied Energy, Vol. 190, pp. 43–56, 2017. (cited in p. 81)

Li Y., Zhang X., Wang Y., Sun J. and Fan X.
Experimental study on premixed combustion characteristics of methane-air under dual spark plug ignition strategy in a closed spherical chamber.
Fuel, Vol. 314 n^o January, pp. 123093, 2022. (cited in p. 179)

Li Y., Zhao H., Stansfield P. and Freeland P.
Synergy between Boost and Valve Timings in a Highly Boosted Direct Injection Gasoline Engine Operating with Miller Cycle.
SAE Technical Paper, 2015. (cited in p. 75)

Liang B., Ge Y., Tan J., Han X., Gao L., Hao L., Ye W. and Dai P.
Comparison of PM emissions from a gasoline direct injected (GDI) vehicle and a port fuel injected (PFI) vehicle measured by electrical low pressure impactor (ELPI) with two fuels: gasoline and M15 methanol gasoline.
Journal of Aerosol Science, Vol. 57, pp. 22–32, 2013. (cited in p. 69)

Livengood J. C. and Wu P. C.
Correlation of Autoignition Phenomena in Internal Combustion Engines and Rapid Compression Machines.
5th Symp. (International) on Combustion, pp. 347–356, 1955. (cited in p. 52)

Lou Z., Wen S., Qian J., Xu H., Zhu G. and Sun M.
Camless Variable Valve Actuator with Two Discrete Lifts.
SAE Technical Paper, 2015. (cited in p. 74)

Lou Zheng and Zhu Guoming.
Review of advancement in variable valve actuation of internal combustion engines.
Applied Sciences (Switzerland), Vol. 10 n^o 4, 2020. (cited in p. 74)

Luján J. M., Bermúdez V., Dolz V. and Monsalve-Serrano J.
An assessment of the real-world driving gaseous emissions from a Euro 6 light-duty diesel vehicle using a portable emissions measurement system (PEMS).
Atmospheric Environment, Vol. 174 n^o July 2017, pp. 112–121, 2018. (cited in p. 68)

Luján J. M., Climent H., Novella R. and Rivas-Perea M. E.
Influence of a low pressure EGR loop on a gasoline turbocharged direct injection engine.
Applied Thermal Engineering, Vol. 89, pp. 432–443, 2015.
(cited in pp. 61, 81, 82, 83, 89)

Luján J. M., Climent H., Pla B. and Rivas-Perea M. E.
Exhaust gas recirculation dispersion analysis using in-cylinder pressure measurements in automotive diesel engines.
Applied Thermal Engineering, Vol. 89, pp. 459–468, 2015. (cited in p. 34)

Luján J. M., Guardiola C., Pla B. and Reig A.
Switching strategy between HP (high pressure)- and LPEGR (low pressure exhaust gas recirculation) systems for reduced fuel consumption and emissions.
Energy, Vol. 90, pp. 1790–1798, 2015. (cited in p. 88)

LujÃ¡n J. M., Dolz V., Monsalve-Serrano J. and Bernal Maldonado M. A.
High-pressure exhaust gas recirculation line condensation model of an internal combustion diesel engine operating at cold conditions.
International Journal of Engine Research, 2019. (cited in p. 178)

Lumsden G., Eddleston D. and Sykes R.
Comparing lean burn and EGR.
SAE Technical Paper n. 970505, 1997. (cited in p. 70)

Lumsden G., Oudenijeweme D., Fraser N. and Blaxill H.
Development of a turbocharged direct injection downsizing demonstrator engine.
SAE Technical Papers, Vol. 2 n^o 1, pp. 1420–1432, 2009. (cited in p. 78)

Luttermann C., Schunemann E. and Klauer N.
Enhanced VALVETRONIC Technology for Meeting SULEV Emission Requirements.
SAE Technical Paper, 2006. (cited in p. 74)

Malaquias A. C. T., Netto N. A. D., da Costa R. B. R. and Baêta J. G. C.
Combined effects of internal exhaust gas recirculation and tumble motion generation in a flex-fuel direct injection engine.
Energy Conversion and Management, Vol. 217 n^o March, pp. 113007, 2020.
(cited in pp. 85, 173, 175, 178)

Malaquias A. C. T., Netto N. A. D., da Costa R. B. R. and Baêta J. G. C.
Combined effects of internal exhaust gas recirculation and tumble motion generation in a flex-fuel direct injection engine.
Energy Conversion and Management, Vol. 217 n^o March, pp. 113007, 2020.
(cited in p. 86)

Marchitto L., Tornatore C., Valentino G. and Teodosio L.
Impact of Cooled EGR on Performance and Emissions of a Turbocharged Spark-Ignition Engine under Low-Full Load Conditions.
SAE Technical Paper, 2019. (cited in pp. 58, 80, 82)

Martín J.
Aportación al diagnóstico de la combustión en motores Diesel de inyección directa.
2007. (cited in p. 129)

Masumitsu N., Otsuka S., Fujikura R., Imai Y. and Endo T.
Analysis of the pressure drop increase mechanism by ash accumulated of coated GPF.
SAE Technical Papers, Vol. 2019-April n^o April, pp. 1–7, 2019. (cited in p. 40)

Mathis U., Mohr M. and Forss A.
Comprehensive particle characterization of modern gasoline and diesel passenger cars at low ambient temperatures.
Atmospheric Environment, Vol. 39 n^o 1, pp. 107–117, 2005. (cited in pp. 65, 67)

Mauro S., cSener R., Gül M. Z., Lanzafame R., Messina M. and Brusca S.
Internal combustion engine heat release calculation using single-zone and CFD 3D numerical models.
International Journal of Energy and Environmental Engineering, Vol. 9 n^o 2, pp. 215–226, 2018. (cited in p. 128)

McCaffery C., Zhu H., Li C., Durbin T. D., Johnson K. C., Jung H., Brezny R., Geller M. and Karavalakis G.
On-road gaseous and particulate emissions from GDI vehicles with and without gasoline particulate filters (GPFs) using portable emissions measurement systems (PEMS).
Science of the Total Environment, Vol. 710, pp. 136366, 2020. (cited in p. 40)

Michaels H. C. and Fulper B. K.
Nitrous oxide emission factors for mobile sources USEPA.
In AWMA emissions inventory conference, New Orleans, USA, 1998., 1998. (cited in p. 62)

Middleton R. J., Manofsky L. K., Lavoie G. A., Wooldridge M. S., Assanis D. N. and Martz J. B.
The effect of spark timing and negative valve overlap on Spark Assisted Compression Ignition combustion heat release rate.
Proceedings of the Combustion Institute, Vol. 35 n^o 3, pp. 3117–3124, 2015. (cited in p. 53)

Miklanek L., Vitek O., Gotfryd O. and Klir V.
Study of Unconventional Cycles (Atkinson and Miller) with Mixture Heating as a Means for the Fuel Economy Improvement of a Throttled SI Engine at Part Load.
SAE International Journal of Engines, Vol. 5 n^o 4, pp. 1624–1636, 2012. (cited in p. 75)

Mikulski M., Balakrishnan P. R. and Hunicz J.
Natural gas-diesel reactivity controlled compression ignition with negative valve overlap and in-cylinder fuel reforming.
Applied Energy, Vol. 254 n^o July, pp. 113638, 2019. (cited in p. 86)

Miller R. H.
Supercharging and Internal Coolimg Cycle for High Output.
Trans. ASME, Vol. 69, 1947. (cited in p. 74)

Mohr M., Forss A. and Lehmann U.
Particle emissions from diesel passenger cars equipped with a particle trap in comparison to other technologies.
Environmental Science and Technology, Vol. 40 n^o 7, pp. 2375–2383, 2006. (cited in p. 65)

Momenimovahed A., Handford D., Checkel M. D. and Olfert J. S.
Particle number emission factors and volatile fraction of particles emitted from on-road gasoline direct injection passenger vehicles.
Atmospheric Environment, Vol. 102, pp. 105–111, 2015. (cited in p. 69)

Mori S. and Shimizu R.
Analysis of EGR cyclic variations in a direct injection gasoline engine by using raman scattering method.
SAE Technical Papers, n^o 724, 2002. (cited in p. 71)

Moriya Y., Watanabe A., Uda H. and Kawamura H.
A Newly Developed Intelligent Variable Valve Timing System - Continuously Controlled Cam Phasing as Applied to a New 3 Liter Inline 6 Engine.
SAE Technical Paper, 1996. (cited in p. 73)

Nates, R. J. Yates A. D. B.
Knock damage mechanisms in spark-ignition engines.
SAE Technical Paper n. 942064, 1994. (cited in p. 51)

Nishiyama A., Le M. K., Furui T. and Ikeda Y.
The Relationship between In-Cylinder Flow-Field near Spark Plug Areas, the Spark Behavior, and the Combustion Performance inside an Optical S.I. Engine.
Applied Sciences, Vol. 9 n^o 8, pp. 1545, apr 2019. (cited in pp. 151, 166)

Novella Ricardo, De la Morena JoaquÃn, Pagano Vincenzo and Pitarch Rafael.
Optical evaluation of orifice orientation and number effects on active pre-chamber spark ignition combustion.
Fuel, Vol. 338, pp. 127265, 2023.

Ntziachristos L., Amanatidis S., Samaras Z., Janka K. and Tikkanen J.
Application of the pegasor particle sensor for the measurement of mass and particle number emissions.
SAE Technical Papers, Vol. 2, 2013. (cited in p. 65)

Oceanic National and Administration Atmospheric.
Trends in Atmospheric Carbon Dioxide.
ESRL Global Monitoring Division, 2019. (cited in pp. 13, 14)

Odell P. R.
Why carbon fuels will dominate the 21st century's global energy economy.
Geopolitics of Energy, Vol. 26 n^o 3-4, pp. 2–8, 2004. (cited in p. 64)

Oh H. and Bae C.
Effects of the injection timing on spray and combustion characteristics in a spray-guided DISI engine under lean-stratified operation.
Fuel, Vol. 107, pp. 225–235, 2013. (cited in pp. 70, 72)

Oh H., Lee J., Woo S. and Park H.
Effect of synergistic engine technologies for 48 V mild hybrid electric vehicles.
Energy Conversion and Management, Vol. 244 n^o May, pp. 114515, 2021.
(cited in pp. 74, 79, 80)

Ohgami E., Ohsawa N. and Saito T.
Nissan's new V8 and L4 aluminum cylinder block - Design and production.
SAE Technical Paper n. 910431, 1991. (cited in p. 8)

Ortiz-Imedio R., Ortiz A. and Ortiz I.
Comprehensive analysis of the combustion of low carbon fuels (hydrogen, methane and coke oven gas) in a spark ignition engine through CFD modeling.
Energy Conversion and Management, Vol. 251, pp. 114918, 2022. (cited in p. 179)

Ortiz-Soto E. A., Vavra J., and Babajimopoulos A.
Assessment of Residual Mass Estimation Methods for Cylinder Pressure Heat Release Analysis of HCCI Engines With Negative Valve Overlap.
J. Eng. Gas Turbines Power, n^o 134, pp. 9, 2012. (cited in p. 86)

Ouellette P., Douville B., Hill P. G. and Ursu B.
NOx reduction in a directly injected natural gas engine.
American Society of Mechanical Engineers, Internal Combustion Engine Division (Publication) ICE, Vol. 31-33 n^o 3, pp. 59–71, 1998. (cited in p. 62)

Pairy F. and Desantes J. M.
Motores de combustión interna alternativos.
Editorial Reverté and Editorial UPV, 2011. (cited in pp. 33, 35, 39, 45, 48, 56, 63)

Pallotti P., Torella E., New J., Criddle M. and Brown J.
Application of an Electric Boosting System to a Small, Four-Cylinder S.I. Engine.
SAE Technical Paper n. 2003-32-0039, 2003. (cited in p. 79)

Palma A., Del Core D. and Esposito C.
The HCCI concept and control, performed with multiair technology on gasoline engines.
SAE Technical Papers, 2011. (cited in p. 74)

Park C., Kim S., Kim H. and Moriyoshi Y.
Stratified lean combustion characteristics of a spray-guided combustion system in a gasoline direct injection engine.
Energy, Vol. 41 n^o 1, pp. 401–407, 2012. (cited in pp. 68, 70)

Park Y. and Bae C.
Experimental study on the effects of high/low pressure EGR proportion in a passenger car diesel engine.
Applied Energy, Vol. 133, pp. 308–316, 2014. (cited in p. 80)

Parker M. C., Jiang C., Butcher D., Spencer A., Garner C. P. and Witt D.
Impact and observations of cylinder deactivation and reactivation in a downsized gasoline turbocharged direct injection engine.
International Journal of Engine Research, Vol. 22 n^o 4, pp. 1367–1376, 2021.
(cited in p. 75)

Parsons D., Orchard S., Evans N., Ozturk U., Burke R. and Brace C.s.
A comparative study into the effects of pre and post catalyst exhaust gas recirculation on the onset of knock.
International Journal of Engine Research, 2020. (cited in p. 80)

Patterson D. J.
Cylinder pressure variations, a fundamental combustion problem.
SAE Technical Paper n. 290016, 1966. (cited in p. 46)

Peckham M. S., Finch A. and Campbell B.
Analysis of Transient HC, CO, NOx and CO_2 Emissions from a GDI Engine using Fast Response Gas Analyzers.
SAE International Journal of Engines, Vol. 4 n^o 1, pp. 1513–1522, 2011. (cited in p. 65)

Peckham M. S., Finch A., Campbell B., Price P. and Davies M. T.
Study of particle number emissions from a turbocharged gasoline direct injection (GDI) engine including data from a fast-response particle size spectrometer.
SAE 2011 World Congress and Exhibition, 2011. (cited in pp. 65, 70)

Pešić R. B., Milojević S. T. and Veinović S. P.
Benefits and challenges of variable compression ratio at diesel engines.
Thermal Science, Vol. 14 n^o 4, pp. 1063–1073, 2010. (cited in p. 77)

Peters N.
Laminar flamelet concepts in turbulent combustion.
Symposium (International) on Combustion, Vol. 21 n^o 1, pp. 1231–1250, 1988.
(cited in p. 48)

Peters N. and Williams F. A.
Premixed combustion in a vortex.
Symposium (International) on Combustion, Vol. 22 n^o 1, pp. 495–503, 1989.
(cited in p. 48)

Pham A. and Jeftic M.
Characterization of Gaseous Emissions from Blended Plug-In Hybrid Electric Vehicles during High-Power Cold-Starts.
SAE Technical Papers, Vol. 2018-01-0428 n^o 2018-01-0428, pp. 1–9, 2018.
(cited in pp. 16, 21)

Pinterits M.
EU National Greenhouse Gas Inventory Report May 2014.
Number 09. 2014. (cited in p. 21)

Piqueras P., De la Morena J., Sanchis E. J. and Pitarch R.
Impact of Exhaust Gas Recirculation on Gaseous Emissions of Turbocharged Spark-Ignition Engines.
Applied Sciences, pp. 1–17, 2020. (cited in pp. 21, 34, 56, 58, 81, 82, 119, 182)

Pla B., De la Morena J., Bares P. and Jiménez I.
Knock Analysis in the Crank Angle Domain for Low-Knocking Cycles Detection.
SAE Technical Papers, Vol. 2020-April n^o April, pp. 1–11, 2020.
(cited in pp. 51, 117, 128)

Pope C. A. and Dockery D. W.
Health effects of fine particulate air pollution: Lines that connect.
Journal of the Air and Waste Management Association, Vol. 56 n^o 6, pp. 709–742, 2006.
(cited in pp. 9, 66)

Potteau S., Lutz P., Leroux S., Moroz S. and Tomas E.
Cooled EGR for a Turbo SI Engine to Reduce Knocking and Fuel Consumption.
SAE Technical Papers, 2007. (cited in p. 82)

Preussner C., Döring C., Fehler S. and Kampmann S.
GDI: Interaction between mixture preparation, combustion system and injector performance.
SAE Technical Papers, n^o 724, 1998. (cited in p. 45)

Price P., Stone R., Oudenijeweme D. and Chen X.
Cold start particulate emissions from a second generation di gasoline engine.
SAE Technical Paper n. 2007-01-1931, 2007. (cited in p. 70)

Pulkrabek W. W.
Engineering Fundamentals of the Internal Combustion Engine.
Upper Saddle River, New Jersey 07548, 1997. (cited in pp. 43, 51)

Puranam S. V. and Steeper R. R.
The Effect of Acetylene on Iso-octane Combustion in an HCCI Engine with NVO.
SAE International Journal of Engines, Vol. 5 n^o 4, pp. 1551–1560, 2012. (cited in p. 86)

Qu W., Fang Y., Wang Z., Sun H. and Feng L.
Optimization of injection system for a medium-speed four-stroke spark-ignition marine hydrogen engine.
International Journal of Hydrogen Energy, Vol. 47 n^o 44, pp. 19289–19297, 2022.
(cited in p. 196)

R. Maly.
Initiation and Propagation of Flame Fronts in Lean CH4-Air Mixtures by the Three Modes of Ignition Spark in Fuel Economy in Road Vehicles Powered by Spark-Ignition Engines.
Hilliard, J. C. and Springer, G. S. Plenum Press, New York, 1984. (cited in p. 45)

R. Maly.
Spark Ignition: Its Physics and Effect on the Internal Combustion Engine in Fuel Economy in Road Vehicles Powered by Spark-Ignition Engines.
Hilliard, J. C. and Springer, G. S. Plenum Press, New York, 1984. (cited in p. 45)

Radu, B. Martin G. Chiriac R. Apostolescu N.
On the knock characteristics of LPG in a spark ignition engine.
SAE Technical Paper n. 2005-01-3773, 2005. (cited in p. 52)

Randolph E., Fieseler K., Conway G., Alger T. and Chadwell C.
The Effects of EGR Composition on Combustion Performance and Efficiency.
SAE Technical Papers, n^o 2020, pp. 1–12, 2020. (cited in p. 119)

Reihani A., Hoard J., Klinkert S., Kuan C. K., Styles D. and McConville G.
Experimental response surface study of the effects of low-pressure exhaust gas recirculation mixing on turbocharger compressor performance.
Applied Energy, Vol. 261 n^o December 2019, pp. 114349, 2020. (cited in p. 89)

Ribbens W. B.
The Basics of Electronic Engine Control.
2017. (cited in p. 41)

Ritchie H. and Roser M.
CO_2 and Greenhouse Gas Emissions.
Our World in Data, 2017. (cited in p. 20)

Roberts M.
Benefits and challenges of variable compression ratio (VCR).
SAE Technical Papers, n^o 724, 2003. (cited in p. 77)

Rodriguez J. F. and Cheng W.
Potential of Negative Valve Overlap for Part-Load Efficiency Improvement in Gasoline Engines.
SAE International Journal of Engines, Vol. 11 n^o 6, pp. 657–668, 2018. (cited in p. 86)

Roth D. B., Gonzalez Tabares I. and Sotelo Álvarez A.
Condensing LPL EGR Mixer with Mid-Pressure Loop.
SAE International Journal of Engines, Vol. 8 n^o 4, 2015. (cited in p. 84)

Roy M. M., Tomita E., Kawahara N., Harada Y. and Sakane A.
Comparison of performance and emissions of a supercharged dual-fuel engine fueled by hydrogen and hydrogen-containing gaseous fuels.
International Journal of Hydrogen Energy, Vol. 36 n^o 12, pp. 7339–7352, 2011.
(cited in p. 80)

Sadakane S., Sugiyama M., Kishi H., Abe S., Harada J. and Sonoda Y.
Development of a new V-6 high performance stoichiometric gasoline direct injection engine.
SAE Technical Papers, Vol. 2005 n^o 724, 2005. (cited in pp. 71, 74)

Saito C., Nakatani T., Miyairi Y., Yuuki K., Makino M., Kurachi H., Heuss W., Kuki T., Furuta Y., Kattouah P. and Vogt C. D.
New Particulate Filter Concept to Reduce Particle Number Emissions.
SAE Technical Papers, 2011. (cited in p. 40)

Saito H., Shirasuna T. and Nomura T.
Extension of Lean Burn Range by Intake Valve Offset.
SAE Technical Paper n. 2013-32-9032, 2013. (cited in p. 70)

Sakai S. and Rothamer D.
Impact of ethanol blending on particulate emissions from a spark-ignition direct-injection engine.
Fuel, Vol. 236 n^o October 2018, pp. 1548–1558, 2019. (cited in p. 69)

Salvi B. L. and Subramanian K. A.
A novel approach for experimental study and numerical modeling of combustion characteristics of a hydrogen fuelled spark ignition engine.
Sustainable Energy Technologies and Assessments, Vol. 51 n^o January, pp. 101972, 2022. (cited in pp. 179, 196)

Samsudin D., Anuar M. D., Othman S., Manshoor B. and Khalid A.
Application of Schlieren Optical Visualization System in External Combustion and Internal Combustion Engine: A Review.
Applied Mechanics and Materials, Vol. 773-774 n^o July, pp. 535–539, 2015. (cited in p. 46)

Santodonato J., Basu D. and Howard P.
Health effects associated with diesel exhaust emissions, literature review and evaluation.
National Academy of Sciencies, Engineering and Medicine, n^o EPA/600/1-78/063, 1978-11. (cited in p. 9)

Sarikoc F., Kettner M., Velji A., Spicher U., Krause A. and Elsaesser A.
Potential of reducing the NO_x emissions in a spray guided DI gasoline engine by stratified exhaust gas recirculation (EGR).
SAE Technical Papers, n^o 2006-01-1261, 2006. (cited in p. 62)

Schwaderlapp M., Habermann K. and Yapici K.
Variable Compression Ratio - A Design Solution for Fuel Economy Concepts.
SAE Technical Papers, 2002. (cited in p. 77)

Schwarz C., Schünemann E., Durst B., Fischer J. and Witt A.
Potentials of the Spray-Guided BMW DI Combustion System Reprinted From : SI Combustion and Direct Injection SI Engine Technology.
SAE International, Vol. 328 n^o 724, pp. 145–149, 2006. (cited in p. 45)

Sellnau M., Kunz T., Sinnamon J., and Burkhard J.
2-step Variable Valve Actuation: System Optimization and Integration on an SI Engine.
SAE Technical Paper, 2006. (cited in p. 73)

Serrano J., Climent H., Navarro R. and González-Domínguez D.
Methodology to Standardize and Improve the Calibration Process of a 1D Model of a GTDI Engine.
SAE Technical Papers, Vol. 2020-April n^o April, pp. 1–13, 2020. (cited in pp. 132, 133)

Serrano J. R., Arnau F. J., García-Cuevas L. M., Gómez-Vilanova A., Guilain S. and Batard S.
A Methodology for Measuring Turbocharger Adiabatic Maps in a Gas-Stand and Its Usage for Calibrating Control Oriented and One-Dimensional Models at Early ICE Design Stages.
Journal of Energy Resources Technology, Vol. 143 n^o 4, pp. 1–11, 2021. (cited in p. 132)

Serrano J. R., Piqueras P., De la Morena J. and Ruiz M. J.
Influence of pre-turbine small-sized oxidation catalyst on engine performance and emissions under driving conditions.
Applied Sciences (Switzerland), Vol. 10 n^o 21, pp. 1–17, 2020. (cited in p. 40)

Shahbaz M. A., Shawal S. and Kaiser S. A.
Endoscopic visualization of the early premixed flame kernel in an SI engine by high-speed chemiluminescence imaging and.
Experiments in Fluids, Vol. March, 2017. (cited in p. 46)

Shen K., Li F., Zhang Z., Sun Y. and Yin C.
Effects of LP and HP cooled EGR on performance and emissions in turbocharged GDI engine.
Applied Thermal Engineering, Vol. 125 n^o x, pp. 746–755, 2017. (cited in pp. 80, 83)

Shen Kai, Xu Zishun, Chen Hong and Zhang Zhendong.
Investigation on the EGR effect to further improve fuel economy and emissions effect of Miller cycle turbocharged engine.
Energy, Vol. 215, pp. 119116, 2021. (cited in p. 80)

Sher E. and Keck J. C.
Spark ignition of combustible gas mixtures.
Combustion and Flame, Vol. 66 n^o 1, pp. 17–25, 1986. (cited in p. 45)

Shiao Y. and Moskwa J. J.
Cylinder Pressure and Combustion Heat Release Estimation for SI Engine Diagnostics Using Nonlinear Sliding Observers.
IEEE Transactions on Control Systems Technology, Vol. 3 n^o 1, pp. 70–78, 1995. (cited in p. 128)

Shojaeefard M. H., Tahani M., Etghani M. M. and Akbari M.
Cooled EGR for a Turbo Charged SI Engine to Reduce Knocking and Fuel Consumption.
Int. Journal of Automotive Engineering, Vol. 3 n^o 4, 2013. (cited in p. 68)

Shu G., Pan J. and Wei H.
Analysis of onset and severity of knock in SI engine based on in-cylinder pressure oscillations.
Applied Thermal Engineering, Vol. 51 n^o 1-2, pp. 1297–1306, 2013. (cited in pp. 21, 68, 127)

Sick V., Drake M. C. and Fansler T. D.
High-speed imaging for direct-injection gasoline engine research and development.
Experiments in Fluids, Vol. 49 n^o 4, pp. 937–947, 2010. (cited in p. 46)

Sivak M. and Schoettle B.
Fuel sources for electricity in the individual countries of the world and the consequent emissions from driving electric vehicles.
Sustainable Worldwide Transportation, 2017. (cited in pp. 16, 17)

Sjerić M., Taritaš I., Tomić R., Blažić M., Kozarac D. and Lulić Z.
Efficiency improvement of a spark-ignition engine at full load conditions using exhaust gas recirculation and variable geometry turbocharger - Numerical study.
Energy Conversion and Management, Vol. 125, pp. 26–39, 2016. (cited in pp. 21, 80)

Smith K. R., Jerrett M., Anderson H. R., Burnett R. T., Stone V., Derwent R., Atkinson R. W., Cohen A., Shonkoff S. B., Krewski D., Pope C. A., Thun M. J. and Thurston G.
Public health benefits of strategies to reduce greenhouse-gas emissions: health implications of short-lived greenhouse pollutants.
The Lancet, Vol. 374 n^o 9707, pp. 2091–2103, 2009. (cited in p. 9)

Solomon A. S., Anderson R. W., Najt P. M. and Zhao F.
Direct fuel injection for gasoline engines.
SAE progress in technology series PT - 80, 2000. (cited in p. 45)

Soltic P. and Hausberger S.
On-Road Emission Measurements and emission modeling results for a tractor-semi trailer in Trans-Alpine operation.
13th International Scienfftic Symposium Transport and Air Pollution Boulder, September 13-15, 2004. (cited in p. 62)

Song H. and Song S.
Numerical investigation on a dual loop EGR optimization of a light duty diesel engine based on water condensation analysis.
Applied Thermal Engineering, Vol. 182, pp. 116064, 2021. (cited in pp. 178, 179)

Song X., Myers J. and Sarnia S.
Integrated Low Temperature Cooling System Development in Turbo Charged Vehicle Application.
SAE International Journal of Passenger Cars - Mechanical Systems, Vol. 7 n^o 1, pp. 163–173, 2014. (cited in p. 34)

Splitter D. A. and Szybist J. P.
Experimental investigation of spark-ignited combustion with high-octane biofuels and EGR. 2. Fuel and EGR effects on knock-limited load and speed.
Energy and Fuels, Vol. 28 n^o 2, pp. 1432–1445, 2014. (cited in pp. 54, 55, 80)

Stephanie, M. Bourgoin G., Lujan J. and Pla B.
Acidic Condensation in Low Pressure EGR Systems using Diesel and Biodiesel Fuels.
SAE Technical Papers, 2009. (cited in p. 179)

Stober W. and Abel U.
Lung cancer due to diesel soot particles in ambient air.
International Archives of Occupational and Environmental Health, Vol. 68, pp. S3–S61, 1996. (cited in p. 66)

Stone R.
Introduction to Internal Combustion Engines.
4th edition, 2012. (cited in p. 74)

Su J., Xu M., Li T., Gao Y. and Wang J.
Combined effects of cooled EGR and a higher geometric compression ratio on thermal efficiency improvement of a downsized boosted spark-ignition direct-injection engine.
Energy Conversion and Management, Vol. 78, pp. 65–73, 2014. (cited in p. 80)

Su J., Xu M., Zhang Y., Hung D. and Li T.
Soot emission reduction using cooled EGR for a boosted spark-ignition direct-injection (SIDI) engine.
Proceedings of the 8th International Conference on Modeling and Diagnostics for Advanced Engine Systems, COMODIA 2012, pp. 98–103, 01 2012. (cited in p. 81)

Szczepanski D.
Factors influencing NOx emissions at Tarong and Stanwell power stations.
PhD-Thesis. The University of Queensland, 1998. (cited in p. 62)

Szwaja S., Ansari E., Rao S., Szwaja M., Grab-Rogalinski K., Naber J. D. and Pyrc M.
Influence of exhaust residuals on combustion phases, exhaust toxic emission and fuel consumption from a natural gas fueled spark-ignition engine.
Energy Conversion and Management, Vol. 165 n^o December 2017, pp. 440–446, 2018.
(cited in pp. 86, 173, 178)

Szybist J. P. and Splitter D. A.
Pressure and temperature effects on fuels with varying octane sensitivity at high load in SI engines.
Combustion and Flame, Vol. 177, pp. 49–66, 2017. (cited in p. 53)

Szybist James P, Wagnon Scott W, Splitter Derek, Pitz William J and Mehl Marco.
The Reduced Effectiveness of EGR to Mitigate Knock at High Loads in Boosted SI Engines.
SAE Technical Paper 2017-24-0061, 2017. (cited in p. 80)

Takaki D., Tsuchida H., Kobara T., Akagi M., Tsuyuki T. and Nagamine M.
Study of an EGR system for downsizing turbocharged gasoline engine to improve fuel economy.
SAE Technical Papers, Vol. 1, 2014. (cited in pp. 80, 91)

Tang Q., Liu J., Zhan Z. and Hu T.
Influences on Combustion Characteristics and Performances of EGR vs. Lean Burn in a Gasoline Engine.
SAE Technical Papers, Vol. 2013-April, 2013. (cited in p. 86)

Tanoue Kimitoshi, Kimura Takanori, Jimoto Taishu, Hashimoto Jun and Moriyoshi Yasuo.
Study of prechamber combustion characteristics in a rapid compression and expansion machine.
Applied Thermal Engineering, Vol. 115, pp. 64–71, 2017. (cited in p. 72)

Teodosio L., De Bellis V. and Bozza F.
Fuel Economy Improvement and Knock Tendency Reduction of a Downsized Turbocharged Engine at Full Load Operations through a Low-Pressure EGR System.
SAE International Journal of Engines, Vol. 8 n^o 4, pp. 2015–01–1244, 2015.
(cited in pp. 21, 68)

Tomazic D. and Pfeifer A.
Cooled EGR - A Must or an Option for 2002/04 Reprinted From: Compression Ignition Combustion and In-Cylinder Diesel Particulates and NOx Control.
SAE Technical Papers, Vol. 2002-01-00962, 2002. (cited in p. 83)

Turner J. W. G., Popplewell A., Patel R., Johnson T. R., Darnton N. J., Richardson S., Bredda S. W., Tudor R. J., Bithell C. I., Jackson R., Remmert S. M., Cracknell R. F., Fernandes J. X., Lewis A. G. J., Akehurst S., Brace C. J., Copeland C., Martinez-Botas R., Romagnoli A. and Burluka A. A.
Ultra Boost for Economy: Extending the Limits of Extreme Engine Downsizing.
SAE Technical Paper n. 2014-01-1185, 2014. (cited in p. 78)

U.S. EPA.
Final rulemaking to establish light-duty vehicle greenhouse gas emission standards and corporate average fuel economy standards.
Joint Technical Support Document, 2010. (cited in p. 69)

Valero J.
Analysis of the potential of SI lean combustion and CAI combustion in a two-stroke spark-assisted gasoline engine.
PhD-Thesis. Universitat Politècnica de València, Departamento de Máquinas y Motores Térmicos, 2020. (cited in pp. 49, 50, 57)

Van Der Wege B. A., Han Z., Iyer C. O., Muñoz R. H. and Yi J.
Development and analysis of a spray-guided DISI combustion system concept.
SAE Technical Papers, n^o 724, 2003. (cited in p. 45)

Varnier O.
Trends and Limits of Two-Stage Boosting Systems for Automotive Diesel Engines.
PhD-Thesis. Universitat Politècnica de València, Departamento de Máquinas y Motores Térmicos, 2012. (cited in p. 43)

Vaudrey Alexandre.
Thermodynamics of indirect water injection in internal combustion engines: Analysis of the fresh mixture cooling effect.
International Journal of Engine Research, Vol. 20 n^o 5, pp. 527–539, 2019. (cited in p. 179)

Vianna J. N. De S., Reis A. Do V., Oliveira A. B. De S., Fraga A. G. and De Sousa M. T.
Reduction of pollutants emissions on SI engines - Accomplishments with efficiency increase.
Journal of the Brazilian Society of Mechanical Sciences and Engineering, Vol. 27 n^o 3, pp. 217–222, 2005. (cited in p. 119)

Vijayaraghavan K., Lindhjem C., DenBleyker A., Nopmongcol U., Grant J., Tai E. and Yarwood G.
Effects of light duty gasoline vehicle emission standards in the United States on ozone and particulate matter.
Atmospheric Environment, Vol. 60 n^o 2012, pp. 109–120, 2012. (cited in p. 9)

Wandell J. L.
Shot peening of engine components.
American Society of Mechanical Engineers, Internal Combustion Engine Division (Publication) ICE, Vol. 29, pp. 101–108, 1997. (cited in p. 8)

Wang C., Daniel R. and Ma X.
Comparison of Gasoline (UGL), 2,5-Dimethylfuran (DMF) and Bio-Ethanol in a DISI Miller Cycle with Late Inlet Valve Closing Time.
SAE Technical Paper, 2012. (cited in p. 76)

Wang X., Zhang X., Wang M., Han Y. and Chen H.
Numerical Simulation of Knock Combustion in a Downsizing Turbocharged Gasoline Direct Injection Engine.
Applied Sciences, Vol. 9 n^o 19, pp. 4133, oct 2019. (cited in p. 80)

Wang Y., Conway G. and Chadwell C.
Combined benefits of variable valve actuation and low-pressure egr on si engine efficiency part 2: High load.
SAE Technical Papers, Vol. 2019-April n^o April, pp. 1–9, 2019. (cited in p. 73)

Wang Y., Wei H., Zhou L., Zhang X. and Zhong L.
Effects of reactivity inhomogeneities on knock combustion in a downsized spark-ignition engine.
Fuel, Vol. 278 n^o May, pp. 118317, 2020. (cited in p. 77)

Warey A., Huang Y., Matthews R., Hall M. and Ng H.
Effects of piston wetting on size and mass of particulate matter emissions in a DISI engine.
SAE Technical Papers, Vol. 2002 n^o 724, 2002. (cited in p. 65)

Warnatz J., Maas U. and Dibble R. W.
Combustion: Physical and chemical fundamentals, modeling and simulation, experiments, pollutant formation.
2006. (cited in p. 51)

Watanabe I., Kawai T., Yonezawa K. and Ogawa T.
The New Toyota 2.0-Liter Inline 4-Cylinder ESTEC D-4ST Engine - Turbocharged Direct Injection Gasoline Engine.
23rd Aachen Colloquium Automobile and Engine Technology, 2014. (cited in p. 74)

Weernink W. O.
Europeans, Japanese intensify hybrid, diesel debate.
Europe: Automotive News, Vol. 8, 2003. (cited in p. 41)

Wei H., Zhu T., Shu G., Tan L. and Wang Y.
Gasoline engine exhaust gas recirculation - A review.
Applied Energy, Vol. 99, pp. 534–544, 2012. (cited in pp. 62, 83, 88, 177)

Weltens H., Garcia P. and Walther H.
Internal and External corrosion of exhaust systems for passenger vehicles - test procedures, laoratory and field results.
Materials and Corrosion, pp. 31–42, 1999. (cited in p. 179)

Westbrook, C. K. Pitz W. J. Leppard W. R.
The autoi-gnition chemistry of paraffinic fuels and pro-knock and anti-knock additives: a detailed chemical kinetic study.
SAE Technical Paper n. 912314, 1991. (cited in p. 51)

Wheeler J., Polovina D., Ramanathan S., Roth K., Manning D. and Stein J.
Increasing EGR tolerance using high tumble in a modern GTDI engine for improved low-speed performance.
SAE Technical Papers, Vol. 2, 2013. (cited in p. 83)

Whitaker P., Kapus P., Ogris M. and Hollerer P.
Measures to Reduce Particulate Emissions from Gasoline DI engines.
SAE Technical Paper n. 2011-01-1219, 2011. (cited in p. 70)

Williams F. A.
An approach to turbulent flame theory.
Journal of Fluid Mechanics, Vol. 40 n^o 2, pp. 401–421, 1970. (cited in p. 48)

Wirth M., Piock W. F., Fraidl G. K., Schoeggl P. and Winklhofer E.
Gasoline di engines: The complete system approach by interaction of advanced development tools.
SAE Technical Papers, n^o 724, 1998. (cited in p. 71)

Wirth M., Zimmermann D., Friedfeldt R., Caine J., Schamel A. and Storch A.
The next generation of gasoline direct injection: improved fuel economy and optimized system cost.
Advance engine design and performance, pp. 52–139, 2003. (cited in p. 45)

Xie F., Li X., Su Y., Hong W., Jiang B. and Han L.
Influence of air and EGR dilutions on improving performance of a high compression ratio spark-ignition engine fueled with methanol at light load.
Applied Thermal Engineering, Vol. 94, pp. 559–567, 2016. (cited in pp. 62, 71, 88, 177)

Xiong Y., Roberts W. L., Drake M. C. and Fansler T. D.
Investigation of pre-mixed flame-kernel/vortex interactions via high-speed imaging.
Combustion and Flame, Vol. 126 n^o 4, pp. 1827–1844, 2001. (cited in p. 46)

Yamada H., Inomata S. and Tanimoto H.
Particle and VOC Emissions from Stoichiometric Gasoline Direct Injection Vehicles and Correlation Between Particle Number and Mass Emissions.
Emission Control Science and Technology, Vol. 3 n^o 2, pp. 135–141, 2017.
(cited in pp. 16, 21, 69)

Yu C., Kim T., Yi Y., Lee J., Noh S. and Choi K.
Development of kmc 2.4l Lean burn engine.
SAE Technical Paper n. 950685, 1995. (cited in p. 70)

Yu C., Zhao Z., Wang L., Cui H. and Zhang F.
The effect of cooled EGR on combustion and load extension in a kerosene spark-ignition engine.
Fuel, Vol. 280 n^o March, pp. 118681, 2020. (cited in p. 88)

Yu X., Zhao Z., Huang Y., Shi W., Guo Z., Li Z., Du Y., Jin Z., Li D., Wang T. and Li Y.
Experimental study on the effects of EGR on combustion and emission of an SI engine with gasoline port injection plus ethanol direct injection.
Fuel, Vol. 305 n^o August, pp. 121421, 2021. (cited in p. 80)

Zaccardi J. M., Pagot A., Vangraefschepe F., Dognin C. and Mokhtari S.
Optimal design for a highly downsized gasoline engine.
SAE Technical Papers, Vol. 4970, 2009. (cited in p. 69)

Zamboni G. and Capobianco M.
Experimental study on the effects of HP and LP EGR in an automotive turbocharged diesel engine.
Applied Energy, Vol. 94, pp. 117–128, 2012. (cited in p. 88)

Zareei J. and Kakaee A. H.
Study and the effects of ignition timing on gasoline engine performance and emissions.
European Transport Research Review, Vol. 5 n^o 2, pp. 109–116, 2013. (cited in p. 54)

Zhang M., Chen W., Shen X., Zhao H., Gao C., Zhang X., Liu W., Yang C., Qin Y., Zhang S., Fu J., Tong D. and Xiu A.
Comprehensive and high-resolution emission inventory of atmospheric pollutants for the northernmost cities agglomeration of Harbin-Changchun, China: Implications for local atmospheric environment management.
Journal of Environmental Sciences (China), Vol. 104, pp. 150–168, 2021. (cited in p. 9)

Zhang S., Li Y., Wang S., Zeng H., Liu J., Duan X. and Dong H.
Experimental and numerical study the effect of EGR strategies on in-cylinder flow, combustion and emissions characteristics in a heavy-duty higher CR lean-burn NGSI engine coupled with detail combustion mechanism.
Fuel, Vol. 276 n^o February, pp. 118082, 2020. (cited in p. 80)

Zhang Z., Wang T., Jia M., Wei Q., Meng X. and Shu G.
Combustion and particle number emissions of a direct injection spark ignition engine operating on ethanol/gasoline and n-butanol/gasoline blends with exhaust gas recirculation.
Fuel, Vol. 130, pp. 177–188, 2014. (cited in pp. 21, 66, 69, 82, 119)

Zhang Z., Zhang H., Wang T. and Jia M.
Effects of tumble combined with EGR (exhaust gas recirculation) on the combustion and emissions in a spark ignition engine at part loads.
Energy, Vol. 65 n^o x, pp. 18–24, 2014. (cited in p. 80)

Zhao J.
Research and application of over-expansion cycle (Atkinson and Miller) engines - A review.
Applied Energy, Vol. 185 n^o January 2017, pp. 300–319, 2017. (cited in p. 76)

Zhao L., Su X. and Wang X.
Comparative study of exhaust gas recirculation (EGR) and hydrogen-enriched EGR employed in a SI engine fueled by biobutanol-gasoline.
Fuel, Vol. 268 n^o October 2019, pp. 117194, 2020. (cited in p. 90)

Zhao X., Zhu Z., Zheng Z., Yue Z., Wang H. and Yao M.
Effects of flame propagation speed on knocking and knock-limited combustion in a downsized spark ignition engine.
Fuel, Vol. 293 n^o January, pp. 120407, 2021. (cited in p. 77)

Zhen X., Tian Z., Wang Y., Xu M., Liu D. and Li X.
Knock analysis of bio-butanol in TISI engine based on chemical reaction kinetics.
Energy, Vol. 239, pp. 122190, 2022. (cited in p. 80)

Zhen X., Wang Y., Xu S., Zhu Y., Tao C., Xu T. and Song M.
The engine knock analysis - An overview.
Applied Energy, Vol. 92, pp. 628–636, 2012. (cited in pp. 51, 127)

Zhou L., Dong K., Hua J., Wei H., Chen R. and Han Y.
Effects of applying EGR with split injection strategy on combustion performance and knock resistance in a spark assisted compression ignition (SACI) engine.
Applied Thermal Engineering, Vol. 145 n^o 2011, pp. 98–109, 2018. (cited in pp. 81, 86)

Zhou Lei, Song Yuntong, Hua Jianxiong, Liu Fengnian, Liu Zongkuan and Wei Haiqiao.
Effects of different hole structures of pre-chamber with turbulent jet ignition on the flame propagation and lean combustion performance of a single-cylinder engine.
Fuel, Vol. 308, 1 2022. (cited in p. 73)

Zhu Z., Wei Y., Mu Z., Du R., Guan W. and Liu S.
Cylinder-to-cylinder variation of knock and effects of mixture formation on knock tendency for a heavy-duty spark ignition methanol engine.
Energy, Vol. 254, pp. 124197, 2022. (cited in p. 179)

Zinola S., Raux S. and M Leblanc.
Persistent Particle Number Emissions Sources at the Tailpipe of Combustion Engines.
SAE Technical Papers, Vol. 2016-01-2283 n^o 2016-01-2283, pp. 1–10, 2016.
(cited in pp. 16, 21)